National Library of Canada
Canadian Theses Service
Ottawa, Canada
K1A 0N4

Bibliothèque nationale du Canada
Services des thèses canadiennes

CANADIAN THESES

THÈSES CANADIENNES

NOTICE

The quality of this microfiche is heavily dependent upon the quality of the original thesis submitted for microfilming. Every effort has been made to ensure the highest quality of reproduction possible.

If pages are missing, contact the university which granted the degree.

Some pages may have indistinct print especially if the original pages were typed with a poor typewriter ribbon or if the university sent us an inferior photocopy.

Previously copyrighted materials (journal articles, published tests, etc.) are not filmed.

Reproduction in full or in part of this film is governed by the Canadian Copyright Act, R.S.C. 1970, c. C-30.

AVIS

La qualité de cette microfiche dépend grandement de la qualité de la thèse soumise au microfilmage. Nous avons tout fait pour assurer une qualité supérieure de reproduction.

S'il manque des pages, veuillez communiquer avec l'université qui a conféré le grade.

La qualité d'impression de certaines pages peut laisser à désirer, surtout si les pages originales ont été dactylographiées à l'aide d'un ruban usé ou si l'université nous a fait parvenir une photocopie de qualité inférieure.

Les documents qui font déjà l'objet d'un droit d'auteur (articles de revue, examens publiés, etc.) ne sont pas microfilmés.

La reproduction, même partielle, de ce microfilm est soumise à la Loi canadienne sur le droit d'auteur, SRC 1970, c. C-30.

THIS DISSERTATION
HAS BEEN MICROFILMED
EXACTLY AS RECEIVED

LA THÈSE A ÉTÉ
MICROFILMÉE TELLE QUE
NOUS L'AVONS REÇUE

NL-339 (r. 86/06)

Canada

THE UNIVERSITY OF ALBERTA

INTERPRETATION OF TUNNEL CONVERGENCE MEASUREMENTS

by

JOHN PETER BARLOW

A THESIS

SUBMITTED TO THE FACULTY OF GRADUATE STUDIES AND RESEARCH

IN PARTIAL FULFILMENT OF THE REQUIREMENTS FOR THE DEGREE

OF MASTER OF SCIENCE

DEPARTMENT OF CIVIL ENGINEERING

EDMONTON, ALBERTA

SPRING 1986

Permission has been granted to the National Library of Canada to microfilm this thesis and to lend or sell copies of the film.

The author (copyright owner) has reserved other publication rights, and neither the thesis nor extensive extracts from it may be printed or otherwise reproduced without his/her written permission.

L'autorisation a été accordée à la Bibliothèque nationale du Canada de microfilmer cette thèse et de prêter ou de vendre des exemplaires du film.

L'auteur (titulaire du droit d'auteur) se réserve les autres droits de publication; ni la thèse ni de longs extraits de celle-ci ne doivent être imprimés ou autrement reproduits sans son autorisation écrite.

ISBN 0-315-30254-2

THE UNIVERSITY OF ALBERTA

RELEASE FORM

NAME OF AUTHOR JOHN PETER BARLOW

TITLE OF THESIS INTERPRETATION OF TUNNEL CONVERGENCE MEASUREMENTS

DEGREE FOR WHICH THESIS WAS PRESENTED MASTER OF SCIENCE

YEAR THIS DEGREE GRANTED SPRING 1986

Permission is hereby granted to THE UNIVERSITY OF ALBERTA LIBRARY to reproduce single copies of this thesis and to lend or sell such copies for private, scholarly or scientific research purposes only.

The author reserves other publication rights, and neither the thesis nor extensive extracts from it may be printed or otherwise reproduced without the author's written permission.

(SIGNED) ....J.B. Barlow.....

PERMANENT ADDRESS:
10207 - 107 AVENUE APT #6
EDMONTON, ALBERTA
T5H 0V6

DATED MARCH 27 1986

THE UNIVERSITY OF ALBERTA

FACULTY OF GRADUATE STUDIES AND RESEARCH

The undersigned certify that they have read, and recommend to the Faculty of Graduate Studies and Research, for acceptance, a thesis entitled INTERPRETATION OF TUNNEL CONVERGENCE MEASUREMENTS submitted by JOHN PETER BARLOW in partial fulfilment of the requirements for the degree of MASTER OF SCIENCE.

.....

Supervisor

.....

.....

Date March 27, 1986

ABSTRACT

An increasing number of tunnels are being designed according to observational methods, where a preliminary design is modified to suit the conditions observed during tunnel excavation. Deformation monitoring plays a central role in any observational design method, but unfortunately, in present practice monitoring results are not utilized to their full potential. Design decisions are often based totally on experience, or on a simplistic interpretation of the monitoring results.

A method has been developed for the interpretation of tunnel convergence measurements to provide a rational basis for the decisions that are made during the construction of a tunnel. This method is applied by fitting a series of semi-empirical equations to the convergence measurements near the tunnel face. The parameters that are determined by this process characterize the response of the rock mass to tunnel excavation, and are related to important physical quantities such as the extent of the yielded zone and the time-dependent properties of the rock mass. This method has been applied to laboratory tests and field observations from a large highway tunnel, to determine the best method of presenting convergence data, and the best procedure for determining the parameters.

It has been found that the use of this method in the interpretation of tunnel convergence measurements provides important information to guide design decisions. The size of

the zone of yielded material can be estimated with the measurements taken within one tunnel radius of the face. This enlightens the dimensioning and design of rock bolt systems. Furthermore, this method can be used to predict the ultimate behavior of the tunnel, and the effect that a variety of support systems could have on the tunnel. This allows the designer to fine tune the design of the support system to achieve the desired effect.

ACKNOWLEDGEMENTS

This research has been conducted under the supervision of Dr. P.K. Kaiser. His guidance and assistance are deeply appreciated. His generosity with time, and enthusiasm for the subject made the research an enjoyable and rewarding experience. Dr. N.R. Morgenstern and Dr. S. Thomson have also provided me with guidance and inspiration throughout my education at the University of Alberta. I would also like to express my appreciation for the help that Dr. D. Chan, S. Maloney and T. Casey have given me at various stages of this research.

The financial assistance that has been provided by the Natural Sciences and Engineering Research Council, Dr. P.K. Kaiser and various teaching assistantships is greatfully acknowledged.

I am especially grateful for the assistance and friendship of my fellow graduate students. Special thanks are extended to G. Pollock, T. Eaton, H. Plewes, R. Wong, F. Pelli, and H. Christian.

I would also like to thank my parents for their love, encouragement and support throughout my education.

Finally, I would like to thank my wife, Joan. She has been extremely supportive, and has assisted me in every possible way. I am deeply indebted to her for her love, understanding and continued encouragement.

Table of Contents

Chapter		Page
1.	INTRODUCTION	1
2.	REVIEW OF TUNNEL CONVERGENCE SOLUTIONS	5
	2.1 Introduction	5
	2.2 Physical Processes Causing Convergence	6
	2.3 Comparison of Existing Methods	8
	2.4 Presentation of Approach by Guenot, Panet and Sulem (1985).	11
	2.4.1 Time-Independent Convergence	12
	2.4.2 Time-Dependent Convergence	13
	2.4.3 Limitations of Approach	15
3.	EXTENSION OF CONVERGENCE EQUATION	22
	3.1 Introduction	22
	3.2 Extension for Pre-face Convergence.	23
	3.3 Extension for a Supported Tunnel	27
	3.3.1 Approach by Sulem (1983)	27
	3.3.2 Proposed Extension to Include Tunnel Support	28
	3.4 Numerical Analysis	32
	3.4.1 Description of Finite Element Analysis	32
	3.4.2 Presentation of Results	35
	3.4.3 Interpretation of Results	36
	3.4.4 Application to Convergence Confinement Method.	47
4.	APPLICATION OF CONVERGENCE SOLUTION TO LABORATORY TESTS	72
	4.1 Introduction	72
	4.2 Description of Laboratory Testing	72
	4.3 Logic of Data Presentation	78

4.4 Adaptation of Convergence Solution 81

4.5 Fitting The Convergence Solution to Laboratory Results 85

4.5.1 Example Fit 85

4.5.2 Discussion of Example Fit 89

4.5.3 Fit of Solution to Convergence Measurements 91

4.5.4 Presentation of Curve Fitting Results 92

4.6 Interpretation of Results 94

5. APPLICATION OF CONVERGENCE SOLUTION TO ENASAN TUNNEL (JAPAN) 117

5.1 Introduction 117

5.2 Description of Enasan Tunnel Project 117

5.2.1 Excavation and Support Placement Procedure 118

5.2.2 Instrumentation 120

5.3 Application of Convergence Solution to Sequentially Staged Excavations 121

5.4 Fit of Convergence Solution to Measurements 126

5.4.1 Example Fit 128

5.4.2 Presentation of Curve Fitting Results 135

5.5 Summary and Conclusions 140

6. CONCLUSIONS AND PRACTICAL IMPLICATIONS 166

6.1 Introduction 166

6.2 Summary of Conclusions 167

6.2.1 Finite Element Analyses 167

6.2.2 Laboratory Test Results 168

6.2.3 Enasan Tunnel 169

6.3 Practical Implications 170

6.3.1 Data Collection and Presentation 170

6.3.2 Applications of the Convergence Solution .172

6.4 Advantages of Convergence Solution 180

REFERENCES 185

APPENDIX A
Description of Computer Program SAFE. 189

APPENDIX B
Derivation of Equation 3.6. 192

APPENDIX C
Documentation of Computer Program CONRATE 193

C.1 Program Listing 194

C.2 Sample Input 200

C.3 Sample Output 201

APPENDIX D
Excavation Steps in Finite Element Analyses 202

APPENDIX E
Convergence Curves from Finite Element Analyses 210

APPENDIX F
Plots of Radial Strain vs Time; Excavation Simulation Test 7.13 221

APPENDIX G
Adaptation of Convergence Solultion for a Supported Tunnel. 226

APPENDIX H
Extension of Convergence Solution to Model Yield Zone Propagation. 232

List of Tables

Table		Page
3.1	Material Properties used in Finite Element Analysis	34
3.2	Compressibility Ratios for Liner Cases #1 to #5	46
3.3	Comparison of Convergence Solution and the Traditional RSS	48
5.1	Input Parameters for Convergence Solution; Support Analysis	133

List of Figures

Figure		Page
2.1	Stress Changes Associated With Tunnel Excavation.	18
2.2	Radial Displacements Behind Advancing Tunnel Face (Modified from Panet and Guenot, 1982).	18
2.3	Components of the Convergence Equation by Guenot et al. (1985).	19
2.4	Normalized Convergence Curves Given by Convergence Equation (Guenot et al., 1985), with a Variation in R.	20
2.5	Normalized Convergence Curves Given by Convergence Equation (Guenot et al., 1985), with a Variation in T.	21
3.1	Components of Convergence Solution for Unlined Tunnel.	52
3.2	Pre-face Convergence Curves from an Unlined Tunnel.	53
3.3	Convergence Confinement Method Diagram with Corresponding Convergence Curves.	54
3.4	Finite Element Mesh.	55
3.5	Unsupported Length Between Liner and Face.	56
3.6	Comparison of Unlined Tunnel Finite Element Analysis with Analyses by Others.	57
3.7	Convergence Data from Finite Element Analyses, for Liner #3.	58
3.8	Smoothed Convergence Curves from Finite Element Analyses, for Liner #3.	59
3.9	Smoothed Convergence Curves from Finite Element Analyses, for L_d = 0.25 a.	60
3.10	Comparison of Finite Element Results and Convergence Solution for Unlined Case.	61
3.11	Comparison of Finite Element Results and Convergence Solution, for Liner #3.	62

Figure Page

3.12 Convergence Curves from Elasto-Plastic Finite Element Analysis (Modified from Rankine and Ghaboussi, 1975). 63

3.13 Convergence Curves from 3-D Finite Element Analysis (after Kaiser,1983). 64

3.14 Supporting Arch Generated in the Rock Mass. 65

3.15 Equivalent Support Pressure Associated with Tunnel Excavation. 66

3.16 Equivalent Lining Pressure from Finite Element Analysis, for Liner #3. 67

3.17 Comparison of Equivalent Lining Pressures from Finite Element Analysis for Liner #3, and the Convergence Solution. 68

3.18 Normalized Pre-liner Equivalent Lining Pressure from Finite Element Analyses vs Normalized Support Delay. 69

3.19 Comparison of Convergence Curves from Finite Element Analyses and Convergence Solution, for Liner #3. 70

3.20 Convergence Confinement Method Diagram with Convergence Curves, for New and Traditional Solutions. 71

4.1 Laboratory Sample MC-6 Instrumentation (modified from Maloney, 1984). 101

4.2 Radial Strain vs Time - Test MC-6.02 (after Kaiser et al., 1982). 102

4.3 Radial Strain vs Time - Test MC-6.02 (after Kaiser et al., 1982). 103

4.4 Laboratory Sample MC-7 Instrumentation (modified from Kaiser et al., 1983b). 104

4.5 Radial Strain vs Time - Test MC-6.02 (Maloney, 1984). 105

4.6 Averaged Radial Strain vs Time, Test MC-6.02. 106

4.7 Averaged Radial Strain vs Time, Test MC-7.13. 106

Figure Page

4.8 Normalized Strain Rate vs Time, Test MC-6.02. 107

4.9 Radial Strain Rate Compared to Convergence Rate, Test MC-6.02, Station 81. 107

4.10 Comparison of Smoothed and Measured Normalized Strain Rate, Test MC-6.02, Station 81. 108

4.11 Fit of Convergence Solution to Strain Data, X Varied. 108

4.12 Fit of Convergence Solution to Strain Data, T Varied. 109

4.13 Fit of Convergence Solution to Strain Data, A^* Varied. 109

4.14 Fit of Convergence Solution to MC-6.02-81 Strain Data. 110

4.15 Fit of Convergence Solution to Convergence Data, MC-6.02-81. 111

4.16 Fit of Convergence Solution to MC-6.02-106 Strain Data. 112

4.17 Fit of Convergence Solution to MC-7.13-56 Strain Data. 113

4.18 Fit of Convergence Solution to MC-7.13-81 Strain Data. 114

4.19 Fit of Convergence Solution to MC-7.13-106 Strain Data. 115

4.20 Yielding associated with Test MC-7.13. 116

5.1 Plan View of East Section of Enasan Tunnel Project. 141

5.2 Cross Section of Enasan Tunnel. 142

5.3 Temporary Support System for Enasan Tunnel, Station A (Modified from Ito, 1983). 143

5.4 Temporary Support System for Enasan Tunnel, Station B (Modified from Ito, 1983). 144

Figure Page

5.5 Position of Convergence Measurements at Enasan Tunnel. 145

5.6 Convergence and Face Progress, Station A, Enasan Tunnel (after Kaiser, 1984). 146

5.7 Convergence and Face Progress, Station B, Enasan Tunnel (Modified from Ito, 1983). 147

5.8 Superposition of Convergence Curves from Excavation Stages. 148

5.9 Convergence from BIEM program for 3 Excavation Stages. 149

5.10 Convergence Solution with R/a Varied, Compared to Data from Station A-H2. 150

5.11 Convergence Solution with T Varied, Compared to Data from Station A-H2. 151

5.12 Convergence Solution with A^* Varied, Compared to Data from Station A-H2. 152

5.13 Fit of Convergence Solution to Data from Station A-H2. 153

5.14 Fit of Convergence Solution with Yield Zone Propagation to Data from Station A-H2. 154

5.15 Effect of Liner on Convergence Solution; Idealized Excavation. 155

5.16 Fit of Convergence Solution to Data from Station A-H1. 156

5.17 Fit of Convergence Solution to Data from Station A-Roof. 157

5.18 Fit of Convergence Solution to Data from Station A-D1. 158

5.19 Fit of Convergence Solution to Data from Station A-D2. 159

5.20 Fit of Convergence Solution to Data from Station B-H1. 160

5.21 Fit of Convergence Solution to Data from Station B-H1. 161

Figure Page

5.22 Fit of Convergence Solution to Data from Station B-H2. 162

5.23 Fit of Convergence Solution to Data from Station B-Roof. 163

5.24 Fit of Convergence Solution to Data from Station B-D1. 164

5.25 Fit of Convergence Solution to Data from Station B-D2. 165

6.1 Fit of Convergence Solution to Data from Enasan Tunnel, Station A-Roof (same as Fig. 5.17). 182

6.2 Convergence Solution Curves, Liner Thickness Varied; Idealized Excavation. 183

6.3 Convergence Solution Curves, Liner Placement Varied; Idealized Excavation. 184

D.1 Portion of Finite Element Mesh. 203

E.1 Convergence Curves from Finite Element Analysis; Liner #1. 211

E.2 Convergence Curves from Finite Element Analysis; Liner #2. 212

E.3 Convergence Curves from Finite Element Analysis; Liner #3. 213

E.4 Convergence Curves from Finite Element Analysis; Liner #4. 214

E.5 Convergence Curves from Finite Element Analysis; Liner #5. 215

E.6 Smoothed Convergence Curves based on Finite Element Analysis; Liner #1. 216

E.7 Smoothed Convergence Curves based on Finite Element Analysis; Liner #2. 217

E.8 Smoothed Convergence Curves based on Finite Element Analysis; Liner #3. 218

E.9 Smoothed Convergence Curves based on Finite Element Analysis; Liner #4. 219

E.10 Smoothed Convergence Curves based on Finite Element Analysis; Liner #5. 220

Figure Page

F.1 Radial Strain vs Time - Test MC-7.13; Station 81 (Maloney, 1984). 222

F.2 Radial Strain vs Time - Test MC-7.13; Station 81 (Maloney, 1984). 223

F.3 Radial Strain vs Time - Test MC-7.13; Station 106 (Maloney, 1984). 224

F.4 Radial Strain vs Time - Test MC-7.13; Station 106 (Maloney, 1984). 225

List of Symbols

a	Radius of tunnel
A	Ultimate time-dependent convergence
A^*	Ratio of $A/C_{x\infty}$
A_s	Cross sectional area of support per unit length
B	Curve fit parameter from convergence equation (Guenot et al., 1985)
C	Tunnel wall convergence
ΔC_k	Difference between unsupported and supported convergence at point of liner installation
ΔC_l	Convergence of tunnel liner
C_s	Convergence at point of tunnel support installation
$C_{x\infty}$	Ultimate time-independent convergence
$C_1(x)$	Time-independent convergence function, after face
$C_2(t)$	Time-dependent convergence function
C_{pf}	Time-independent convergence function, before face
C^*	Compressibility ratio
E	Young's Modulus of the ground
E_s	Young's Modulus of the support
G	Shear modulus
K	Parameter that reflects stiffness of liner
K_o	Ratio of horizontal to vertical earth pressure
k_p	Constant in convergence equation by Guenot et al. (1985)
K_s	2-D ring stiffness of a circular liner

L_d	Distance between face and point of liner installation
p_k	Equivalent lining pressure exerted before point of liner installation
p_l	Equivalent radial support pressure contributed by liner
p_o	Initial pressure in ground
p_r	Total equivalent radial support pressure
p_s	Actual pressure exerted on tunnel wall by support
$P_{k+}(x)$	Function to correct convergence before point of liner installation
$P_{k-}(x)$	Function to correct convergence after point of liner installation
$P_s(C)$	Function that pressure exerted by support
Q_1	Proportion of ultimate time-independent convergence that occurs ahead of the face
Q_2	Proportion of ultimate time-independent convergence that occurs after the face
Q_k	p_k/p_o
Q_b	Ratio of ultimate bench convergence to ultimate heading convergence
Q_i	Ratio of ultimate invert convergence to ultimate heading convergence
r	Distance from center of tunnel to point of interest
R	Radius of yield zone
T	Parameter that governs time-dependent convergence
t_f	Time at which the face passes the monitoring section
t_s	Thickness of liner

u	Radial displacement of tunnel wall
v	Velocity of tunnel excavation
x_f	Value of x at tunnel face
x_s	Value of x at point of liner installation
X	Parameter that governs time-independent convergence
a	Exponent of functions P_{k+} and P_{k-}
ϵ_r	Radial strain
λ	Fictitious support pressure (Guenot et al., 1985)
ν	Poisson's ratio of the ground
ν_s	Poisson's ratio of the tunnel support

1. INTRODUCTION

The design of a structure that interacts with the ground has traditionally followed the pattern of: sampling and testing to determine ground properties; modelling the response of the ground to the structure by using an appropriate model that incorporates the ground properties; and then designing the structure, based on the results of the analysis, to ensure adequate performance. This traditional approach is often poorly suited to the design of a tunnel for several reasons. First, obtaining a representative number of samples can be very difficult, especially in a mountainous environment. Second, the response of the ground to tunnel excavation is not easily modelled with analytical or numerical methods, due to the complexity of the tunneling environment. Factors that are difficult to quantify, such as the presence of joints and fractures and the method of construction, often exert a dominant influence on the behavior of the ground. In addition, there is an important interaction between the ground and the supporting elements of a tunnel that is not considered in the traditional design approach. The loads that must be carried by the tunnel supports are a product of this interaction. These difficulties have precluded the use of the traditional design approach in most tunneling projects.

A popular alternative to the traditional approach is the Observational Design Method. The general pattern that is

followed when the Observational Method is employed is to make a preliminary design based on the available information, and make necessary modifications to the preliminary design based on field observations. The importance of field observations in this method necessitates a thorough tunnel monitoring program. It is important to note the different purposes for monitoring a tunnel. If the safety of the opening is the only concern, a relatively sparse monitoring program could be adequate. However, if the monitoring program is to provide information on the behavior of the ground for the design of the support system, a much more comprehensive program is required. Only the tunnel monitoring results taken for the latter purpose are considered in this thesis.

Unfortunately, the present application of the Observational Method to tunneling projects falls short of the potential that exists within the method. Monitoring data, that is routinely taken, is not fully utilized, as design decisions are either based totally on experience, or on simplistic interpretations of the monitoring data. *The objective of this thesis is to develop a rational framework for the interpretation of tunnel monitoring results to provide information for the dimensioning of supports and the evaluation of the performance of existing supports.*

Monitoring programs typically include measurements of the ground deformation in response to the excavation, and the pressures that develop in the supports. The most common

measurement taken is the convergence of the tunnel walls, because it is the easiest to measure. Measurements of the deformation within the ground, using extensometers and inclinometers, are less common, but very informative. Pressures are typically monitored with gauges imbedded within the liner, or load cells at the ground liner interface. However, load cells are very sensitive to installation procedure, and often give unreliable results. *The method proposed in this thesis to interpret monitoring results will focus solely on convergence measurements, because they are the most easily obtained and universally measured.* In addition, convergence is a good indicator of the overall response of the ground because it is not dominated by localized processes as the other types of measurements mentioned above are (Kaiser et al., 1982).

The method proposed in this thesis for the interpretation of convergence measurements is based on an approach developed by Guenot et al. (1985). In this approach, a semi-empirical equation is fitted to the convergence measurements by adjusting parameters, that then characterize the response of the ground. These parameters are related to important physical quantities, such as the time-dependent properties of the ground and the extent of the yielding zone. This information provides valuable input into the Observation Design Method for the refinement of support design, and evaluation of support performance.

The approach by Guenot et al. (1985) is an important step toward a more rational interpretation of convergence data, but it is not applicable to many realistic tunneling conditions. It does not incorporate the influence that a tunnel support has on convergence, and it is unable to model sequentially staged excavations. This approach has been expanded in this thesis, to encompass these two effects to broaden its application to more realistic tunneling conditions. The most logical manner of presenting convergence data and of performing the curve fitting procedure has also been investigated, using data from laboratory tunnel excavation simulation tests (Kaiser et al., 1983a). Finally, the use of the proposed method as a practical design tool has been demonstrated on the Enasan Tunnel in Japan (Ito, 1983).

2. REVIEW OF TUNNEL CONVERGENCE SOLUTIONS

2.1 Introduction

There are many factors which influence the convergence of the walls of a tunnel. The excavation of a tunnel causes a redistribution of the existing stresses in the ground which causes elastic deformation, time dependent deformation and plastic deformation if yielding of the rock occurs. The convergence of a tunnel is a result of an interplay between the physical processes mentioned above. It is a formidable task to model the convergence of a tunnel taking all of the above factors into account. It is necessary to use a three dimensional visco-elastic or visco-plastic finite element analysis.

The major limitation of this type of rigorous analysis for practical use, is that the material properties required as input parameters are often difficult to determine and vary widely within the rock mass. The presence of discontinuities also limits the usefulness of the results as they often exert a controlling influence on the deformation mode of the rock mass. In addition, if the rock exhibits strain weakening behavior, the number of input parameters required is greatly increased. As a result of these difficulties associated with the realistic modelling of tunnel convergence, several authors have resorted to solutions that involve simplifying assumptions. These solutions often contain parameters that are determined by

curve fitting field measurements, rather than actual material properties.

This chapter contains a discussion of the physical processes that cause convergence, followed by a comparison of the existing methods that have been proposed to model convergence. The solution by Guenot, Panet and Sulem (1985) that has been adopted in the present study is then presented in detail along with a discussion of its advantages and limitations.

2.2 Physical Processes Causing Convergence

As a tunnel is excavated, the stresses that originally existed in the excavated core of material are transferred to the rock mass adjacent to and ahead of the excavation. The compressive stresses generate an arch that permits the rock to reach a new stable equilibrium condition. Any such stress change or stress redistribution process results in ground deformation and causes tunnel wall convergence. The stress change near an opening is illustrated by Figure 2.1 showing a rectangular element of rock at the tunnel wall. The initial stress of p_o before excavation is relieved in the radial direction during excavation and disappears, if the tunnel is unsupported. The tangential stress increases simultaneously due to arching and may eventually exceed the strength of the rock. For a ground stress condition of K_o=1.0, shown in Fig. 2.1, the tangential stress will eventually increase to $2p_o$ when the face is far away.

These stress changes cause immediate elastic deformation and may initiate creep deformation which continues at a decreasing rate until a new state of equilibrium is reached in the long term (unless accelerating creep leads to a collapse of the opening). If the stresses generated by the excavation exceed the yield strength of the rock, a plastic or yielded zone will propagate from the tunnel wall until a new state of stress equilibrium is achieved. This produces a decompressed annulus of yielded rock surrounding the excavation and additional convergence. The associated redistribution of stresses in turn affects the elastic and creep response of the rock inside and outside of the yielded rock mass.

The amount of convergence produced by the interplay of these processes at a given section along the tunnel is controlled by the position and shape of the tunnel face. When the face is close, it carries some of the additional stresses caused by excavation. As the face advances, its supporting effect decreases, and the stress in the rock adjacent to the excavation increases until it is bearing all of the additional stresses. This total stress change produces the final, maximum convergence.

The various methods that have been proposed to model these processes are compared in the following section.

2.3 Comparison of Existing Methods

Various approximate methods that have been used to model tunnel convergence. They differ not only in the manner they describe the physical processes that cause convergence, but also in how these processes are combined to express the resulting convergence.

A simplifying assumption that is common to all of the following methods, is that deformations only occur in a plane perpendicular to the tunnel axis. This eliminates displacements along the tunnel axis, and makes it possible to reduce the problem from three dimensions to two.

Descoeudres (1977) derived a closed form solution for the convergence of a tunnel in the vicinty of the face assuming that the tunnel face was a spherical cavity at the end of a cylindrical tunnel. This was done to account for the over excavation at the tunnel face that produces a non-planar face, and to assess the effect of damage or yielding of the face. The solution considers the effect of yielding, but neglects the time dependent deformation that invariably occurs in every tunnel, to varying degrees.

Lo and Yuen (1981) developed an explicit closed form solution that describes the time-dependenent response of the rock to the tunnel excavation. They paid particular attention to the stress transfer from the rock to the tunnel support and the effect that this decrease in stress has on the time dependent response of the rock. They did not, however, include the time independent component of

convergence in their solution, which makes it applicable only to cases where the full additional stress has already been transferred to the rock walls. This corresponds to a distance of at least two tunnel diameters past the face. This limitation was justified for the case histories that Lo and Yuen (1981) examined, where they were interested in the deformation of a tunnel support that was installed a long distance behind the face. However, the near face behavior is of primary interest in the present study so the time-independent component of convergence cannot be neglected.

Ladanyi and Gill (1984) went a step further toward developing a more generally applicable formulation of the time-dependent response, by considering the effect of the advancing tunnel face. They realized that the position of the face determines the stress at a given point which causes the rock to creep. They fell short however of fully modelling the interplay between the advancing face and the time-dependent convergence, as they only used the position of the face at the time of lining installation to determine the initial stress for their creep solution. In reality, the convergence continues to be influenced by the position of the face as the stress state is constantly changing until the face is sufficiently distant. In addition to this shortcoming, this approach only considers time-dependent convergence. Also, many input parameters are required including rock properties which are difficult to obtain.

This precludes the use of this method for practical applications where a small number of easily obtained parameters is desirable.

Otsuka and Kondoh (1981) developed an equation that describes convergence due to both the elastic, and time-dependent response of the rock to tunnel excavation. They derived it on the basis of a visco-elastic model, but then simplified it by replacing expressions involving several material properties with four representative parameters. These parameters characterize different aspects of the rock behavior, but are determined by fitting equations to field data rather than by measuring the parameters in field and laboratory tests. However, they do not include the effects of yielding in their equation and also disregard the influence that the position of the face has on the time-dependent behavior.

Sakurai (1978) developed an equation that fit cases generated by elastic and visco-elastic axisymmetric finite element analyses. The solution includes both elastic and time-dependent convergence, and simulates the creep realistically by taking the effect of the advancing face into account. It does not, however, allow for yielding of the rock and is not as easy to apply to a field case as the method by Otsuka and Kondoh (1981).

The method that is adopted for the present study was originally proposed by Panet and Guenot (1982) and later modified by Sulem (1983). They combined elasto-plastic

finite element analyses with field measurements to develop an equation with a similar structure to that proposed by Otsuka and Kondoh (1981). It has also four parameters that are determined by curve fitting. The solution contains elastic, plastic and time-dependent components of convergence and accounts for the influence of the advancing face on time-dependent behavior in a realistic manner. Their approach is described in detail in the following section.

2.4 Presentation of Approach by Guenot, Panet and Sulem (1985).

The general form of the convergence equation proposed by Guenot et al. (1985) is as follows:

$$C(x,t) = C_1(x) \{C_{x\infty} + A\, C_2(t)\} \qquad \text{Eqn 2.1}$$

where: $C_1(x)$ = time-independent, or loading function;

$C_2(t)$ = time-dependent function;

$C_{x\infty}$ = ultimate time-independent convergence (elastic + plastic);

A = ultimate time-dependent convergence; and

$(C_{x\infty} + A)$ = total ultimate convergence.

$C_1(x)$ represents the proportion of the ultimate stress change that has been transferred to the rock at a distance x from the face. The time-independent convergence is given by the product $C_1(x) * C_{x\infty}$, and the time-dependent convergence

is given by $C_1(x) * A * C_2(t)$. Thus, the time-dependent convergence is a function of the position of the face, x (which controls the stress change), and time. The two functions $C_1(x)$ and $C_2(t)$ are described below.

2.4.1 Time-Independent Convergence

The loading function $C_1(x)$ describes the stress increase in the rock surrounding the tunnel excavation as the face advances. Panet and Guenot (1982) simplified this three dimensional process by assuming that the support given by the face was equivalent to a "fictitious" radial support pressure acting on the tunnel walls. This "fictitious" pressure, p_r, varies from the initial stress in the medium, p_o, to zero after tunnel excavation is completed and is described by the function λ. This function is illustrated in Fig. 2.2.

Panet and Guenot (1982) determined the form of the function λ using an axisymmetric elasto-plastic finite element analysis. They found that the distribution of convergence behind the face could be adequately described by the function:

$$C_1(x) = C_{x\infty}\{1-[\frac{1}{1+\frac{x}{a \cdot B}}]^2\} \qquad \text{Eqn 2.2}$$

where: a = tunnel radius; and

B = curve fit parameter.

By varying the strength properties of the ground, they created plastic zones of different sizes, and found that B was almost constant at 0.84 R/a, where R is the radius of the plastic zone. This led to the form of the convergence function that is used in the present study:

$$C_1(x) = C_{x\infty} \{1-[\frac{1}{1 + \frac{x}{X}}]^2\} \qquad \text{Eqn 2.3}$$

where: X = 0.84 R.

This could be of great practical importance, because it makes it possible to determine the radius of the plastic zone by fitting the above function to convergence observations. Unfortunatly, this task is not as simple as Eqn. 2.3 suggests as will be discussed later.

2.4.2 Time-Dependent Convergence

The time-dependent convergence can best be observed during a stoppage of tunnel excavation, when the face advance component of convergence disappears and the remaining convergence is solely due to time-dependent stress redistribution and rock mass creep.

Panet and Guenot (1982) took advantage of one such work stoppage at the Fréjus Tunnel in France and determined that the time-dependent convergence could be adequately described by:

$$C_2(t) = \{1-[\frac{1}{1+\frac{t}{T}}]^{0.3}\} \qquad \text{Eqn 2.4}$$

where: T = parameter reflecting the shape of the creep curve for a particular rock.

Figure 2.3 illustrates the two components of Eqn 2.1 together with the total convergence curve that results from the addition of the two components.

The effect of the extent of the yield zone on the convergence is shown in Fig. 2.4. While the ultimate convergence increases with R, the normalized convergence curve becomes flatter. This corresponds well with field observations as will be demonstrated later. For Fig. 2.5, the parameter T has been varied to illustrate the influence of this creep parameter on the convergence curve. The convergence in both Figures 2.4 and 2.5, were normalized to the ultimate convergence, to demonstrate the dependence of the shapes of the convergence curves on the four parameters X, T, A, and $C_{x\infty}$. It is important to note that the extent of yielding significantly influences the shape of the initial part of the convergence curve (within two diameters of the face). In contrast, the creep characteristics of the rock dominate the shape of the latter part of the convergence curve. As shown later, this allows the determination of one parameter independent of the other.

The equation presented in this section has been successfully used by Sulem (1983) to match convergence measurements from two case histories. He found that fitting the equation to the data yielded a consistent set of parameters that characterized the rock mass.

2.4.3 Limitations of Approach

The major limitation of this approach is that the effect of a tunnel support is not considered. As Ladanyi et al. (1984) and Lo et al. (1981) have demonstrated, a support reduces the additional stress that could be transferred to the rock mass, and in so doing alters the convergence curve. Another limitation is that the approach in its current form does not consider the effect of excavation sequencing, as the approach is only applicable to full face excavation. Many tunnel excavations, particularly in poor ground involve sequential excavation and support techniques that cannot be simulated properly with this approach. All these limitations necessitate an expansion of these otherwise valuable concepts to more realistic conditions.

There is also a fundamental limitation to the manner in which the time-dependent behavior is modelled. The function that governs the time-dependent response of the rock, $C_2(t)$, is a continuous function that is initiated at t=0. The actual time-dependent component of convergence is given by the product of $C_2(t)$, A (the magnitude) and $C_1(x)$, which represents the proportion of the ultimate stress change that

has already developed. The function $C_2(t)$ is not a true creep function, as creep represents the response of a rock to a constant applied stress, which is a material property. Rather, $C_2(t)$ describes the response of the rock to a changing stress, that evolves from zero to the full stress change. It is therefore not a true material property, but a parameter that reflects the creep properties of the rock and the loading history. The function $C_2(t)$ is not only influenced by the rate of excavation, but also by the variations in the excavation rate. A continuous function, $C_2(t)$ will only be produced by a constant excavation rate. Thus, the convergence equation by Guenot et al. (1985) is only applicable to tunnels excavated at a constant rate. Fortunately, $C_2(t)$ (and hence, the parameter T) is relatively insensitive to changes in excavation rate as will be demonstrated later in Chapter 4.

The approach for interpreting convergence measurements proposed by Ladanyi and Gill (1984) involves a completely different method of modelling time-dependent behavior. Rather than commencing at t=0, their time-dependent function is initiated when the support is installed. Clearly, the rock displays time-dependent behavior right from the beginning of excavation, and this time-dependent function is not a pure creep function, as it not only depends on the creep properties of the rock, but also the time of support installation.

The only way of modelling the time-dependent behavior of the rock with a function that depends only on the creep properties, would be to superimpose a series of creep curves that correspond to each incremental increase in stress. This would be a formidable task that is not practically feasible. Thus, the methods mentioned above involve simplifying assumptions that make it possible to model the complex time-dependent response of a rock mass to the excavation of a tunnel. Both methods of modelling time-dependent behavior are a simplification of the actual physical process, and it is important to recognize these limitations.

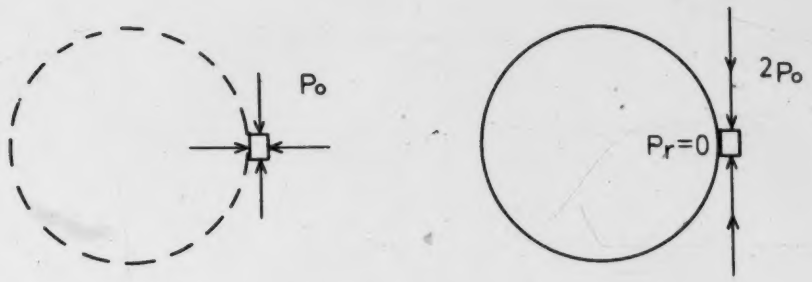

Figure 2.1 Stress Changes Associated With Tunnel Excavation.

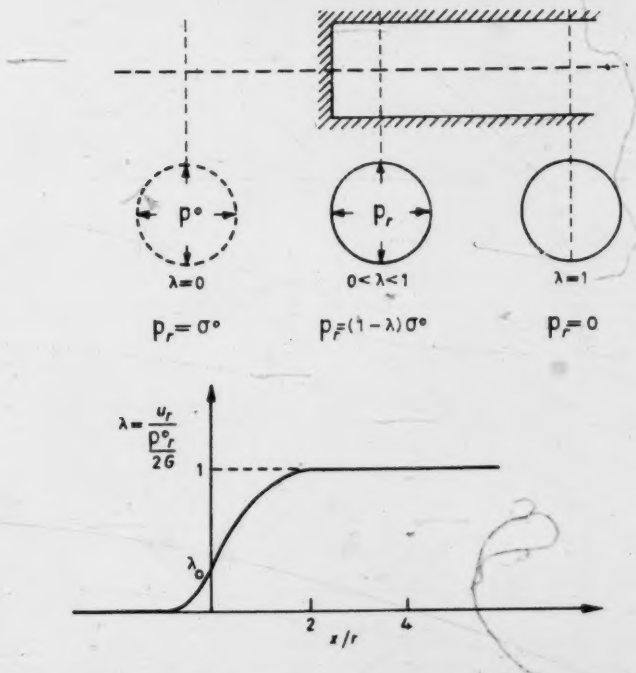

Figure 2.2 Radial Displacements Behind Advancing Tunnel Face (Modified from Panet and Guenot, 1982).

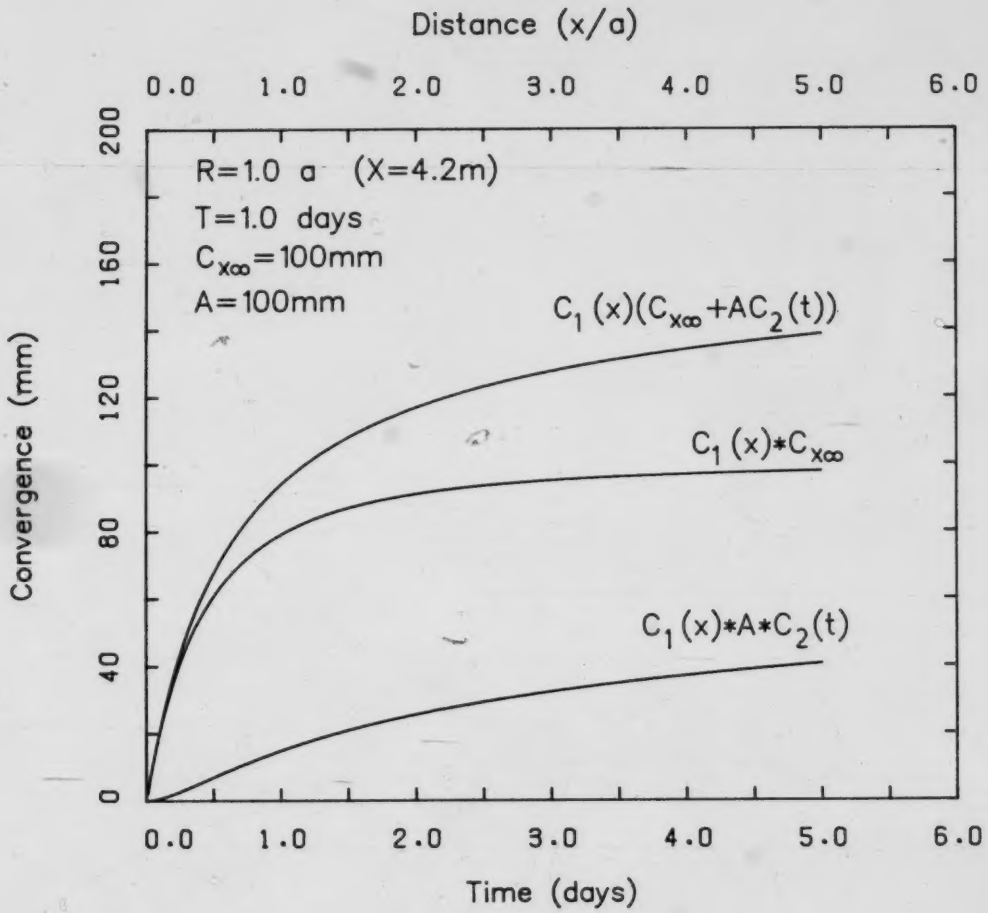

Figure 2.3 Components of the Convergence Equation by Guenot et al. (1985).

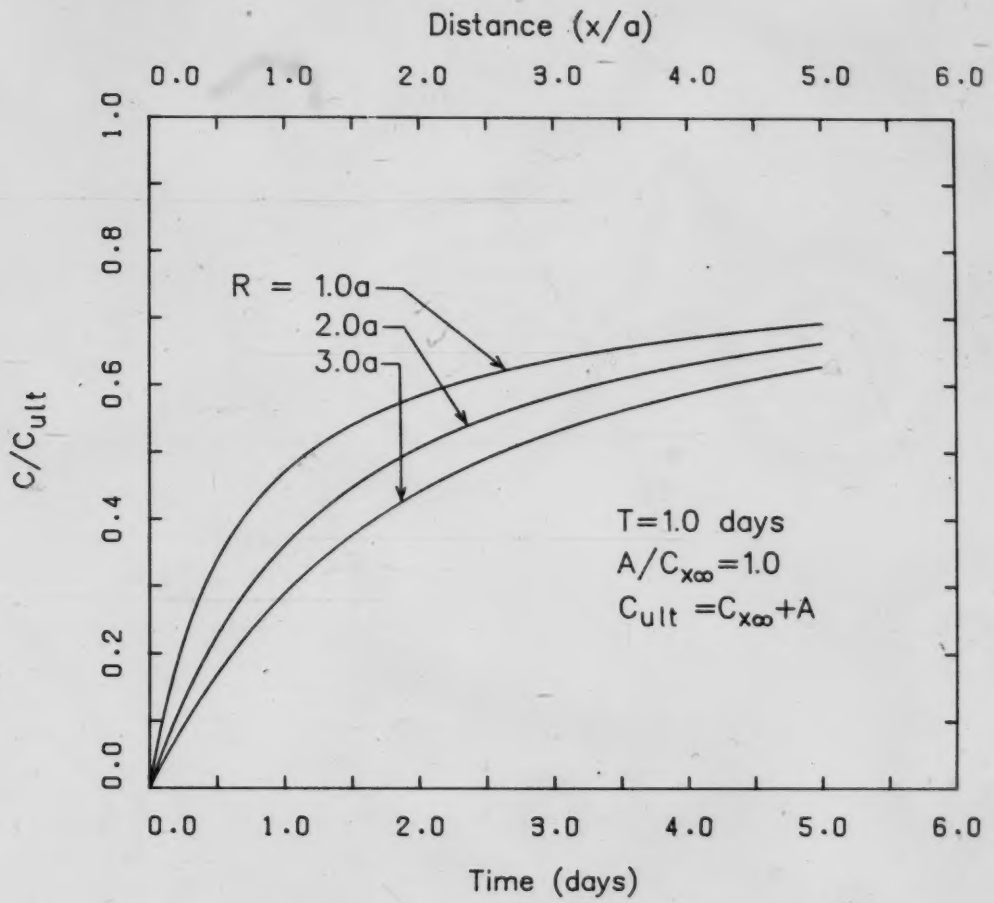

Figure 2.4 Normalized Convergence Curves Given by Convergence Equation (Guenot et al., 1985), with a Variation in R.

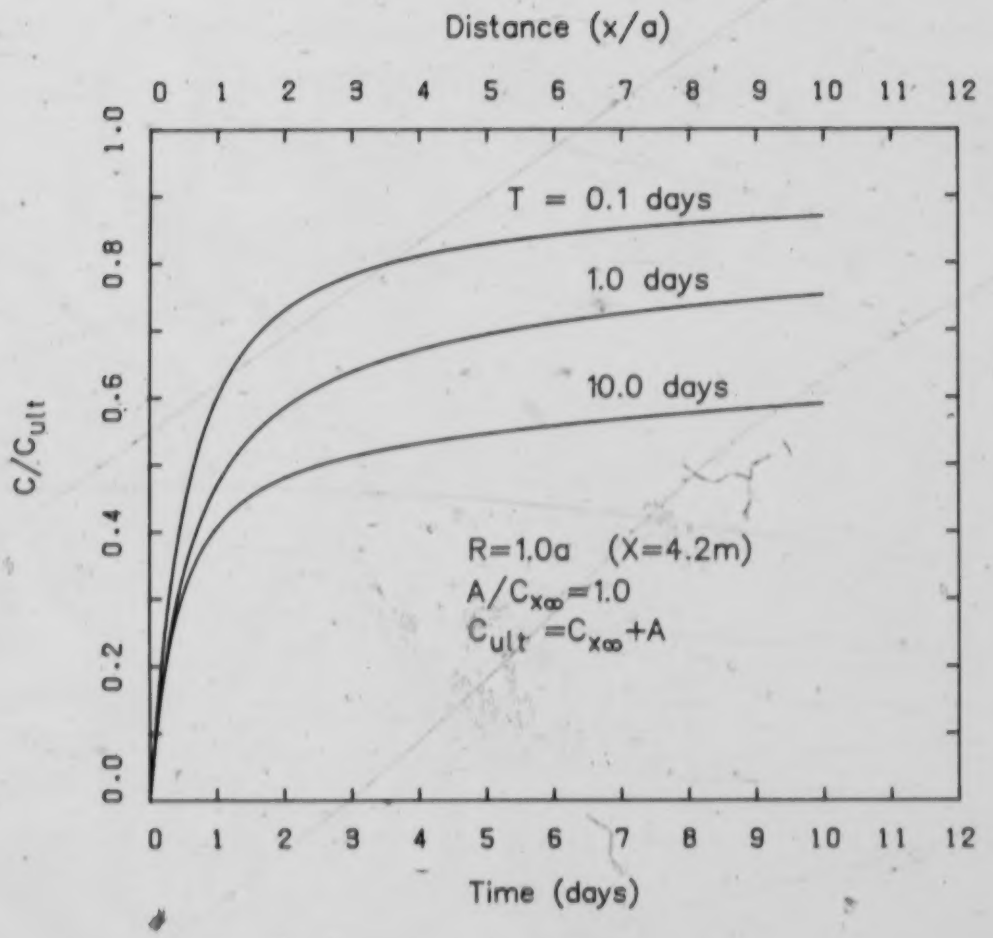

Figure 2.5 Normalized Convergence Curves Given by Convergence Equation (Guenot et al., 1985), with a Variation in T.

3. EXTENSION OF CONVERGENCE EQUATION

3.1 Introduction

The convergence equation by Guenot et al. (1985) is expanded in this section to broaden its application to more realistic tunneling conditions. The objective is is to make it applicable to the conditions present in the Enasan Tunnel case history, examined in Chapter 5. This tunnel, with a diameter of ten meters, was excavated in poor ground in three sequential stages and lined with a temporary support. The full details of the project are given in Chapter 5. Two modifications to the equation are necessary to make it applicable to the Enasan Tunnel. First, it must be extended to describe the convergence ahead of the face for the second and third stages. The tunnel wall exposed by the first excavation is affected by the stress changes that occur both before and after these advancing faces pass. Second, the convergence equation must also be expanded to incorporate the effects of a tunnel support. Both the stiffness of the liner and the distance between the face and the point of installation, influence the wall convergence, and must be included in the equation.

The proposed changes to the convergence equation are verified by comparison with results from a series of finite element analyses.

3.2 Extension for Pre-face Convergence.

The most important aspects of the pre-face convergence are the total amount of convergence that occurs ahead of the face and the slope of the convergence curve immediately ahead of the face. The magnitude of the convergence ahead of the face is important, because it reflects the amount of stress change that occurs ahead of the face. The slope of the convergence curve, or the convergence rate, immediately ahead of the face has an important influence on the shape of the overall convergence rate curve, which will be examined in detail in Chapters 4 and 5. It is not as important to model the exact shape of the pre-face convergence curve, even for a sequential excavation. The primary reason for prediction of the tunnel wall convergence, is to provide information for the design of the support system. Since supports are usually not activated until all of the stages have been excavated at a given section, it is the post-face convergence curve that is of primary interest. Thus, an equation that provides an approximate fit of the pre-face convergence curve, and models correctly the magnitude of convergence at the face, and the rate of convergence immediately ahead of the face, would be adequate.

Several finite element analyses have been performed in this study to model the convergence associated with the excavation of a tunnel. This analysis will be presented in detail in Section 3.4, but the pre-face portion of the convergence curve for the unlined tunnel case will be used

in this section to develop an equation that describes this portion of the curve.

Convergence occurs ahead of the face because the approaching excavation causes a redistribution of stresses that increases the stress in the vicinity of the face. The convergence equation can be used to describe the distribution of this convergence if the pressure term, $C_1(x)$, is altered to reflect the portion of this stress change that occurs ahead of the face. It must increase from zero far ahead of the face to a value at the face that will produce the amount of convergence given by the finite element analyses.

The following equation is proposed to describe the **pre-face portion of the convergence curve**, based on the finite element analysis:

$$C(x,t) = Q_1 \, C_{pf}(x)[C_{x\infty} + A \, C_2(t)] \qquad \text{Eqn 3.1}$$

where: Q_1 = proportion of the total stress change associated with excavation that occurs ahead of the face; and

$$C_{pf}(x) = \left[\frac{1}{1 + \left(\frac{x_f - x}{X}\right)}\right]^{1.2}$$

where: x_f = value of x at tunnel face.

The **post-face portion of the convergence curve** would now be described by:

$$C(x,t) = [Q_1 + Q_2\, C_1(x)][C_{x\infty} + A\, C_2(t)] \qquad \text{Eqn 3.2}$$

where: Q_2 = proportion of the total stress change associated with excavation that occurs after the face.

Note that $C_{x\infty}$ and A now represent the total (pre-face + post-face) time-independent and time-dependent components of convergence, respectively.

Equations 3.1 and 3.2 describe the entire range of convergence, and will be referred to jointly as the "Convergence Solution" in the remainder of this thesis.

The proportion of the total stress change, given by the pressure term in Eqn 3.1, gradually increases from zero, far ahead of the face, to Q_1 at the face. This stress change produces a time-independent convergence of $C_{x\infty} * Q_1$ at the face and initiates the time-dependent convergence. The proportion of the total time-dependent convergence that has occurred at the face depends, therefore, on the rate of excavation. The maximum time-dependent convergence that could occur at the face is $Q_1 * A$. This would only occur if the excavation rate was infinitely slow. At regular advance rates, the time-dependent deformation at the face will be small because insufficient time will be available to reach the ultimate creep level. The time-independent and time-dependent components of convergence given by the Convergence Solution (Eqns 3.1 and 3.2) are illustrated in Fig. 3.1. The convergence curves produced by the Convergence

Solution in Fig. 3.1 were calculated by the computer program CONRATE. This program calculates convergence curves according to the Convergence Solution presented above for any given set of input parameters. A full description of the capabilities of CONRATE, along with a program listing and an example run are contained in Appendix C.

In Fig. 3.2, Eqn 3.1 is compared to the pre-face portion of the convergence curve from the finite element analysis of an unsupported tunnel. The equation satisfies the criteria outlined earlier, i.e., it produces the correct magnitude of convergence at the face and fits the slope of the convergence curve immediately ahead of the face. The time-dependent behavior is not included in this figure because the FE analysis did not consider the effect of time.

The value of Q_1 determined in the finite element analysis was 0.27, which corresponds to the value given by Panet and Guenot (1982). However, in their elasto-plastic analyses, they discovered that Q_1 increased with an increase in the radius of the plastic zone. For example, a radius of the plastic zone, R, of 2.15a produced a Q_1=0.58. The effect that yielding has on the value of Q_1 is an important consideration, that will influence the application of this method in Chapters 4 and 5.

In summary, the convergence equation by Guenot et al. (1985) has been expanded to describe the full range of convergence, both ahead of, and after the face. This is an essential modification for the application of the

Convergence Solution to tunnels excavated in sequential stages. The other modification that will broaden the application of the Convergence Solution to more realistic conditions, is the incorporation of the effect of a tunnel support.

3.3 Extension for a Supported Tunnel

3.3.1 Approach by Sulem (1983)

Sulem (1983) outlined a proposal for incorporating the effect of a support into the convergence equation (Guenot et al. 1985). He modelled a supported tunnel with a series of finite element analyses in which he varied the stiffness of the liner, K_s, and the distance between the face and the point of liner installation, L_d. He fitted the convergence equation to each of these cases, and found that a variation in support stiffness was reflected in a variation in the parameters T, A and $C_{x\infty}$. The parameter X, and the ratio $A/C_{x\infty}$ remained more or less constant. He also found that a variation in L_d caused a variation in A and $C_{x\infty}$, but X and T remained constant. From these findings he suggested that the effect of a support could be introduced into the convergence equation through the parameters T, $C_{x\infty}$ and A. He did not, however, propose any generally applicable relationship between the liner properties and these parameters, that could be used for the interpretation of convergence data from other lined tunnels.

Sulem's approach constitutes an important step toward incorporating the effect of a support into the convergence equation, but it contains some inconsistencies that have precluded its use in the present study. The parameters in the convergence equation all reflect certain physical properties of the rock: T characterizes the time-dependent properties of the rock; $C_{x\infty}$ and A represent the magnitude of the immediate and time-dependent convergence, respectively, that occur in response to the stress change associated with tunnel excavation. The introduction of a support doesn't change the properties of the rock, but alters the stress state. Therefore, introducing the effect of a support by altering these parameters changes their original physical meaning.

The approach developed in the following section attempts to reflect more accurately the effect of the actual physical process of support installation sequence and support stiffness.

3.3.2 Proposed Extension to Include Tunnel Support

The excavation of a tunnel causes a gradual transfer of stress from the original unexcavated core of rock to the surrounding rock mass, as tunnel excavation proceeds. When a tunnel support is introduced, it alters this process of stress transfer, by sharing the load with the rock mass as it evolves with the advance of the tunnel face. This reduces the amount of additional load carried by the rock mass, and

hence decreases the convergence of the walls of the tunnel. The Convergence Confinement Method (CCM), summarized by Hoek and Brown (1980), provides a useful illustration of this process of load sharing. The method is illustrated in Fig. 3.3, where the equivalent radial support pressure, p_r, is plotted against the convergence of the tunnel wall. These two quantities are normalized to the initial pressure, p_o, and the ultimate time-independent convergence, $C_{x\infty}$, respectively. Also shown are the convergence curves that correspond to the CCM diagram. The Ground Convergence Curve (GCC) in Fig 3.3 gives the relationship between equivalent support pressure and convergence. When there is no support installed, the equivalent support pressure represents the three dimensional support provided by the ground ahead of the tunnel face. This is identical to the "fictitious" support pressure of Panet and Guenot (1982), described in the preceeding chapter. This pressure decreases from the initial stress before excavation, at u=0, to zero when the excavation is completed, and the face is far enough away that it provides no supporting influence. At this point, the rock mass is bearing all of the additonal load, and the ultimate time-independent convergence ($C_{x\infty}$) is reached. However, when a support is installed, it gradually takes on load as the walls converge until a new state of stress equilibrium is reached. At this point, the support bears the pressure p_s(final), and the rock mass is bearing the pressure difference: [p_o - p_s(final)], shown in Fig. 3.3.

The slope of the Support Confinement Curve (SCC) is dictated by the stiffness of the support. For a circular liner, this is termed the ring stiffness and is given in Eqn 3.3 (Hoek and Brown, 1980).

$$K_s = \frac{E_s[a^2-(a-t_s)^2]}{(1+\nu_s)[(1-2\nu_s)a^2+(a-t_s)^2]} \qquad \text{Eqn 3.3}$$

where: E_s = Young's modulus of the liner;

a = tunnel radius;

t_s = Liner thickness; and

ν_s = Poisson's ratio of the liner.

The support pressure for a given liner convergence, ΔC_l, is given by:

$$P_s(C(x,t)) = K_s \frac{\Delta C_l}{2a} \qquad \text{Eqn 3.4}$$

The finite element analyses (described in Section 3.4) that generated the convergence curves in Fig. 3.3 do not include time-dependent convergence. The introduction of a support also decreases the time-dependent convergence. Without a support, time-dependent convergence is driven by the full stress change, p_o, after the face is far away. When a support is introduced, it is the new ultimate pressure, $[p_o - p_s(final)]$, that causes the time-dependent convergence of the rock mass, and the pressure p_s drives the creep of

the liner material, if it exhibits creep.

The most logical way of introducing the effect of the support into the Convergence Solution is to subtract the amount of pressure taken by the support, $P_s(C(x,t))$, from the total pressure that has been transferred to the rock mass from the face, $(Q_1 + Q_2 C_1(x))$, as follows:

$$C(x,t) = [Q_1 + Q_2 C_1(x) - \frac{P_s(C(x,t))}{P_o}][C_{x\infty} + AC_2(t)] \quad \text{Eqn 3.5}$$

The support pressure, $P_s(C(x,t))$, is normalized to the initial stress, p_o, to be compatible with $C_1(x)$, which is also normalized to p_o. Substituting Eqn 3.4 into Eqn 3.5 and simplifying (Appendix B) leads to:

$$C(x,t) = \frac{[Q_1 + Q_2 C_1(x) + KC_s]}{[1 + K(C_{x\infty} + AC_2(t))]}[C_{x\infty} + AC_2(t)] \quad \text{Eqn 3.6}$$

where: C_s = Convergence at the point of liner installation;
and

$$K = \frac{K_s}{2ap_o}$$

Thus, the Convergence Solution for a supported tunnel is now described by three equations: Equations 3.1 and 3.2 give the convergence before the liner is installed, and Eqn 3.6 applies after liner installation.

In contrast to the method proposed by Sulem (1983) for handling the influence of a support, this introduces the effect of the support in one additional parameter, K, which can be related directly to the liner properties. Furthermore, the other parameters remain unchanged and retain their original physical meaning.

A further modification of the Convergence Solution will be given later, that reflects the influence that a support has ahead of the point of support installation.

3.4 Numerical Analysis

A numerical analysis has been performed to establish a basis for the parameters needed in the modified Convergence Solution. The convergence curve for the unlined case has already been presented in Section 3.2 to aid in the development of the pre-face portion of the Convergence Solution. This section contains a description of the numerical analysis, a presentation of the results, and the application of the results to the supported tunnel case.

3.4.1 Description of Finite Element Analysis

Finite element analyses were performed using the program SAFE (Soil Analysis by Finite Element), developed by Chan (1985) at the University of Alberta. A brief description of this program is contained in Appendix A. The ground was modelled as an axisymmetric medium, with a stress condition of K_o=1.0. A linear elastic constitutive

relationship has been used throughout. The mesh and the boundary conditions are shown in Fig. 3.4. The top boundary of the mesh is a pressure boundary with displacements restrained in the horizontal direction. This simulates a deep tunnel where the top boundary is within the rock mass and is therefore not free to move horizontally.

The left side boundary is initially a pressure boundary, to create an isotropic stress state in the ground, but it is changed to a boundary with zero horizontal displacement for all following steps. This simulates more accurately the conditions that would exist on such a plane in a rock mass, where the pressure does not remain constant, but changes in response to the excavation of the tunnel. No horizontal displacements on the right side nor vertical displacements on the bottom boundary were allowed.

The analyses model six cases: an unlined tunnel, and five lined tunnels with liners of various stiffnesses. The properties of the rock and each of the liners are summarized in Table 3.1.

Table 3.1. Material Properties used in Finite Element Analysis.

	E (GPa)	ν	Liner Thickness (mm)	t_c* (mm)
Rock**	0.5	0.40	-	
Liner #1	2.5	0.15	625	52
Liner #2	5.0	0.15	625	104
Liner #3	10.0	0.15	625	208
Liner #4	30.0	0.15	625	625
Liner #5	60.0	0.15	625	1250

a = 5.0 m; p_o= 11.25 MPa

* Thickness of a circular concrete liner that would provide the equivalent support.

** Selected to represent conditions at Enasan Tunnel (see Chapter 5)

Each of the lined tunnel cases consisted of four runs in which the distance between the face and the point of liner installation changes. These four gaps, termed L_d, are 0.25,0.75,1.25, and 1.75 radii. Due to the discrete nature of the excavation and lining placement process, L_d is an equivalent unsupported length, illustrated in Fig. 3.5. L_d is the sum of the distance between the face and the front of

the liner, and half of the round length. This is the same definition adopted by Einstein and Schwartz (1979). The sequence of steps involved in these analyses are summarized in Appendix D.

3.4.2 Presentation of Results

The distribution of convergence along the tunnel axis given by the finite element analysis for the unlined tunnel case is shown in Fig. 3.6 together with results from similar analyses found in the literature (Kaiser, 1983) and (Panet and Guenot, 1982). There is very close agreement with the other analyses.

Typical convergence curves from the analysis are shown in Fig. 3.7. The convergence curve of the unlined tunnel is shown together with the four curves from the tunnel lined with Liner #3. The four curves correspond to four different support delays. The figure shows that a decrease in support delay reduces the ultimate convergence, and affects the shape of the convergence curve. For a detailed discussion of the influence of a finite element mesh on convergence curves, see Pelli et al. (1986).

The waviness of the curves is a result of the discrete, step-wise excavation and lining placement process followed in the analysis. Both the Convergence Solution that these results are to be compared to, and observations made in real tunnel projects are more continuous in nature. Thus, to allow a better comparison, smooth curves were created by

visually fitting a curve to the FE data. Figure 3.8 contains the smoothed curves for Liner #3 that correspond to the data shown in Fig. 3.7. The original and smoothed convergence curves for each liner case are given in Appendix E.

The effect that the stiffness of the liner has on convergence distribution is illustrated by Fig. 3.9. The convergence curve for the unlined case is shown together with the curves from the five lined tunnel cases for a support delay of 0.25 radii. This shows that an increase in stiffness causes a significant reduction in convergence. For the remainder of this chapter only the smoothed convergence curves will be used.

3.4.3 Interpretation of Results

The purpose of performing the numerical analysis was to evalute the modifications proposed for the Convergence Solution. In Fig. 3.10, the unlined case is compared to the convergence curve, produced by the Convergence Solution for an unlined tunnel (Eqns 3.1 and 3.2). The program CONRATE (Appendix C) was used to generate the Convergence Solution curve. Good agreement between the results of the FE analysis and the Convergence Solution for the unlined case can be observed. The solution slighty overpredicts the convergence from one to two radii from the face, but this fit is considered adequate for practical purposes, and is comparable to the fit that Panet and Guenot (1982) achieved.

The Convergence Solution for a supported tunnel (Eqns 3.1, 3.2, and 3.6) is compared to the convergence curve from the finite element analysis, with Liner #3, in Fig. 3.11. Again, the program CONRATE (Appendix C) was used to generate the Convergence Solution curves. The convergence produced by the FE analysis is significantly less than the convergence predicted by the solution. These two curves diverge even before the point of liner installation, x_s. The portion of the curve for $x < x_s$ was described by the Convergence Solution for the unlined case.

This phenomenon can be observed in other numerical analyses of this nature. Fig. 3.12 shows the lined and unlined convergence curves from an axisymmetric, elasto-plastic, finite element analysis by Rankine and Ghaboussi (1975). A major convergence difference, ΔC_k, also exists between the two curves at the point of liner installation. The convergence curves from a three dimensional, linear elastic, finite element analysis performed by Kaiser (1983) are shown in Fig. 3.13. The unlined and lined curves in this figure also diverge before the point of liner installation.

It follows from these examples, that the assumption of equal wall convergence for a lined tunnel and an unlined tunnel before the point of liner installation, is not appropriate. However, this is an assumption that is commonly adopted for the use of the Convergence Confinement Method. It is also implicit in the Relative Stiffness Solution

proposed by Einstein and Schwartz (1979). The application of this finding to the CCM will be discussed in more detail in Section 3.6.

This result is, however, consistent with the actual physical process of stress transfer near the face. The effect that a liner has on the rock is not confined to the area behind the liner installation point. It is distributed along the tunnel axis, ahead of, and after x_s, in the same manner that the supporting influence of the rock at the face is distributed before and after the face. Figure 3.14 illustrates the supporting effect that the face and the liner have on the unsupported gap between the face and x_s through the process of arching.

A further modification of the Convergence Solution is therefore required to incorporate this effect. It should reflect the actual physical process that occurs in the rock. Fig. 3.15 provides a helpful illustration of the effect that the supporting components have on the equivalent radial support pressure, p_r. This is not an actual pressure, but is the equivalent two dimensional radial pressure that would produce the observed convergence. This figure shows the interaction between the equivalent support provided by the rock ahead of the advancing tunnel face (p_f), and the equivalent support provided by the liner (p_l). The quantities shown in Fig. 3.15 were calculated from the finite element analysis, Liner #3, with a support delay of 0.25 radii. The curve labelled p_f is the equivalent support

provided by the face that decreases with tunnel excavation from 1.0 before the face to zero after the face is far away. The curve labelled p_s represents the actual pressure at the rock/liner interface that is generated by the liner as it is compressed by the converging walls. The curve p_l represents the equivalent radial pressure that is felt by the rock mass in response to the liner.

Thus, p_l is the equivalent two dimensional radial support pressure that would produce the same effect as the actual liner pressure, p_s. The quantity p_l was calculated from the convergence curves for the lined and unlined tunnel cases in Fig. 3.8. The difference between these two curves reflects the impact that the liner has on tunnel wall convergence. Consequently, the equivalent effect of the liner, p_l, is obtained by expressing this difference as a proportion of $C_{x\infty}$, on the assumption that equivalent pressure is proportional to time-independent convergence. This assumption is central to the development of the original convergence equation by Panet and Guenot (1982).

The sum of p_f and p_l yields p_{total}, which is the total equivalent support pressure that produces the actual time-independent convergence in a supported tunnel. This is the equivalent pressure that reflects the stress change that drives the time-dependent convergence.

The difference between the curves p_s and p_l indicates that there is a transfer of stress from the unsupported gap to the liner. This stress transfer will now be described for

a point (A) on the tunnel wall (Fig. 3.15). The pressure experienced at this point, as it moves from Position 1, to Position 4, reflects the sequence of events that would occur at a stationary point as the excavation-lining placement process proceeds through the rock mass.

At Position 1, p_f is decreasing due to the unloading of the approaching excavation and p_l is increasing as the supporting effect of the approaching liner is just being felt. At Position 2, both the rock ahead of the face, and the liner are working together to support a rock arch. The pressure p_f is decreasing rapidly as the face is advancing, and p_l is increasing rapidly as the liner is approaching. p_l increases to p_k at the point of liner installation. Thus, the total amount of equivalent pressure that has been transferred to Point A before liner installation is p_k. At Position 3, the liner has been installed, and is generating the actual pressure, p_s, as it deforms with the tunnel walls. The pressure, p_s, that the liner is exerting on the rock mass at Point A is inhibiting the displacement of Point A, and is therefore increasing the equivalent support pressure, p_l. However, it is also partially supporting the rock arch which is inhibiting displacements of the present unsupported length, which is now to the left of Point A. Thus, the pressure p_s at Point A increases more than the equivalent support pressure p_l, as only a portion of p_s is inhibiting displacement at Point A. At Position 4, p_s and p_l are equal, which means that the full pressure, p_k, that was

transferred to Point A while it was ahead of the liner has now been transferred to the liner at point A as it has supported subsequent unsupported lengths. The equivalent pressure provided by the face, p_f, has almost vanished, as the face has advanced more than four radii past point A. When the face becomes sufficiently distant, that it provides no support, p_s and p_{total} are equal.

This transfer of the equivalent pressure, p_k, must be incorporated into the series of equations that constitute the Convergence Solution. This has been done by introducing another term into the two equations that describe convergence before x_s (Eqns. 3.1 and 3.2). This term gradually applies an equivalent support pressure ahead of the liner, up to a value of p_k at x_s. Furthermore, a similar term must also be added to the last equation such that this pressure p_k is gradually applied to the liner.

The additional term that applies pressure before x_s must fit the p_1 curve, shown in Fig. 3.15, up to x_s. Thus, a term is required that starts at zero and increases to p_k at x_s. An equation similar in form to the pre-face Eqn 3.1 would accomplish this. However, the shape of the p_1 curve depends on the support delay, as illustrated in Fig. 3.16. This figure shows the p_1 curves for the four delay cases of Liner #3, (finite element analyses). For a delay of 0.25 radii, the pre-liner portion of the p_1 curve rises very steeply. As the delay increases, the curves rise much more gradually. Hence, it was decided to approximate this effect

by an equation similar in form to Eqn 3.1. The exponent will depend on the magnitude of the delay.

The exponent shown in the following equation provides an adequate fit to the p_1 curves of Fig. 3.15.

$$Q_k * P_{k+}(x) = Q_k\left[\frac{1}{1 + \left(\frac{x_s - x}{x}\right)}\right]^a \qquad \text{Eqn 3.7}$$

where: $a = 1 + \frac{a}{L_d}$.

The function $P_{k+}(x)$ gradually increases from zero to a value of 1.0 at x_s. The parameter Q_k is the equivalent pressure, p_k, normalized to the total pressure p_o. Hence, the product of Q_k and $P_{k+}(x)$ yields a function that increases from zero to Q_k at the face.

The exponent (a) of Eqn 3.7 is large for small support delays, which gives a more gradually rising function. The curves generated by this equation are compared to the finite element p_1 curve for a delay of 0.25 radii, in Fig. 3.17. This shows that Equation 3.7 is only an approximation of the pre-liner portion of the p_1 curve. The p_1 curve has an abrupt change in slope at the face, but is approximated by one continuous function (Eqn 3.7). The reason for this approximation is that it is desirable to express this effect in one term involving as few additional parameters as possible. As will be shown later, this approximation produces convergence curves that adequately fit the finite

element convergence curves.

The new term given by Eqn 3.7 is incorporated into Eqns 3.1 and 3.2 in the following manner:

- for $x < x_{face}$:

$$C(x,t) = [Q_1 C_{pf}(x) - Q_k P_{k+}(x)][C_{x\infty} + AC_2(t)] \qquad \text{Eqn 3.8}$$

- for $x_{face} < x < x_s$:

$$C(x,t) = [Q_1 + Q_2 C_1(x) - Q_k P_{k+}(x)]\,[C_{x\infty} + AC_2(t)] \qquad \text{Eqn 3.9}$$

$Q_k P_{k+}(x)$ is subtracted from the loading terms in the above equations to simulate the influence that the liner has ahead of the point of liner installation. This decreases the amount of pressure transferred to the rock mass from the advancing face, given by $Q_1 C_{pf}(x)$ in Eqn 3.8 and $Q_1 + Q_2 C_1(x)$ in Eqn 3.9. The result of this decrease in the pressure that acts on the rock mass is a decrease in both time-independent and time-dependent convergence.

The term that reapplies the pressure, p_k, onto the lined portion of the tunnel must now be added to Eqn 3.6, which describes the lined portion of the convergence curve ($x > x_s$). This is accomplished by decreasing this extra support pressure that was applied ahead of the liner from a value of p_k at x_s to zero at large x. The reverse of the function given in Eqn 3.7 is proposed as follows:

$$Q_k * P_{k-}(x) = Q_k\left[\frac{1}{1 + \left(\frac{x-x_s}{X}\right)}\right]^a \qquad \text{Eqn 3.10}$$

This function decreases from a value of $\frac{p_k}{p_o}$ (or Q_k) at x_s to zero at large x. This is incorporated into Eqn 3.6 in the following manner:

• for $x > x_s$:

$$C(x,t) = [Q_1 + Q_2C_1(x) - P_s(C(x,t)) - Q_kP_{k-}(x)]\,[C_{x\infty} + AC_2(t)]$$

$$= \frac{[Q_1 + Q_2C_1(x) + KC_s - Q_kP_{k-}(x)]}{[1 + K(C_{x\infty} + AC_2(t))]}\,[C_{x\infty} + AC_2(t)] \qquad \text{Eqn 3.11}$$

The simplification to obtain Eqn 3.11 follows the same procedure as that found in Appendix B.

The term $Q_kP_{k-}(x)$ transfers the extra pressure p_k onto the lined portion of the tunnel as it decreases from a value of $\frac{p_k}{p_o}$ ($=Q_k$) to zero.

The elimination of this pre-liner support pressure increases the total equivalent pressure that causes convergence to $Q_1 + Q_2C_1(x)$. This increase in total equivalent pressure causes increased liner deformation, and hence, a greater liner pressure, p_s. In this manner, the equivalent support pressure, p_k, that acts ahead of the liner to inhibit convergence is transferred to the liner.

The equivalent support pressure is given by the terms $[P_s(C(x,t)) - Q_k P_{k-}(x)]$ in Eqn 3.11. This sum is plotted in Fig. 3.17 to describe the p_l curve after the point of liner installation. This figure illustrates the equivalent support pressure that is produced by the Convergence Solution with the new terms introduced above. As shown in Fig. 3.17 the predicted p_l curve gives an adequate fit of the curve given by the finite element analyses.

The application of this series of equations requires a knowledge of the parameter Q_k. The values of Q_k that have been derived from the finite element analyses are shown in Fig. 3.18. This figure shows that Q_k decreases with a decrease in liner stiffness and with an increase in support delay. These results can be generalized beyond the specific conditions of this analysis by expressing the stiffness of the liner relative to the stiffness of the ground. A useful ratio that has been used to express the relative stiffness of the ground and liner is the compressibility ratio, C^* (Einstein and Schwartz, 1979):

$$C^* = \frac{E\ a\ (1 - \nu_s^2)}{E_s\ A_s (1 - \nu^2)} \qquad \text{Eqn 3.12}$$

where: E = Young's Modulus of the Ground;

ν = Poisson's Ratio of the Ground;

E_s = Young's Modulus of the Support;

ν_s = Poisson's Ratio of the Support; and

A_s = Cross Sectional Area of the Support/Unit Length.

The Compressibility ratios that correspond to each of the five liner cases are given in Table 3.2.

Table 3.2 Compressibility Ratios for Liner Cases #1 to #5.

	E (GPa)	C^*
Liner #1	2.5	1.86
Liner #2	5.0	0.93
Liner #3	10.0	0.47
Liner #4	30.0	0.16
Liner #5	60.0	0.08

By substituting C^* for E in Fig. 3.18, it becomes a chart that applies to a range of ground and liner conditions. It should be noted that this chart has been developed on the basis of elastic conditions.

The Convergence Solution (Eqns 3.8, 3.9, and 3.11) has been fitted to two finite element convergence curves from Liner #3 with support delays of 0.25 and 1.25 radii. These curves are compared in Fig. 3.19. The Convergence Solution curves in this figure were generated using the program CONRATE (Appendix C). Now, excellent agreement between the finite element results and the proposed Convergence Solution can be observed.

3.4.4 Application to Convergence Confinement Method.

The results presented in this chapter have important implications for the use of the Convergence Confinement Method (CCM) in design. Although the method is generally applied in a qualitative manner to examine the tunnel supporting process, it has also been used quantitatively as a design tool. A notable example of this is the Relative Stiffness Solution (RSS) (Einstein and Schwartz, 1979). They used the CCM to determine the pressure acting on the support, which is then used to calculate final displacements, thrusts and bending moments within the liner. A typical CCM diagram that would be used in the RSS was shown in Fig. 3.3, together with the corresponding convergence curve. Einstein and Schwartz (1979) only dealt with cases that have no support delay (L_d) in their presentation of the RSS. However, a common application of this method when there is a support delay is as shown in Figs 3.3 and 3.20. The SCC is placed at the convergence value on the horizontal axis that corresponds to the convergence curve at the point of liner installation (see Fig. 3.3). The assumption that is commonly employed, is that the walls converge as an unsupported tunnel until the point of liner installation, when the convergence is inhibited by the liner. The behavior of this post-liner portion is described by the RSS (Einstein and Schwartz, 1979). The commonly accepted use of the RSS described above will be termed the Traditional RSS in the discussion that follows.

The results presented in this chapter show that the Traditional RSS portrays the convergence of a supported tunnel in an incorrect manner. It assumes that the lined convergence curve follows the unlined convergence curve up to the point of liner installation. However, it has been demonstrated that the lined convergence curve falls below the unlined curve before the point of liner installation (C_s).

The error that results from this incorrect assumption is illustrated in Fig. 3.20, where the Traditional RSS from Fig. 3.3 is compared to the Convergence Solution. The convergence curves in this figure were calculated for the conditions of the tunnel with Liner #3. The two convergence curves yield two different equilibrium points on the GCC. The differences between these two solutions are summarized in Table 3.3.

Table 3.3 Comparison of Convergence Solution and the Traditional RSS.

	$C(x_s)$ (mm)	C(final) (mm)	Lining Pressure (MPa)
Traditional RSS	185	212	4.0
Convergence Solution	143	181	5.0

The Traditional RSS overestimates the ultimate convergence, and underestimates the ultimate lining pressure. The latter error is unconservative, as it could lead to the selection of a support with insufficient capacity.

Two methods of representing the effect of the liner with the new solution are presented in Fig. 3.20. The traditional Support Confinement Curve (SCC) that corresponds to the new solution is given by the dashed line. This is calculated in a similar manner to the RSS, except that the initial convergence is corrected by the amount C_k ($= Q_k * C_{x=}$), shown in this figure. The value of C_k that applies to any given set of ground/liner conditions can be determined from the chart in Fig. 3.18.

The new method of representing the effect of a liner on the CCM diagram is given by the solid p_1 curve. This represents the equivalent radial support pressure that is felt by the rock in response to the liner. This concept has been introduced in Section 3.4. The p_1 curve in Fig. 3.20 is plotted against convergence, whereas earlier it was plotted against distance along the tunnel axis, x, in Fig. 3.15.

These two methods yield the same equilibrium point, but they represent two different quantities. The SCC shows the actual two dimensional radial pressure (p_s) that the liner exerts as it deforms. The p_1 curve gives the equivalent radial support pressure that would cause the observed convergence. Thus it is the equivalent three dimensional

effect that the liner has on the rock. The GCC represents the equivalent radial support pressure provided by the rock at the tunnel face as excavation proceeds. A comparison of the equivalent support pressures provided by the liner, and the rock at the face, gives a more consistent representation of the interaction between the liner and the rock. It is a comparison of like quantities, in contrast to the Traditional RSS which compares equivalent support pressure to actual two dimensional lining pressure.

The CCM diagram can be used for different purposes. It can predict the pressure that a given liner would experience for a given set of conditions, to furnish the required liner capacity for design. For this purpose, the Convergence Solution can be used to predict the convergence curve and hence, the p_1 curve, or the SCC. The CCM diagram can also be used to evaluate the effectiveness of support measures. This can be accomplished by plotting the measured convergence data on the CCM diagram.

For both of these purposes, the representation of the effect of the liner with the p_1 curve has distinct advantages. It provides a more realistic, consistent illustration of the actual effect of a liner on the rock. It also allows a comparison of the effectiveness of many different types of supports. Supports such as rock anchors are difficult to evaluate using a SCC, but the equivalent effect they have on the rock can be translated onto the CCM diagram by plotting the p_1 curve, based on the observed

convergence. Thus, the equivalent supporting effect that any type of support provides can be evaluated using the p_1 curve.

In summary, the convergence equation developed by Guenot et al. (1985) has been expanded to describe the convergence of the walls of a supported tunnel in response to excavation, both ahead of, and after the face. The convergence ahead of the face is given by Eqn 3.8; the convergence after the face but before the liner is given by Eqn 3.9; and the convergence after the liner is installed is given by Eqn 3.11. Also, the chart in Figure 3.18 is to be used in conjunction with Eqn 3.11 to furnish the parameter Q_k, that corresponds to the support conditions.

While the original equation has grown from one to three equations, it has only gained one additional parameter, K. This parameter reflects the stiffness of the support system, and can be determined directly from the liner properties. If the support system is other than a circular liner, K may be determined by fitting the solution to convergence data. Thus, for a circular liner, the application of the Convergence Solution is no more complex than the original equation, as both involve the determination of four parameters by curve fitting. The expansion of the Convergence Solution (Eqns 3.8, 3.9, and 3.11) makes it applicable to a wide range of realistic tunneling conditions.

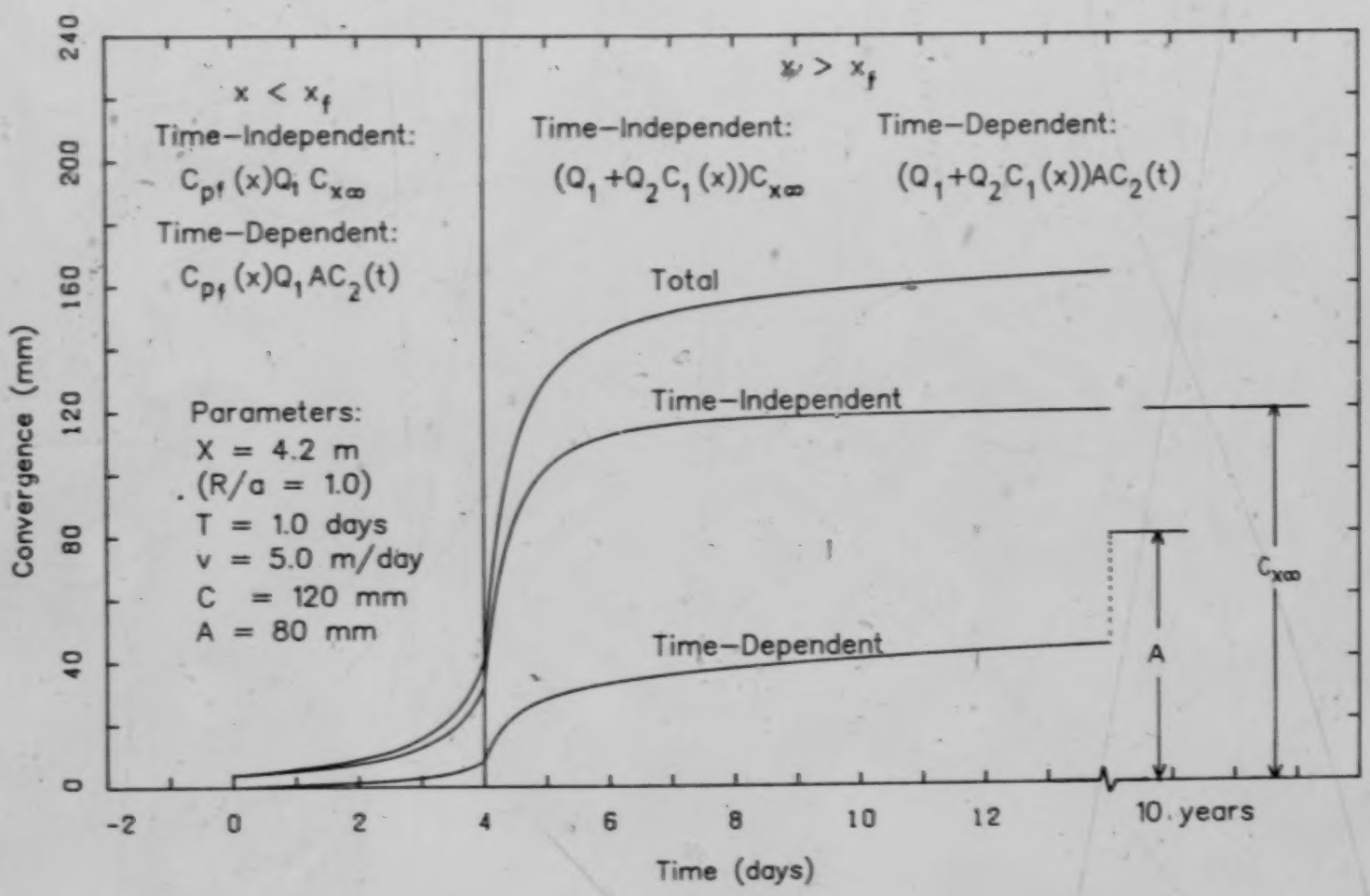

Figure 3.1 Components of Convergence Solution for Unlined Tunnel.

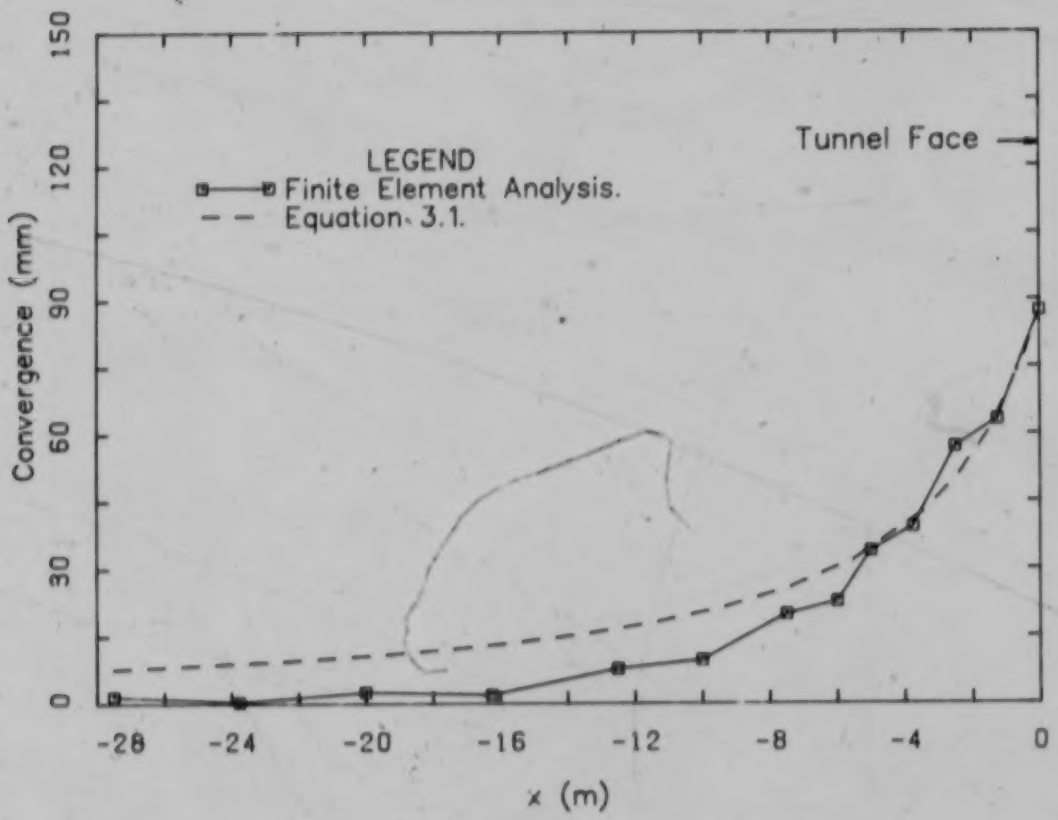

Figure 3.2 Pre-face Convergence Curves from an Unlined Tunnel.

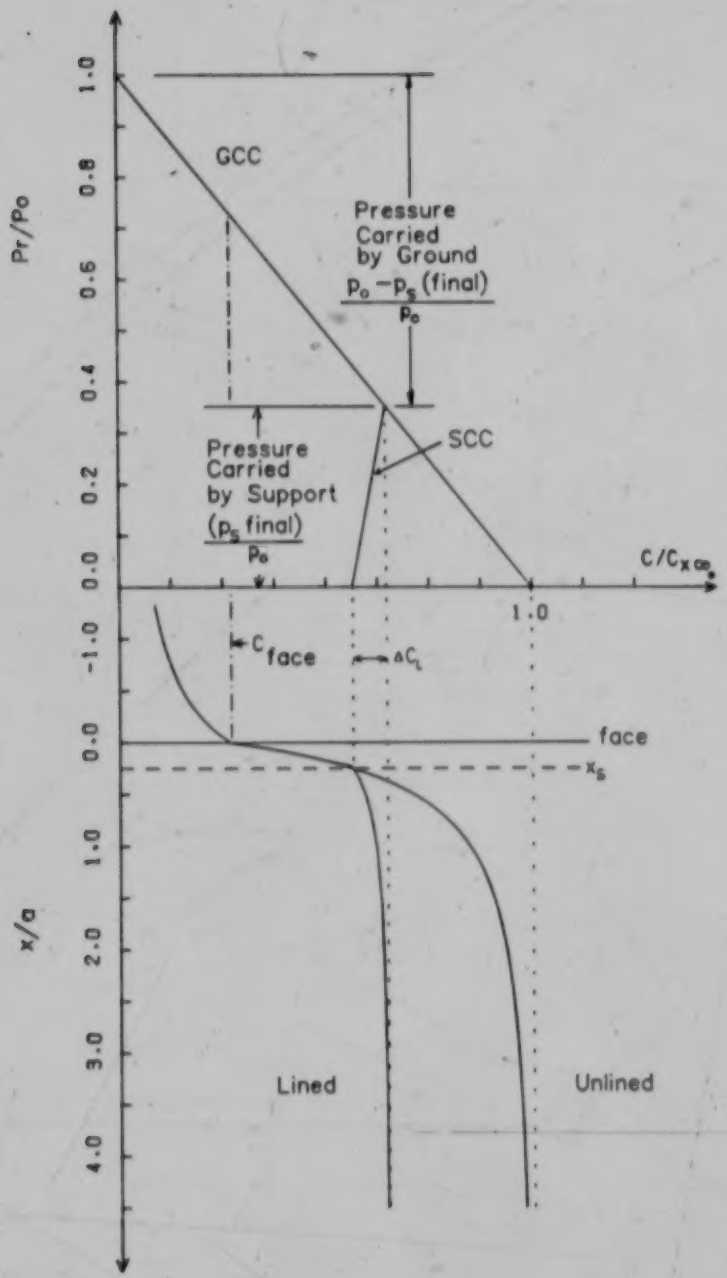

Figure 3.3 Convergence Confinement Method Diagram with Corresponding Convergence Curves.

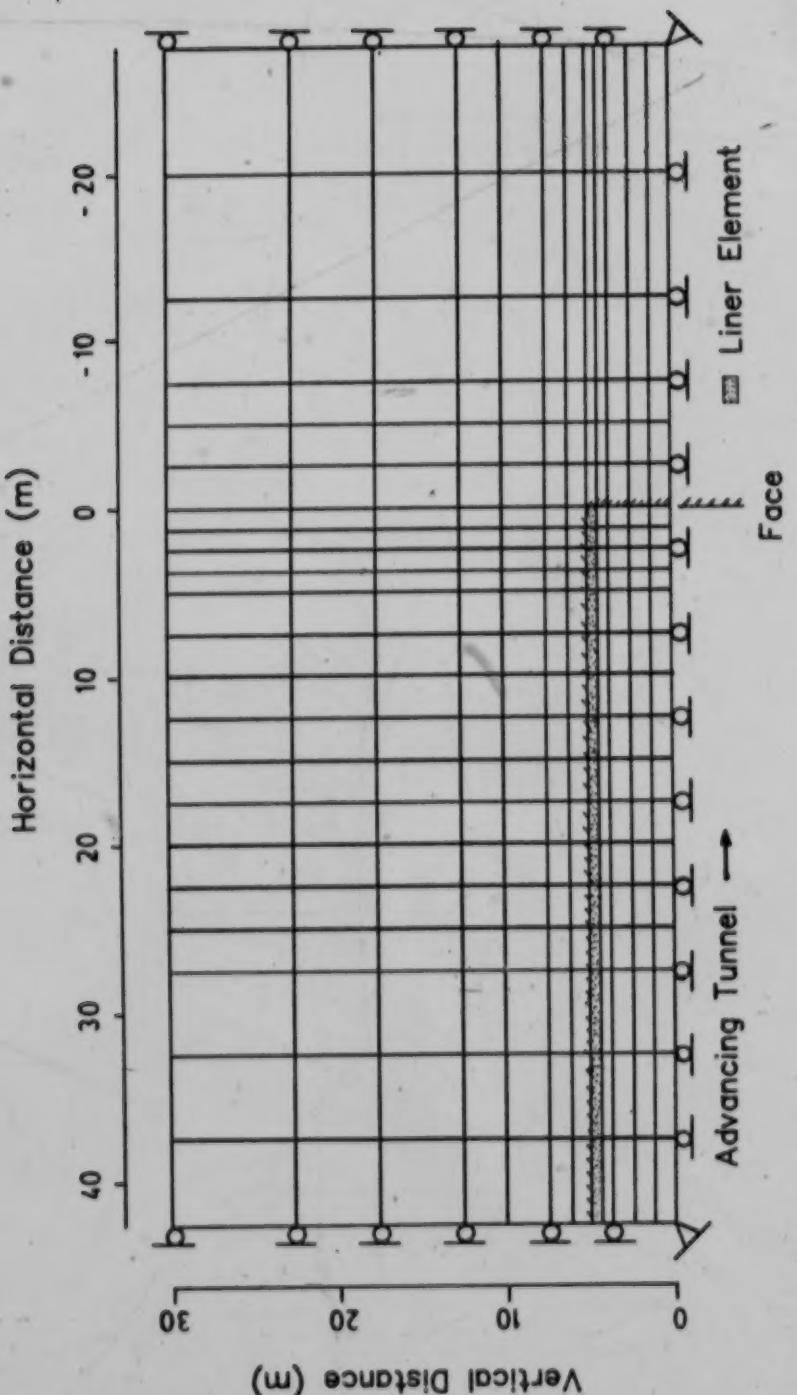

Figure 3.4 Finite Element Mesh.

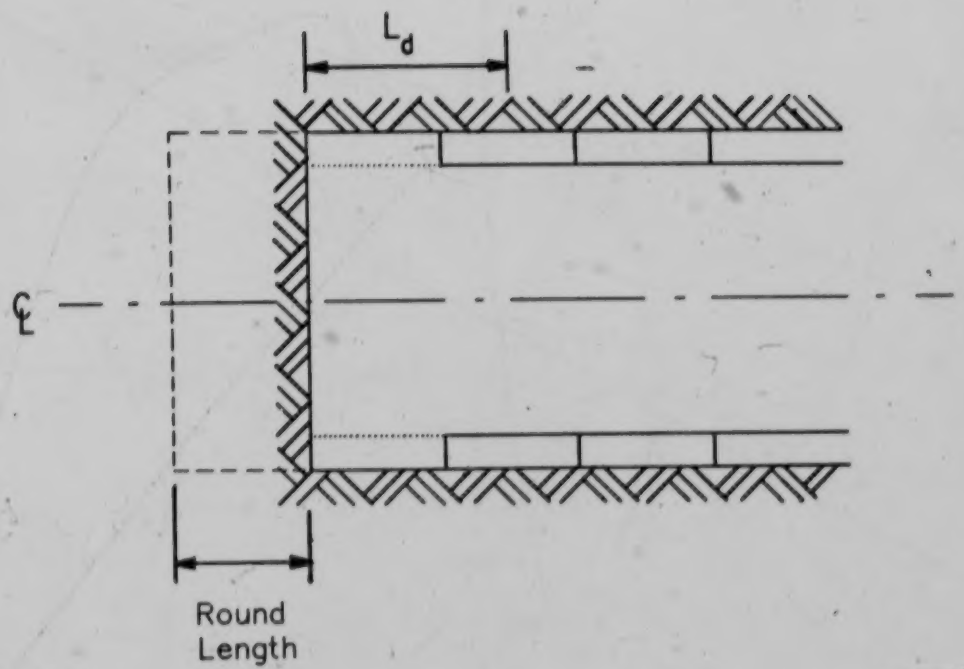

Figure 3.5 Unsupported Length Between Liner and Face.

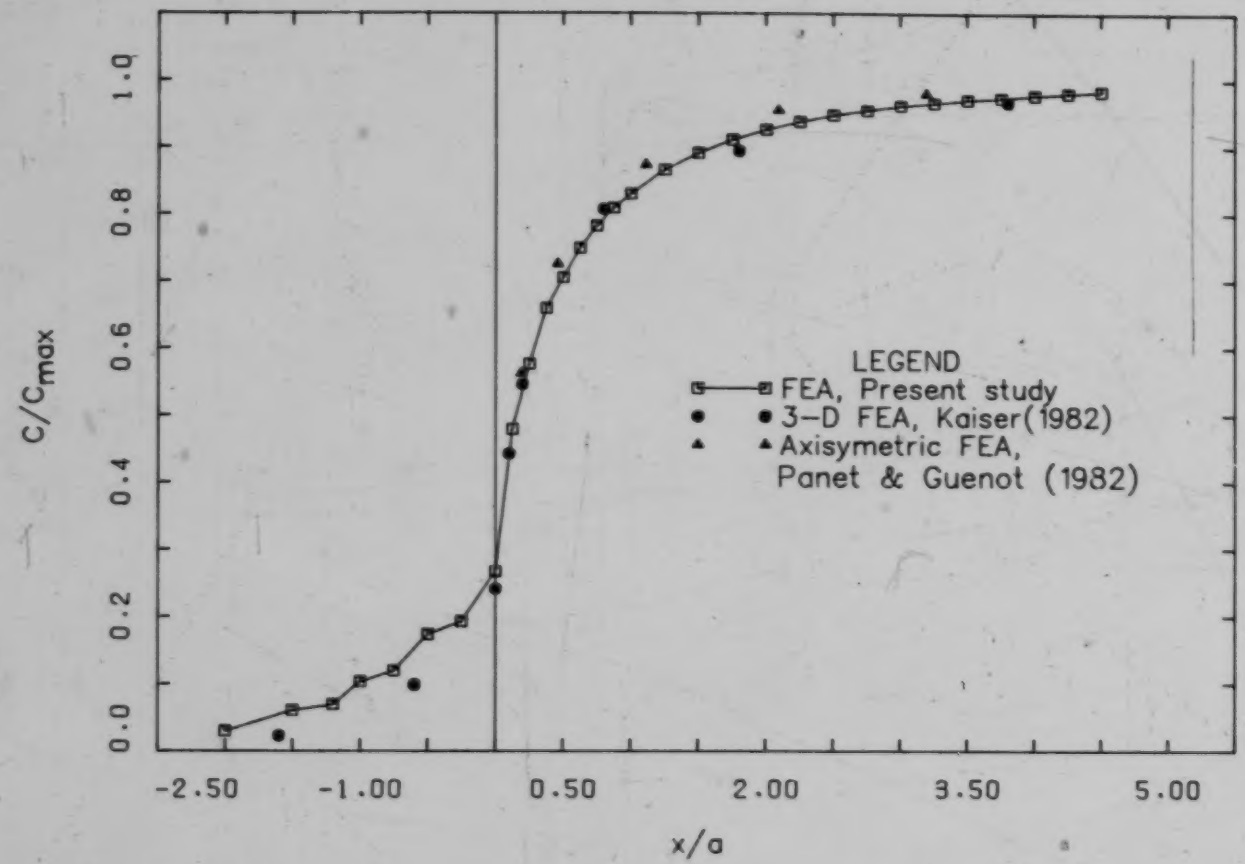

Figure 3.6 Comparison of Unlined Tunnel Finite Element Analysis with Analyses by Others.

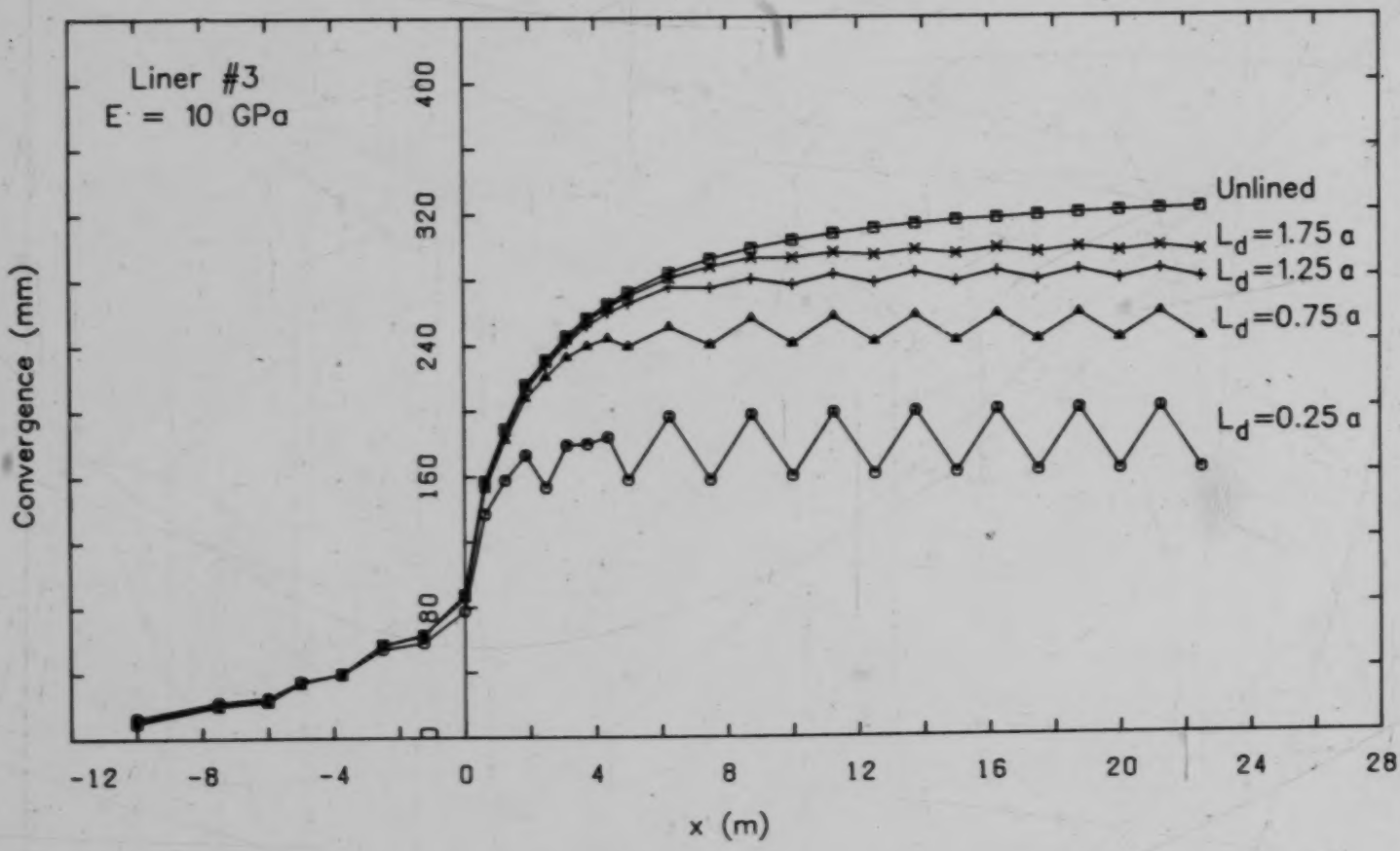

Figure 3.7 Convergence Data from Finite Element Analyses, for Liner #3.

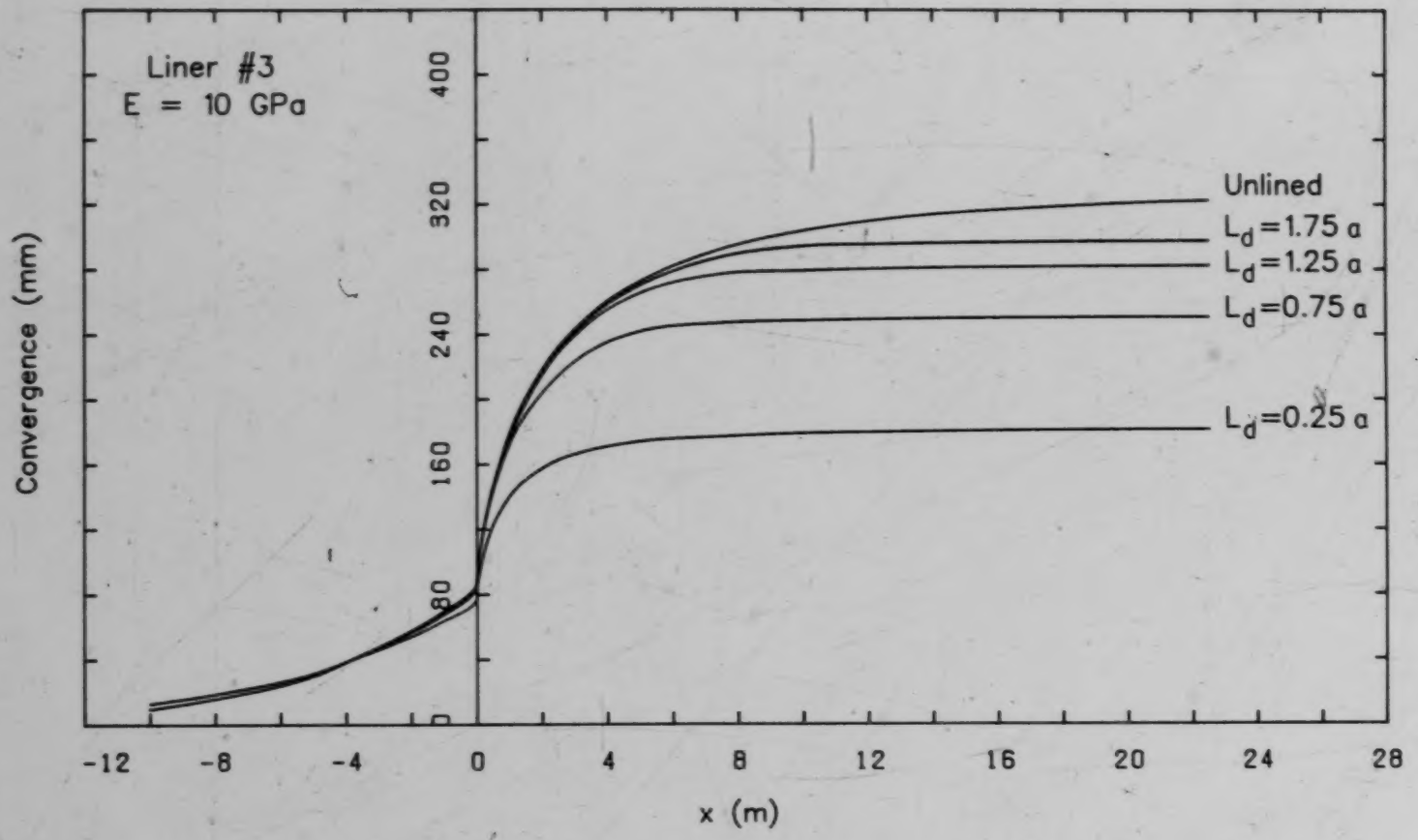

Figure 3.8 Smoothed Convergence Curves from Finite Element Analyses, for Liner #3.

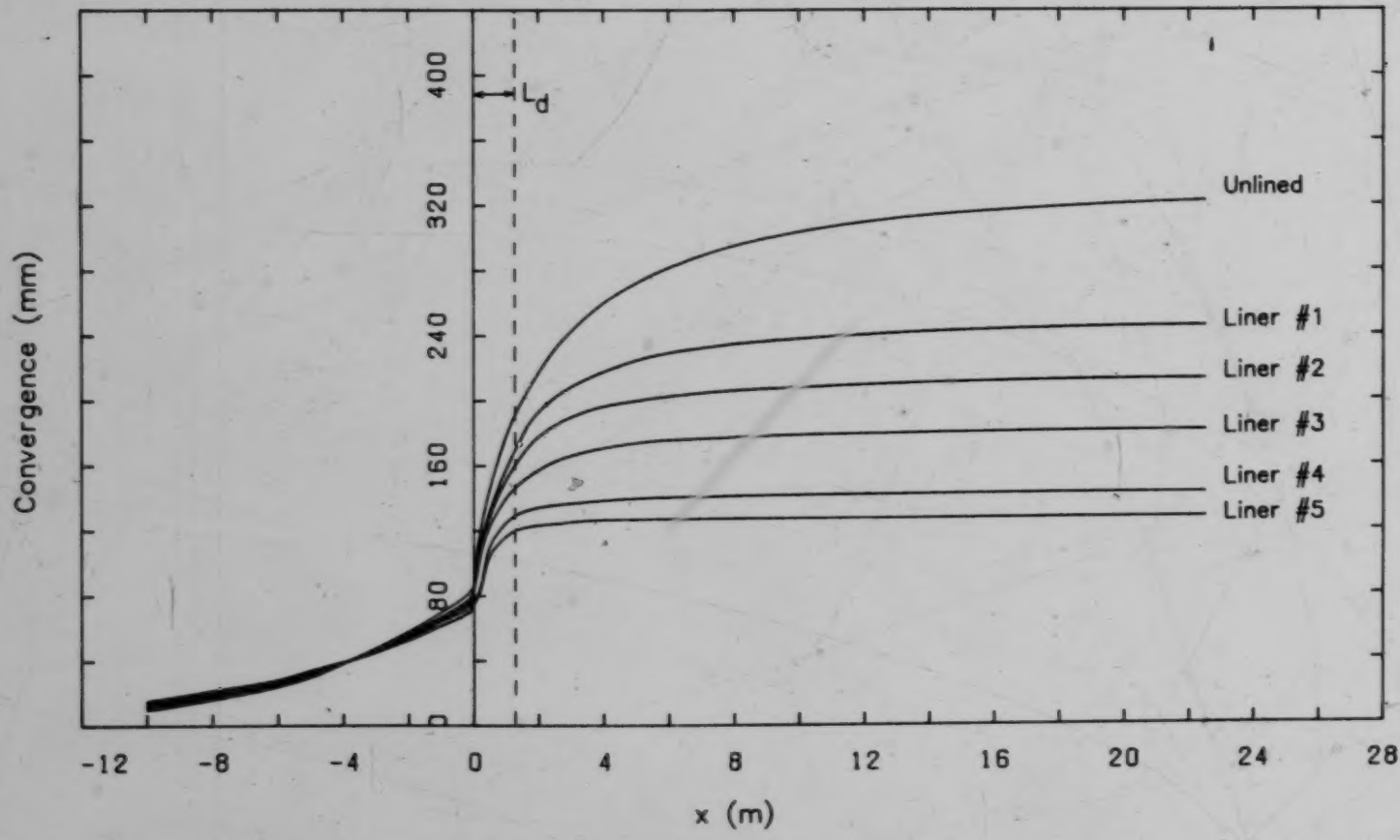

Figure 3.9 Smoothed Convergence Curves from Finite Element Analyses, for L_d = 0.25 a.

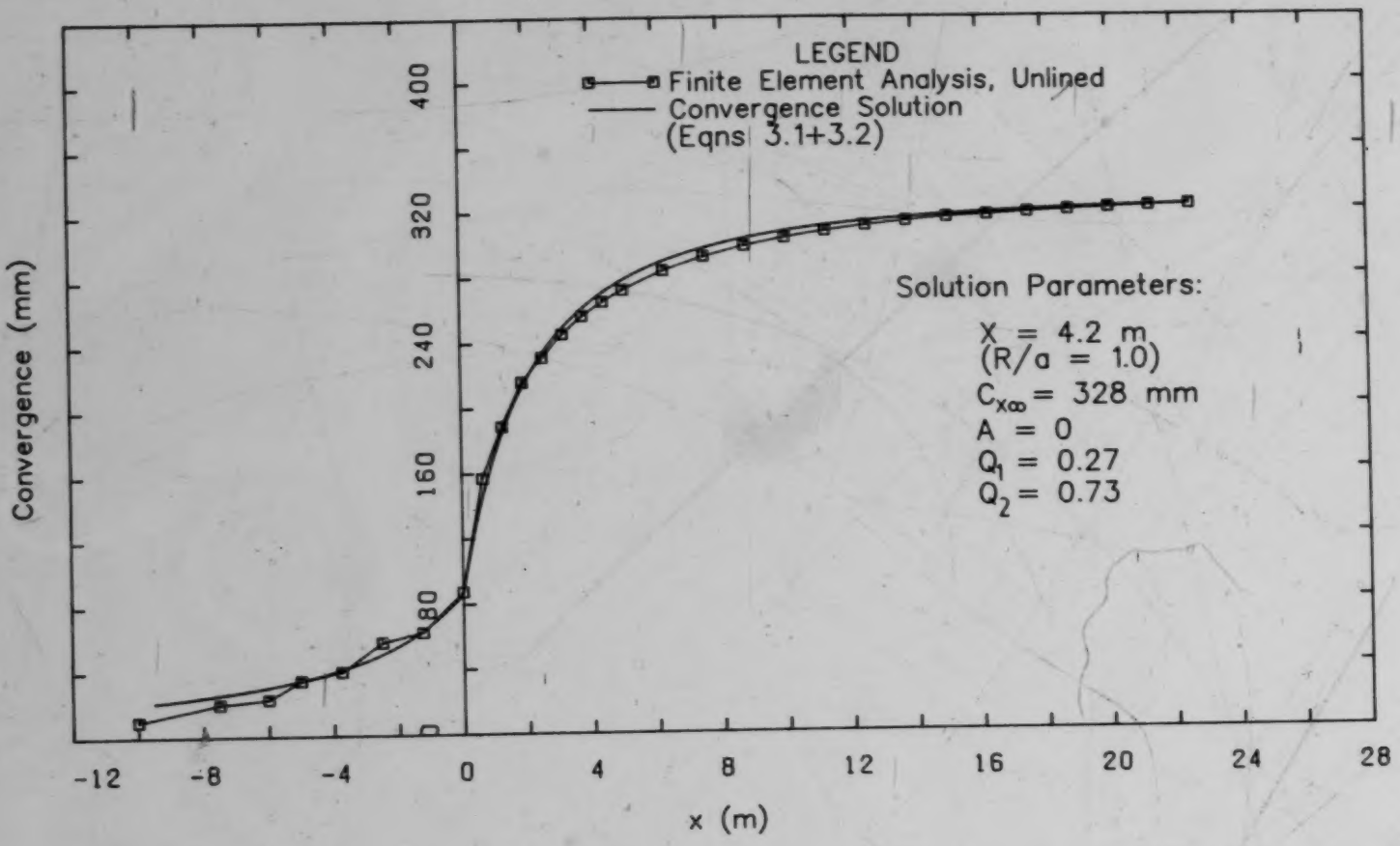

Figure 3.10 Comparison of Finite Element Results and Convergence Solution for Unlined Case.

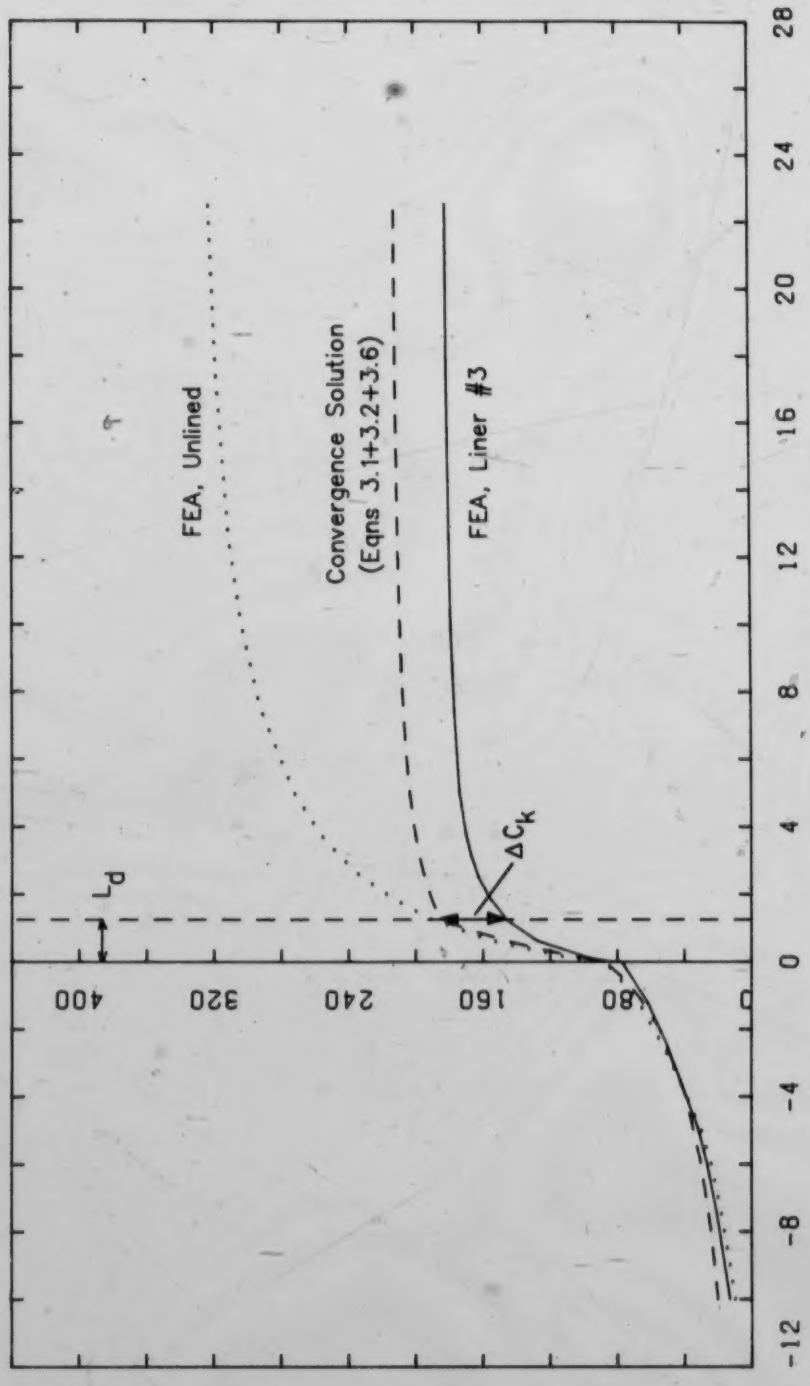

Figure 3.11 Comparison of Finite Element Results and Convergence Solution, for Liner #3.

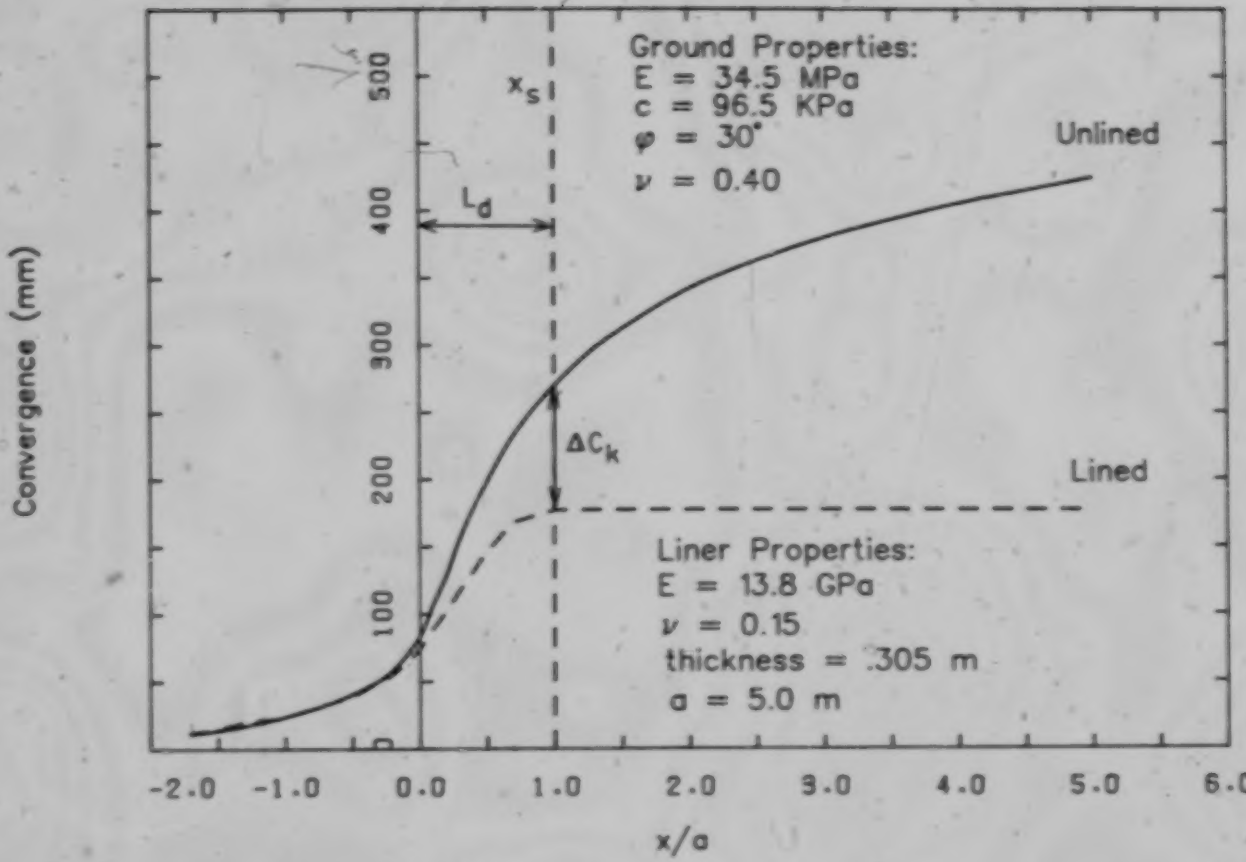

Figure 3.12 Convergence Curves from Elasto-Plastic Finite Element Analysis (Modified from Rankine and Ghaboussi, 1975).

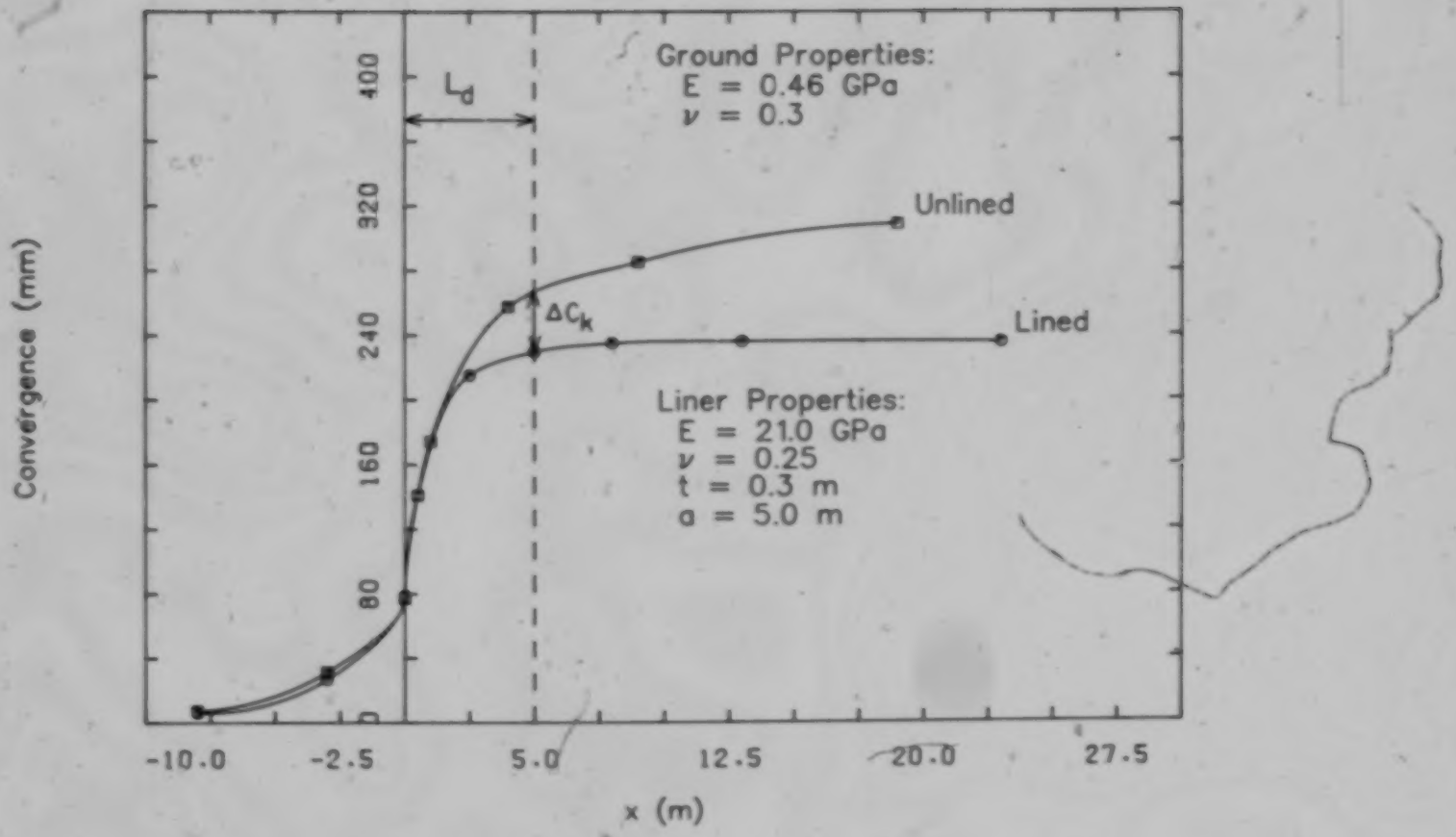

Figure 3.13 Convergence Curves from 3-D Finite Element Analysis (after Kaiser, 1983).

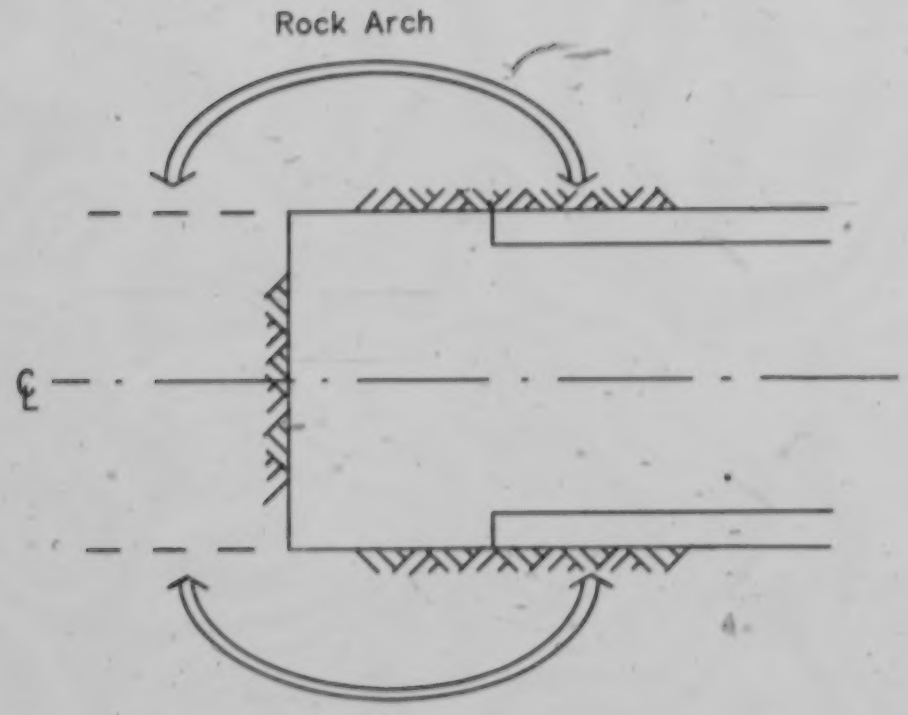

Figure 3.14 Supporting Arch Generated in the Rock Mass.

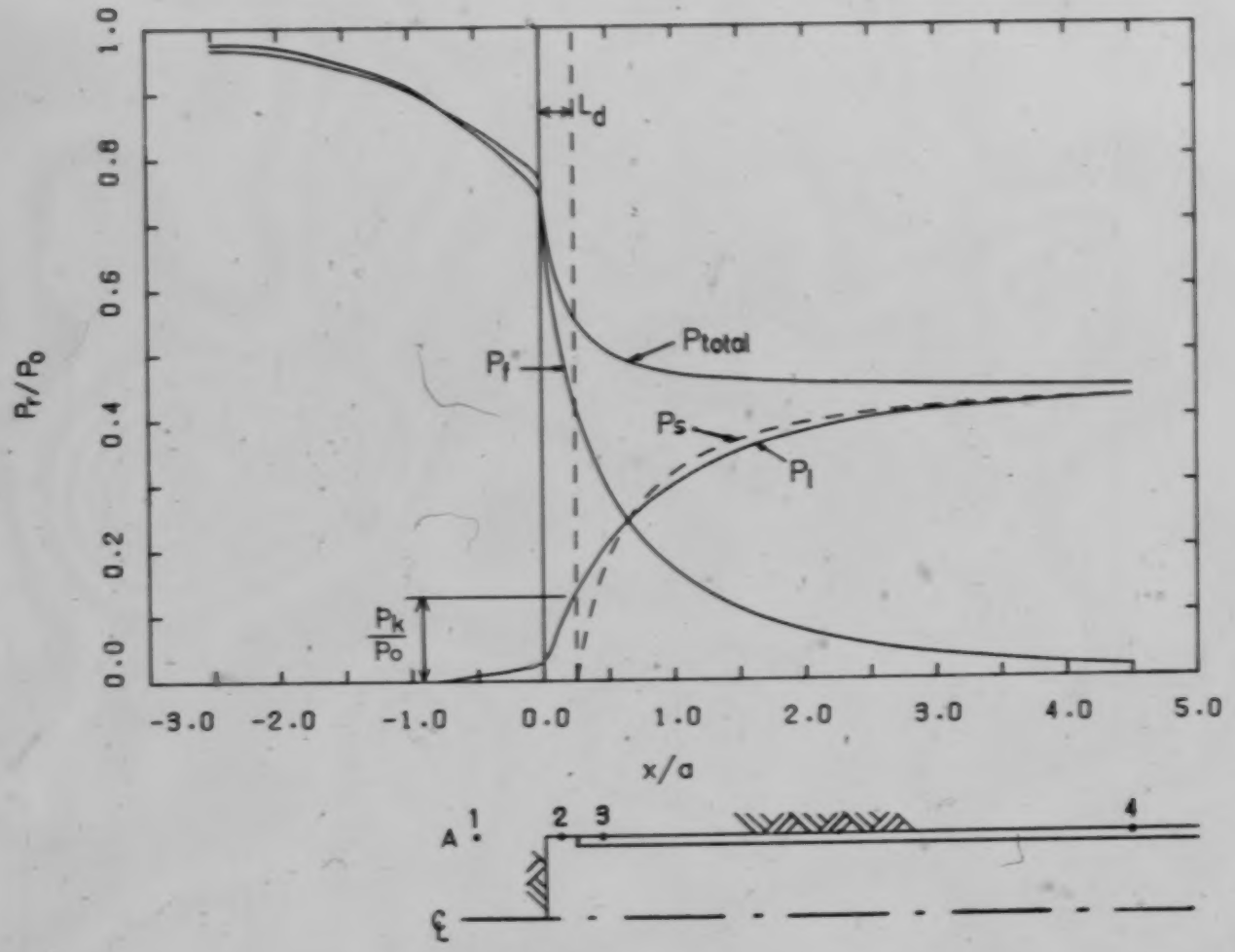

Figure 3.15 Equivalent Support Pressure Associated with Tunnel Excavation.

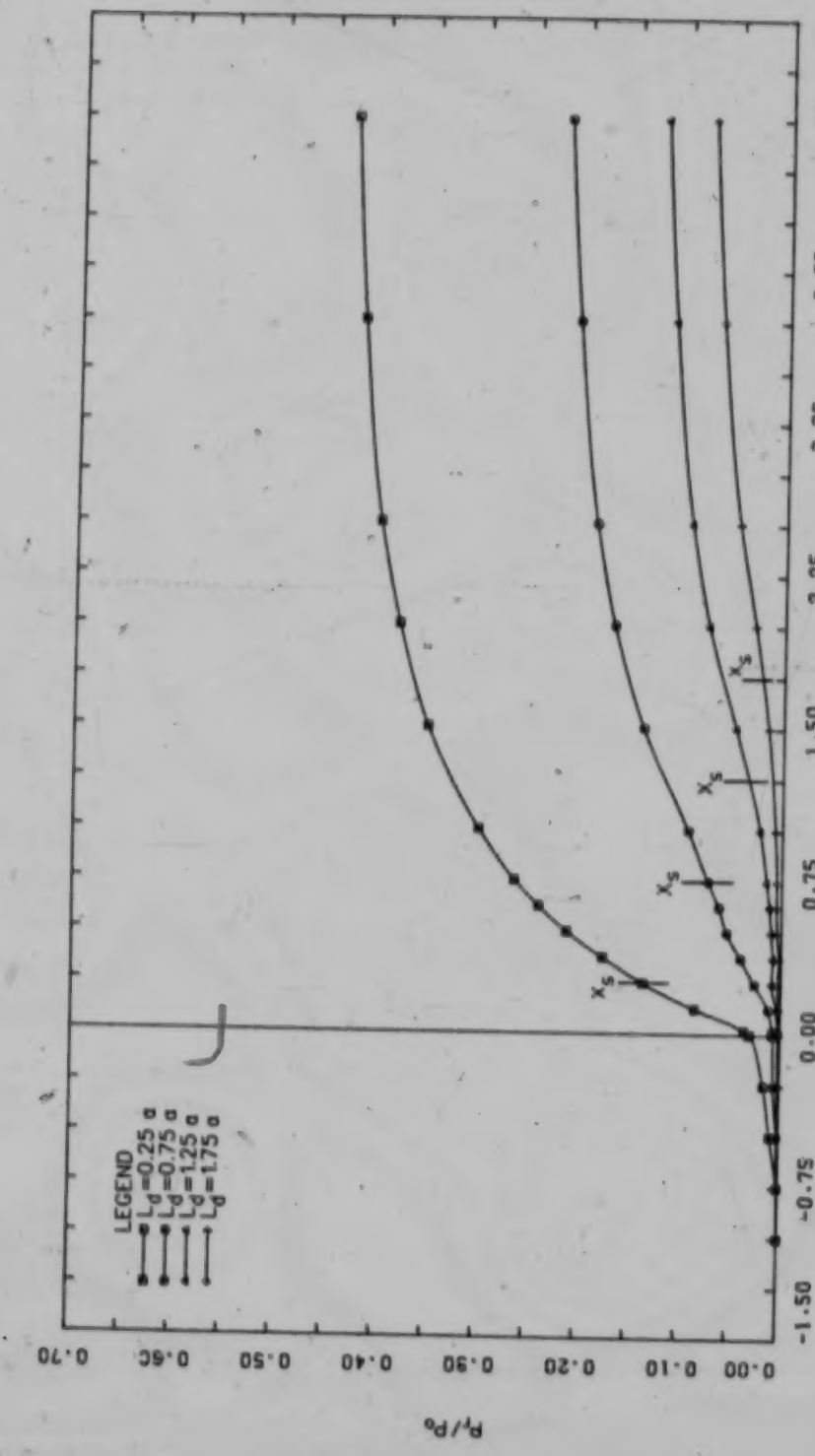

Figure 3.16 Equivalent Lining Pressure from Finite Element Analysis, for Liner #3.

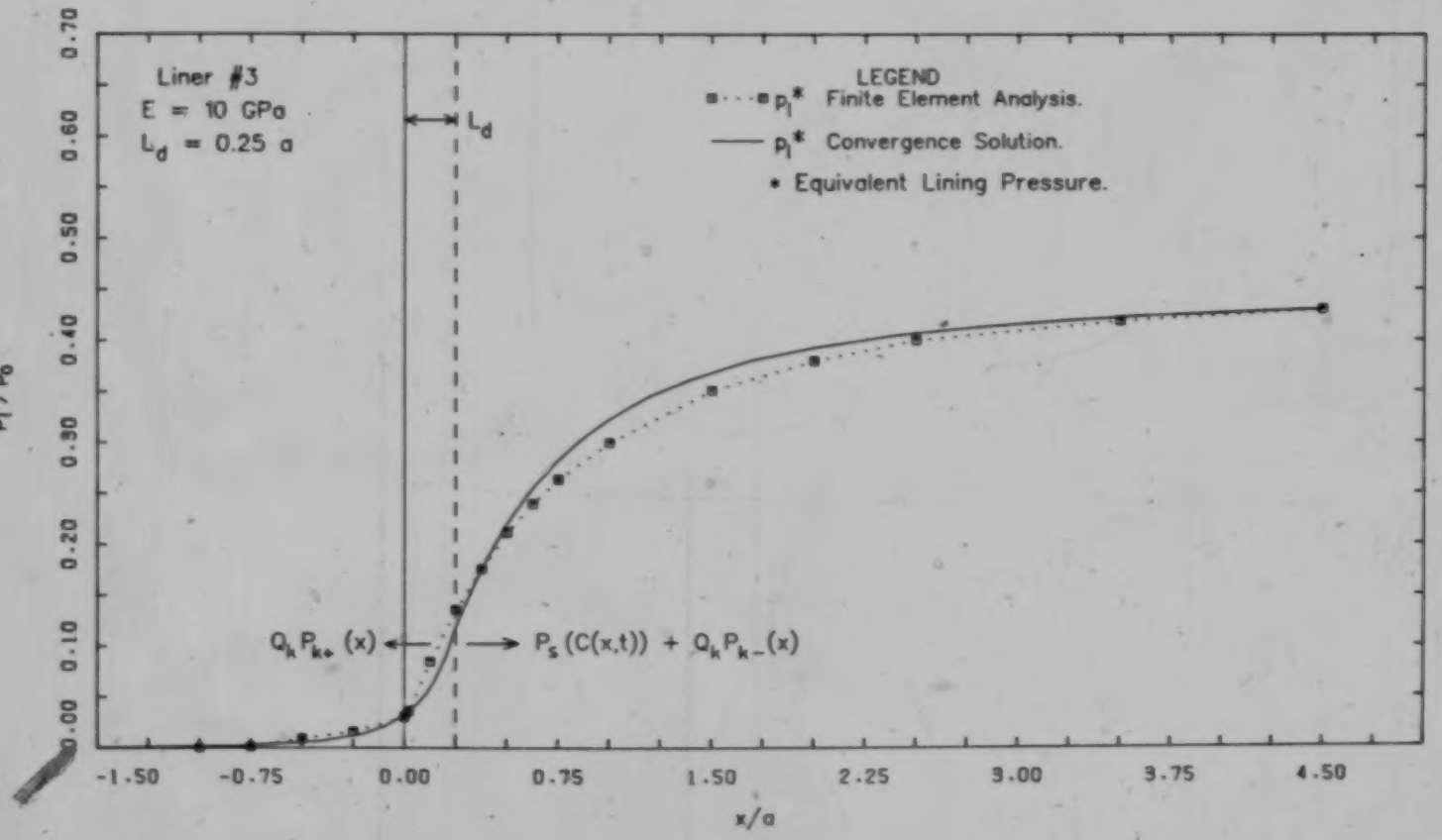

Figure 3.17 Comparison of Equivalent Lining Pressures from Finite Element Analysis for Liner #3, and the Convergence Solution.

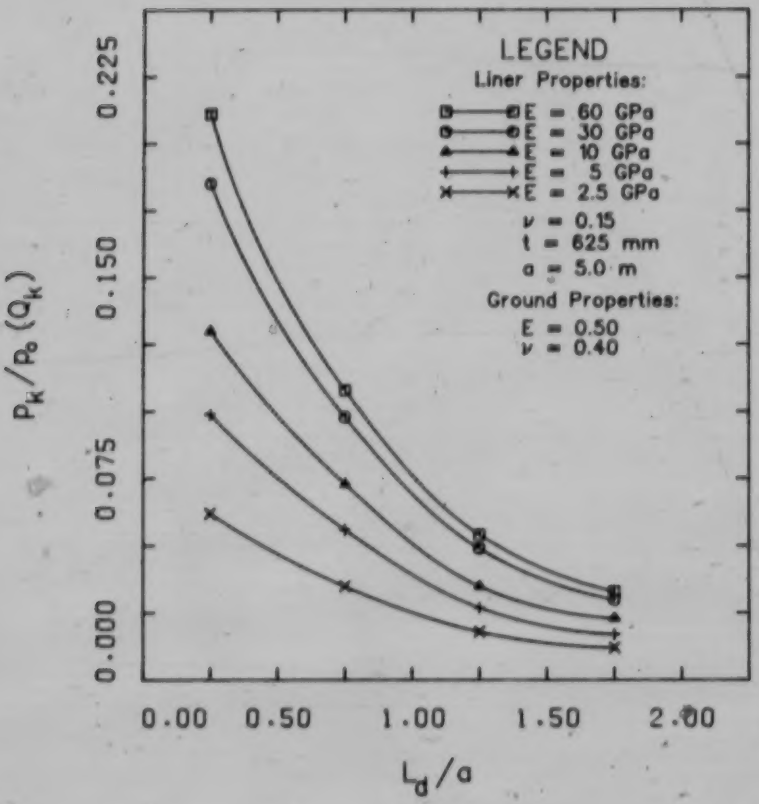

Figure 3.18 Normalized Pre-liner Equivalent Lining Pressure from Finite Element Analyses vs Normalized Support Delay.

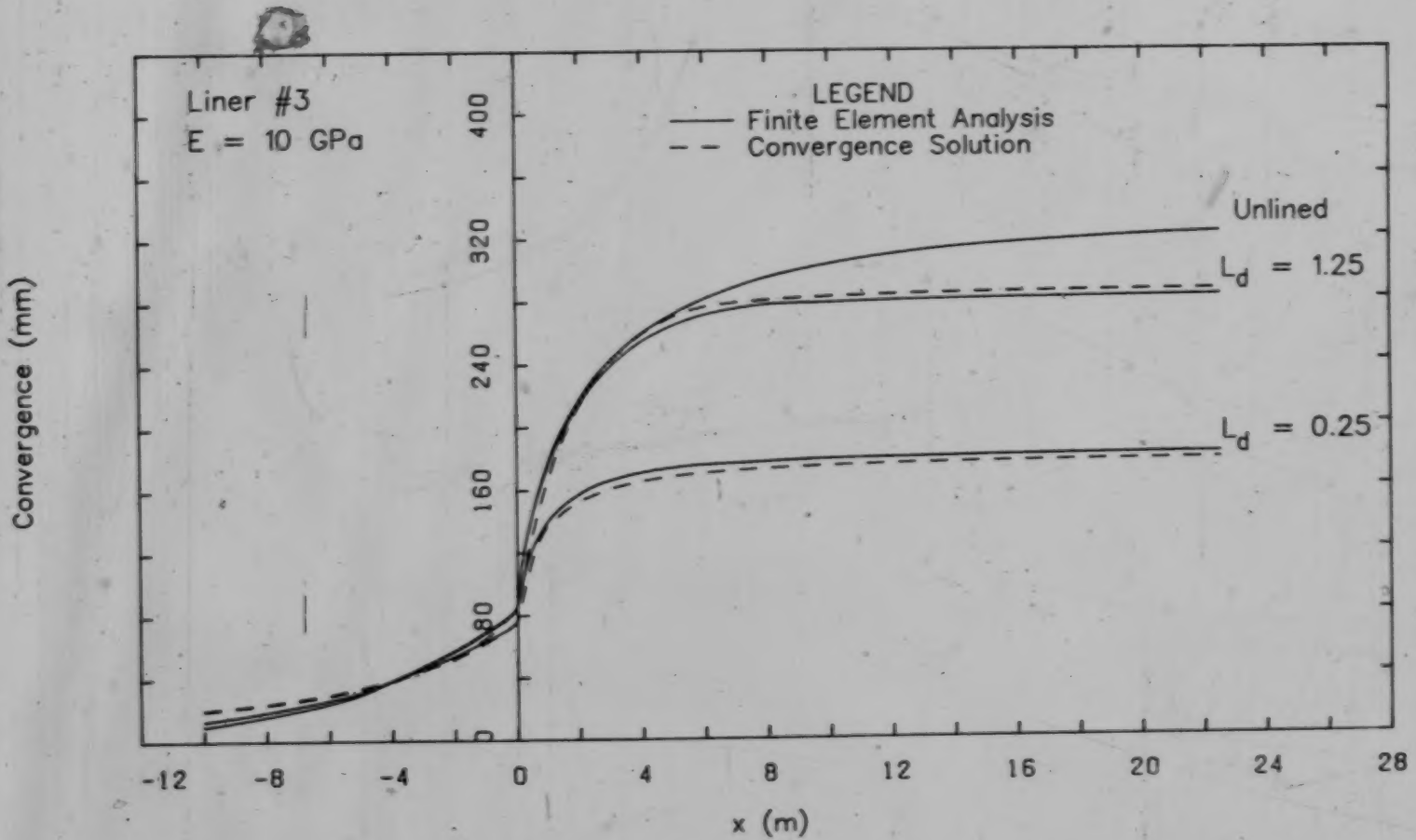

Figure 3.19 Comparison of Convergence Curves from Finite Element Analyses and Convergence Solution, for Liner #3.

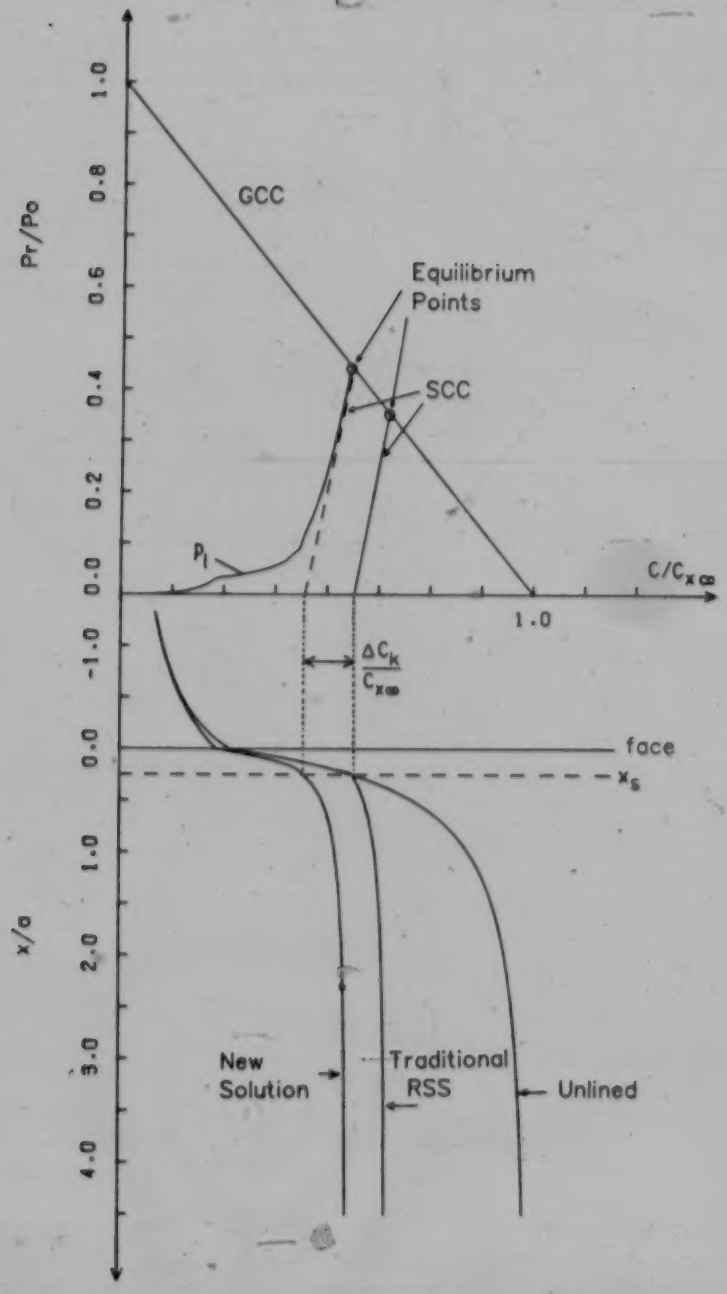

Figure 3.20 Convergence Confinement Method Diagram with Convergence Curves, for New and Traditional Solutions.

4. APPLICATION OF CONVERGENCE SOLUTION TO LABORATORY TESTS

4.1 Introduction

There are a variety of different ways to present convergence data measured in tunneling projects. The method of data presentation that is best suited to a particular project depends on the purpose of the tunnel monitoring program. If safety monitoring was the only concern, the data would be presented in a different manner than if the data were to be used as input to the Convergence Solution for the observational design approach. For this latter purpose, it is desirable to present the data in a manner that simplifies the task of fitting the solution to the data. It is proposed in this chapter that convergence rates, normalized to the maximum rate, be plotted against time. This format enables a set of independent parameters that describe the Convergence Solution to be determined from the data. The benefit of this method of data presentation is demonstrated using data from a tunnel excavation simulation test, conducted in the laboratory.

4.2 Description of Laboratory Testing

A series of laboratory tests were conducted at the University of Alberta (Kaiser et al., 1983a) to simulate tunneling in a weak rock mass. Tunnel excavation was simulated by drilling a hole through a block of coal while it was under pressure. Each block of coal was instrumented

to monitor the deformation of the coal in response to the excavation.

The coal samples were taken from the Highvale mine, approximately 75 kilometers west of Edmonton. Each sample was cut to the size: 62 cm x 62 cm x 21 cm. The two samples that are considered in this study contained non-linear joint sets trending at 45 degrees to the axis of the principal stresses. The joint spacing ranged from about 5 to 20 mm.

The coal samples were mounted in a large testing frame that applied a pressure of 12.5 MPa on the sides of the sample. The top and bottom of each sample were loaded in such a manner that no movement occurred. This created a condition of plane strain with no strain along the axis of the tunnel. Diamond bit core barrels of varying diameter were used to drill holes, or overcore existing holes through the center of each sample. This simulated the excavation of an unsupported tunnel.

The positions of the instruments in Sample MC-6 are shown in Fig. 4.1. Three concentric rings of extensometers are indicated in the figure by R1, R2, and R3. Average radial strains were derived from the relative displacements of anchor points 35 mm apart, measured by LVDTs connected to each extensometer. A multidirectional gauge was inserted into the hole after excavation was completed to measure the actual convergence. Unfortunately, this convergence measurement does not include the time-independent component of convergence that occurs near the tunnel face, but only

measures the time-dependent convergence that occurs after the excavation is complete. Thus, only the radial strains measured by the extensometers can be used in this analysis, as they are the only measurements that include both time-independent and time-dependent behavior.

The excavation simulation on Sample MC-6 that has been analyzed here is Test MC-6.02. In this test, a 108 mm diameter hole was drilled through the center of the sample, indicated by D1 in Fig. 4.1, at an average rate of 12.5 mm/min. The field stress of 12.5 MPa was applied to the sample 2.8 days prior to drilling. This allowed the hydrostatic creep caused by this load to dissipate to a sufficiently low level that it would not interfere with the response of the coal to the excavation. The radial strains measured during the excavation by the gauges in Rings R1 and R2 are plotted in Figures 4.2 and 4.3 (Kaiser et al., 1982) against time. Ring R1, represented by the solid lines is at a depth of 81 mm (Station 81), and Ring R2, indicated by the dashed lines is at a depth of 106 mm (Station 106). The widening of this hole to the diameter D2, shown in Fig. 4.1 was not analyzed in this study.

The second test that has been analyzed in this study is Test MC-7.13 on Sample MC-7. The layout of the instrumentation in this sample is shown in Fig. 4.4. The markers indicate the position of the extensometers at each of the three measuring locations that are analyzed in this study. The excavation history prior to Test MC-7.13 is

considerably more complex than that of MC-6.02. An initial hole of 42 mm diameter was drilled in a similar manner to the excavation in MC-6.02. This hole was subsequently widened to a 108 mm diameter, and then to a 152 mm diameter. The positions of the three holes in the sample are shown in Fig. 4.4. Only Test MC-7.13, during the final widening, is analyzed in this study, due to several problems encountered during the first two excavations. The first excavation of 42 mm diameter produced a poor response in the extensometers, probably due to the relatively large distance between this hole and the extensometers. The widening to 108 mm was plagued with many stoppages in excavation due to interruptions in the power supply. This produced fluctuations in the radial strain with time that make it difficult to apply the Convergence Solution.

The final widening of the opening, to a 152 mm diameter (MC-7.13) was drilled continuously at the rate of 1.22 mm/min, an order of magnitude lower than in Test MC-6.02. This took place after the sample had been allowed to creep for 1.2 days under a pressure of 12.5 MPa with the 108 mm diameter hole in it. The time-dependent response of the sample under load was recorded for 3.5 days after the final widening was completed. The response of four extensometers to the excavation for the first 3.5 hours is shown in Fig. 4.5 for Station 56. The data from Stations 81, and 106 are given in Appendix F.

The response of the coal to the excavation in both of the tests described above was recorded only by extensometers that measured radial strain at varying distances to the tunnel wall. However, the Convergence Solution proposed in Chapter 3 applies to the convergence of the actual tunnel walls. It is necessary therefore, to relate radial strain within the rock mass to tunnel wall convergence. The radial strain that occurs in an elastic rock mass (with K_o=1.0) in response to tunnel excavation is given by:

$$\epsilon_r = \frac{p_o(\frac{a}{r})^2}{2G} \qquad \text{Eqn 4.1}$$

where: r = distance from center of tunnel to point of measurement;

p_o = inital uniform ground stress (K_o=1.0); and

G = Shear modulus.

The convergence of the tunnel walls for the same conditions is given by:

$$C = \frac{p_o a}{G} \qquad \text{Eqn 4.2}$$

A comparison of Eqns 4.1 and 4.2 shows that radial strain in the rock mass differs from the convergence of the walls by a constant factor, $\frac{a}{2r^2}$. In both tests, MC-6.02 and MC-7.13, all of the gauges in any given measuring section

are equidistant from the center of the tunnel. Thus, the radial strains measured in these tests can be converted to equivalent convergence measurements by dividing them by $\frac{a}{2r^2}$, provided that the behavior is elastic. There was not a significant amount of nonrecoverable strains observed for either of these tests. In the absence of more detailed information about the radial strain to convergence ratio, $\frac{a}{2r^2}$ was assumed. Kaiser et al. (1982) made the same assumption.

It has been demonstrated by Kaiser et al. (1982) that there is one important difference between radial strains and tunnel wall convergence. Radial strains are sensitive to local processes that are occuring within the rock mass and are extremely variable. In contrast, convergence measurements fail to detect localized processes but reflect the global response of the rock mass. Convergence then, seems to reflect an average of all of the localized processes surrounding a tunnel. For this reason, it was assumed that an average of the radial strains at a given measuring section would best reflect the convergence behavior.

The averaged radial strain curves are given in Figures 4.6 and 4.7 for Tests MC-6.02 and MC-7.13, respectively. The analysis in this chapter is based on the curves presented in these two figures. The validity of taking averaged radial strain multiplied by the ratio $\frac{a}{2r^2}$ as equivalent to convergence will be examined in the following section.

4.3 Logic of Data Presentation

A format for the presentation of the laboratory results is proposed here that will aid in the interpretation of the results with the Convergence Solution.

Convergence measurements may either be plotted with respect to time, or distance to the face. When the excavation rate is constant, these two plots will be identical. However, if there are interruptions in excavation, the convergence vs distance plot would become discontinuous if the material exhibits time-dependent convergence. This would yield infinite convergence rates, and would be difficult to analyze. Thus, the laboratory results will be plotted with respect to time to give continuous plots.

It is desirable to normalize the convergence curves to make them independent of the magnitude of convergence. The main assumption that the Convergence Solution is based on, is that the behavior of the rock mass can be characterized by the *shape* of the convergence curve. Both the parameter X, which indicates the amount of yielding, and the parameter T, which characterizes the time-dependent behavior, are determined by the shape of the convergence curve. This was demonstrated in Figures 2.4 and 2.5. It would be advantageous, therefore, to plot convergence such that the shapes of various curves could be compared, independent of differences in magnitude. This was accomplished in Figures 2.3 to 2.5 where the convergence curves were normalized to

the ultimate convergence. Guenot et al. (1985) and Sulem (1983) also present their convergence curves in this manner. Unfortunately, in the observational design method, observations must be interpreted before the ultimate convergence is known. Thus, normalizing in this manner is best suited to a back analysis, where the ultimate convergence is known. However, the ultimate convergence is the only appropriate quantity to normalize the convergence, to achieve independence from magnitude.

This problem can be circumvented by plotting convergence rates, instead of actual convergence, and normalizing to the maximum rate. The maximum convergence rate is a convenient quantity to normalize the rate to, because it occurs at or near the face, and hence can always be observed early in a monitoring program. Thus, the shape of the convergence rate curves can be compared for measurements with different magnitudes of convergence rate. This also provides independence from the magnitude of convergence, as the maximum convergence and the maximum convergence rate are proportional. This will be demonstrated in Section 4.4 with the Convergence Solution. Figure 4.8 shows the normalized strain rate curves that correspond to the two radial strain curves shown in Fig. 4.6. This shows that the shape of two curves that have different magnitudes of convergence can be readily compared when presented in this manner. It is necessary to plot the logarithm of strain rate to present the enormous range of data on one graph.

It was assumed earlier that the averaged radial strain shown in Figures 4.6 and 4.7 differed from equivalent tunnel wall convergence by the constant factor, $\frac{a}{2r^2}$. The validity of this assumption can be examined in Fig. 4.9, where the averaged radial strain rate is compared to the tunnel wall convergence rate for Test MC-6.02, Station 81. As mentioned earlier, the tunnel wall convergence measurements did not commence until sometime after drilling was complete, which corresponds to t=100 min in Fig. 4.9. According to the above assumption, the convergence rate should differ from the radial strain rate by the amount indicated in the figure. The radial strain rate is slightly higher than the assumed rate based on the convergence measurements (indicated by the dashed line), but the slope and shape of the two curves are similar. Thus, the averaged radial strains, adjusted with the factor $\frac{a}{2r^2}$, give a reasonable approximation of tunnel wall convergence. These convergence measurements will also be compared to the Convergence Solution in Section 4.5.

In summary, when convergence measurements are presented on a normalized convergence rate versus time diagram, a continuous curve is obtained that is independent of the magnitude of convergence. This facilitates a comparison of the shapes of various curves, which is desirable for the application of the Convergence Solution to field data interpretation. It is now necessary to alter the Convergence Solution to fit data presented in the normalized convergence rate format.

4.4 Adaptation of Convergence Solution

The Convergence Solution for an unsupported tunnel consists of Equations 3.1 and 3.2, which give convergence as a function of x and t. There are three steps involved in converting these equations from predicting convergence to predicting normalized convergence rate.

First, they must be expressed as a function of time alone. This is accomplished by substituting v*t (advance velocity*time) for x. If the excavation does not proceed with constant velocity, it must be divided into a series of constant velocity intervals. In this case, the following substitution would be required:

$$x = \bar{x}_{n-1} + v_n t_n \qquad \text{Eqn 4.3}$$

where: v_n = velocity of n^{th} constant velocity interval;

t_n = time from the beginning of the n^{th} constant velocity interval;

$$\bar{x}_{n-1} = \sum_{i=1}^{n-1} v_i t_i;$$

v_i = velocity of i^{th} constant velocity interval; and

t_i = duration of the i^{th} interval.

This gives the position of the face in the n^{th} constant velocity interval as a function of time.

Second, these equations must be converted from convergence to convergence rates. This is accomplished by taking the first derivative with respect to time, as follows:

- Pre-face equation:

$$\dot{C}(t) = \frac{dC(t)}{dt} = Q_1\dot{C}_{pf}(t)C_{x\infty} + Q_1\dot{C}_{pf}(t)AC_2(t) + Q_1C_{pf}(t)A\dot{C}_2(t) \qquad \text{Eqn 4.4}$$

- Post-face equation:

$$\dot{C}(t) = Q_2\dot{C}_1(t)C_{x\infty} + Q_2\dot{C}_1(t)AC_2(t) + Q_2C_1(t)A\dot{C}_2(t) + Q_1A\dot{C}_2(t) \qquad \text{Eqn 4.5}$$

where: $$C_{pf}(t) = \left[\frac{1}{1 + \left[\frac{x_f - (\bar{x}+vt)}{\bar{X}}\right]}\right]^{1.2};$$

$$\dot{C}_{pf}(t) = \frac{1.2v}{\bar{X}}\left[\frac{1}{1 + \left[\frac{x_f - (\bar{x}+vt)}{\bar{X}}\right]}\right]^{2.2};$$

$$C_1(t) = 1 - \left[\frac{1}{1 + \left[\frac{(\bar{x}+vt) - x_f}{\bar{X}}\right]}\right]^{2};$$

$$\dot{C}_1(t) = \frac{2v}{X}\left[\frac{1}{1 + \left[\frac{(\bar{x}+vt)-x_f}{X}\right]}\right]^3; \text{ and}$$

$$\dot{C}_2(t) = \frac{0.3}{T}\left[\frac{1}{1 + \frac{t}{T}}\right]^{1.3}.$$

The final step is to normalize both equations to the maximum convergence rate, which occurs at the face (Eqn 4.5) Substituting $t=t_f$ into Eqn 4.5 yields:

$$\dot{C}_{max} = \frac{2Q_2v}{X} C_{x\infty} + \frac{2Q_2v}{X} A\dot{C}_2(t_f) + Q_1A\dot{C}_2(t_f) \qquad \text{Eqn 4.6}$$

The magnitude can be factored out of this equation as follows:

$$\dot{C}_{max} = C_{x\infty}\left[\frac{2Q_2v}{X} + \frac{2Q_2v}{X} A^*\dot{C}_2(t_f) + Q_1A^*\dot{C}_2(t_f)\right]$$

$$= C_{x\infty} * [N] \qquad \text{Eqn 4.7}$$

where: $A^* = \frac{A}{C_{x\infty}}$; and

$$N = \left[\frac{2Q_2v}{X} + \frac{2Q_2v}{X} A^*\dot{C}_2(t_f) + Q_1A^*\dot{C}_2(t_f)\right].$$

Normalizing equations 4.4 and 4.5 to Eqn 4.7 yields:

- Pre-face equation:

$$\frac{\dot{C}(t)}{\dot{C}_{max}} = \frac{Q_1}{N}[\dot{C}_{pf}(t) + \dot{C}_{pf}(t)A^*C_2(t) + C_{pf}(t)A^*\dot{C}_2(t)]$$

Eqn 4.8

- Post-face equation:

$$\frac{\dot{C}(t)}{\dot{C}_{max}} = \frac{Q_2}{N}[\dot{C}_1(t) + \dot{C}_1(t)A^*C_2(t) + C_1(t)A^*\dot{C}_2(t) + \frac{Q_1}{Q_2}A^*\dot{C}_2(t)]$$

Eqn 4.9

It is important to note that Eqns 4.8 and 4.9 are independent of the magnitude of the ultimate convergence ($C_{x\infty}$) and the maximum convergence rate, because these two quantities are proportional, as can be seen in Eqn 4.7. The number of parameters in the solution has now been reduced from four to three: X, T, and A^*. Although these equations have been normalized to $\dot{C}_{max}$, the convergence rate at anytime could have been used, and it would still be independent of magnitude. This is an important result, as it introduces a degree of flexibility to the interpretation of convergence measurements. It is no longer necessary to prosess the entire convergence curve to use the Convergence Solution. If the convergence measurements do not commence until a distance after the face, the data can be normalized to the initial rate measured, and the corresponding time can be input into Eqn 4.9. This was one of the main factors that limited the application of the original equation by Guenot

et al. (1985), because the convergence right at the face is often difficult to obtain in a tunneling environment.

The form of the Convergence Solution that includes the effect of a tunnel support (Eqns 3.8, 3.9 and 3.11) may be converted to give normalized convergence rates in a manner similar to that presented here. The derivation is summarized in Appendix G. This form of the Convergence Solution is not applicable to the model test, which simulates an unsupported tunnel. The altered form of these equations, expressing normalized convergence rate for a supported tunnel, are not completely independent of magnitude. The last equation, that gives convergence after the support is installed, requires an estimate of $C_{x\infty}$.

The computer program, CONRATE, in addition to calculating convergence, also calculates the normalized convergence rate curves. A listing of this program is given in Appendix C, together with a description of its capabilities and an example run.

4.5 Fitting The Convergence Solution to Laboratory Results

4.5.1 Example Fit

The process of fitting the Convergence Solution to the data will be demonstrated with the measurements from test MC-6.02, Station 81. It was necessary to make some assumptions regarding the processing and interpretation of the data as outlined below.

The extensometers did not seem to accurately portray the response of the coal in the latter portion of the test, where the strains are very small. Instead of recording a continuous increase in strain, they recorded discrete jumps in strain, followed by periods of no movement at all. This resulted in wild fluctuations in the strain rate curve, making it difficult to analyze. This is illustrated in the normalized convergence rate versus time diagram in Fig. 4.10, where the actual data is represented by the dashed line. It was assumed that the true strain behavior is continuous, so a smoothing routine has been used to average out these fluctuations in the strain rates. This smoothing routine eliminates all the strain rates of zero through an averaging process that has been proposed by Cruden (1971). An example of data that has been smoothed by this process is shown in Figure 4.10, where it is compared to the actual data. This eliminates the fluctuations, and gives a curve that is more representative of the true strain behavior. Both of the stations in MC-6.02 have been smoothed. Test MC-7.13 did not require smoothing.

The other assumption that has been employed pertains to the position of the advancing face. Figure 4.10 shows that the maximum convergence rate occurs before the face passes the station (indicated by the solid vertical line). This differs from the Convergence Solution, which predicts that the maximum rate coincides with the passing of the face. While in a real excavation the maximum convergence rate

could occur ahead of the face due to yielding ahead of the face, the cause of this apparent discrepancy arises from the limitations of the testing facility. The bottom boundary of the sample was prepared in a manner that produces very low shear stresses. In contrast, a real tunnel excavated in a continuous rock mass would not posess a low shear stress boundary in a plane perpendicular to the tunnel axis. Consequently, the rock ahead of the tunnel face in the model test provides less support than it would in a continuous rock mass. This skews the convergence curve, causing the coal to respond as if the face was ahead of its actual position. Therefore, in the analysis of these curves the effective position of the face will be taken at the location of the maximum rate, ahead of the actual face. This involves an element of judgement, as the maximum rate is sometimes poorly defined, e.g., Figure 4.8. The effective position of the face that has been adopted for MC-6.02, Station 81 is indicated in Fig. 4.10 by the vertical dashed line.

The process of fitting the Convergence Solution to the strain rate data consists of determining the values of the three parameters that fit the data the best. As will be demonstrated in the following, it is actually possible to obtain independent estimates of the parameters, because each parameter influences a different portion of the convergence rate curve. This will be demonstrated below in an outline of the step by step fitting procedure. All of the Convergence Solution curves for each of the cases below have been

generated using the computer program CONRATE (Appendix C).

First, determine the value of X that best describes the initial portion of the curve. The curves produced by a range in values of X, together with reasonable estimates of A^* and T, are compared to the data in Fig. 4.11. In this figure, X=0.03 provides the best fit of the cases shown. The fit of the portion of the curve before the face (Zone I) is neglected for reasons that will be explained in the next section. Time is portrayed on an arithmetic scale in this figure to emphasize the near face behavior. The initial portion of the curve, that is in the vicinity of the face, is dominated by the time-independent response of the rock. The parameter X has a dominant influence on this portion of the curve because it reflects the time-independent behavior of the rock. In contrast, T and A^* have virtually no influence over this portion of the curve. This is demonstrated in Figures 4.12 and 4.13, where a range of values for T and A^* were used. Thus, a value of 0.03 has been determined for X, independent of T and A^*, based on fitting the initial portion of the curve.

The next step is to determine the value of T that best describes the *shape* of the final portion of the curve. The parameter T alone governs the shape of this portion of the curve, because it is beyond the influence of the face, where only time-dependent convergence occurs. T is determined by plotting the curves produced by a range in T, together with the value of X found in the previous step, and a reasonable

estimate of A^*. These curves are shown in Fig. 4.12. A range in T from 700 to 1000 best reflects the shape of the final portion of the curve. Zone II is neglected for reasons that will be explained later.

The final step is to determine the value of A^*. This parameter controls the vertical position of the final portion of the curve. Figure 4.13 shows the curves produced by the values of X and T determined above, and a range in A^*. A value of $A^* = 0.5$ appears to give the best fit of the cases shown.

The final fit that is produced by the set of parameters determined above, is compared to the data in Fig. 4.14. The semi-logarithmic plot, Fig. 4.14A, is included to better portray the initial portion of the curve.

4.5.2 Discussion of Example Fit

The Convergence Solution provides a close fit to the strain rate data, shown in Fig. 4.14, with the exception of two discrepancies. The solution does not accurately predict the behavior of the sample just ahead of the effective face (Zone I, Fig. 4.14A), and immediately after the drill exits the sample (Zone II). These two discrepancies are caused by certain aspects of the laboratory tests that are outlined separately below.

The Convergence Solution predicts a sharp point of inflection as the face passes the measuring section (Zone I). The extensometers however, recorded a more gradual,

rounded peak at the location of the effective face. The major cause of this rounded peak probably arises from a basic difference between radial strain and tunnel wall convergence; radial strain is measured a distance away from the tunnel wall, whereas the convergence is measured right at the wall. The distance between the extensometers and the tunnel wall likely moderates the abruptness of the stress change associated with the passing of the face. A true convergence measurement, right at the tunnel wall would undoubtedly record a much sharper peak. In addition, this rounded peak could also be caused by yielding in the vicinity of the face, in response to the stress concentrations that occur there. This would cause a more gradual transition from the intact core of undisturbed rock ahead of the face, to the excavated cavity after the face passes.

The discrepancy in Zone II reveals a limitation of the Convergence Solution that was discussed in Chapter 2. It was stated there that the Convergence Solution was derived for tunnels excavated at a constant rate. The time-dependent component, $C_2(t)$, was formulated on the basis of the continuous stress change that results from a constant excavation velocity. When the velocity decreases, the solution underpredicts the convergence rate. Conversely, when the velocity increases, the solution overpredicts the convergence rate. In the laboratory test, the exit of the drill is analogous to a sudden increase to an infinite

velocity, followed by a velocity of zero. This is reflected in the Convergence Solution, shown in Fig. 4.14, where the rate increases suddenly, overpredicting the measured rate as the drill exits the sample. The rate then decreases suddenly after the drill exits the sample, giving an underprediction of the actual rate. However, the difference between the solution and the measured rates in this case is much worse than what would be observed in the field. When the drill exits the sample, the supporting effect of the rock at the face vanishes instantaneously. This abrupt increase in stress is peculiar to the test conditions, and would not occur in the field. Any change in velocity in a real tunnel would produce a deviation from the solution that would be less severe than that observed in Fig. 4.14. In addition, the magnitude of the drop in rate predicted by the solution is actually correct, even though it was not reached immediately but only after about 40 min.

Thus, the Convergence Solution can be used for tunnels with variable excavation rate, with the caution that abrupt changes in convergence rate associated with rate changes will not be reflected immediately in the data.

4.5.3 Fit of Solution to Convergence Measurements

At the beginning of this chapter it was assumed that the averaged radial strain could be substituted for tunnel wall convergence, using the factor $\frac{a}{2r^2}$. This was a necessary assumption, because the convergence measurements were only

commenced after tunnel excavation was complete, whereas the radial strain was measured over the entire duration of the tests. The final check on the validity of this assumption is whether or not the parameters that fit the radial strain measurements give a good prediction of the convergence measurements. Figure 4.15 shows the measured convergence rates compared to the convergence rate curve that was fit to the radial strain data of Test MC-6.02, Station 81, in the preceding section. It was not possible to normalize the convergence measurements to the maximum convergence rate, because it wasn't measured. Consequently, both the Convergence Solution, and convergence measurements have been normalized to the convergence rate at t=105 min, when the convergence measurements commenced. As shown in Fig. 4.15, the Convergence Solution prediction is very close to the actual convergence behavior over the region that it was measured.

4.5.4 Presentation of Curve Fitting Results

TEST MC-6.02

The curve produced by the final fit of the Convergence Solution to the data from Station 106 is shown in Fig. 4.16. The choice of the effective position of the face is even more ambiguous here, than with Station 81. This is caused by a distinct separation in time between the responses of the various gauges at this station, illustrated in Figs 4.2 and

4.3. This was probably caused by heterogeneities in the sample. The result of this behavior is the two peaked maximum rate observed in Fig. 4.16, which is difficult to fit with one curve. The effective face has been placed between these two peaks, and the resulting fit is only approximate. The Convergence Solution parameters that characterize the two stations of MC-6.02 are summarized below:

	X (m)	T (min)	A*
Station 81	0.03	700 - 1000	0.5
Station 106	0.03	300	0.2

TEST MC-7.13

The final fit of the Convergence Solution to each of the stations of Test MC-7.13 are shown in Figures 4.17 to 4.19. The effective position of the face, indicated by the dashed line, was placed at the maximum rate. This consistently occured 10 to 25 mm ahead of the actual face, indicated by the solid line. The exception to this is Station 81, where the maximum rate occurred at the actual face. This however is a spurious maximum, as it is caused by a jump in only one of the eight gauges in the ring. Therefore, the effective face has been placed at the maximum rate that occurred before the actual face, consistent with

the other stations.

The parameters determined in the fitting process are summarized below:

	X (m)	T (min)	A^*
Station 56	0.05	1000	0.35
Station 81	0.09	1000	0.80
Station 106	0.06	700	0.40

4.6 Interpretation of Results

The validity of the parameters that have been determined by fitting the Convergence Solution to the test data will now be discussed. This will be accomplished by relating the physical meaning of the parameters to the experimental observations. In addition, the results will be compared to two projects; the Fréjus tunnel, and the Las Planas tunnel, where the original form of this approach has been applied. These were analyzed by Sulem(1983) with the form of the convergence equation developed by Guenot et al. (1985).

TEST MC-6.02

A completely consistent set of parameters was not obtained in this test. The value of X was the same for both stations, but A^* and T for Station 81 were more than 100

percent greater than those for Station 106. The difference between these two is a result of the poor quality of the data from Station 106. The extensometers at this station were 86 mm away from the tunnel wall, compared to 35 mm for Station 81. This increased distance makes the gauges less responsive to movement. The initial part of the curve, described by X, was similar to Station 81 in shape, because the strains in this region were well within the range of the instruments. The latter part of the curve however, deviated from that of Station 81, because the strains were close to the sensitivity of the instruments. These strains were two orders of magnitude smaller than the strains at Station 81. Hence, the results from Station 81 will be adopted as more representative of the actual behavior.

The value of X, determined in the analysis is 0.03. Panet and Guenot (1982) defined X as:

$$X = k_p R \qquad \text{Eqn 4.10}$$

where: R = Radius of plastic, or yielded zone; and

k_p = constant.

They found that k_p=0.84 gave the best fit to the range of cases they modelled with finite element analyses. In Test MC-6.02, there was little, or no observed yielding which suggests that R=a=0.054 m (no yield case). On the basis of this no yield case, and X=0.03, the value of k_p for Test

MC-6.02 is 0.6, which is lower than the value k=0.84 determined by Panet and Guenot (1982). This discrepancy results from the limitation of the laboratory test that it is not infinite in extent, as a rock mass is. When a tunnel is excavated in a rock mass the stress transfer associated with excavation is felt over a distance of approximately two tunnel diameters on either side of the face. In the laboratory tests however, the samples are only 1.4 and 1.9 tunnel diameters thick for Tests MC-6.02 and MC-7.13 respectively. Consequently, all of the stress transfer must take place within this reduced distance. This produces steeper stress gradients, and hence steeper convergence gradients. This is reflected in a lower value of k_p. Thus, a k_p of 0.6 will be used to interpret the laboratory results, but k_p=0.84 will be used for the Enasan Tunnel, analyzed in Chapter 5.

The value of the parameter T found in the analysis is on average about 800. This is well within the range of 140 to 5000 found by Sulem (1983) for both of the tunnels he analyzed.

The value of A^*=0.5, determined from this test, is significantly less than the range of 2 to 5.6, obtained by Sulem. A difference of this order suggests that the coal used in the laboratory test displayed much less time-dependent behavior that either the schist at the Fréjus tunnel, or the marl at the Las Planas tunnel. This is unlikely, since coal is a material that displays significant

time-dependent behavior. The major reason for this discrepancy arises from the difference between the convergence equation of Guenot et al. (1985) used by Sulem, and the new Convergence Solution, presented in this study. The original equation did not account for convergence ahead of the face. Thus, their value of A^* is the ratio of the ultimate time-dependent to time-independent convergence that occured after the face ($A/C_{x\infty}$). $C_{x\infty}$ after the face is approximately 70 percent of the total $C_{x\infty}$, but almost all of the ultimate time-dependent convergence, A, occurs after the face. Thus, when the pre-face convergence is included, the ratio A^* is a smaller number. In addition, the laboratory test recorded the entire range of movement, but in a real tunnel project, the convergence is seldom measured starting right from the face. When a portion of the near face behavior is neglected, A^* increases significantly. This increase is caused by a proportionally larger reduction in $C_{x\infty}$ than A, because the time-independent convergence occurs near the face. Consequently, the value of A^* becomes larger the further back the convergence measurements are commenced. Thus, the range in A^* found by Sulem (1985) likely overestimates the true A^*, as a portion of the near face convergence was likely missed.

MC-7.13

A relatively consistent set of parameters was obtained from the three stations analyzed from test MC-7.13. The

parameters X and A^* from Station 81 were higher than either of the other two stations, but this difference is likely due to local variations in rock properties or the amount of local yielding.

The values of X determined in this test correspond to plastic radii predictions that are supported by the experimental observations. It is not possible to determine the exact shape, and extent of the plastic zone from the extensometers, but they do give an approximate indication of the extent of yielding. Figure 4.20 contains the estimated yield zones at each of the three measuring stations of Test MC-7.13, based on the extensometer response. The open circles represent the extensometers that recorded large strains that indicate yielding of the coal. The strain at the end of excavation at each of these gauges is given in the figure as well. The solid circles indicate the position of extensometers that did not record any yielding. The predictions of R are based on k_p, established in Test MC-6.02. The values of R given by the Convergence Solution for each of the stations are:

	R/a
Station 56	1.1
Station 81	2.0
Station 106	1.3

Although it is difficult to relate the localized yielding behavior observed in this test to the uniform annulus of yielded material assumed in the Convergence Solution, an important trend has been identified. The station that displayed the least amount of yielding in Fig. 4.20 (Station 56), corresponded to the lowest R; and as the predicted value of R increased, the observed yielding also increased. Thus, while it was not possible to validate numerically the yield zone predictions, the relative amount of yielding between the stations was correctly indicated by the Convergence Solution.

A consistent set of values of the parameter T was obtained, that correspond to the range found for Test MC-6.02, which are within the range found by Sulem (1983). Even though there was a difference in excavation rate of one order of magnitude between these two tests, the range in T was identical (excluding MC-6.02, Station 106). This suggests that the dependence of the parameter T on excavation rate, explained in Chapter 2, is very minor.

The values of A^* obtained in this test are very close to the value of A^* found for Test MC-6.02. Station 81 had a higher value of A^* than any of the other stations, but this could be a result of the assumption of the maximum rate. The choice of maximum rate, and hence the location of the effective face, was somewhat ambiguous for this station. An error in selecting the maximum rate shifts the entire curve vertically up or down. This shift has a direct impact on A^*,

which reflects the vertical position of the latter portion of the curve. Thus, the A^* values determined at Stations 56 and 106 are likely more representative of the true behavior.

In summary, a consistent set of parameters has been obtained from the application of the Convergence Solution to the data from two laboratory tests. These parameters characterize the response of the coal to the excavation of a tunnel. The two tests that were analyzed yielded remarkably similar parameters, despite the difference in excavation history. MC-6.02 was an initial excavation, but MC-7.13 involved the widening of an existing tunnel.

The similarity between the virgin excavation and the tunnel widening suggests that the main difference between the response of a rock mass to tunnel widening versus a virgin excavation, is the magnitude of the convergence. Thus, when the results are analyzed in the format presented in this chapter, which gives independence from magnitude, these two excavation cases may be treated identically. This has important implications for sequential stage excavations, such as the Enasan Tunnel, that will be analyzed in the following chapter. It implies that each excavation stage can be treated separately as a virgin excavation and the results of each stage superimposed.

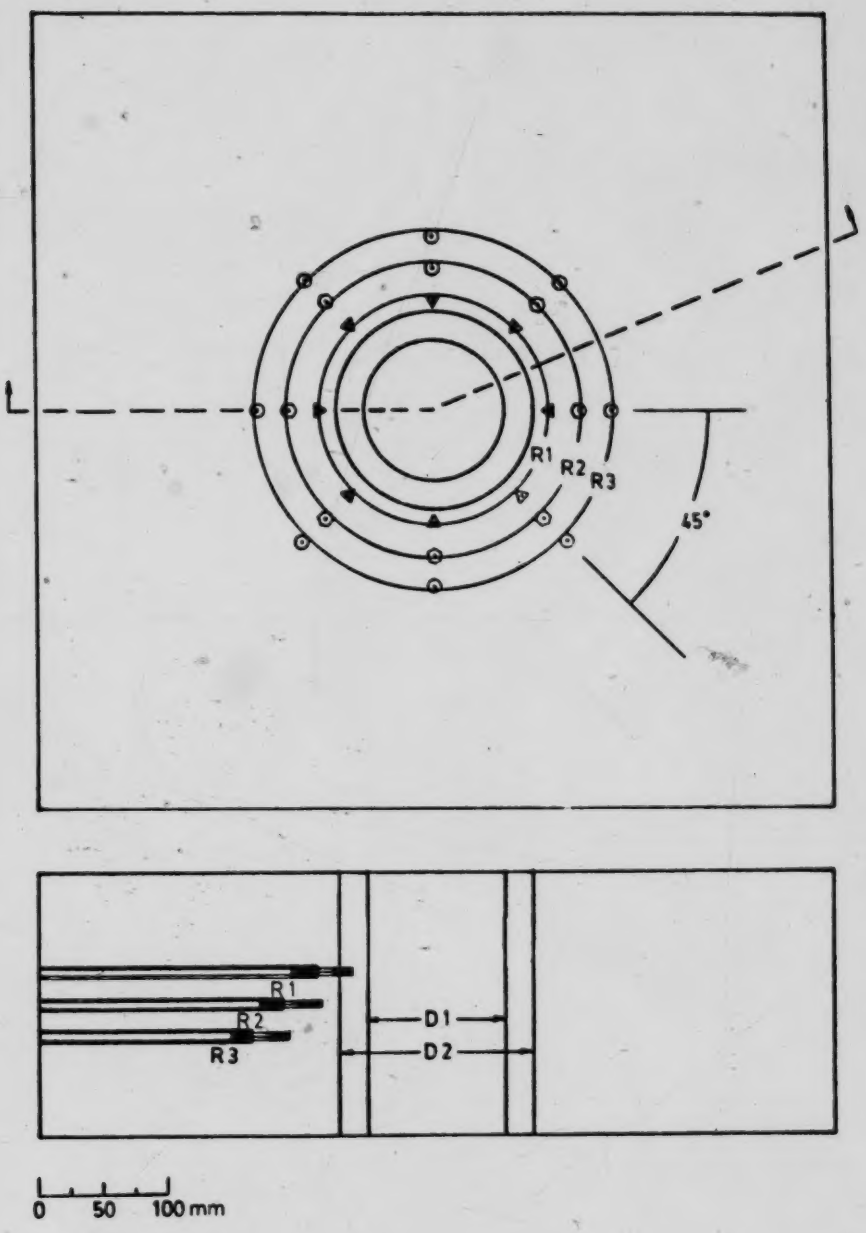

Figure 4.1 Laboratory Sample MC-6 Instrumentation (modified from Maloney, 1984).

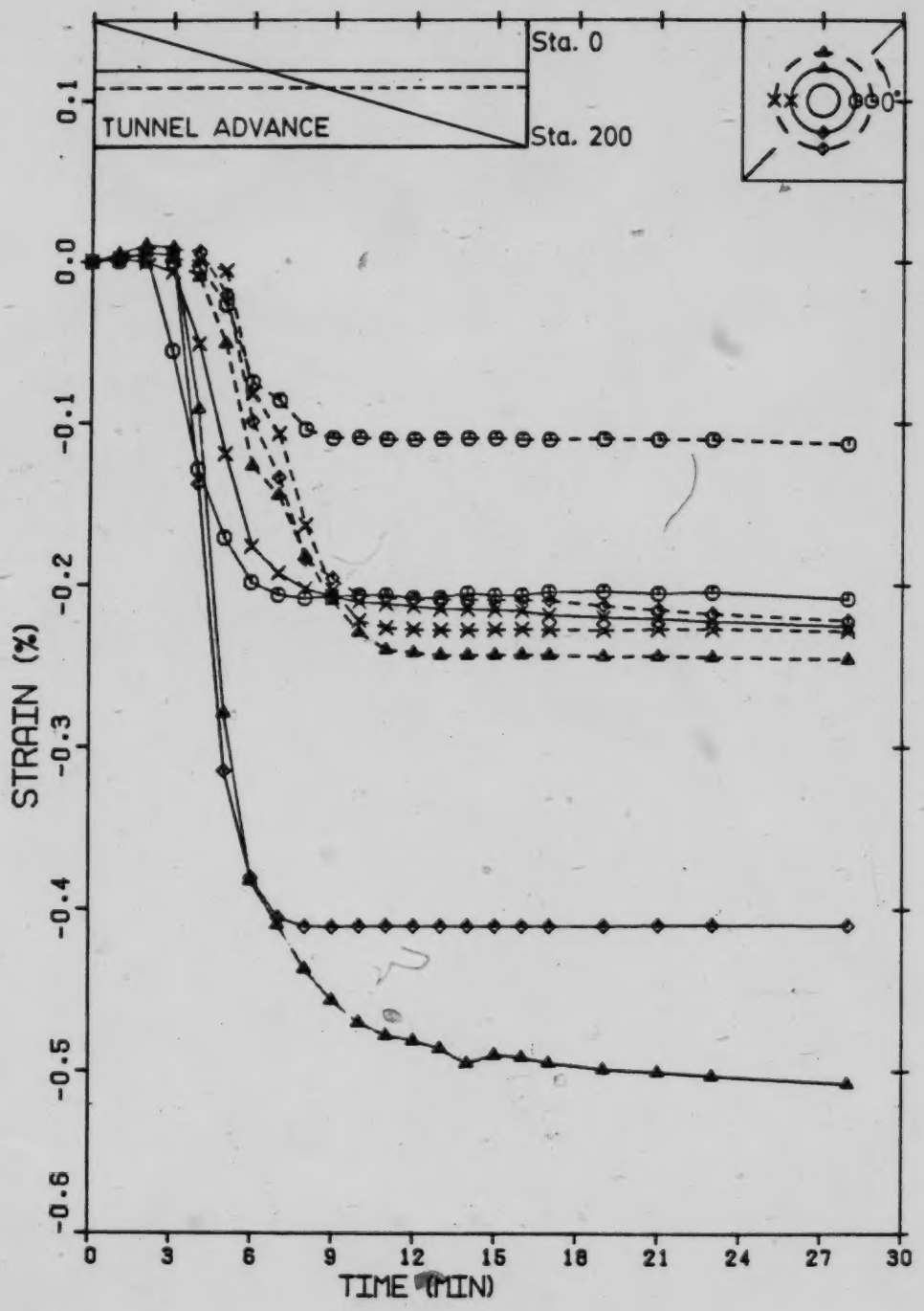

Figure 4.2 Radial Strain vs Time - Test MC-6.02 (after Kaiser et al., 1982).

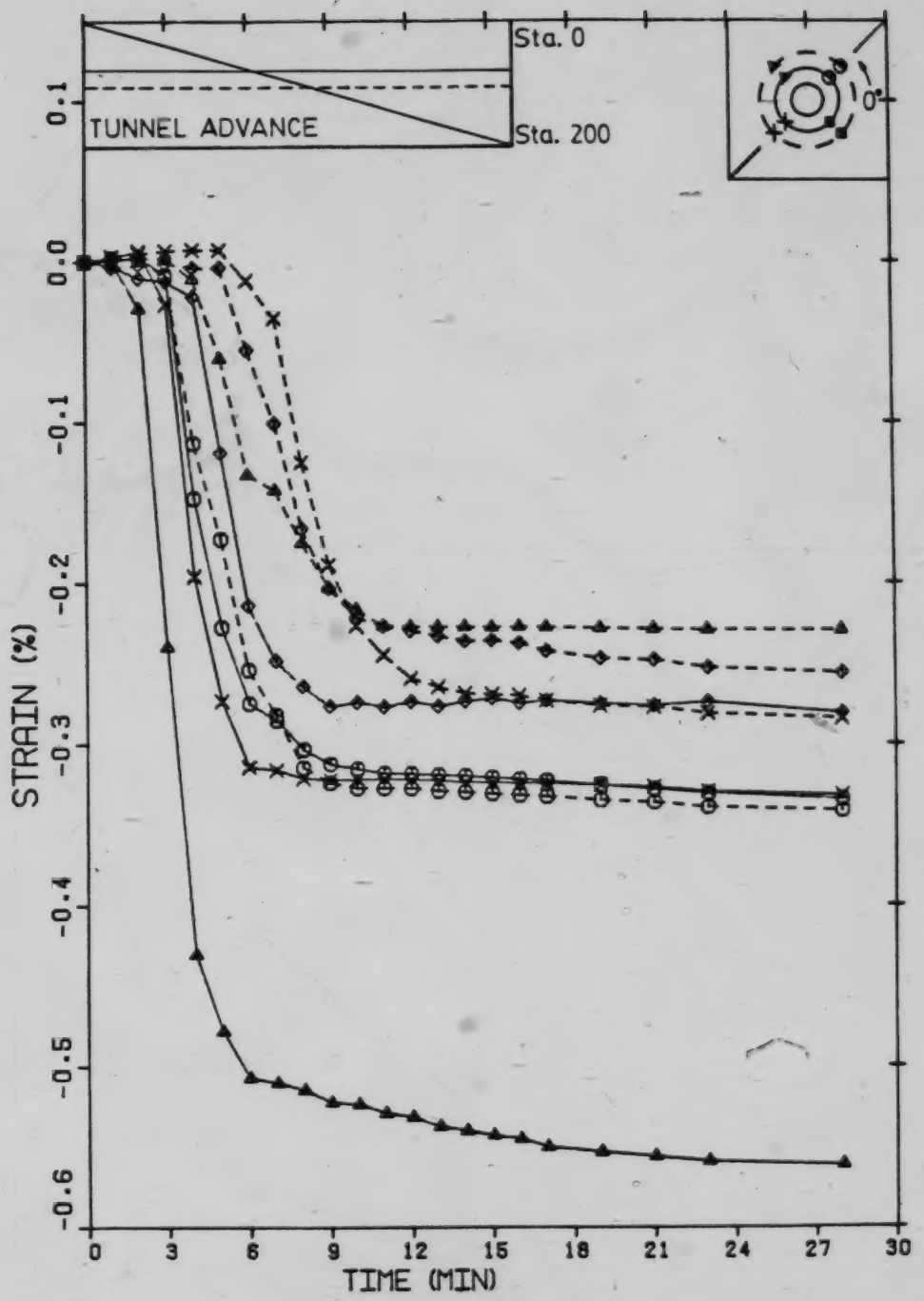

Figure 4.3 Radial Strain vs Time - Test MC-6.02 (after Kaiser et al., 1982).

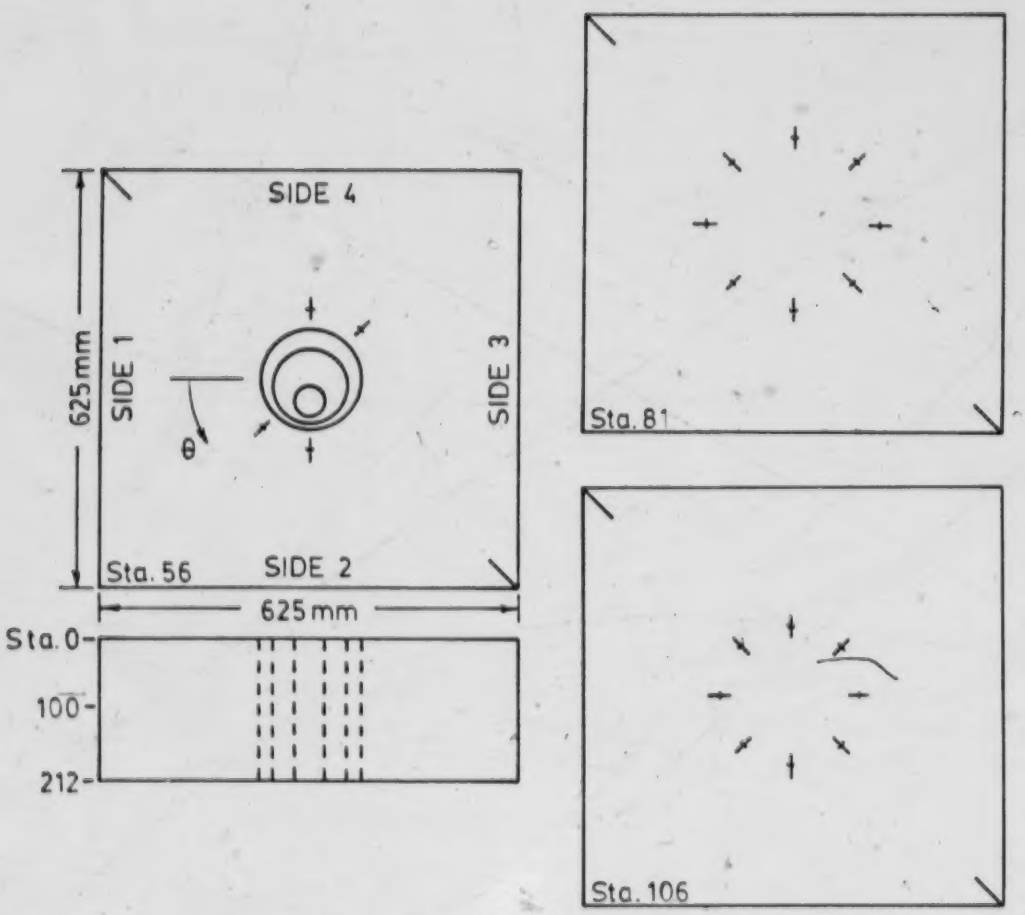

Figure 4.4 Laboratory Sample MC-7 Instrumentation (modified from Kaiser et al., 1983b).

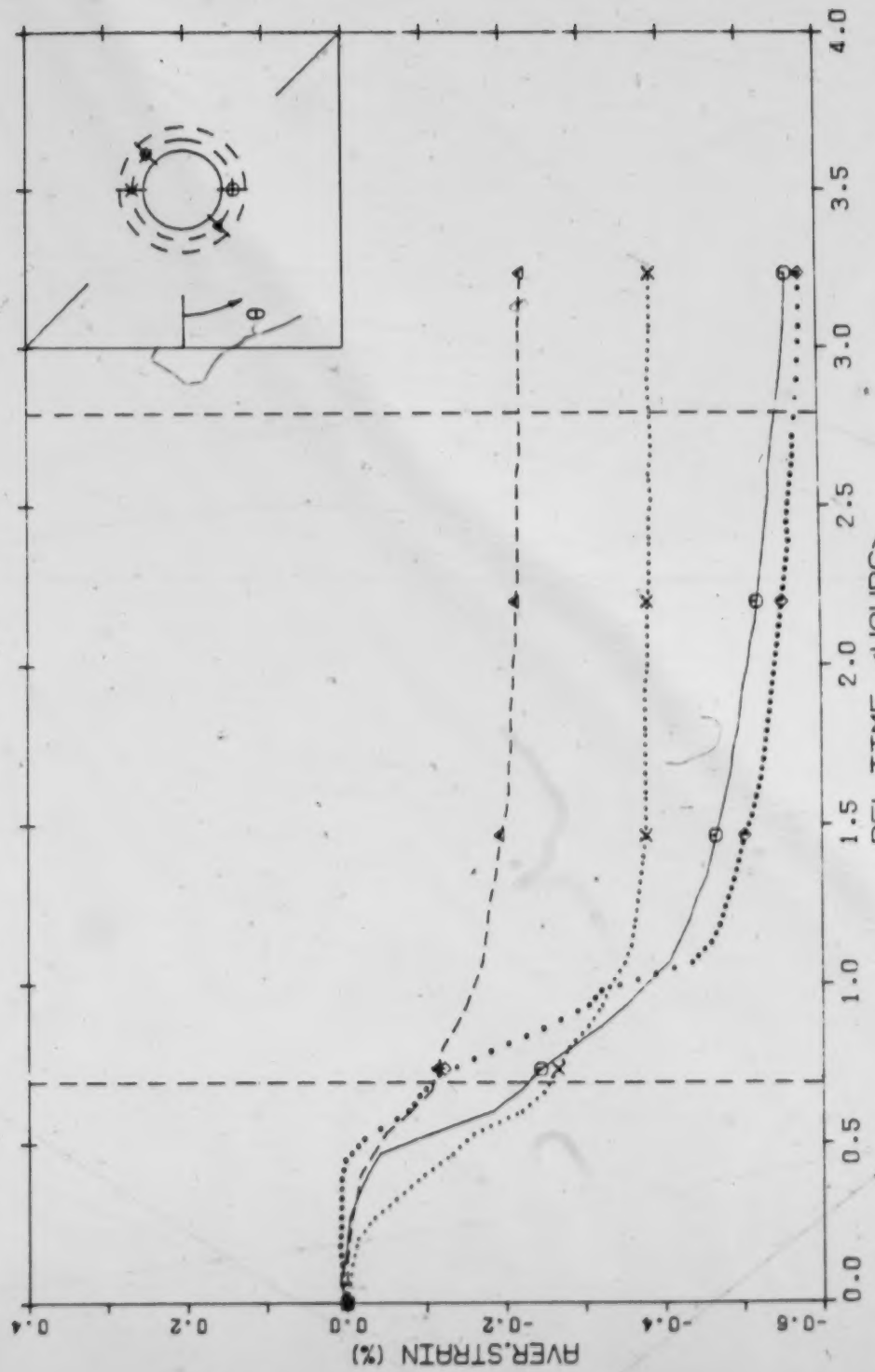

Figure 4.5 Radial Strain vs Time - Test MC-6.02 (Maloney, 1984).

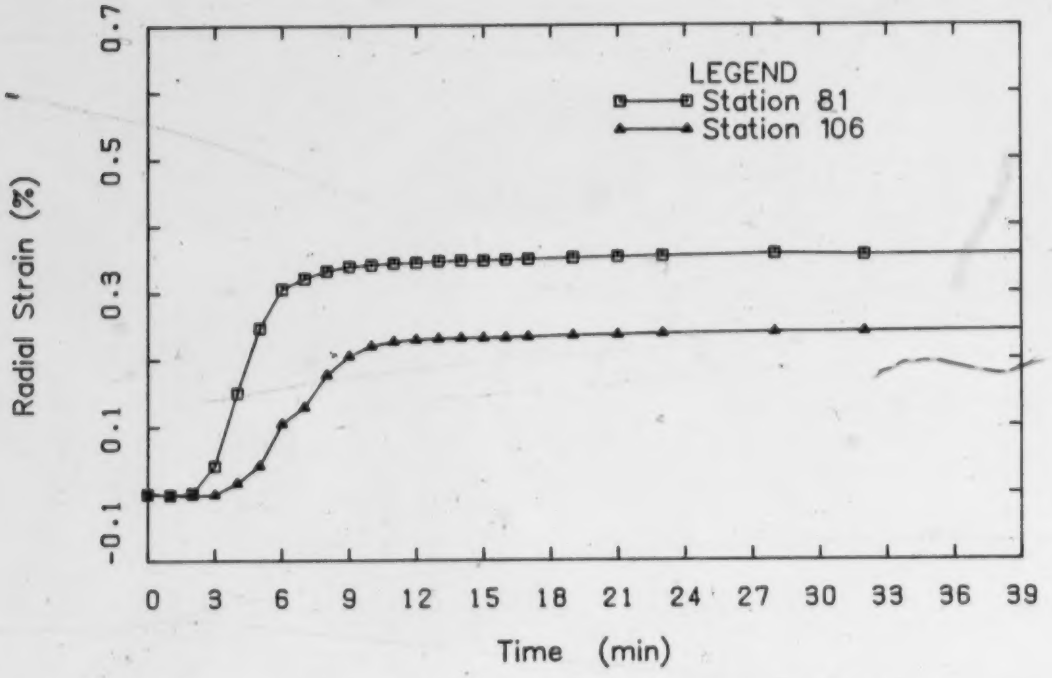

Figure 4.6 Averaged Radial Strain vs Time, Test MC-6.02.

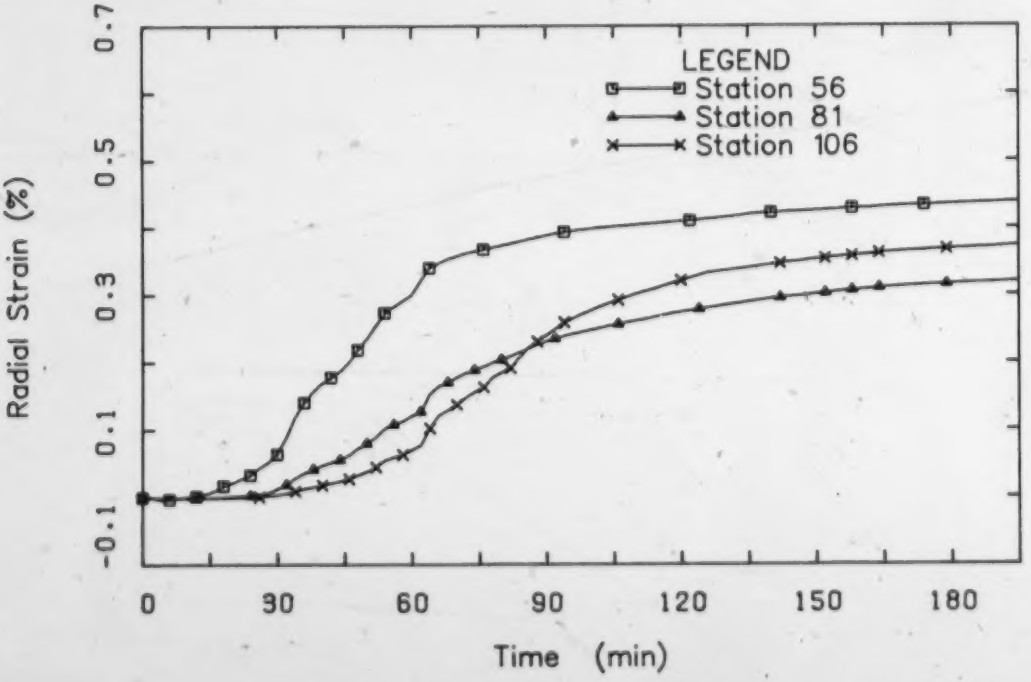

Figure 4.7 Averaged Radial Strain vs Time, Test MC-7.13.

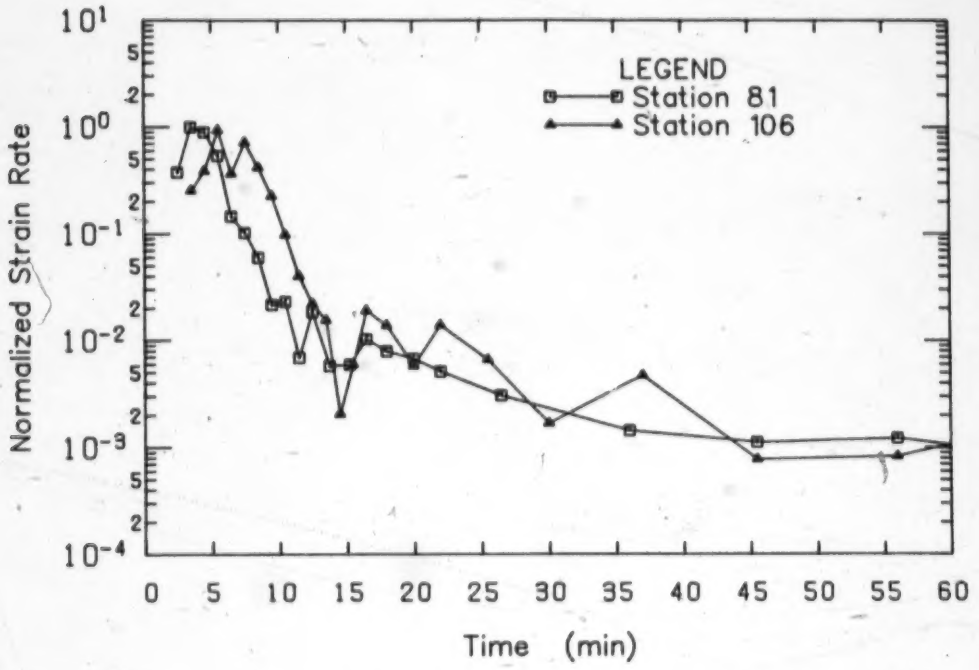

Figure 4.8 Normalized Strain Rate vs Time, Test MC-6.02.

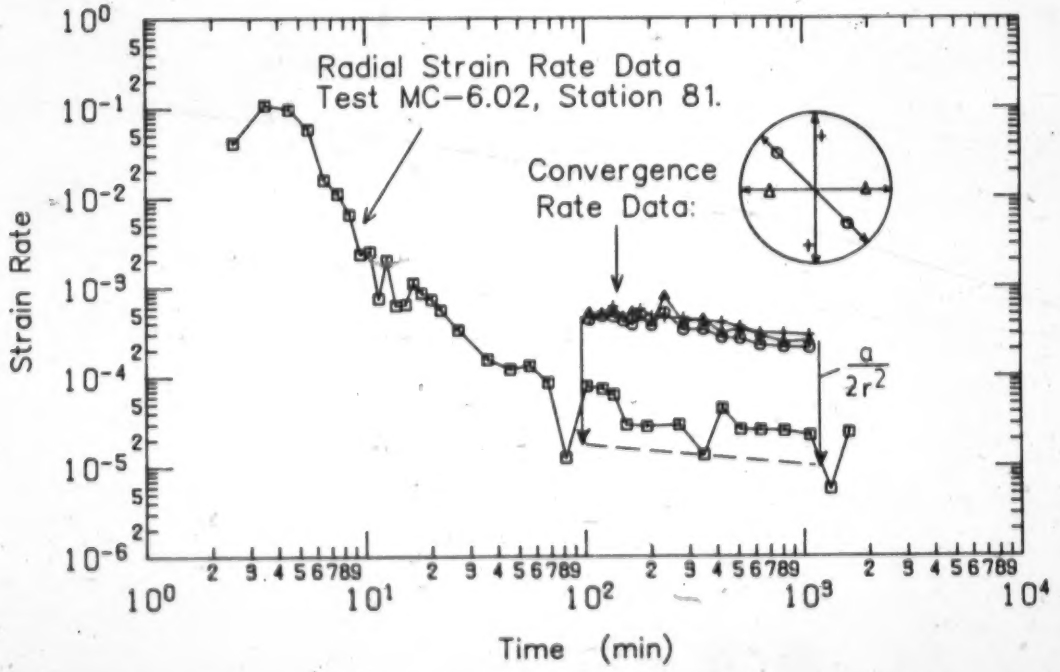

Figure 4.9 Radial Strain Rate Compared to Convergence Rate, Test MC-6.02, Station 81.

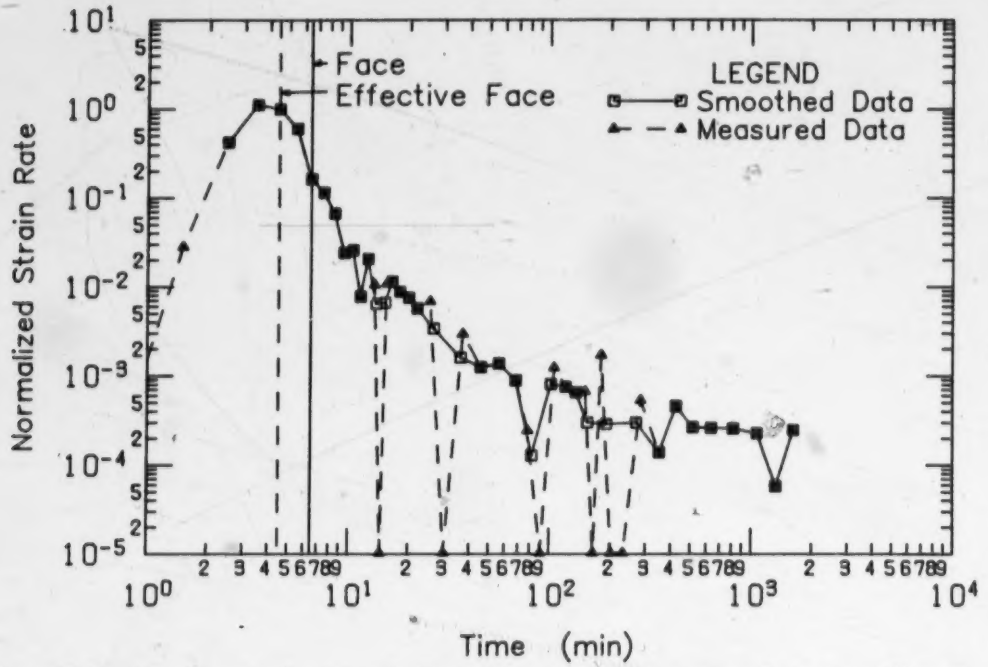

Figure 4.10 Comparison of Smoothed and Measured Normalized Strain Rate, Test MC-6.02, Station 81.

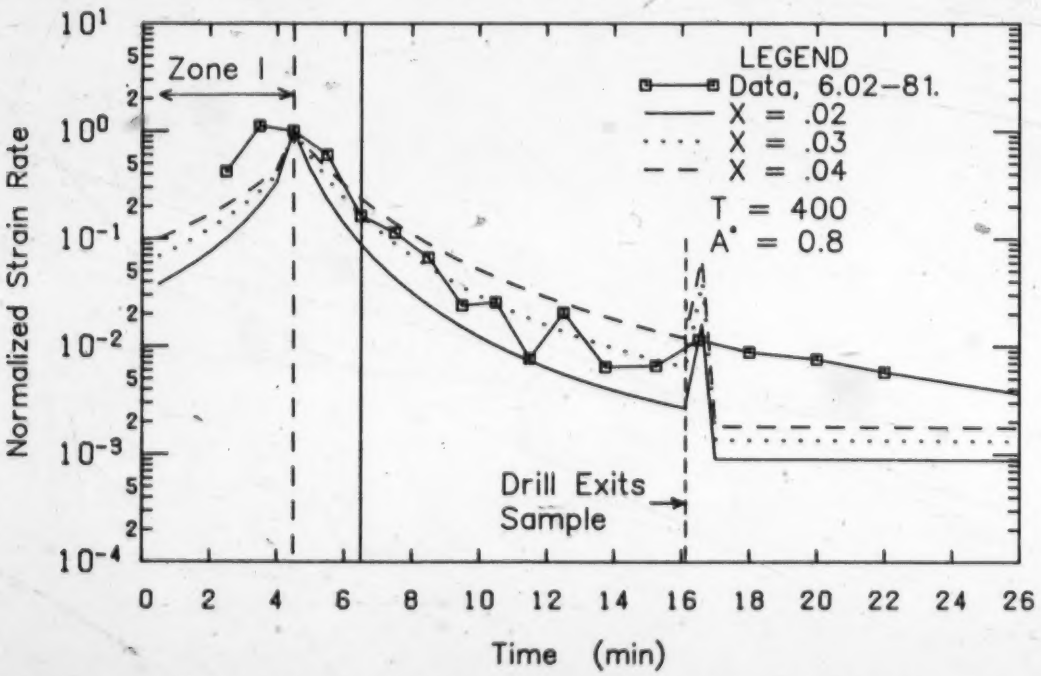

Figure 4.11 Fit of Convergence Solution to Strain Data, X Varied.

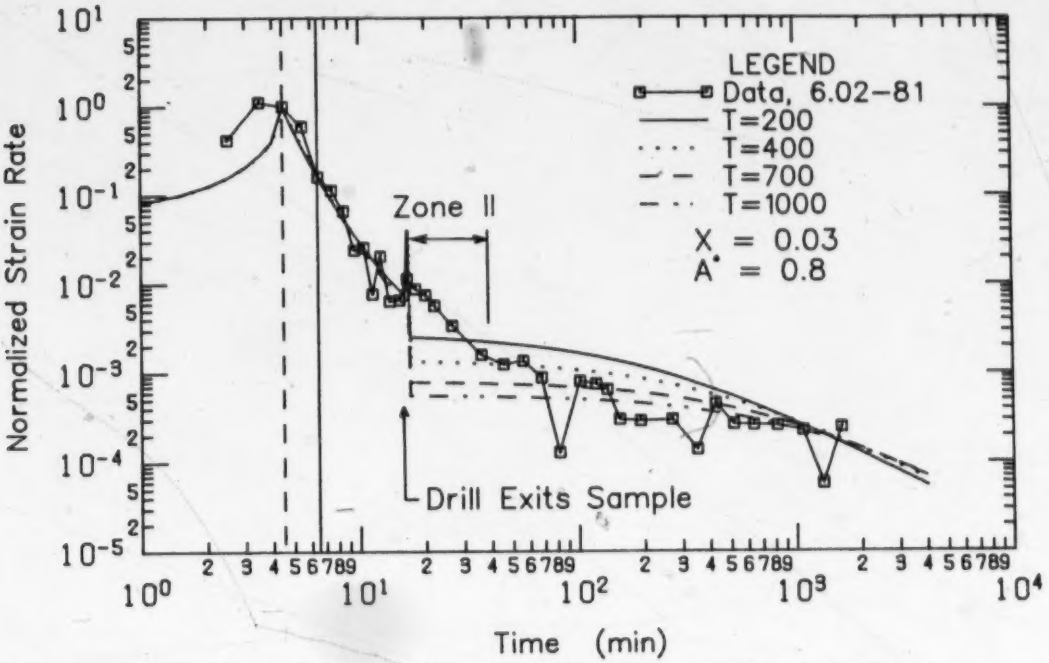

Figure 4.12 Fit of Convergence Solution to Strain Data, T Varied.

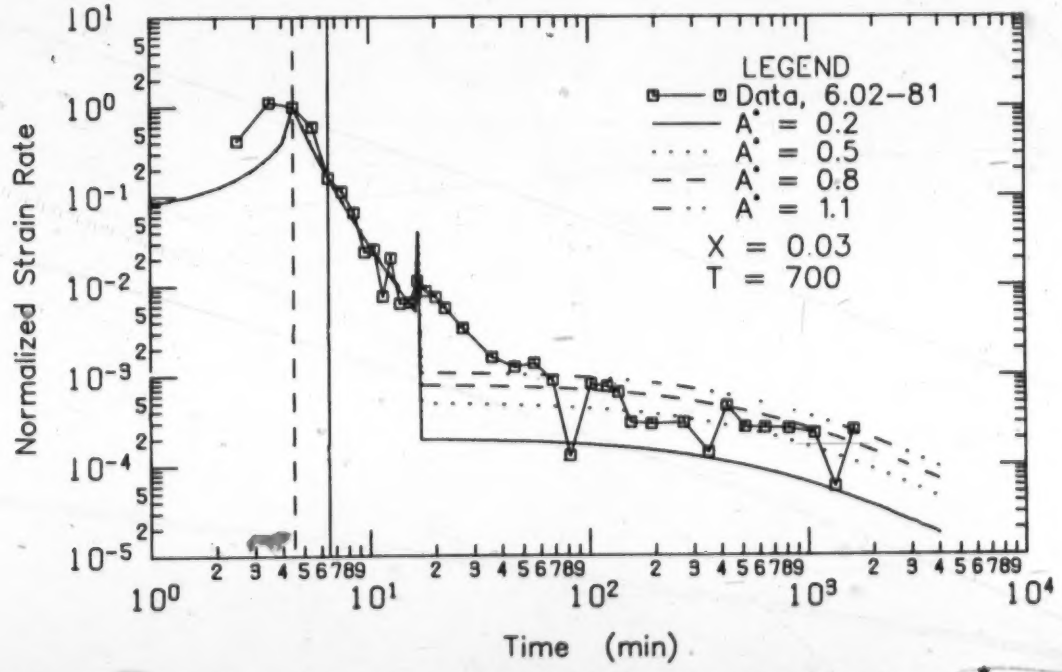

Figure 4.13 Fit of Convergence Solution to Strain Data, A^* Varied.

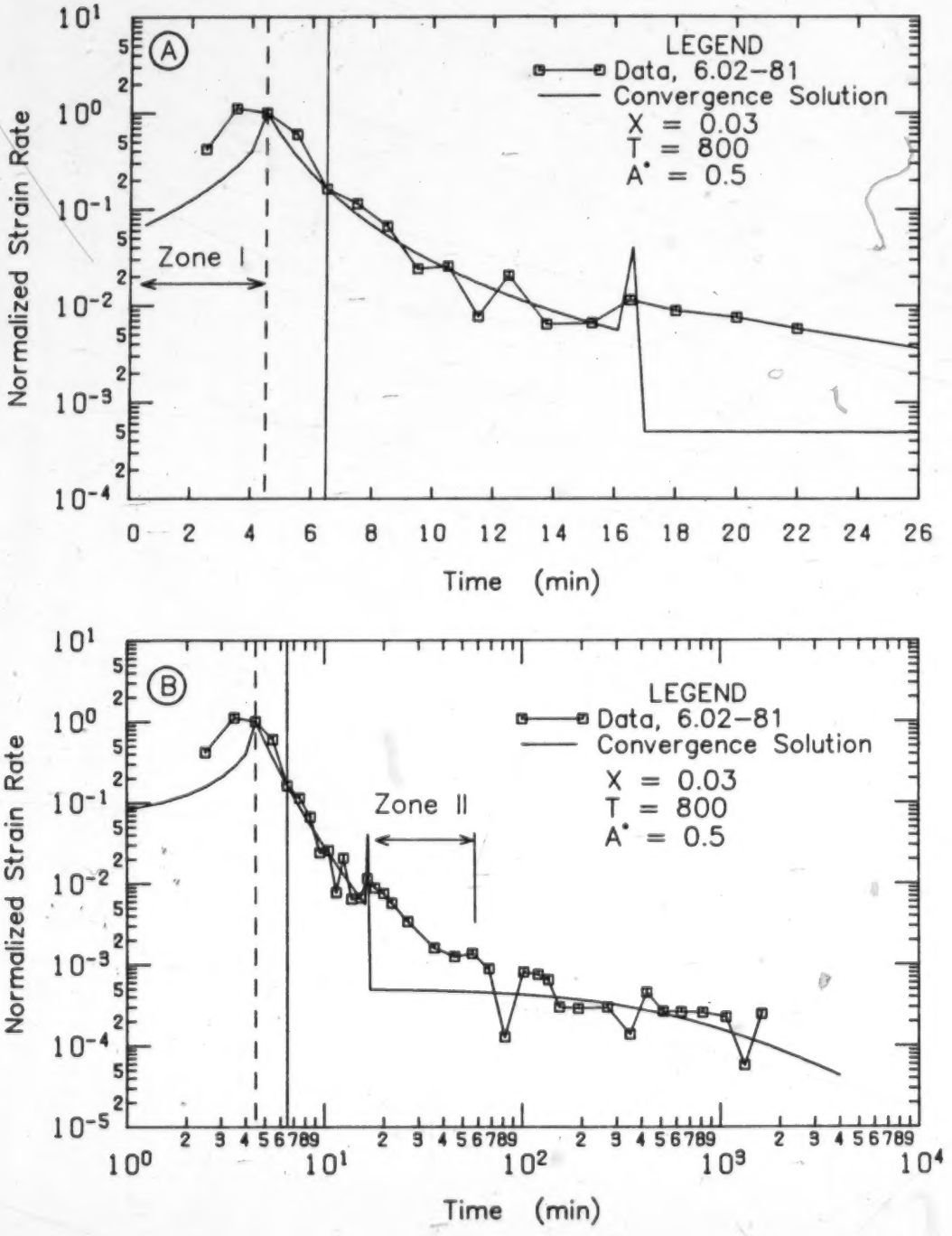

Figure 4.14 Fit of Convergence Solution to MC-6.02-81 Strain Data.

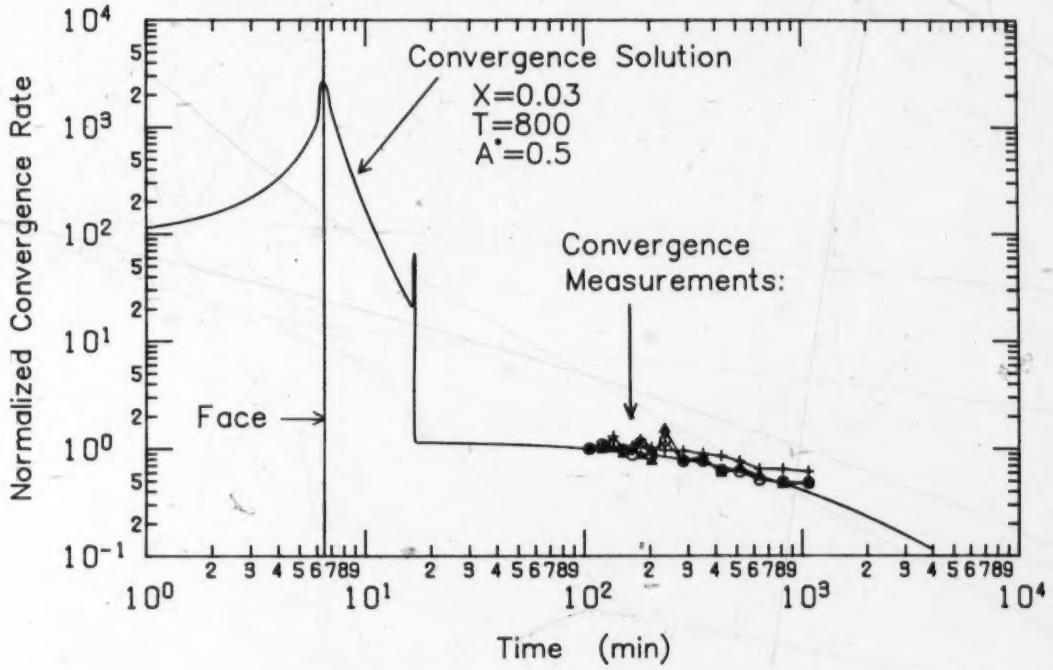

Figure 4.15 Fit of Convergence Solution to Convergence Data, MC-6.02-81.

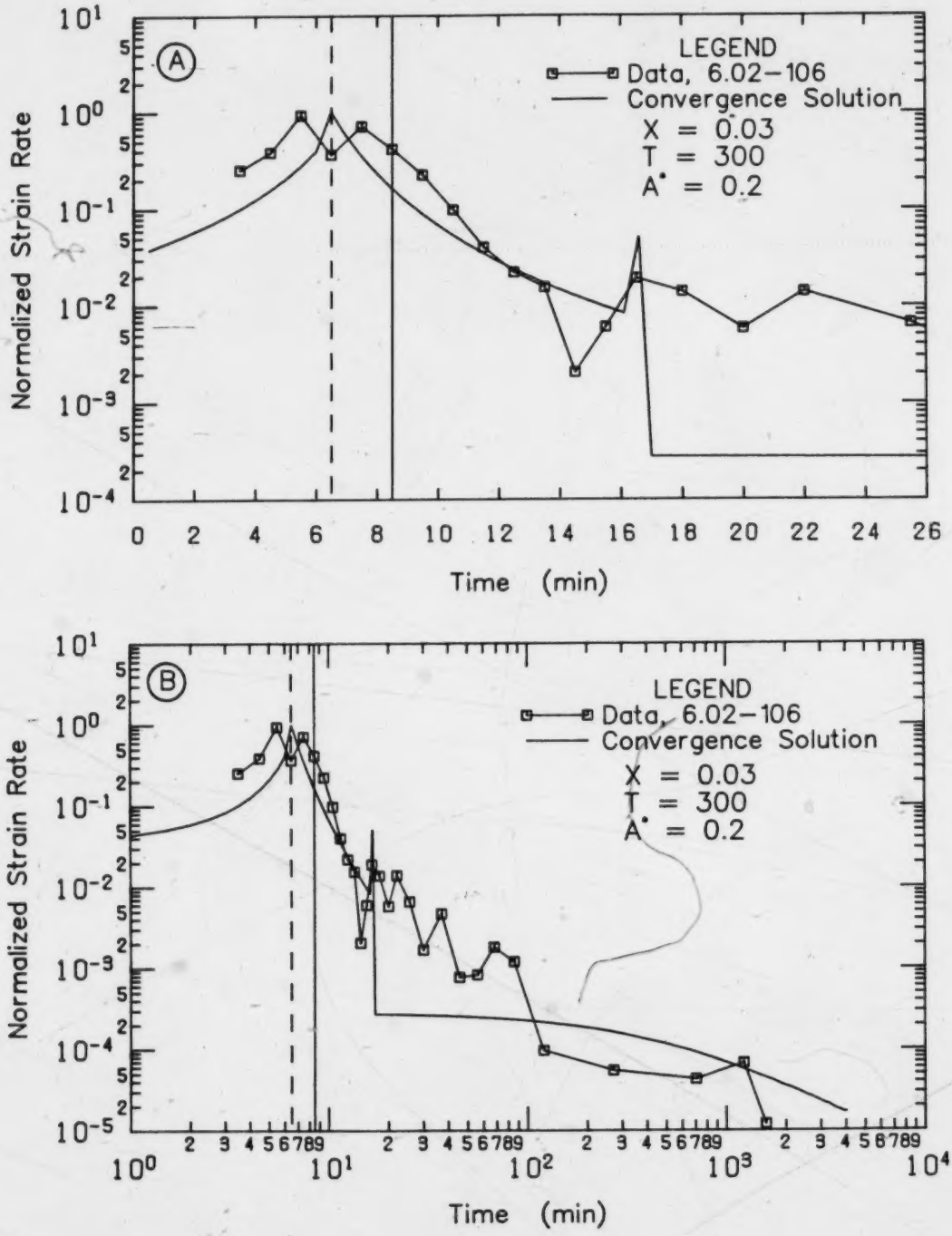

Figure 4.16 Fit of Convergence Solution to MC-6.02-106 Strain Data.

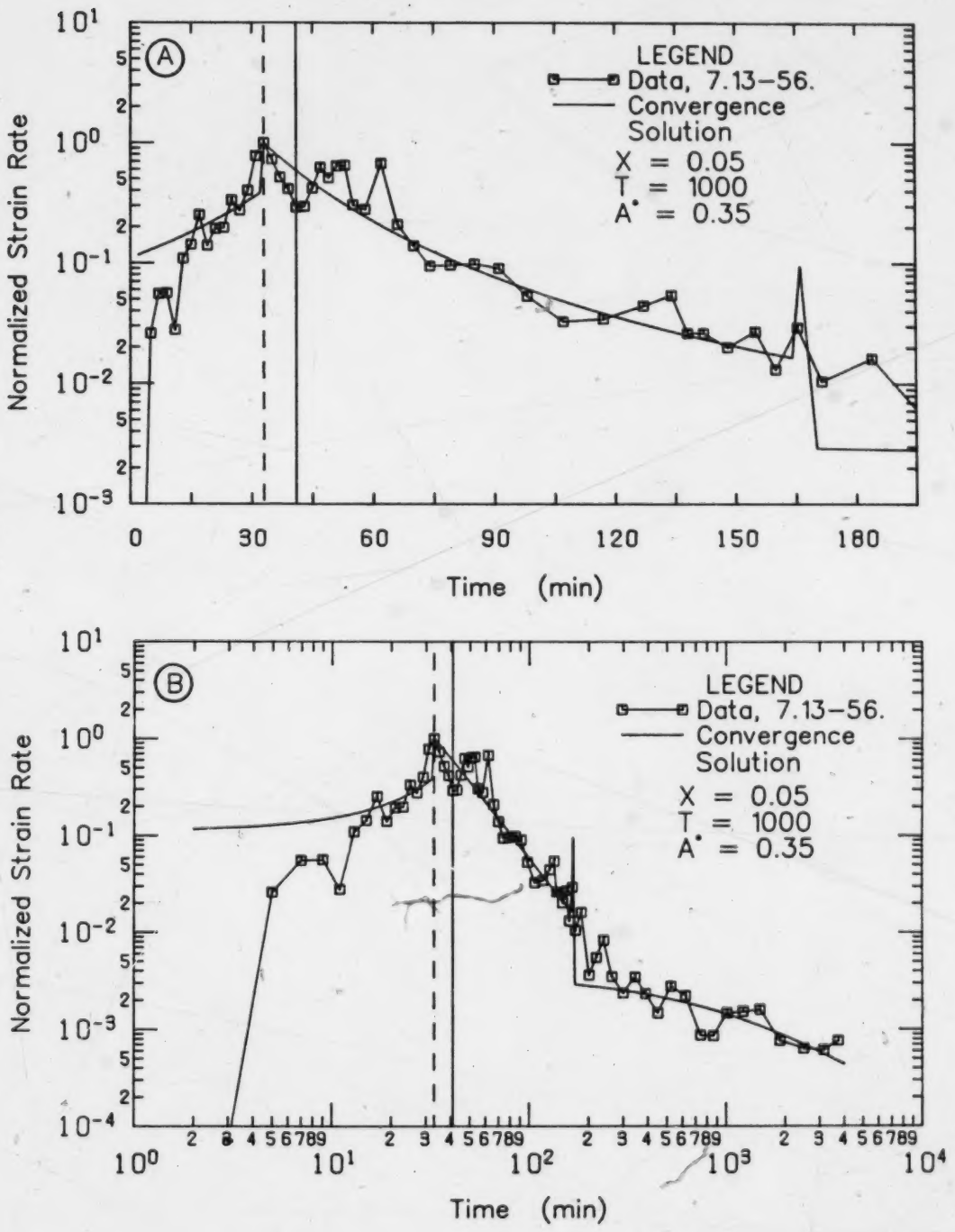

Figure 4.17 Fit of Convergence Solution to MC-7.13-56 Strain Data.

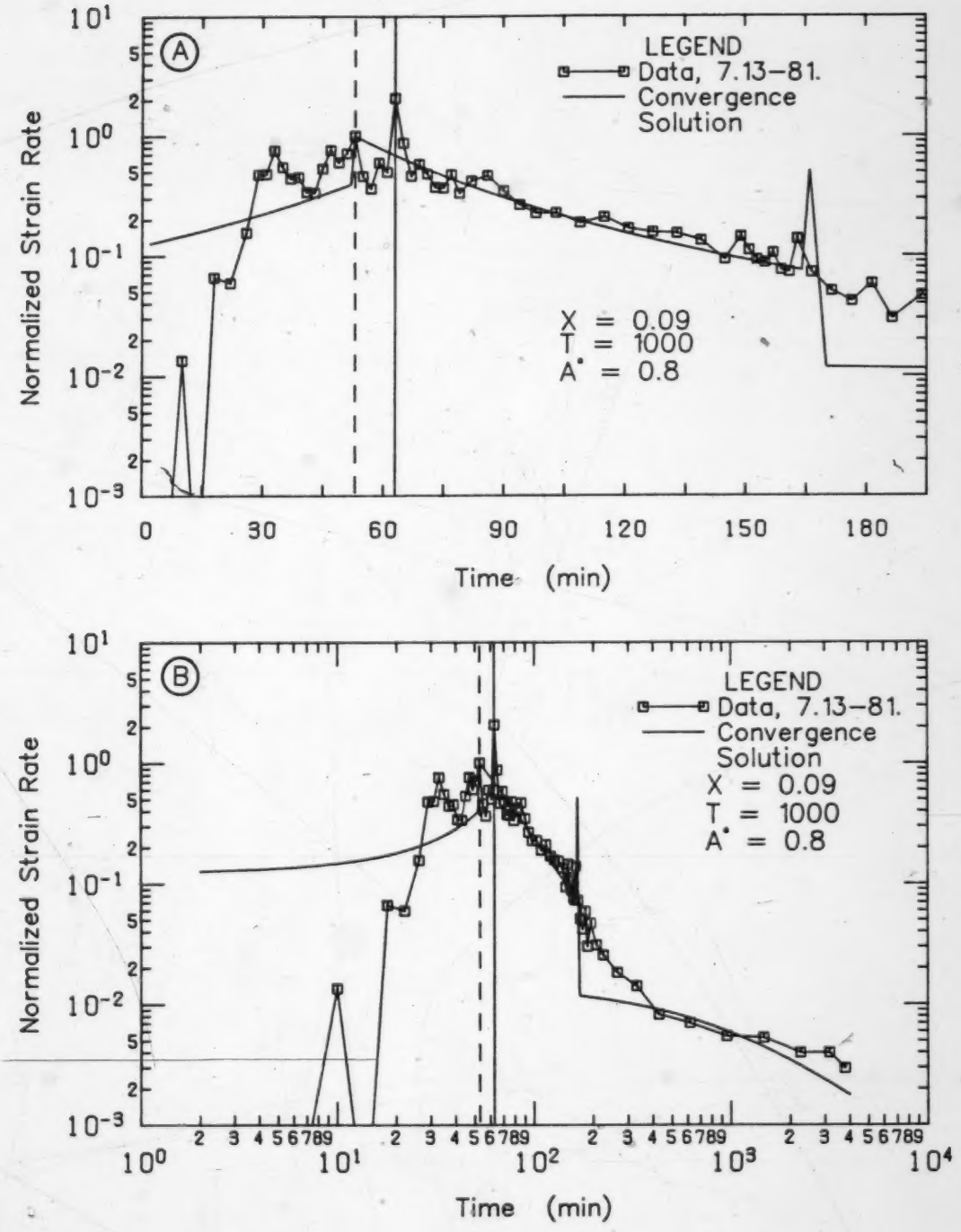

Figure 4.18 Fit of Convergence Solution to MC-7.13-81 Strain Data.

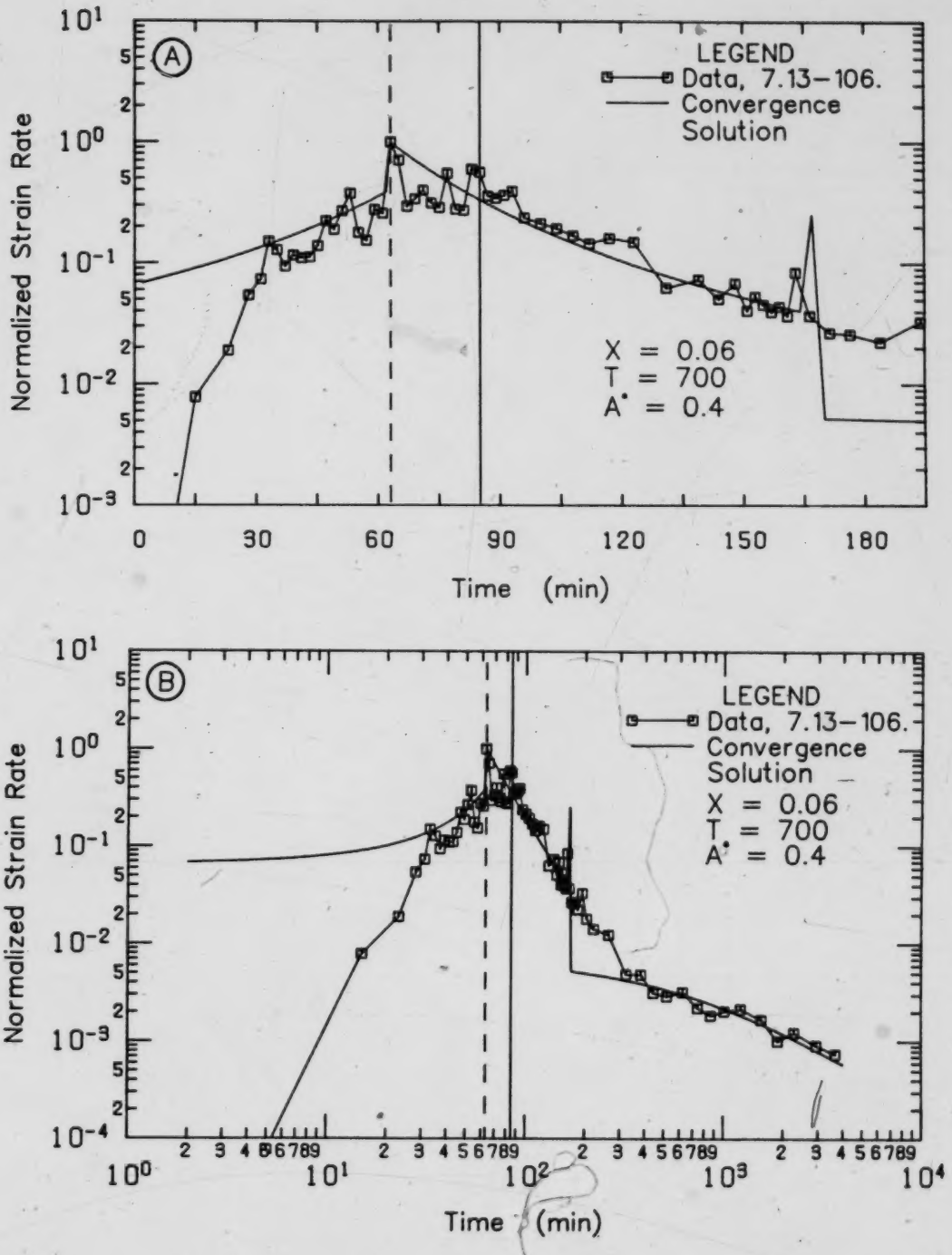

Figure 4.19 Fit of Convergence Solution to MC-7.13-106 Strain Data.

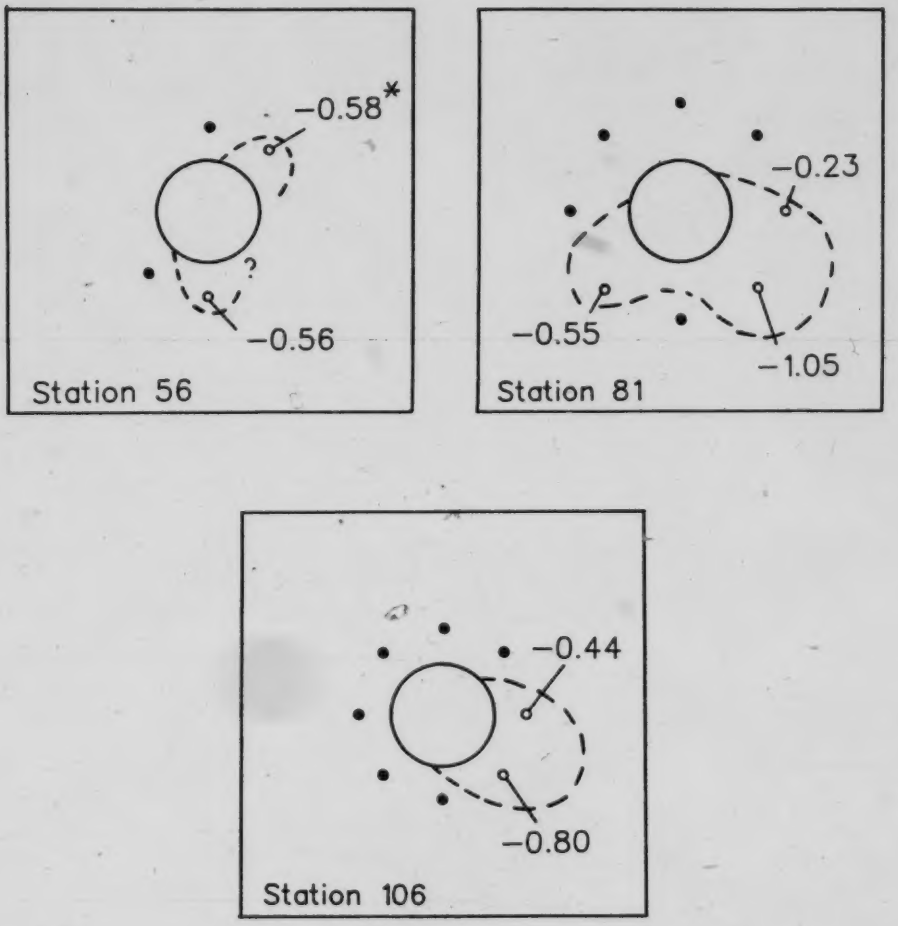

Figure 4.20 Yielding associated with Test MC-7.13.

5. APPLICATION OF CONVERGENCE SOLUTION TO ENASAN TUNNEL (JAPAN)

5.1 Introduction

The Convergence Solution will now be applied to measurements taken from the Enasan tunnel project in Japan (Ito, 1983). This data was received by Kaiser (1984) during site visits in Japan. The thoroughness of the instrumentation program in this project make it particularly amenable to analysis using the Convergence Solution. The tunnel was excavated in three sequential stages. The top portion, or heading, was excavated first, followed by a bench and invert excavation. For the analysis, each excavation stage was treated as a completely separate excavation, and the results of the each stage were superimposed, based on the conclusions of Chapter 4. This necessitated certain assumptions that are outlined in detail in Section 5.3.

5.2 Description of Enasan Tunnel Project

Two parallel highway tunnels were constructed through Mount Enasan as a part of the Chuo expressway that traverses the central Alps of the Honshu Island, in Japan. The two 8.6 km long tunnels are spaced at 60 m center to center, and the maximum depth of cover is approximately 1000 m. These tunnels are located in granite in the vicinity of the active Andera fault. The rock is folded, faulted and heavily

fractured. The New Austrian Tunneling Method (NATM) was used for a 350 m long section of the north tunnel where the rock was heavily overstressed (Takino et al., 1983). The location of this section is indicated on the plan view of the east half of the Enasan tunnel project in Figure 5.1. The response of the rock mass in this 350 m section will be investigated in this chapter.

5.2.1 Excavation and Support Placement Procedure

The tunnel was excavated by drilling and blasting in three sequential stages. The portion of the cross section excavated in each stage is indicated in Figure 5.2. The temporary support system was installed following the procedure outlined below:

- Heading Excavation:
    1. 5 cm of shotcrete was applied to the face and upper arch, exposed by the heading excavation. Longitudinal slots were left in the shotcrete on the walls and roof, to prevent buckling of the shotcrete.
    2. Steel sets were placed at 1.0 m spacing.
    3. A second layer of shotcrete was applied; 5 cm on the face, and 20 cm on the upper arch (with slots).
    4. Spiling with 2.5 m long bolts was used to control the tunnel face.

5. Rock bolts were installed 1.5 m behind the leading steel set.

- Bench Excavation:

Identical procedure to heading excavation without Step #4.

- Invert Excavation:

1. 10 cm of concrete was placed with steel net reinforcing.
2. Rock bolts were installed.
3. An additional 10 cm of concrete was placed.

The purpose of this temporary support system was to strengthen and maintain the integrity of the rock mass, rather than to apply pressure against the rock to limit deformation. Consequently, the components of the support system were designed to reinforce the rock mass, while allowing deformation to occur. This was accomplished by using yielding steel sets, and by leaving longitudinal slots in the shotcrete. These two features allowed deformation to occur without causing failure of the supporting elements.

The configuration of the rock bolts that were installed at the two measuring stations that are analyzed later (Stations A and B in Fig. 5.1), are indicated in Figures 5.3 and 5.4 respectively. The solid lines indicate the position of rock bolts installed according to the above procedure.

The rock bolts are either 6.0, 9.0, or 13.5 m long as illustrated in Figs 5.3 and 5.4. The bolts in the heading and bench are fully grouted, whereas those in the invert are self boring spiral rock bolts. Also shown in Figs 5.3 and 5.4 is the position of the spiling, and the slots that were left open in the shotcrete to allow deformation to occur. Additional rock bolts were installed at a later stage to limit the unexpectedly large deformations. The position of these bolts at Stations A and B are indicated in Figs 5.3 and 5.4, respectively, by the dashed lines.

The final support consisted of a 450 mm thick cast in place reinforced concrete liner that was installed over 300 days after excavation, and does not enter into this analysis.

5.2.2 Instrumentation

The section of the north tunnel that was excavated using the NATM contained three main and 13 supplementary measuring stations. The two stations that are analyzed in this chapter are main measuring Stations A and B, indicated on the plan view in Figure 5.1. As in most Japanese tunneling projects, these monitoring sections were heavily instrumented with a network of convergence anchors and load cells to measure both earth and lining pressure. For the purpose of this thesis, only the convergence of the tunnel walls was analyzed. The convergence was obtained by measuring the change in distance between the various anchor

points placed around the circumference of the tunnel wall. The configuration of the various convergence measurements for Stations A and B is shown in Fig. 5.5.

The convergence measurements that are considered in this analysis are plotted against time in Figures 5.6 and 5.7, respectively. These figures show that the excavation history of the three stages is extremely variable, due to many changes in rate of advance, and work stoppages. The irregular nature of the convergence curves in Figs 5.6 and 5.7 reflects this variability in excavation history. The time at which additional rock bolts were installed is also indicated in both Figs 5.6 and 5.7.

5.3 Application of Convergence Solution to Sequentially Staged Excavations

The Convergence Solution has been developed on the basis of full face excavations. The extension of this solution to model sequentially staged excavations requires some simplifying assumptions, as outlined below.

It was demonstrated in Chapter 4 that the Convergence Solution could be applied to the measurements from tunnel widening by treating it as a full face excavation of the same size. The shape of the convergence curves produced by these two cases is the same, but they differ in magnitude of convergence. Since the convergence measurements are normalized to make them independent of magnitude, these two cases may be treated identically. On this basis, it is

proposed that the Enasan Tunnel be modelled as three separate excavations of sucessively larger diameter, and the results superimposed. This superposition is illustrated schematically in Figure 5.8, where the convergence curves produced by each separate excavation are shown together with the curve produced by their sum. In the case shown in Fig. 5.8, the stress redistribution associated with the excavation has caused yielding of the rock surrounding the tunnel. If the strength of the rock (c and ϕ) is assumed constant, the ratio R/a would also be constant. Hence, the yielding illustrated at the bottom of Fig. 5.8 corresponds to a constant R/a ratio of 2.0. Thus, as the tunnel radius increases with each excavation stage, the plastic zone propagates to maintain a constant R/a ratio.

In Chapter 4 it was demonstrated that normalizing convergence rates to the maximum rate at the face achieved independence from the magnitude of convergence. For a sequentially staged excavation however, each stage has its own peak convergence rate, and ultimate value of convergence. It is most convenient for practical purposes to normalize the entire convergence rate curve to the maximum rate produced by the heading excavation. Consequently, the bench and invert excavations will not be normalized to their own maximum rate, and will therefore not decrease from an initial value of 1.0 at their face locations. However, when each excavation stage is modelled separately by the Convergence Solution, three rate curves are produced that

each decrease from an initial value of 1.0 at their respective faces. It is therefore necessary to multiply the convergence rate curves produced by the bench and invert excavations by the ratios:

$$\frac{\dot{C}_{max}(\text{bench})}{\dot{C}_{max}(\text{heading})}; \text{ and } \frac{\dot{C}_{max}(\text{invert})}{\dot{C}_{max}(\text{heading})}$$

respectively. Since the maximum convergence rate is proportional to the ultimate time-independent convergence ($C_{x\infty}$), the above ratios can be expressed as:

$$Q_b = \frac{C_{x\infty}(\text{bench})}{C_{x\infty}(\text{heading})}; \text{ and } Q_i = \frac{C_{x\infty}(\text{invert})}{C_{x\infty}(\text{heading})}$$

respectively.

These ratios have been determined by simulating the excavation with a two dimensional Boundary Integral Equation Method (BIEM) program (Hoek and Brown, 1980, modified by Simmons, 1983). The material behavior has been modelled as linear elastic even though observations indicate extensive yielding completely surrounding the excavation. This simplification is justified because both the elastic, and yielded case would produce similar final deformed shapes of the tunnel walls. Since the ratios Q_b and Q_i reflect the deformed shapes, rather than the magnitude of convergence the elastic analysis would produce comparable results to a more elaborate elasto-plastic analysis.

The BIEM program was used to determine the ultimate time independent convergence of the tunnel walls in response to the following three cases:

1) Heading excavation.
2) Combined heading and bench excavation.
3) All three excavation stages combined (full face excavation).

The convergence caused by the bench excavation was determined by subtracting case one from case two; and the convergence caused by the invert excavation was determined by subtracting case two from case three.

The distribtion of convergence along the cross section of the tunnel given by the BIEM program for the above three cases are shown in Fig. 5.9. The position of the various convergence measurements is also shown in this figure. The ultimate values of convergence ($C_{x\infty}$) given by the BIEM program caused by each of the excavation stages includes the convergence that occurs both before and after each face. However, it is only the portion of $C_{x\infty}$ that occurs after the face that is proportional to $\dot{C}_{max}$. It has been assumed for this analysis that half of $C_{x\infty}$ occurs before the face and half after the face ($Q_1 = Q_2 = 0.5$) because of the significant amount of yielding that was observed. Thus, the values of $C_{x\infty}$ given by the BIEM for each excavation stage must be multiplied by 0.50.

The following ratios have been calculated on the basis of these results:

Measuring Position	$Q_b = \frac{C_{x\infty}(\text{bench})}{C_{x\infty}(\text{heading})}$	$Q_i = \frac{C_{x\infty}(\text{invert})}{C_{x\infty}(\text{heading})}$
H1	0.629	0.050
H2	1.187	0.085
Roof	0.074	0.061
D1	0.500	0.047
D2	0.500	0.047

These ratios represent the amount of convergence produced by the bench and invert excavations, respectively, relative to the convergence produced by the heading excavation. These ratios are different for each measuring position because the measurements are taken at varying orientations. Each point around the circumference will respond in a different manner to the various excavation stages. For example, Postion H2, shown in Figure 5.5, is much more sensitive to the excavation of the bench than the roof measurement is, due to their relative locations with respect to the bench. This difference is reflected in the higher value of Q_b for Position H2.

In summary, the Convergence Solution has been adapted and simplified to model the sequentially staged excavations of the Enasan Tunnel by modelling the three excavation stages separately and superimposing the results. The normalized convergence rate curves produced by all three

excavations will be normalized to the maximum convergence rate produced by the heading excavation. The convergence rate curves produced by the bench and invert excavations are then multiplied by the ratios Q_b and Q_i, respectively. It was demonstrated earlier that an independence from the magnitude of convergence is attained when the data is analyzed in the normalized convergence rate format. Since the ratios Q_b and Q_i express only the *relative* magnitude of convergence associated with each excavation stage, the method remains independent of the absolute magnitude of convergence.

These modifications enable the Convergence Solution to be fitted to the data measured in the Enasan Tunnel, as will be shown in the following section.

5.4 Fit of Convergence Solution to Measurements

The application of the Convergence Solution to the Enasan Tunnel data differs from the previous application of the Solution to the experimental data in Chapter 4, because the Enasan Tunnel is supported. As mentioned earlier, the final concrete liner does not enter into this analysis, but both the temporary support system, and the additional rock bolts that were installed at a later stage are supporting elements that need to be considered. Since the temporary support system was installed immediately upon the excavation of each stage, and was intended to reinforce rather than apply pressure on the rock mass, it will not be considered

as a true support. Instead, the Convergence Solution will model the Enasan Tunnel as an unsupported, reinforced rock mass. Thus, the parameters will not be characteristic of the rock mass itself, but of the rock mass reinforced by the temporary support system. However, the additional rock bolts that were installed at various intervals after excavation to arrest further convergence, must be considered separately as a support. Since the supporting effect of these additional bolts is difficult to quantify, they will be neglected initially as the Convergence Solution will model an unsupported reinforced rock mass. After this first step, the influence of the additional rock bolts will be assessed separately.

The procedure that has been adopted for fitting the Convergence Solution to the field measurements (from the "reinforced" rock mass) is similar to the procedure followed in Chapter 4. There, each parameter was varied separately to obtain a unique set of parameters that characterized the behavior of the rock mass. It was possible to obtain independent estimates of the parameters because each parameter affected the curve in a different manner. The parameter X controlled the initial (time-independent) portion of the curve, while T and A^* controlled the of the latter (time-dependent) portion of the curve. Even though A^* and T had an overlapping influence on the latter portion of the curve, they could still be determined independently. Both T and A^* affected the vertical translation of the

curve, but only T controlled the shape. Consequently, T was chosen to match the shape of the curve, ignoring the effect it had on vertical translation, and A^* was chosen to match the vertical translation of the data, given the choice of T. At the Enasan Tunnel, however, the extremely slow excavation progress caused an overlap of the time-independent and time-dependent behavior which renders parameter evaluation more ambiguous. Nevertheless, a fitting procedure similar to the one described in Chapter 4 was adopted, even though it is not possible to obtain completely independent estimates of the parameters for each set of measurements.

The data from each of the measuring positions has been smoothed with the technique discussed in Chapter 4. This eliminates the zero convergence rates observed in the latter portion of these curves.

The step by step fitting procedure that was followed is outlined below for the measurements from Position H2, at Station A (see Fig. 5.5).

5.4.1 Example Fit

The first step is to determine the set of three parameters that fits the data that corresponds to the heading excavation (between 0 and 45 days). It is necessary to limit the scope of this first step to the initial (heading) excavation because of the complexity of the multistage excavation.

First, the value of X is investigated by plotting the Convergence Solution for a range in X values, and initial estimates of T and A^*. Figure 5.10 shows the convergence rate data measured at Position H2 compared to the curves produced by a range of X (=0.84 R/a) from R/a=1.0 to R/a=3.0, and an initial estimate of A^*=1.0 and T=1.0 days. These convergence rate curves have been produced by the program computer CONRATE, described in Appendix C. The portion of the curve that is influenced by the advance (and hence R/a) is labelled Zone I. Zone II corresponds to an excavation stoppage and therefore does not display any time-independent behavior. From Fig. 5.10 it appears that R/a=2.5 gives a reasonable fit of the data in Zone I.

The effect of the parameter T on the Convergence Solution is illustrated in Figure 5.11, where a range of T between 0.1 and 10.0 days is combined with R/a=2.5 and the estimate of A^*=1.0. As was noted earlier, T is determined by the *shape* of the time-dependent portion of the convergence rate curve. Unfortunately, the extremely variable excavation history at the Enasan Tunnel has not produced a long enough continuous section that is exclusively controlled by time-dependent material behavior (free from the influence of the face advance). Thus, T must be determined from short excavation stoppages such as Zone II in Fig. 5.11. This figure shows that a range in T of two orders magnitude does not even affect the shape of the curve in Zone II significantly. A comparison of the influence of this range

in T in Figure 5.11, and the influence of A^*, shown in Figure 5.12, reveals that these two parameters have a virtually identical effect on the convergence rate curve. Thus, a range in A^* and T pairs, as opposed to two independent values can be fit to the data. Rather than expressing a range of A^*-T pairs, the value T=1.0 days will be chosen as a representative though not unique quantity. From Figure 5.12, it can be seen that a value of A^*=1.0 gives the best fit of the cases shown to the data in Zone II, based on a T=1.0 days. While this A^*-T pair is not unique, both parameters are within the range of values determined in other applications of this method, such as that found in Chapter 4, and the analysis of the Fréjus Tunnel (Sulem, 1983).

The final fit of the heading excavation that is achieved with the parameters R/a=2.5, T=1.0 days and A^*=1.0, determined in this fashion, is shown in Fig. 5.13 together with the data from Station A, Postion H2. It can be seen in this figure that the Convergence Solution provides a very close fit of the convergence rate curve up to the time when the bench reaches the measuring section. The value of R/a is unique, as it has been determined independently of A^* and T. However, the values of A^* and T are not independent, but they provide a good representation of the response of the reinforced rock mass.

The next step is to examine the portion of the convergence rate curve influenced by the bench and invert

excavations. Figure 5.13 shows that the solution deviates from the bench excavation on (t>45 days). The convergence rate is generally underpredicted and the slope of the rate plot is steeper than the data from 45 to 90 days. This deviation is likely caused by a more than proportional propagation in the yield zone. The almost constant rate between the bench and invert excavation is indicative of yielding behavior. Without additional yielding, the rate would have to drop more rapidly during excavation advance.

In Summary, the fitting exercise to this point has characterized the response of the rock mass to the heading excavation, and has indicated the existence of a yield zone with a radius (R) of about 2.5a. In addition, the propagation of this initial yield zone has been identi[illegible] to a larger yield zone of unknown extent (R/a>2.5a) w[illegible] bench excavation passes the measuring section.

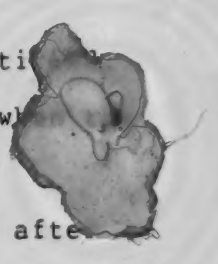

In order to estimate the size of the yield zone afte[illegible] this propagation, some additional simplifying assumptions have been made that enable the Convergence Solution to simulate this propagation behavior. These assumptions are outlined in detail in Appendix H. Both the initial fit, determined above, and the fit with propagation modelled, are compared to the data in Fig. 5.14. An adequate fit of the entire range of data is furnished by the Convergence Solution when a propagation in the yield zone from R/a=2.5 to R/a=4.5 at t=40 days is modelled, as shown in Fig. 5.14. The effect of yield zone propagation shifts the curve up

vertically and produces a much flatter slope from 45 to 90 days.

The final step in the fitting process is to consider the effect of the additional bolts that were added at the times indicated in Fig. 5.5 for Station A. This will be approached by first modelling the excavation, combined with a range of support cases, with the Convergence Solution. The influence that these support cases have on the convergence rate curve will then be compared to the data to see if the additional rock bolts provided any support.

The excavation history of the Enasan Tunnel has been idealized to a constant excavation velocity of 1.0m/day, in order to eliminate the obscurity that is caused by the extremely variable excavation rates. The separation between the three advancing faces was assumed to remain constant at 20 m each, and all three excavations now proceed simultaneously. The selected rate of advance is close to the actual average rate of excavation, if longer stoppages are eliminated.

The parameters that have been used as input into the Convergence Solution for this analysis are tabulated below. These include the parameters determined above, that characterize the response of the reinforced rock mass to the excavation, as well as additional parameters required to model the various support cases.

Table 5.1. Input Parameters for Convergence Solution; Support Analysis.

Parameters for tunnel in reinforced rock mass:

R/a=2.5; T=1.0 days; A^*=1.0;

Q_b=1.187; Q_i=0.085

$C_{x\infty}$(heading)=555 mm (estimate from Fig. 5.5, based on A^*=1.0, and t=190 days)

Liner Parameters for Parametric Study:

Concrete Thickness:	50 mm	200 mm	500 mm
K	0.0019/mm	0.0078/mm	0.0200/mm
Qk(heading)+	0.01	0.04	0.10
Qk(bench)+	0.04	0.10	0.18
Qk(invert)+	0.08	0.18	0.24

+ Extrapolated from Figure 3.18.

Additional rock bolts were installed at Station A according to the schedule tabulated below. Also shown is the corresponding schedule for the idealized excavation.

Time (days)	# Bolts	Length (m)	Idealized Time (days)	# Bolts
51	4	9.0	26	4
82	8	9.0	54	19
98	11	9.0		

The bolts installed at 82 and 98 days correspond to 54 days in the idealized (constant rate) excavation, because both installations occured in one long excavation stoppage.

The major episode of additional bolting (at t=54 days) has been modelled as an equivalent concrete liner with the Convergence Solution. The impact that concrete liners, varying in thickness from 50 to 500 mm, have on the convergence rate curve of the idealized excavation is shown in Figure 5.15. This figure shows that a support reduces the convergence rate curve. Figure 5.15 also indicates that if a support is to have a noticable impact on the convergence rate curve, it must provide the equivalent support of between 50 to 200 mm concrete liner.

The points at which additional bolts were installed at Station A are indicated on the measured convergence rate curve in Fig. 5.14. No clear deviation from the "unsupported" Convergence Solution curve can be detected at any of the support installation points. It is possible that some deviation in the convergence rate curve may have been caused by these support measures but it is obscured by the noise in the data (caused by the stop-go excavation history), but there is no evidence that the extra rock bolts had any impact on the convergence of the tunnel walls. This finding is consistent with the estimate of a large yield zone (approximately 4.0 a, or 24 m) because 9 m rock bolts installed inside an already yielded zone of this size would not be expected to provide a significant amount of

reinforcement, or support.

Since the additional rock bolts do not have a noticeable impact on the convergence rate curve, they may be neglected in the fitting process. Thus, the final fit of the Convergence Solution to this example case is shown in Figure 5.14 where the tunnel was modelled as an unsupported tunnel in a reinforced rock mass.

This fitting procedure has also been used for the data from the remaining measuring positions at Stations A and B, presented below.

5.4.2 Presentation of Curve Fitting Results

The Convergence Solution curves that have been fitted in this manner to the remaining measuring positions at Station A are presented in Figures 5.16 to 5.19. Again, the computer program CONRATE (Appendix C) has been used to generate all of the Convergence Solution curves. As demonstrated by these figures, all of the measuring positions at Station A displayed the yield zone propagation behavior that was shown by Position H2 in the example fit (Fig. 5.15). A summary of the parameters that were determined for each of the measuring positions in Station A is given below:

Measuring Position	T (days)	A*	R/a (t=0-40 days)	R/a (t=40-200 days)
H1	1.0	0.5	2.0	4.0
H2	1.0	1.0	2.5	4.5
Roof+	1.0	0.4	1.5	4.0
D1	1.0	0.6	1.0	2.5
D2	1.0	0.4	2.0	3.5
Average	1.0	0.6	1.8	3.7

+ Roof displacement was measured, rather than convergence, but it is treated in the same manner as the convergence measurements, because it becomes independent of magnitude when normalized.

On average the plastic zone must have propagated from 1.8 to 3.7a during bench excavation at Station A.

The fitting procedure that was followed for Station A was also followed Station B. A comparison of the fit of the Convergence Solution and the data from the Position H1, Station B is shown in Figures 5.20. The initial portion of the data for position H1 is portrayed on an expanded time scale in Fig. 5.21 to give a better representation of the rapidily fluctuating behavior in this region. As for Station A, the Convergence Solution provides a very close fit of the measurements up to a certain point (t=51 days), especially considering the extremely variable excavation history. From this point on, the Solution again under

predicts the results. When the yield zone is modelled as propagating from 1.6 to 4.0a, shown by the dashed line in Figs 5.20 and 5.21, a remarkable fit is achieved.

The additional rock bolts that were installed at Station B are indicated in Figure 5.20. The main episode of extra bolting occured from 130 to 155 days, when 19 9.0m, and 15 13.5m bolts were installed. This additional bolting did not have a ~~noticeable~~ impact on the convergence rate curve in Fig. 5.20 that can be observed beyond the noise of the data. Thus, it is also valid to model the tunnel at Station B as an unsupported tunnel in a reinforced rock mass.

The data from the remaining measuring positions at Station B are fit to the Convergence Solution in Figs 5.22 to 5.25. These figures demonstrate that the same propagation behavior is observed at all locations. A summary of the parameters that were obtained from Station B are tabulated below:

Measuring Position	T (days)	A*	R/a (t=0-51 days)	R/a (t=51-200 days)
H1	1.0	1.0	1.6	4.0
H2	1.0	1.0	2.0	4.0
Roof+	1.0	1.4	1.9	5.0
D1	1.0	1.0	1.4	3.0
D2	1.0	1.4	1.8	4.5
Average	1.0	1.2	1.8	4.1

+ Displacement rather than convergence.

On average the predicted yield zone propagated from 1.8 to 4.1a at Station B during the bench excavation.

Remarkably consistent sets of parameters have been found to characterize the response of the rock mass to the tunnel excavation at both stations. A^* ranged from 0.4 to 1.4, for T=1.0 days, and R/a ranged from 1.0 to 2.5 (average = 1.8) before propagation, and 2.5 to 5.0 (average = 3.9) after propagation. While extensometer measurements were not available at either station there are several indirect indicators that suggest the presence of a very large yield zone. First, if the rock was elastic, the predicted radial displacement would be about 190 mm, for the conditions at the the Enasan Tunnel. Since the rock mass displays creep, and an avèrage A^* of 0.9 was found for the two stations analyzed, the ultimate radial displacement would be expected as:

$$u_{ult} = 190mm + 0.9(190mm) = 361mm.$$

The measured roof displacement at 195 days was 710 mm at Station A and 920 mm at Station B. The measured roof displacements exceed the elastic prediction by at least 100 percent, which suggests that significant plastic deformation occurred that could only be produced by a large yield zone. Secondly, the convergence rate at both stations is sensitive to activities at the tunnel face at locations well removed from the tunnel face. For example, at Station A there is a jump in rate measured at Postion H2 (Fig. 5.15) in response to the advance of the heading 58 m (5 tunnel diameters) away. In elastic rock, the advance of the face should not cause a significant rate increase for more than two diameters past the face. Thus, this observation also suggests the existence of a large zone of yielded rock. In addition to these two points, the decisions made by the engineers on the project reflect a concern for excessive yielding. They increased the length of the rock bolts from the original 6.0 and 9.0m lengths, to 13.5m (at Station B) when the convergence exceeded their expectations. They also installed spiling (ahead of the advancing face), which is usually only adopted to stabilize the face in heavily yielded ground.

5.5 Summary and Conclusions

The application of the Convergence Solution to the measured convergence from the Enasan Tunnel has revealed several important findings. First, the radius of the zone of yielded material surrounding the tunnel was predicted to range initially from 1.0 to 2.5 a. Once the bench and invert were excavated, it is suggested that the yield zone propagated to from 2.5 to 5.0 a. The existence of a very large yield zone is supported by the enormous magnitude of ultimate convergence that was measured, which exceeds the elastic predictions by 100 percent. Also, the influence that the excavation has on the convergence curve is felt as far as five or more tunnel diameters behind the face. This far exceeds the commonly assumed limit of two diameters for elastic rock.

The effectiveness of remedial supporting measures in inhibiting convergence was also investigated using the Convergence Solution. This revealed that the extra support that was introduced to control displacements had little impact on the convergence curve. Furthermore, a support pressure equivalent to the pressure generated by a concrete liner of 50 to 200 mm thickness would have been required to cause a noticeable reduction in the convergence rate.

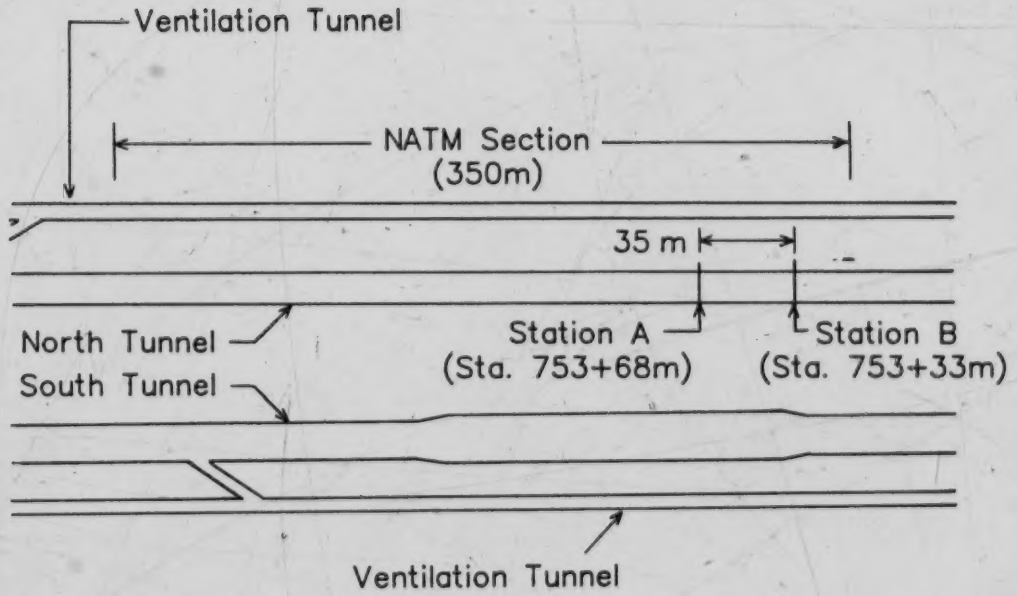

Figure 5.1 Plan View of East Section of Enasan Tunnel Project.

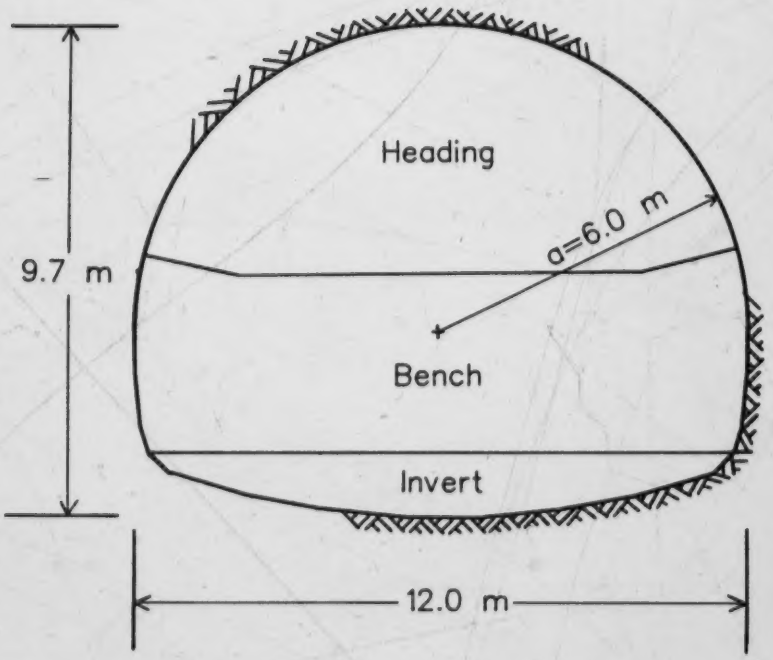

Figure 5.2 Cross Section of Enasan Tunnel.

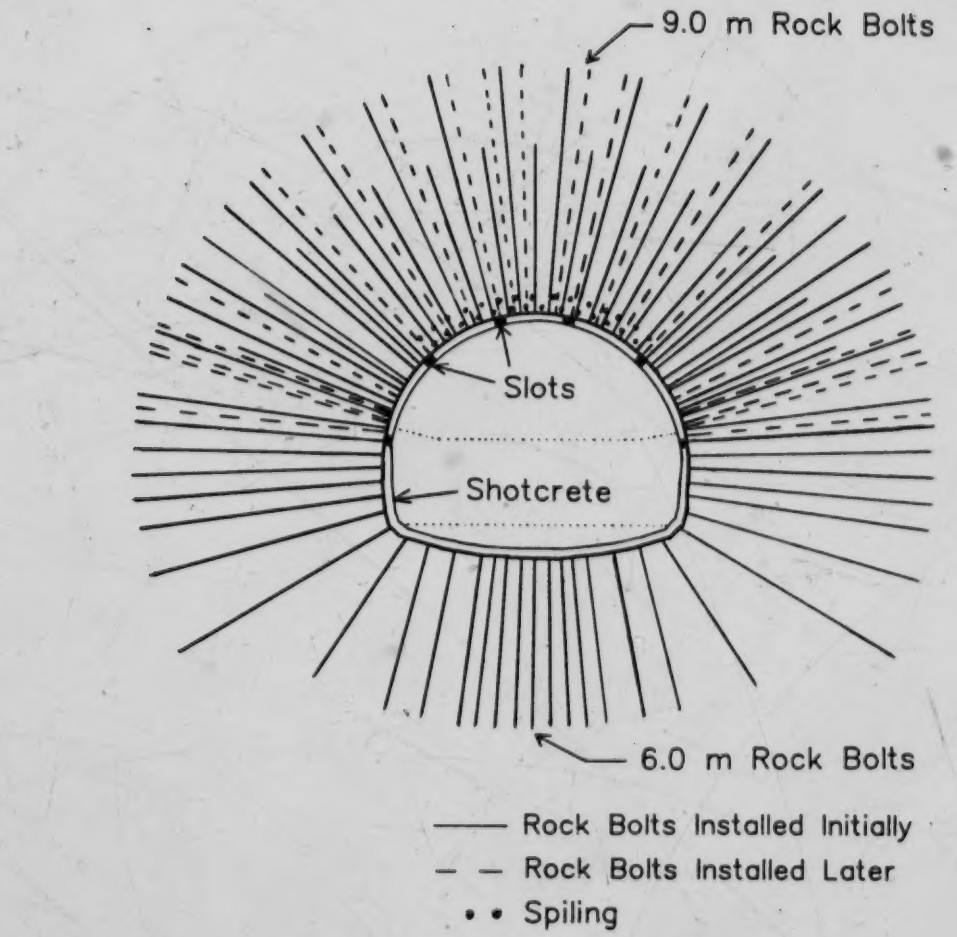

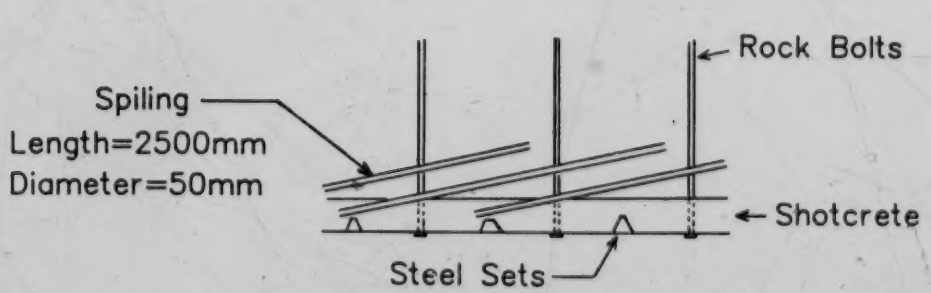

Longitudinal Section at Roof

Figure 5.3 Temporary Support System for Enasan Tunnel, Station A (Modified from Ito, 1983).

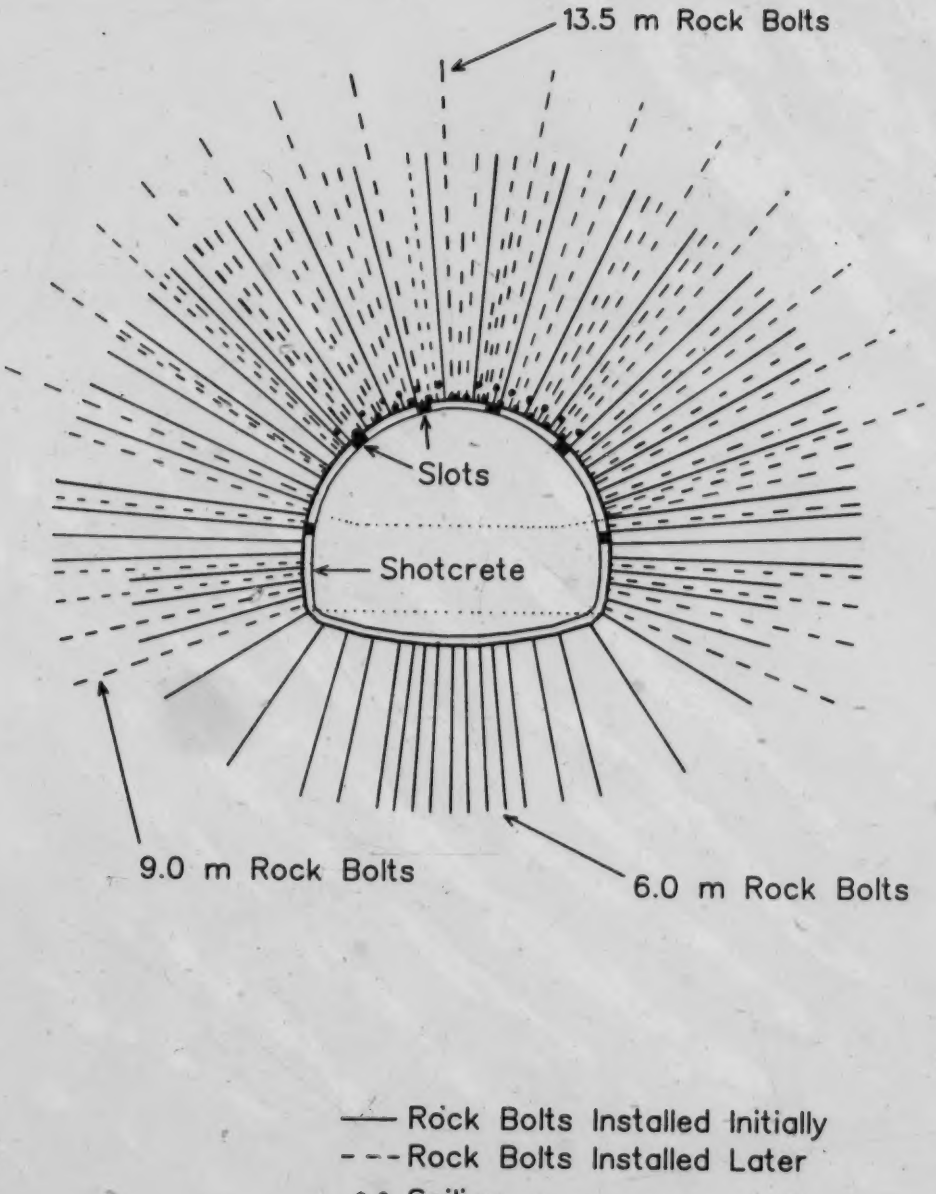

Figure 5.4 Temporary Support System for Enasan Tunnel, Station B (Modified from Ito, 1983).

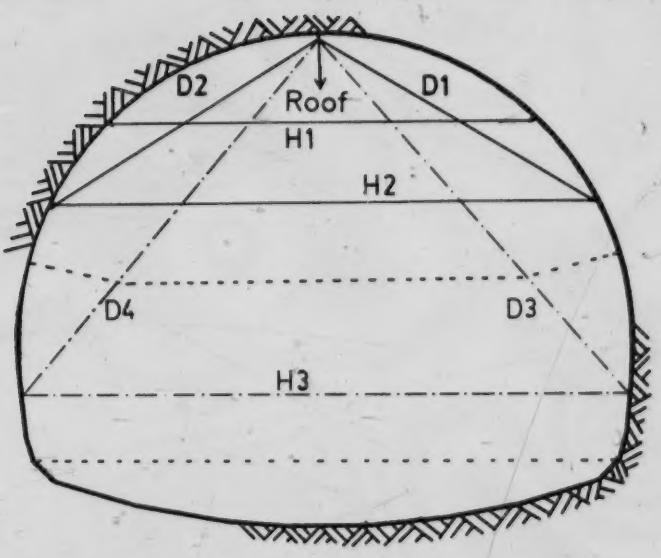

—— Measurements shown in Figs 5.6 and 5.7

—·— Measurements not shown in Fig 5.6 or 5.7

Figure 5.5 Position of Convergence Measurements at Enasan Tunnel.

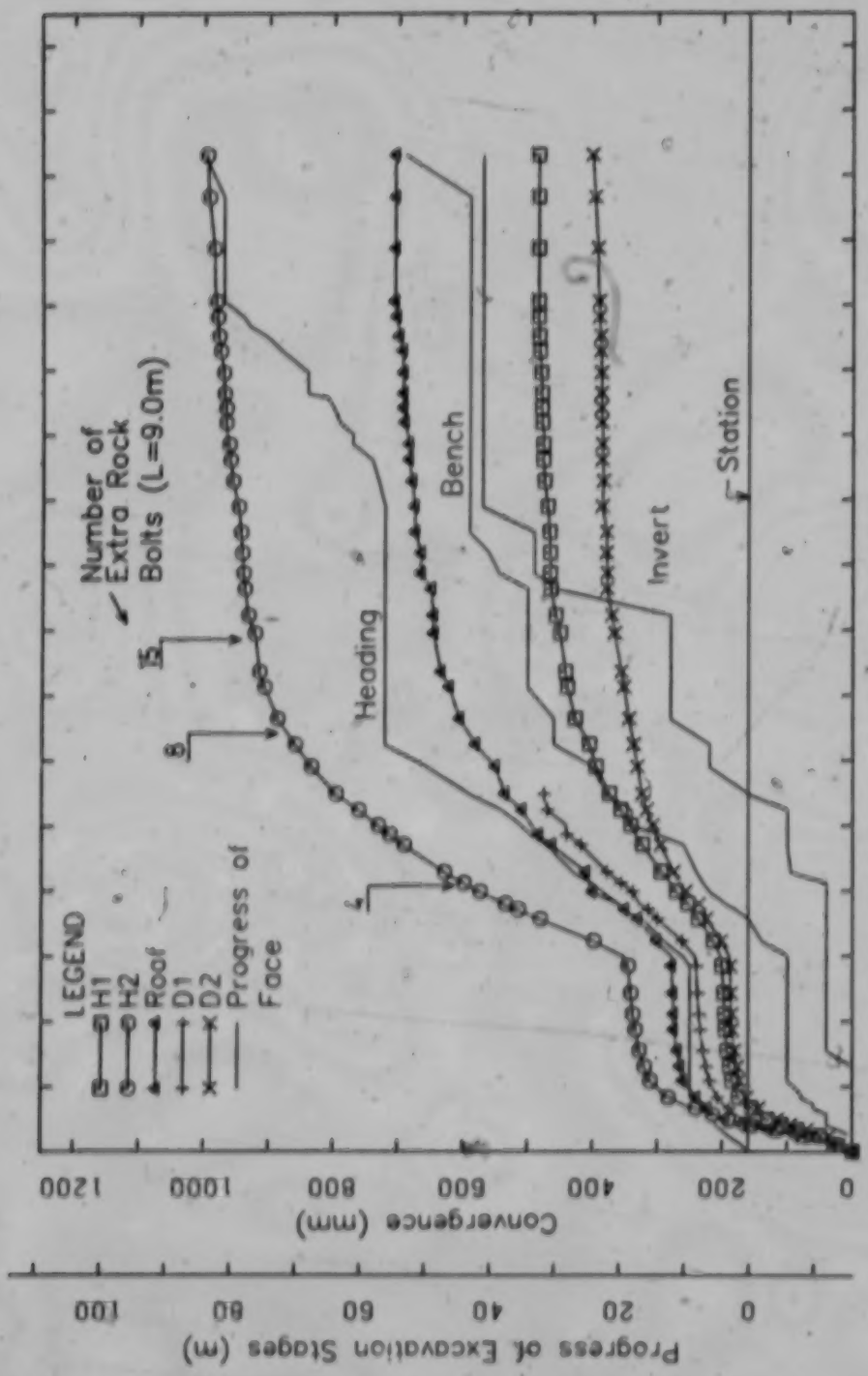

Figure 5.6 Convergence and Face Progress, Station A, Enasan Tunnel (after Kaiser, 1984).

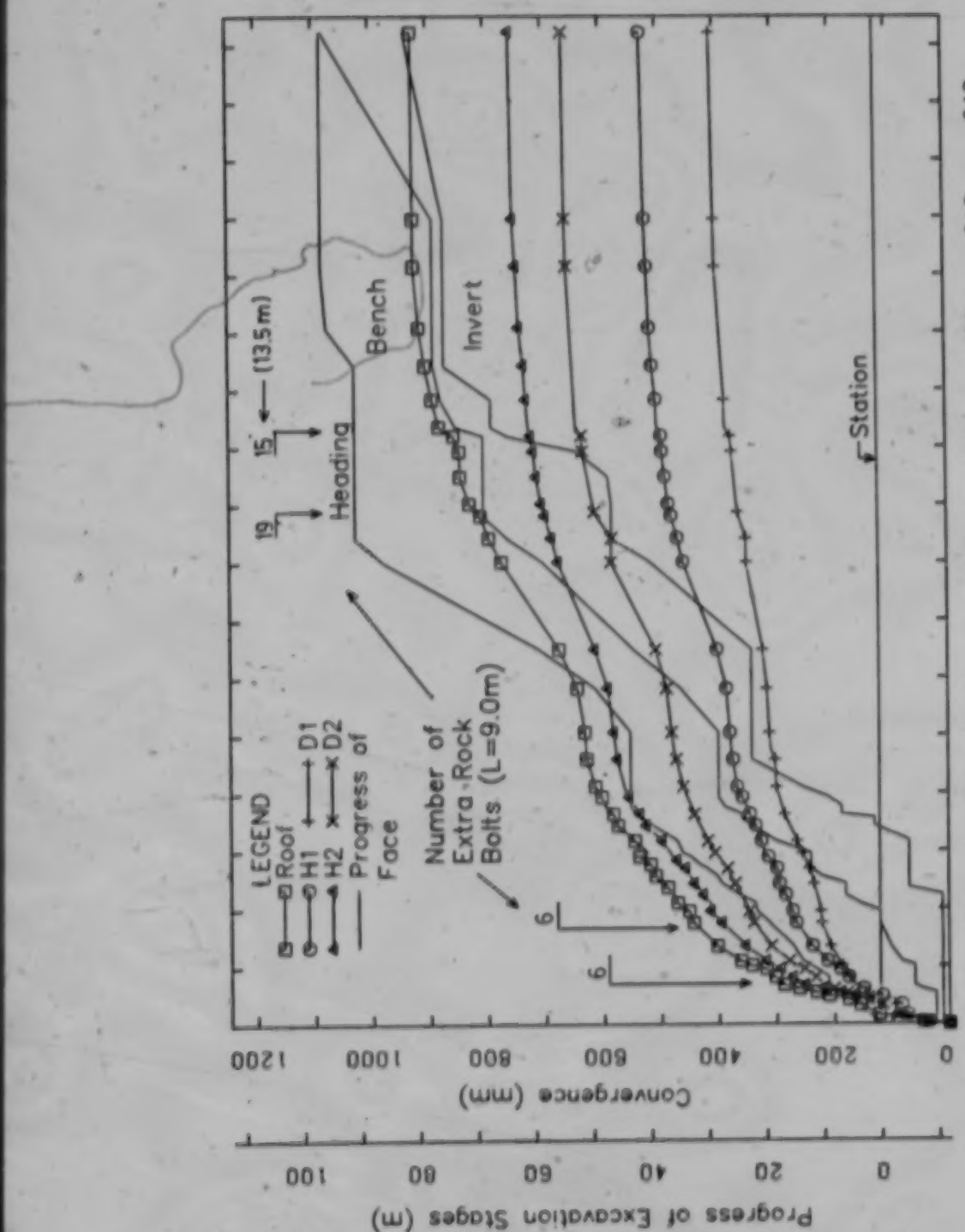

Figure 5.7 Convergence and Face Progress, Station B, Enasan Tunnel (Modified from Ito, 1983).

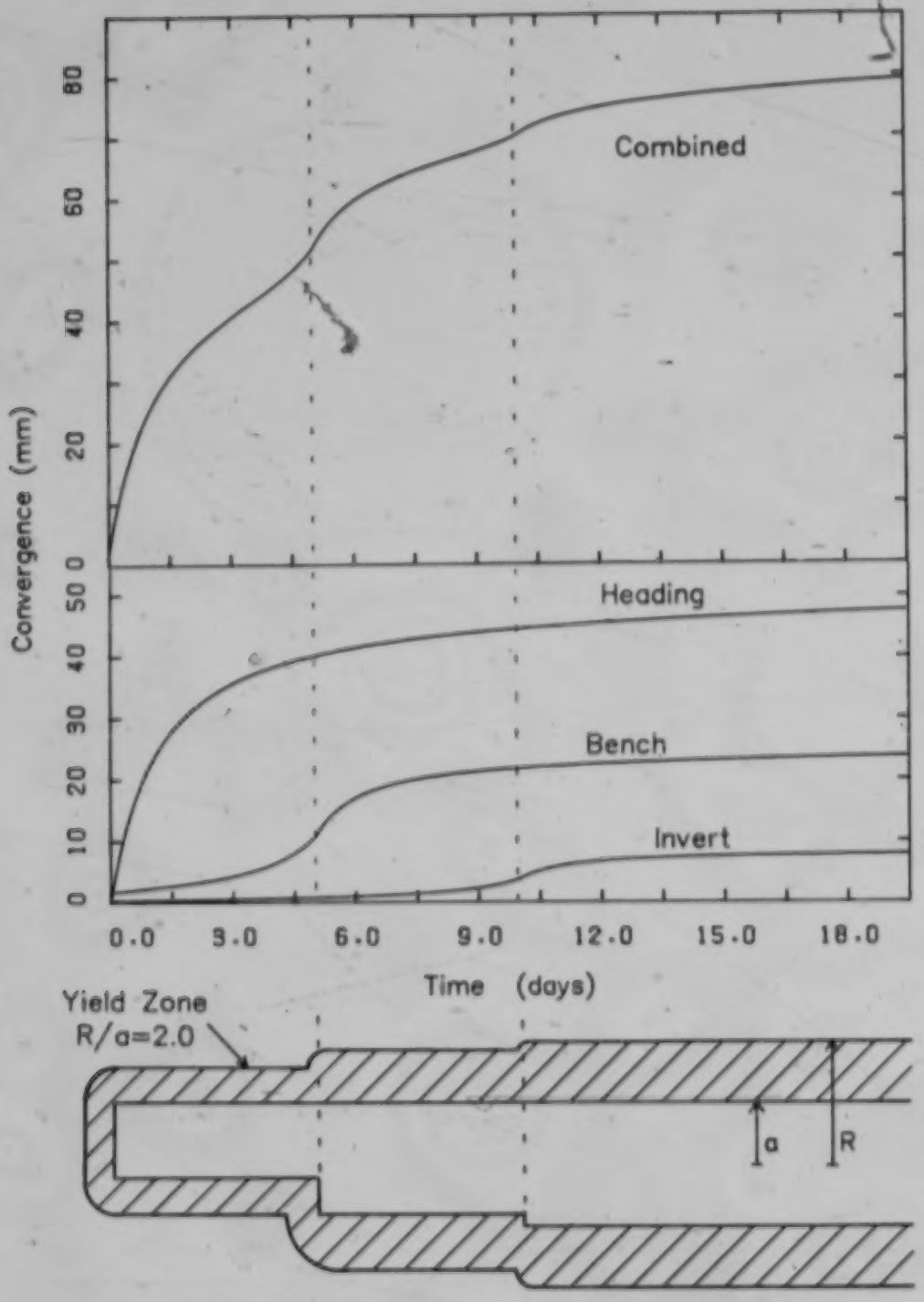

Figure 5.8 Superposition of Convergence Curves from Excavation Stages.

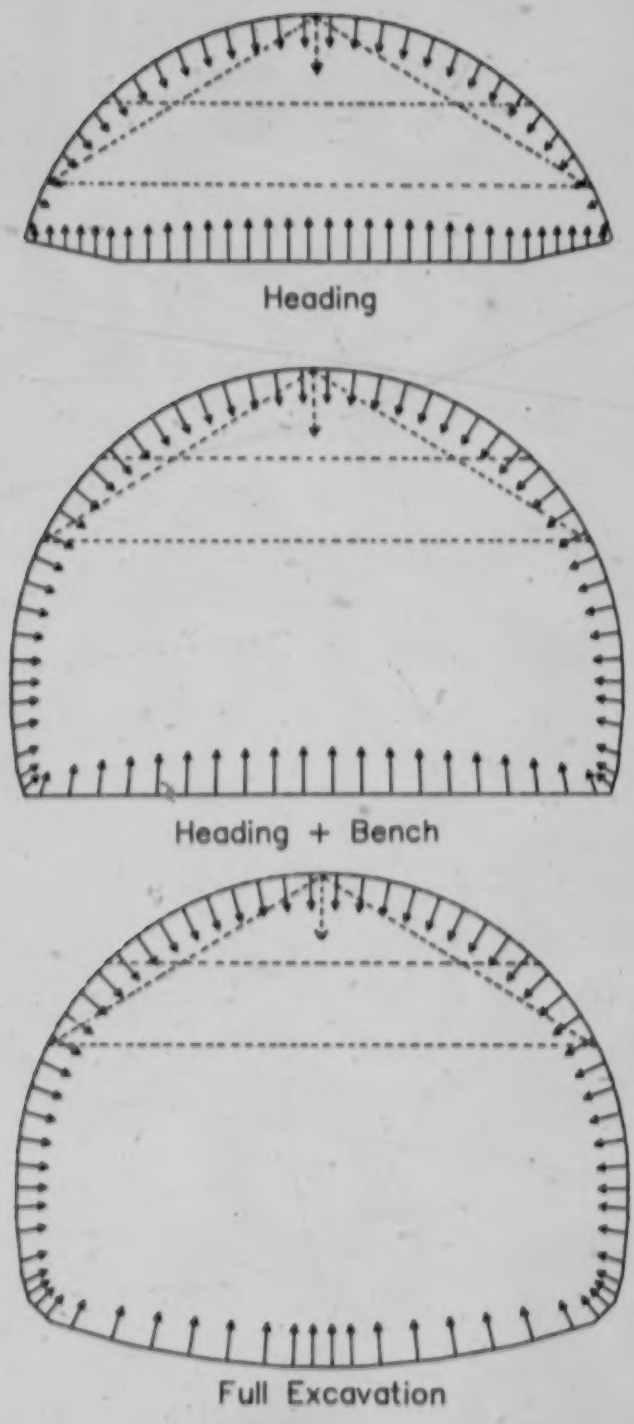

Figure 5.9 Convergence from BIEM program for 3 Excavation Stages.

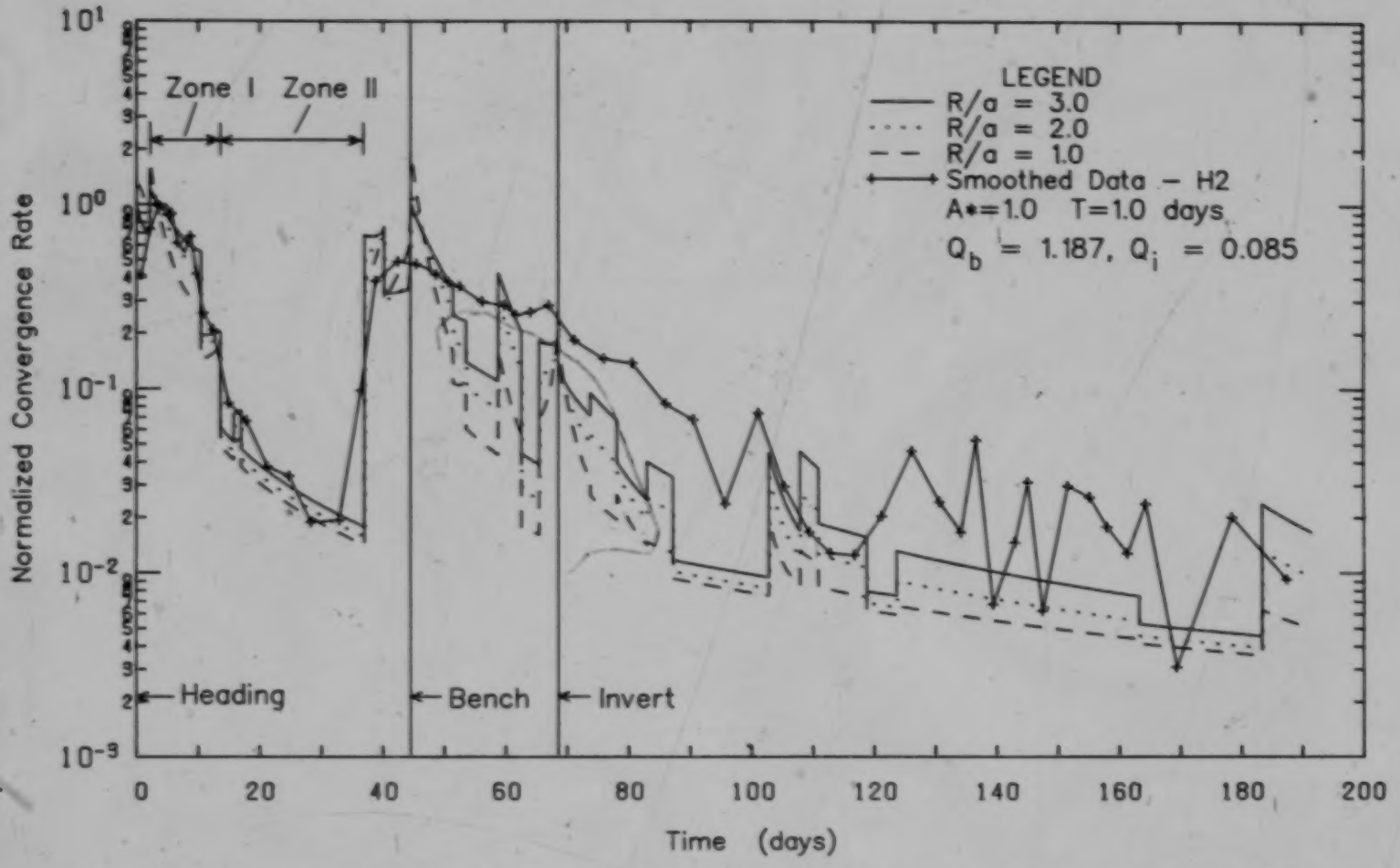

Figure 5.10 Convergence Solution with R/a Varied, Compared to Data from Station A-H2.

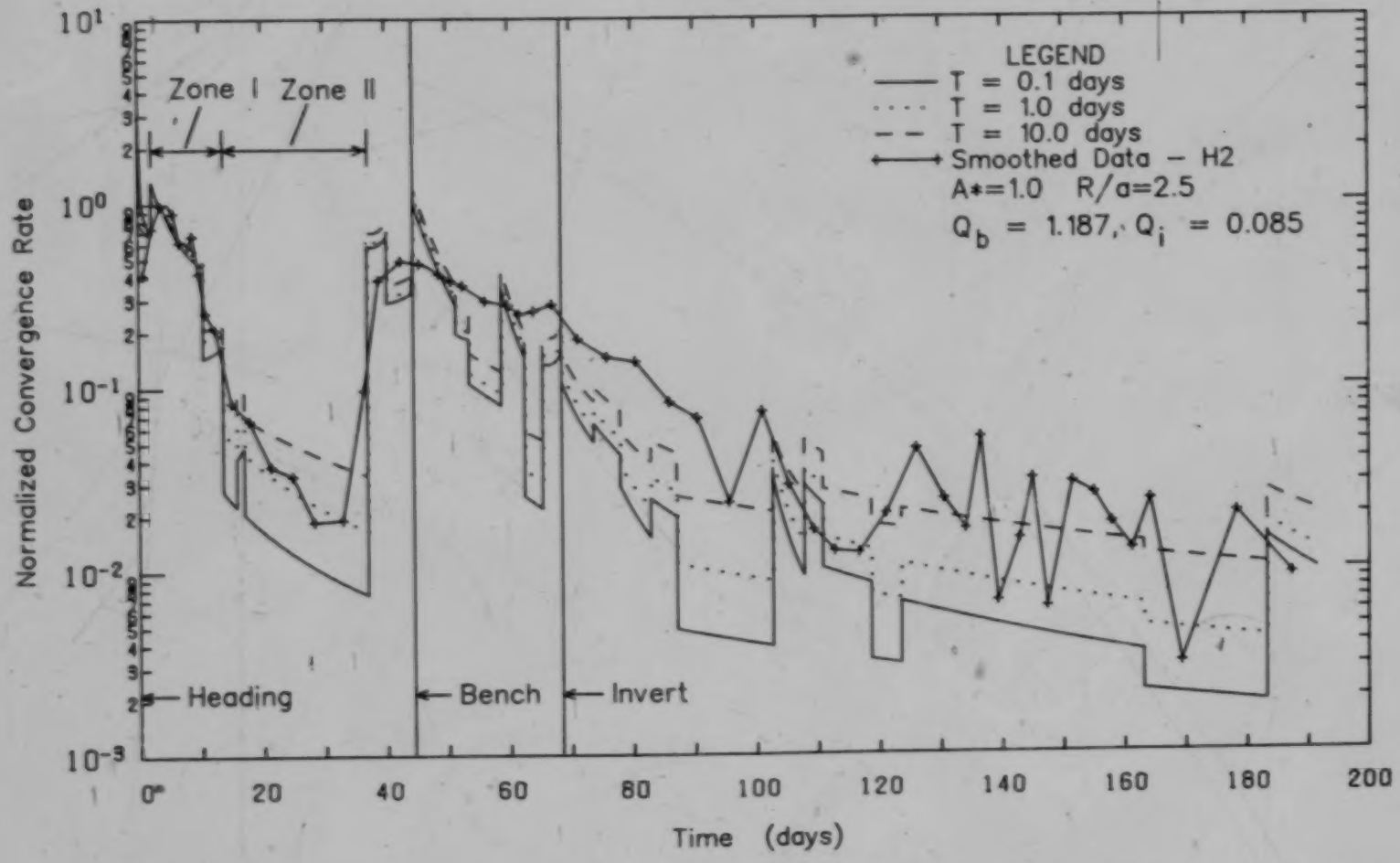

Figure 5.11 Convergence Solution with T Varied, Compared to Data from Station A-H2.

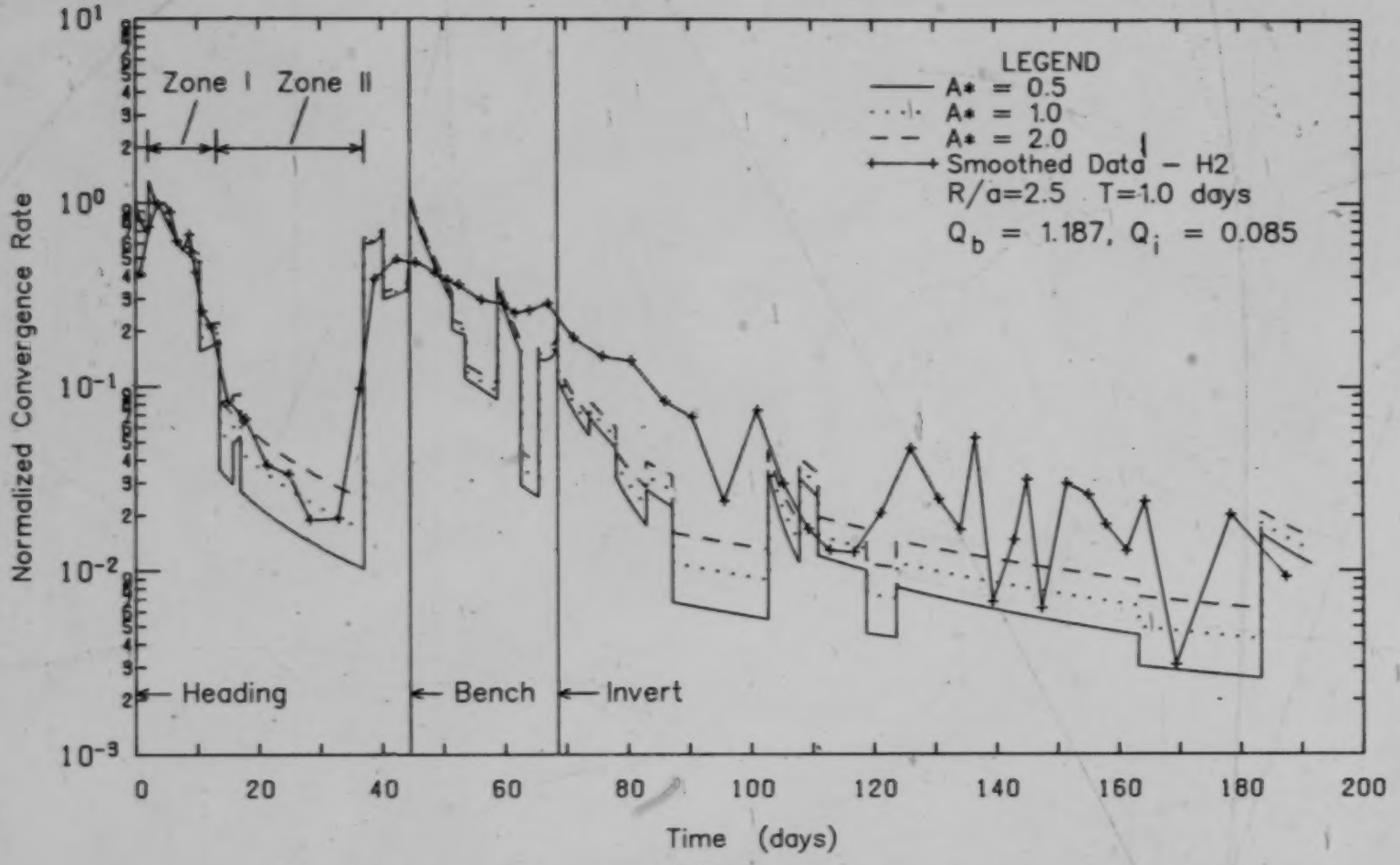

Figure 5.12 Convergence Solution with A^* Varied, Compared to Data from Station A-H2.

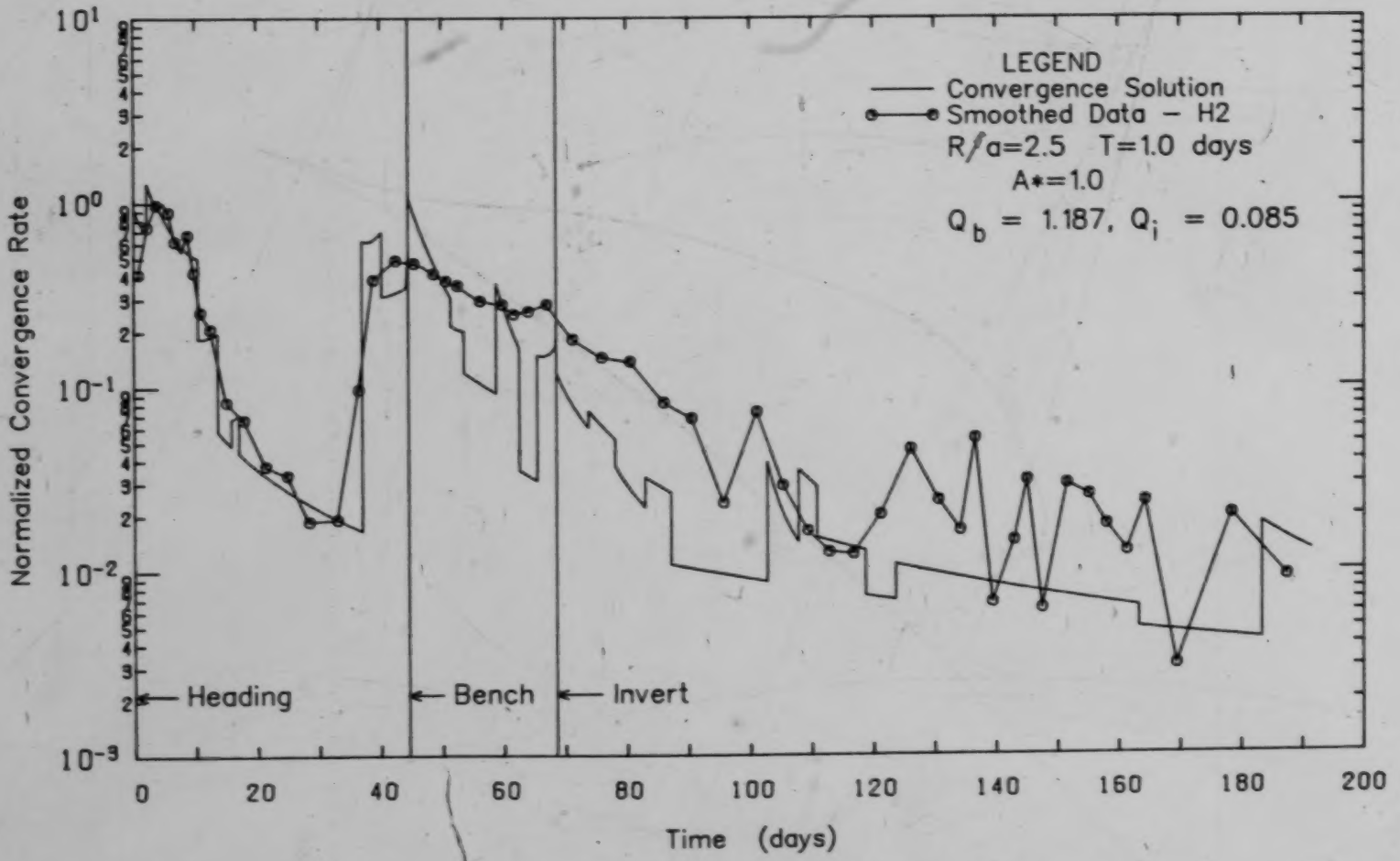

Figure 5.13 Fit of Convergence Solution to Data from Station A-H2.

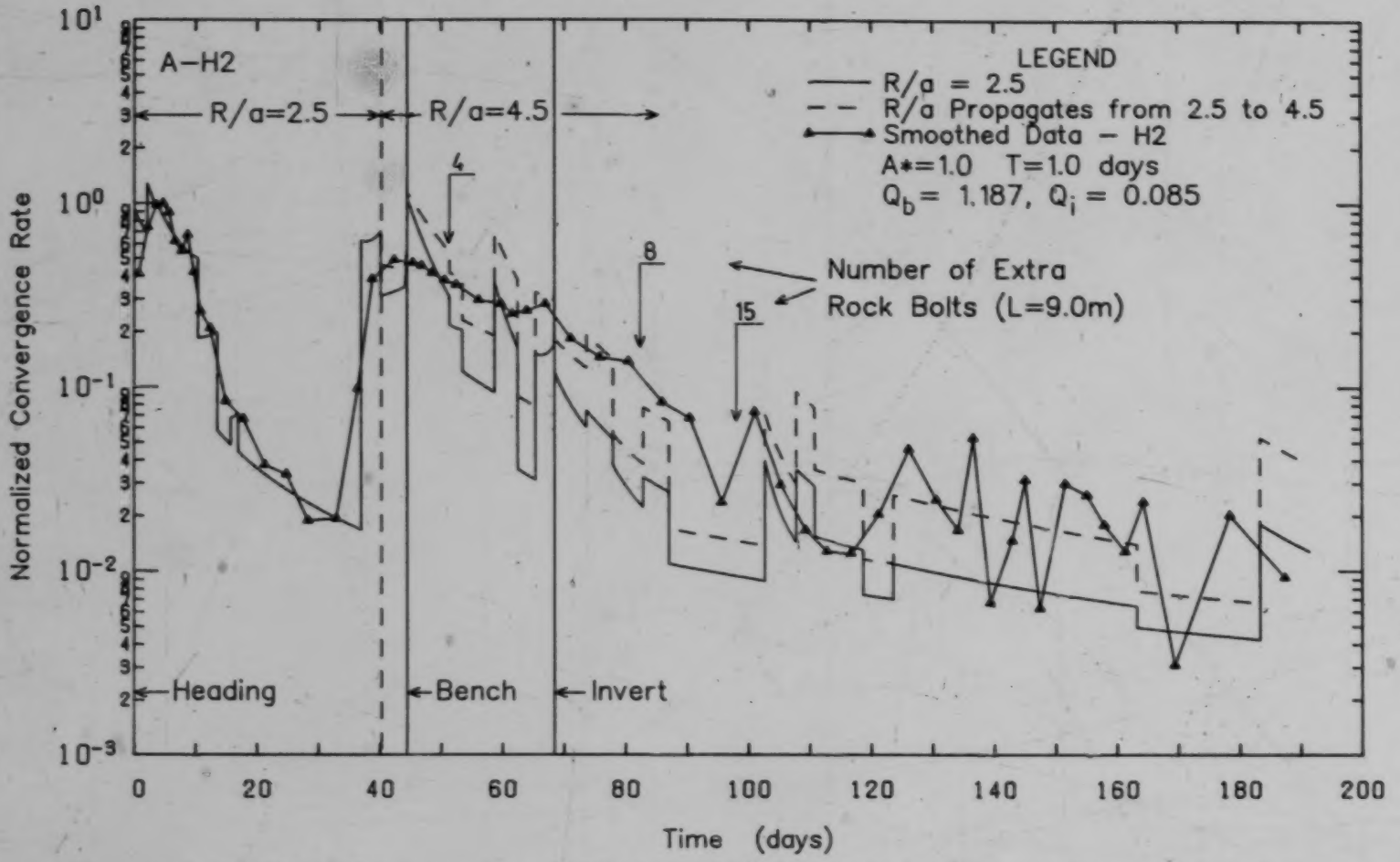

Figure 5.14 Fit of Convergence Solution with Yield Zone Propagation to Data from Station A-H2.

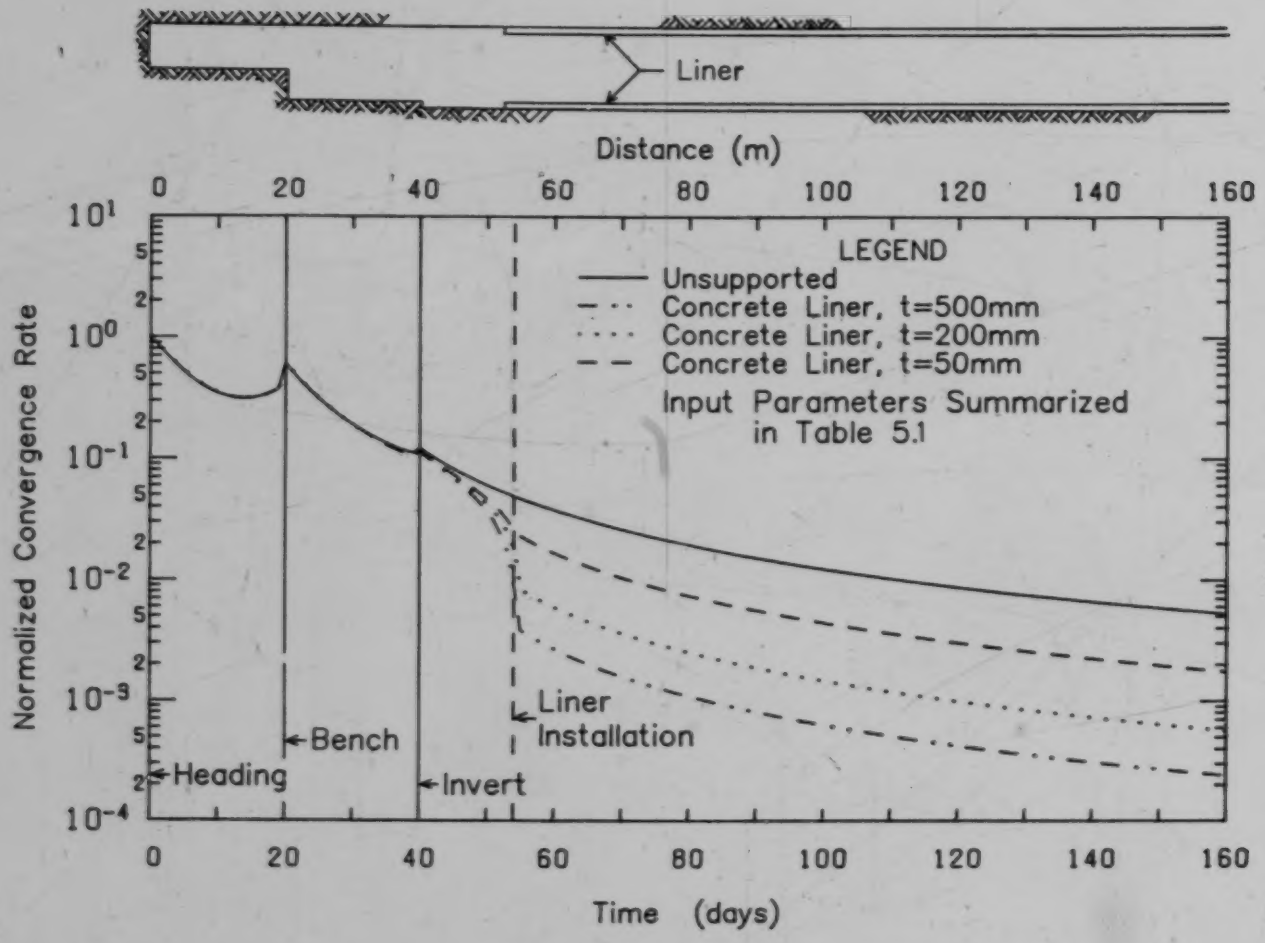

Figure 5.15 Effect of Liner on Convergence Solution; Idealized Excavation.

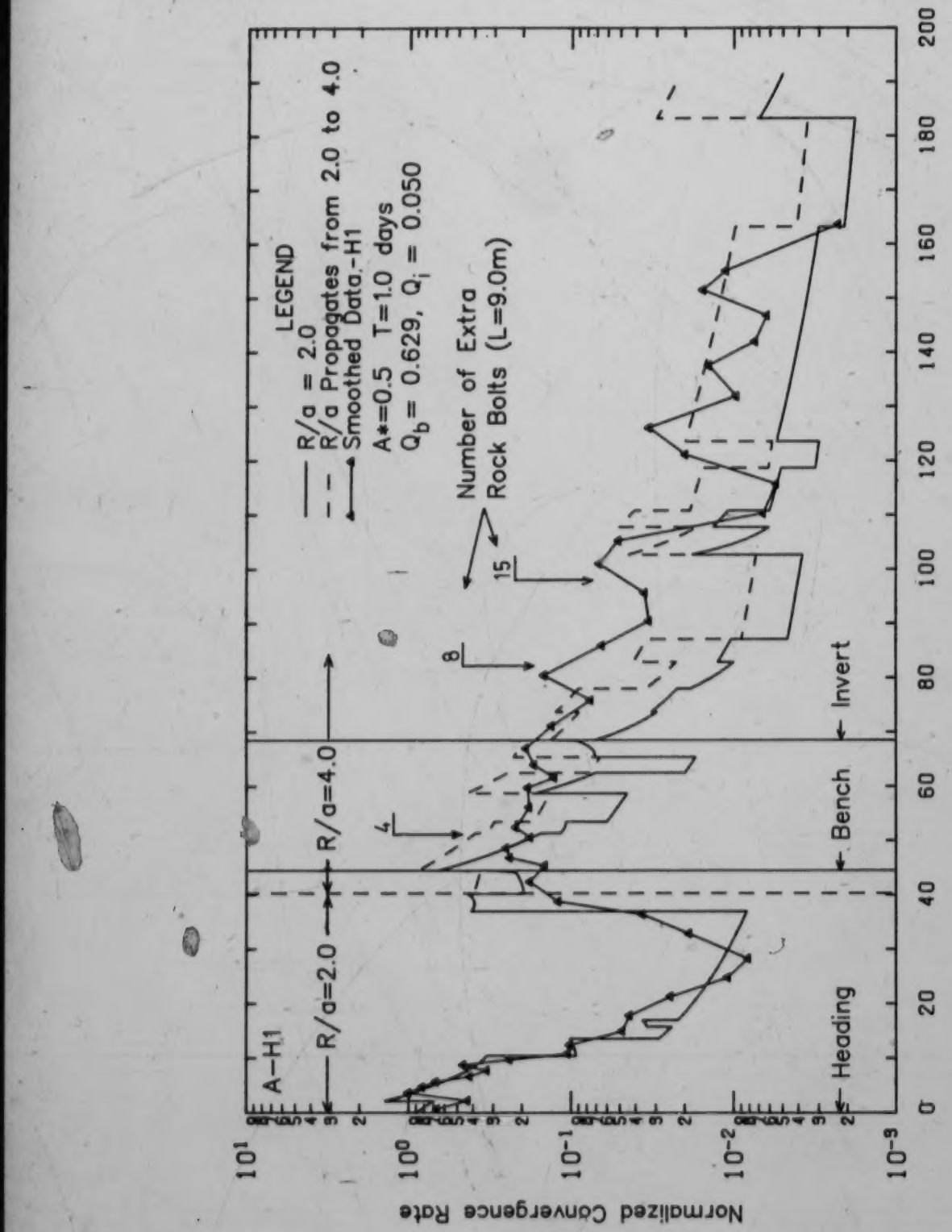

Figure 5.16 Fit of Convergence Solution to Data from Station A-H1.

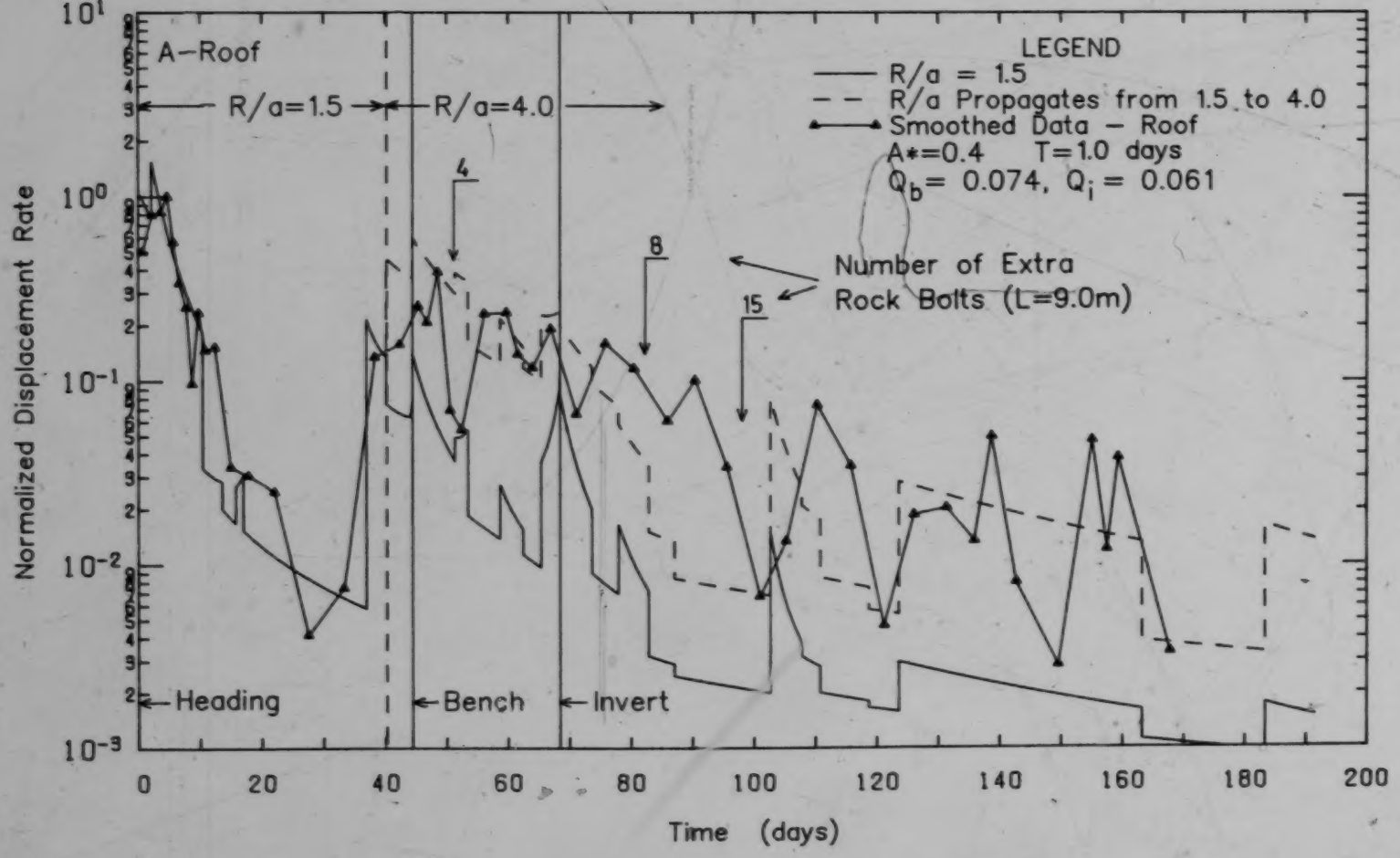

Figure 5.17 Fit of Convergence Solution to Data from Station A-Roof.

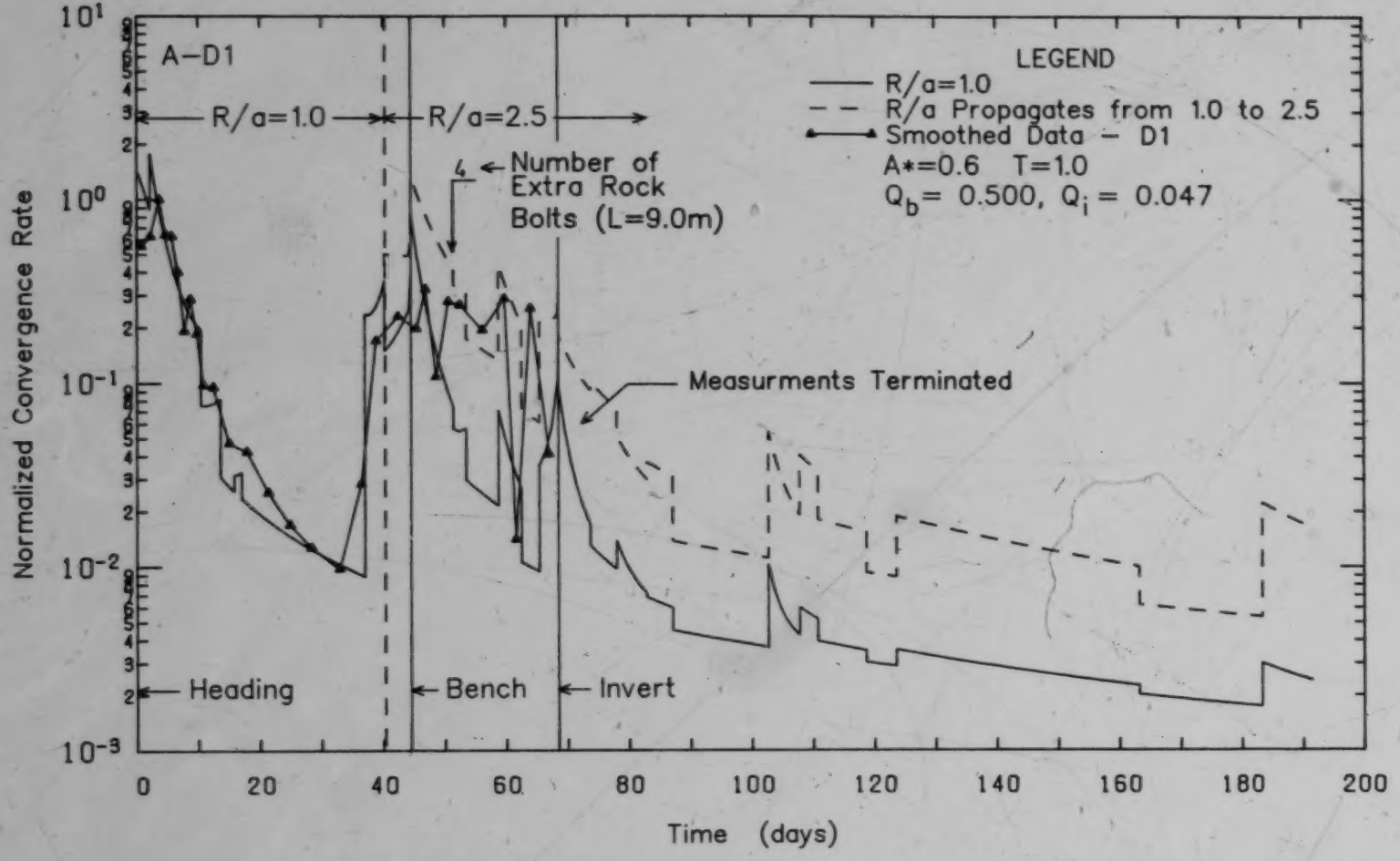

Figure 5.18 Fit of Convergence Solution to Data from Station A-D1.

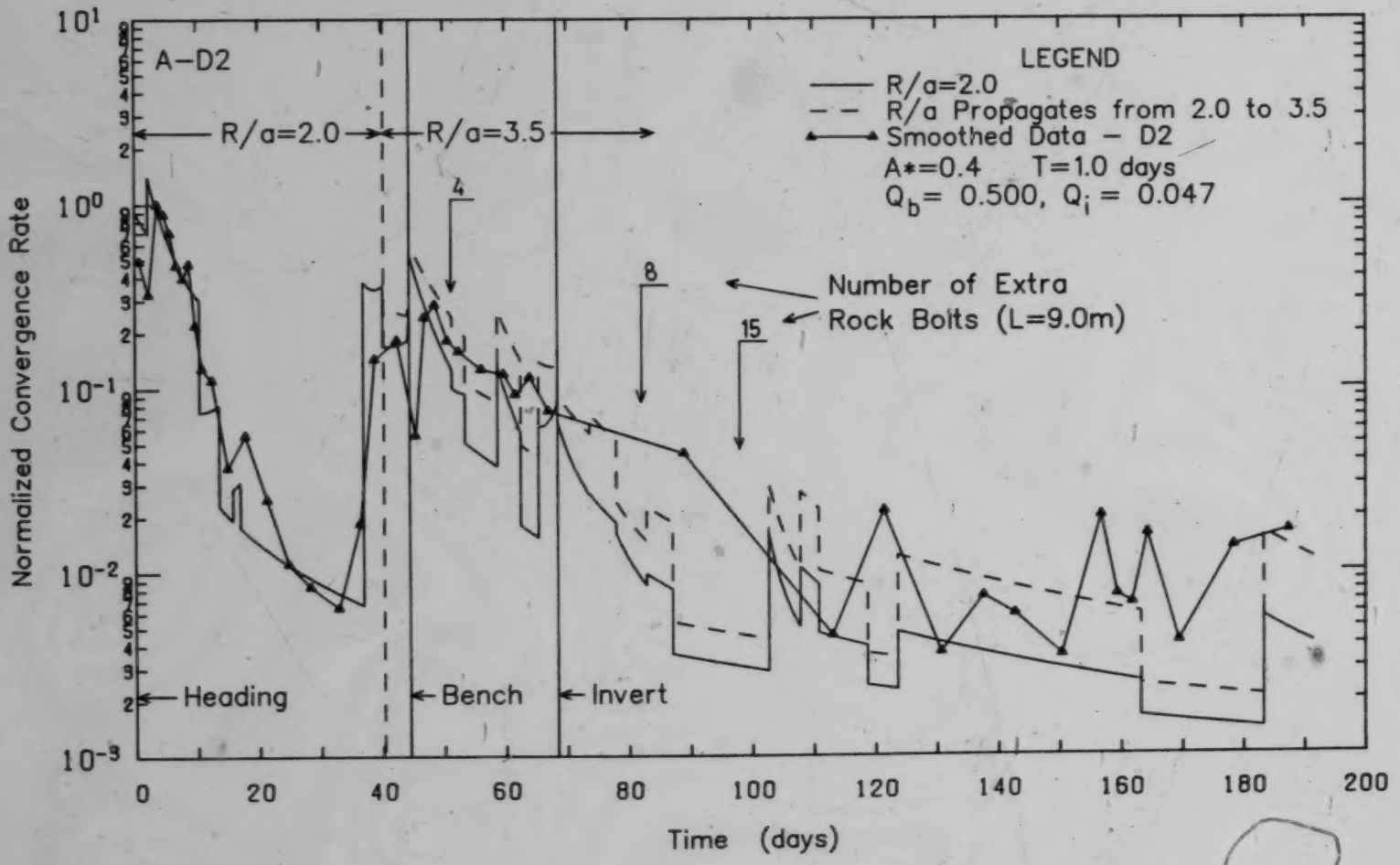

Figure 5.19 Fit of Convergence Solution to Data from Station A-D2.

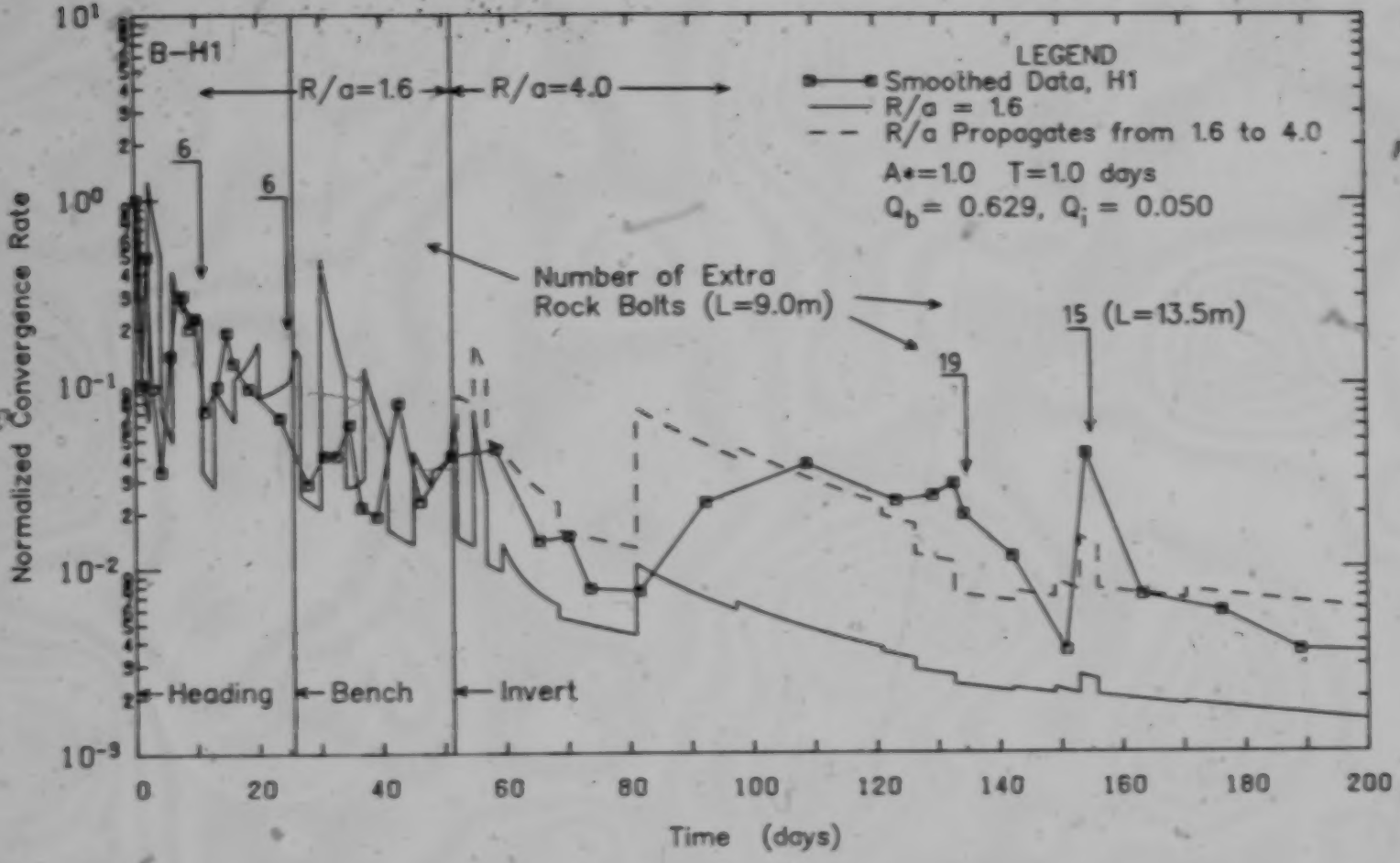

Figure 5.20 Fit of Convergence Solution to Data from Station B-H1.

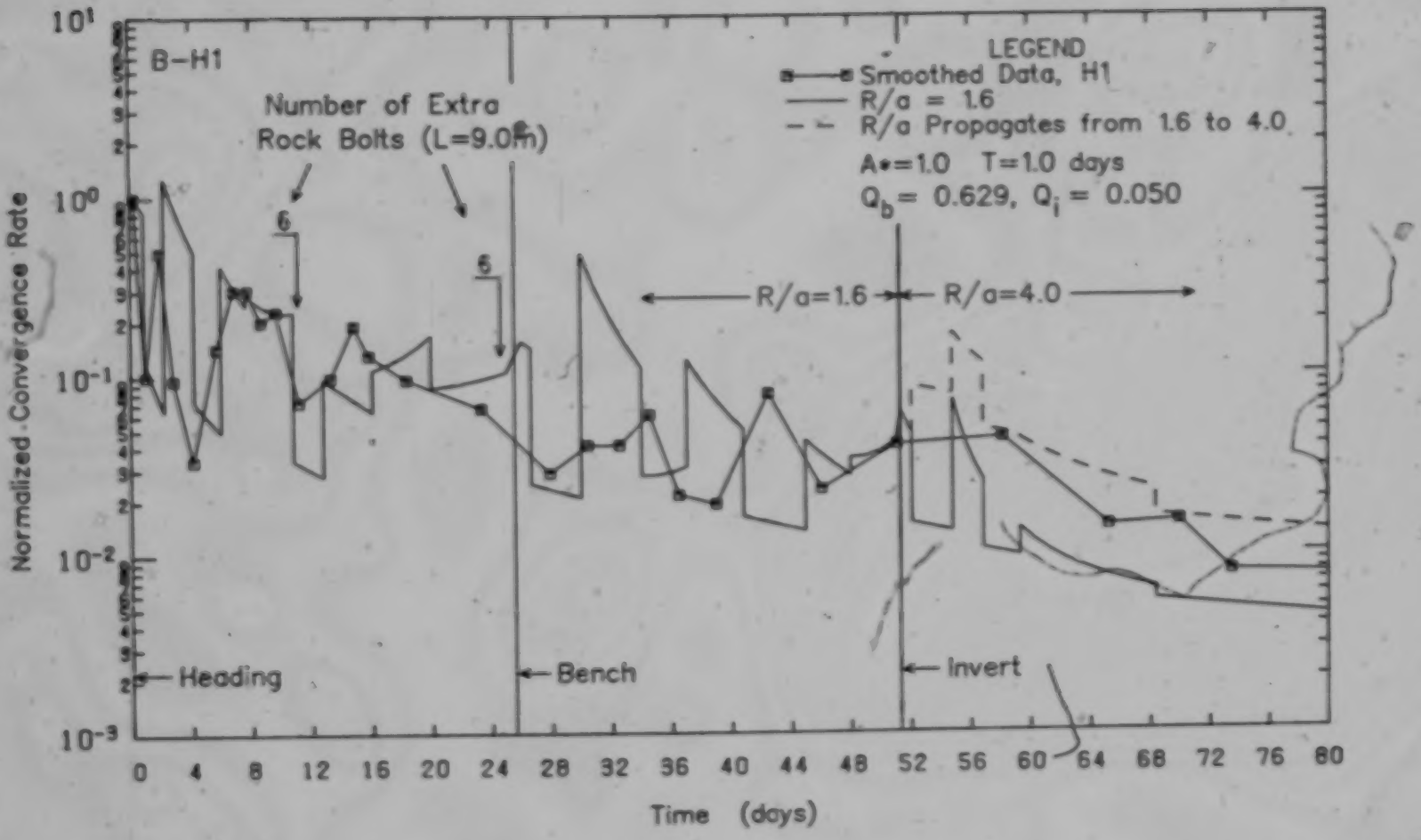

Figure 5.21 Fit of Convergence Solution to Data from Station B-H1.

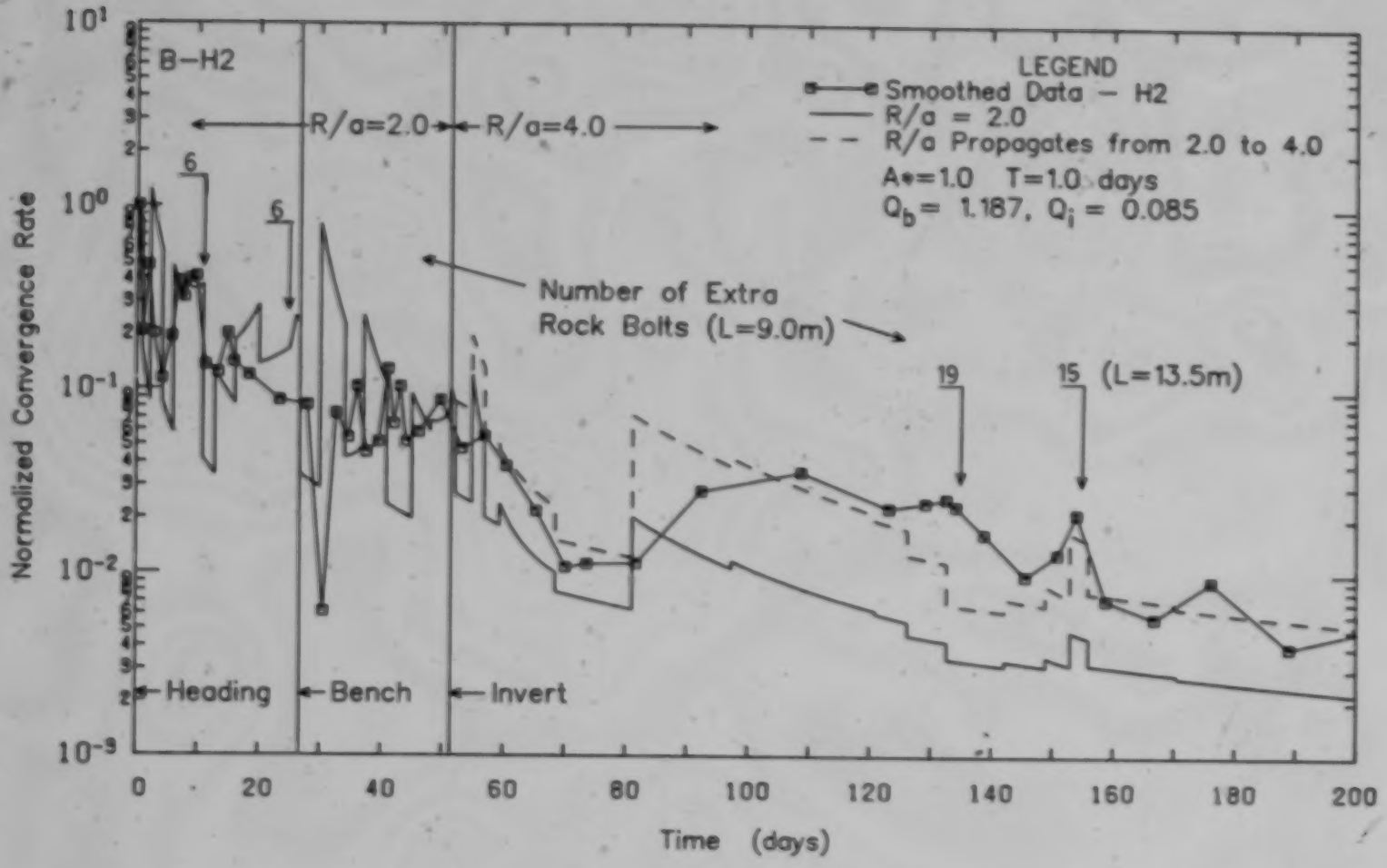

Figure 5.22 Fit of Convergence Solution to Data from Station B-H2.

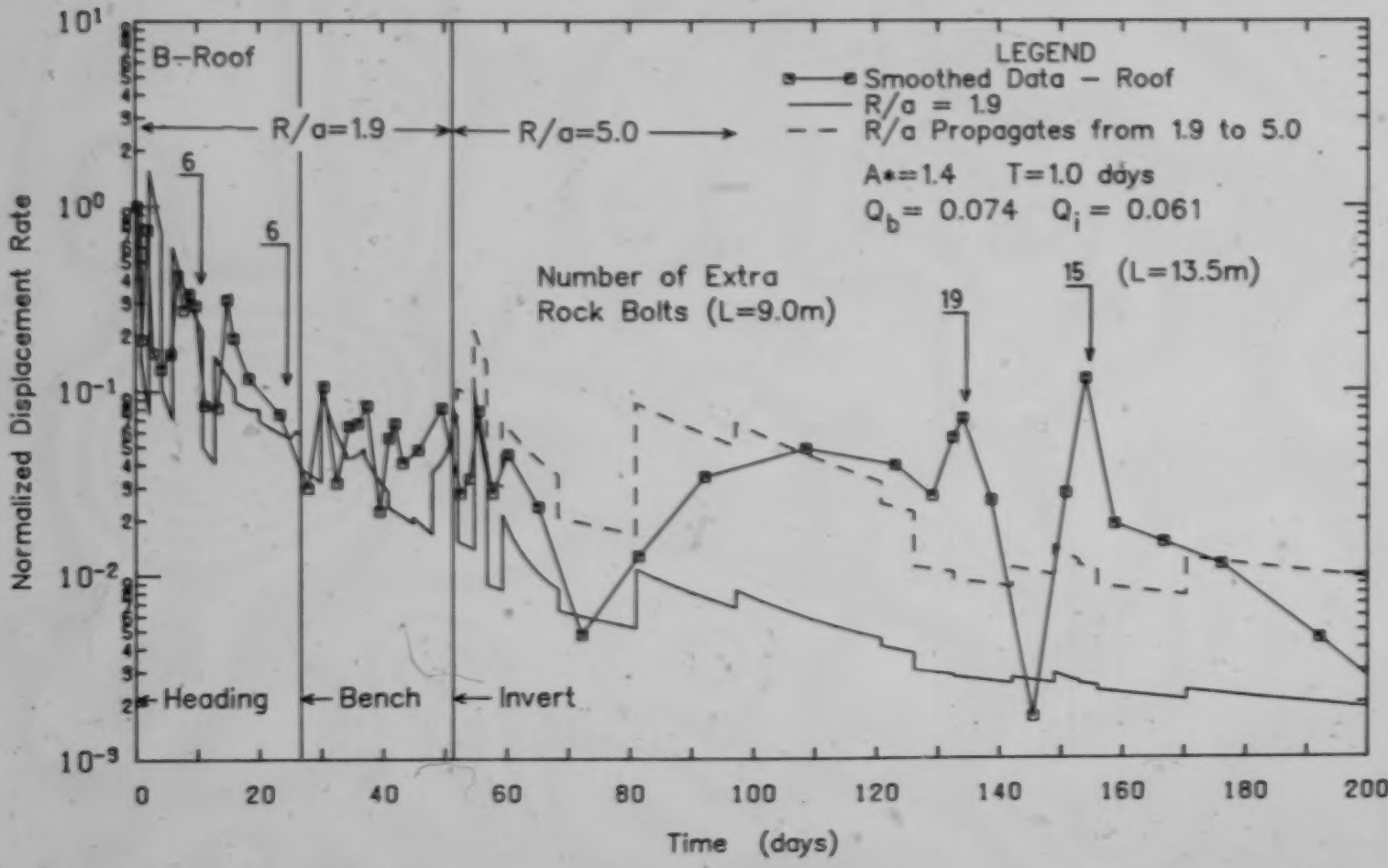

Figure 5.23 Fit of Convergence Solution to Data from Station B-Roof.

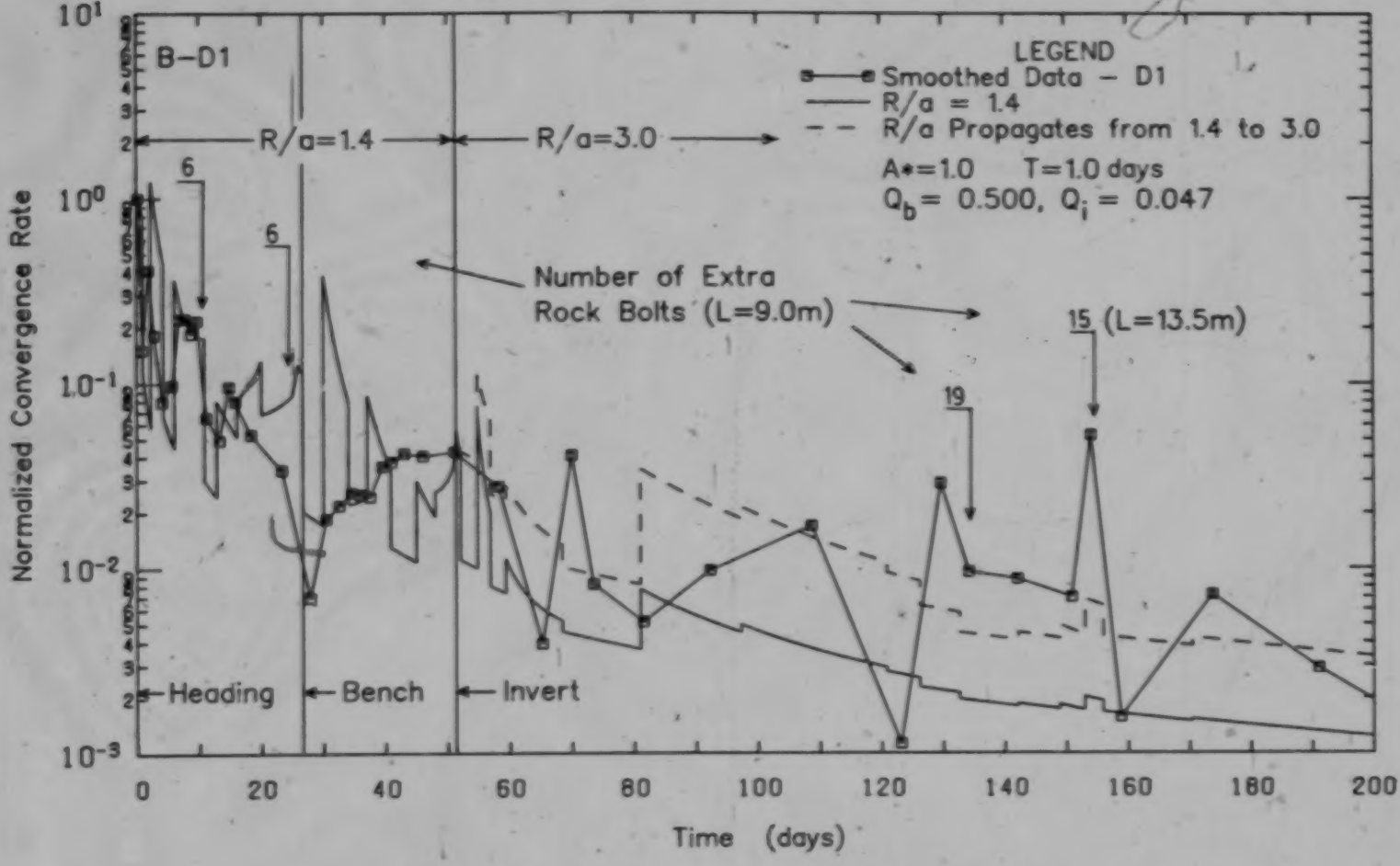

Figure 5.24 Fit of Convergence Solution to Data from Station B-D1.

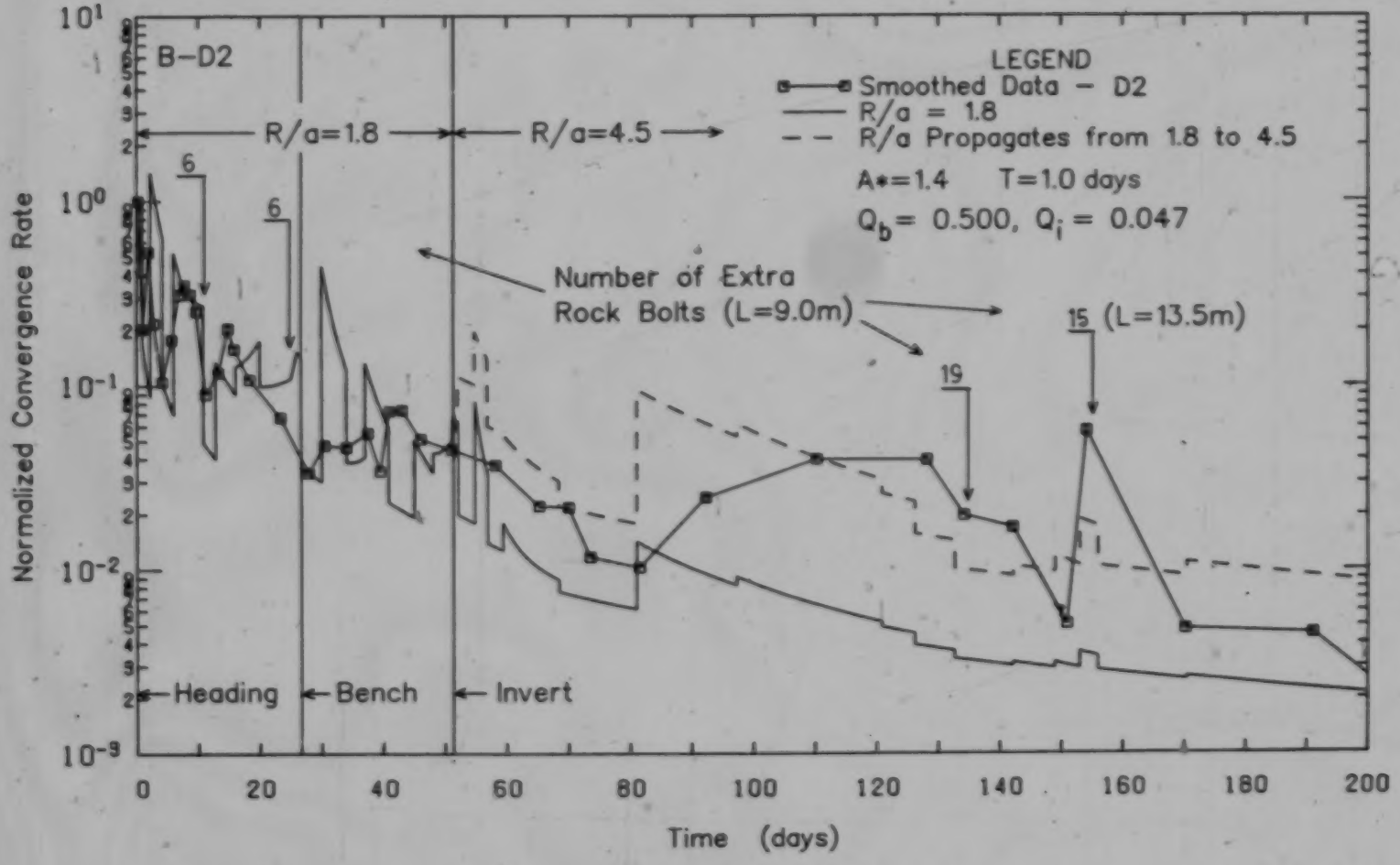

Figure 5.25 Fit of Convergence Solution to Data from Station B-D2.

6. CONCLUSIONS AND PRACTICAL IMPLICATIONS

6.1 Introduction

Tunnel wall convergence is routinely monitored in almost every tunneling project, but unfortunately the results are extremely under-utilized. If interpreted properly, convergence measurements can give important information regarding yielding of the rock mass, the validity of design assumptions, and the effectiveness of support measures. Valuable guidance can also be gained for support decisions, such as when remedial support measures should be introduced to check excessive deformation, and when the final liner can be installed. At present, these decisions are often based on experience, or on simplistic interpretations of the convergence measurements. For example, at the Arlberg Tunnel in Austria, a maximum convergence rate limit was defined (1 to 2 mm/hr), beyond which additional rock bolts were required, and a lower limit was defined (0.2 to 0.3 mm/day), beyond which the final liner could be installed (John, 1977). In the Enasan Tunnel in Japan, the interpretation of the convergence measurements was based on an extrapolation of the convergence measured in a smaller ventilation tunnel. When the measured convergence exceeded expectations, rock bolts were added to limit the excessive deformation. While these two approachs do provide a much needed framework for the interpretation of the data from their respective tunnels, they ignore the effect that

excavation history and supporting elements have on the convergence. Furthermore, there is no rational approach to date that incorporates these two effects.

An approach has been proposed in this thesis that provides a rational framework for the interpretation of convergence measurements, accounting for the effects that both the excavation sequence, and tunnel supports have on convergence. This approach, termed the Convergence Solution, is an extension of the approach by Guenot et al. (1985) to model more realistic tunneling conditions. The conclusions that follow from the application of the Convergence Solution to the results of a finite element analysis, and to laboratory and field data are summarized below.

6.2 Summary of Conclusions

6.2.1 Finite Element Analyses

The simulation of a variety of supported tunnels with finite element analyses provided important information for the extension of the Convergence Solution to model the effect of a tunnel support. These analyses confirmed the validity of the proposed Convergence Solution for modelling the effect of a support after the point of installation, and revealed the impact that a support has on the convergence curve before its installation point. It has been shown that the introduction of a support causes a deviation in the convergence curve (from the unsupported case) that starts

well before the point of support installation. The magnitude of this deviation depends on the stiffness of the support, and the length of the gap between the face, and the point of support installation (L_d). Figure 3.18 shows the relationship between this deviation (Q_k), the support stiffness (K) and L_d. The parameter Q_k, determined from this chart, is a new parameter used as input for the Convergence Solution.

6.2.2 Laboratory Test Results

The application of the Convergence Solution to data from tunnel simulation tests (Kaiser et al., 1983a) produced a consistent set of parameters that characterized the response of coal samples to small diameter excavations. There was very little variation in the parameters T and A^*, even though the Solution was applied to data from five separate monitoring stations, in two different samples, with different excavation histories, and tunnel diameters. More variation was observed in the parameter X (=0.84R/a), caused by different amounts of yielding at individual stations. The amount of yielding indicated by the Convergence Solution was in agreement with the observed yielding. The consistency of these physically meaningful parameters shows that the Convergence Solution was able to delineate the characteristic response of the coal samples because the differences in geometry and excavation history were correctly modelled.

Both laboratory simulation tests contained changes in excavation rate that produced abrupt changes in the measured convergence rates. As stated in Chapter 2, the Convergence Solution was developed on the basis of a constant excavation rate, and is therefore not applicable to a tunnel excavated at variable rates. However, when the Convergence Solution was applied to these tests it correctly predicted the magnitude of these changes in rate, but it predicted a gradual transition from one rate to the other, rather than the abrupt transitions that actually occured. Thus, with this limitation, the Convergence Solution may be used to model tunnels with variable excavation rates.

6.2.3 Enasan Tunnel

The Convergence Solution was successfully applied to convergence data from the Enasan Tunnel in Japan (Ito, 1983) which was excavated in three sequential stages. The parameters determined from various sets of data predicted a propagation of the annular yield zone from an average radius of 1.8a to 3.9a during the excavation of the second stage (bench). The existence of such a large yield zone is supported by the observed excessive convergence, which exceeded elastic predictions by more than 100 percent (at the roof). Also, the influence of activities at the face were felt at least five tunnel diameters past the face. In elastic rock, the influence of the face usually extends only about two diameters past the face. This has important

implications for the installation of the final liner, as it is desirable to install it beyond the influence of the face, to limit the amount of deformation and hence pressure that the liner incurres.

Once parameters had been determined that characterized the response of the rock, the Convergence Solution was used to demonstrate that the remedial support measures that were adopted to limit the excessive convergence had little or no noticeable effect.

6.3 Practical Implications

6.3.1 Data Collection and Presentation

The application of the Convergence Solution to a tunneling project requires that the convergence measurements be collected and presented in a certain manner. The specific requirements for a given tunneling project depend on the purpose of the monitoring program. A monitoring program that provides information for support decisions should be much more intensive than a program that is providing information for a back analysis. The following recommendations are based on the back analysis of the Enasan Tunnel in Chapter 5, and should be considered as the minimum requirements for the application of this method.

DATA COLLECTION

1) A minimum of six rate determinations should be taken for

each diameter advance of the tunnel within the first five diameters after the face passes the monitoring station.
2) After the face is more than five diameters away, one measurement every four days is sufficient.
3) Frequent measurements should be made during excavation stoppages to identify the time-dependent behavior of the rock mass. Also, readings should always be taken just before and after a change in advance rate (or stoppage).
4) The first measurement should be taken as close to the face as possible, and repeated frequently to establish the maximum rate of deformation.
5) The excavation history must be recorded in detail.
6) It is desirable to measure convergence in a minimum of two different orientations, to have more than one set of measurements to base the interpretation on.

DATA PRESENTATION

1) Plot convergence rate, normalized to the maximum rate, against time. If the tunnel is excavated in sequential stages, normalize the entire range of data to the maximum convergence rate associated with the first excavation.
2) Present both the normalized convergence rate and time on an arithmetic scale. If the range in either quantity is too large it may be necessary to use a logarithmic scale, but this should be avoided if possible, as it is difficult to assess a visual fit on logarithmic scales.

6.3.2 Applications of the Convergence Solution

Five proposed applications of the Convergence Solution to the observational design of a tunnel are discussed below, and illustrated with the analysis of the data from the Enasan Tunnel (see Chapter 5).

YIELD ZONE

The Convergence Solution can be used to gain information about the extent of the yield zone surrounding a tunnel. The parameter X is proportional to the radius, or extent of the Annluar yield zone, R, (X/R is 0.84). It must be noted that R is not necessarily the radius of a zone of yielded material but it gives the extent of a yield related stress redistribution zone. For this reason it is called 'equivalent' yield zone radius. The value of X can be determined from the initial measurements because it characterizes the time-independent response of the rock mass to excavation, which dominates the readings close to the face. The parameters T and A^*, which characterize the time-dependent response of the rock mass have little influence on this initial portion of the curve. Thus, information on the extent of the yield zone can be obtained from the first few readings (within one tunnel diameter from the face).

The prediction of the size of the equivalent yield zone (R) is a valuable component for the selection of rock bolt type and length. For example, if the yield zone is very

large, fully grouted rock bolts could be installed to provide frictional resistance. Conversely, if the yield zone is not large, end grouted or mechanical rock bolts could be installed with a length capable of anchoring into the unyielded rock.

The use of the Convergence Solution to estimate the extent of the yield zone is illustrated now on an example from the Enasan Tunnel.

Convergence data, measured at Station A of the Enasan Tunnel, is shown in the normalized convergence rate format in Figure 6.1, together with the best fit of the Convergence Solution. The portion of the data from 0 to 11 days was sufficient to identify the parameter X as 7.6m (or R/a=1.5). The range in R/a was 1.0 to 2.5 for all of the sets of measurements taken at Station A. This represents a yield zone depth of up to 9.0m from the tunnel wall. Thus, to reinforce the entire yield zone, bolts of at least 9.0m would be needed. The fact that the yield zone propagated later (see below) clearly demonstrates the need for early installation (near the face).

FRAMEWORK FOR INTERPRETATION OF DATA

Once all three parameters (R/a, A^* and T) of the Convergence Solution have been determined, by curve fitting to the field measurements, the Solution can be used to forecast subsequent behavior. This forecast then provides a basis for the interpretation of convergence measurements

taken after that point. This is extremely valuable, as it enables the discernment of jumps in convergence rate that are caused by the excavation activities, from those caused by other processes such as the propagation of a yield zone.

The convergence data that is shown in Fig. 6.1 provides a demonstration of this application of the Convergence Solution. The three parameters were all determined on the basis of the convergence measurements from 0 to 38 days. The solid curve past 38 days is the forecast of the subsequent convergence rate based on these initial parameters. On the basis of this forecast, it was possible to identify a change in the characteristic response of the rock mass from the initial behavior over the first 38 days. As can be seen in Fig. 6.1, the slope of the convergence rate curve past the bench excavation is much more shallow than the predicted slope, and the convergence rates are higher than predicted. This deviation indicates that a change has occurred in the rock mass. A variation of this type can be matched by the Convergence Solution with a variation in R/a, which suggests that the size of the yield zone has changed. The dashed curve in Fig. 6.1 was calculated for a higher value of R/a past t=41 days, which represents the propagation of the initial yield zone from R/a=1.5 to R/a=4.0 at 41 days.

The above deviation would have been very difficult to distinguish from the jumps in the data caused by the variable excavation history without the basis provided by the Convergence Solution. Furthermore, the jumps in the data

at 110 and 126 days could have been interpretted as yield zone propagation, but were clearly a result of the stop-go excavation of the bench, when examined together with the Convergence Solution forecast. These two jumps were measured when the bench was more than three tunnel diameters beyond the monitoring station, and would not likely have been attributed to the excavation activity without the aid of the Convergence Solution. This clearly demonstrates the inadequacy of the convergence rate limit as criteria for support decisions (e.g., Arlberg Tunnel) as will be discussed in Section 6.4.

If there is more than one monitoring location in the same rock type along a tunnel, the parameters determined at the first location could be used to forecast the convergence curve anticipated at subsequent locations before any measurements are taken. Thus, a change in behavior from previous locations could be identified within the first few measurements.

ULTIMATE CONVERGENCE

The ultimate convergence can be estimated once all three parameters (X, T and A^*) have been determined. This is the ultimate convergence that would occur if no additional supports were added to the tunnel. It can be estimated with the three curve fitting parameters, and the latest convergence measurement. For the data shown in Fig. 6.1 the extrapolation of the ultimate roof displacement is 790mm,

based on a displacement of 720mm at 191 days. The calculations to obtain this estimate are given below. In this example, it is roof displacement, rather than convergence that will be calculated, but it is calculated in the same manner as convergence.

Example calculation:

- From Fig. 5.6, the roof displacement at 191 days is 720mm.
- Average distance of three faces from station at 191 days is 60m.
- Parameters for roof data, Station A, are:
  $R/a=4.0$ (after propagation); $A^*=0.4$; and $T=1.0$ days.
- The convergence after the face for an unsupported tunnel is described by Eqn 3.2 as follows:

$$C(x,t) = [Q_1 + Q_2\, C_1(x)]C_{x\infty}[1 + A\, C_2(t)] \qquad \text{Eqn 3.2}$$

Substituting the above quantities in Eqn 3.2 yields:

$$720\text{mm} = [0.50 + 0.50(0.94)]C_{x\infty}[1 + 0.4(0.79)]$$

$$C_{x\infty} = 564\text{mm}$$

Hence;

$$C_{ult} = C_{x\infty} + (A^*)C_{x\infty}$$

$$= 564\text{mm} + (0.4)564\text{mm}$$

$$C_{ult} = 790\text{mm}$$

GUIDANCE FOR SUPPORT DECISIONS

The Convergence Solution can also be used to guide decisions regarding the type of support that should be installed and the optimum installation location. This can be accomplished by examining the impact that variations in support type, and location have on the convergence, once the parameters that characterize the response of the rock mass have been determined. The effect that concrete liners of various thicknesses have on both the convergence and convergence rate curves is shown in Figure 6.2. At first sight it can be seen that the normalized convergence rate is an excellent indicator of support effectiveness.

The curves in Fig. 6.2 depict the response of the rock mass at the Enasan Tunnel to an "idealized" excavation, with all of the stoppages eliminated (see Chapter 5). As expected, Fig. 6.2 shows that an increase in liner thickness causes a downward translation of the convergence rate curve, and hence a lower convergence. The effect that a variation in the installation location has on the convergence curves from the same idealized excavation is shown in Figure 6.3. This figure shows the interesting result that all of the convergence rate curves eventually merge into one curve irrelevant of their respective installation locations. This has implications for the pressure build-up in the liner, as it is proportional to the deformation of the liner. The ultimate rate of pressure increase in the liner is identical, independent of installation location. Only the

initial load increment depends on the location of the installation point. This shows that lining pressure extrapolations, based on the initial load build up must be erroneous.

The ultimate convergence and lining pressure caused by each of the 6 support cases shown in Figs 6.2 and 6.3 are summarized below:

t_s* (days)	x_s+ (m)	Liner Thickness (mm)	C_{ult} (mm)	$C_l(ult)$++ (mm)	p_{liner} (MPa)
54	12	50	937	64	1.37
54	12	200	889	21.4	1.87
54	12	500	873	9.1	2.05
41	1	500	792	12.9	2.91
60	20	500	892	8.2	1.85
80	40	500	932	6.4	1.44

* Time of liner installation.

\+ Distance between excavation and liner installation.

++ Ultimate convergence of liner.

Thus, when the Convergence Solution is used in the above manner, the choice of support type, and installation location can be fine tuned to achieve the desired effect on the convergence. In addition, the ultimate pressure that the support would experience can be calculated to ensure that the support has adequate strength. At this time, the desired

factor of safety for the liner can be evaluated and ensured.

EVALUATION OF SUPPORT PERFORMANCE

The prediction of the influence that a given support should have on the convergence (and convergence rate) curve can be used as a basis to evaluate the performance of a support after it is installed. This can be especially useful for rock reinforcing supports such as rock bolts, where the supporting effect is difficult to quantify otherwise. An example of this application of the Convergence Solution was given in Chapter 5, where the effectiveness of additional rock bolts that were installed in the Enasan Tunnel to combat the excessive convergence was examined. Most of the additional rock bolts (23 of 27) were installed at 82 and 98 days (see Fig. 6.1) which both correspond to 54 days in the "idealized" excavation (as both times were in one long excavation stoppage). The effect that concrete liners of varying thickness, installed at 54 days, would have on the convergence rate curve is shown in Fig. 6.2. An examination of Fig. 6.1 reveals no noticeable change in the convergence rate curve after the additional bolts have been installed. By comparing Figs 6.1 and 6.2 it appears that the net effect that the additional bolts had on the convergence rate curve was less than that produced by a 50mm concrete liner. Any deviation from the convergence rate curve less than that produced by a 50mm concrete liner would be lost in the noise of the data caused by the variable excavation history.

6.4 Advantages of Convergence Solution

There are several distinct advantages in using the Convergence Solution instead of convergence rate criteria to make support decisions. As mentioned earlier, at the Arlberg Tunnel a maximum tolerable convergence rate was defined that indicated whether or not bolting was required, and a lower rate limit was set to indicate when the final liner could be installed.

The use of an absolute, rather than normalized convergence rate, is not a good indicator of the behavior of the rock mass. The magnitude of the convergence rate is influenced by both the geometry of the opening, and the orientation at which the convergence measurements are taken, as was demonstrated in Chapter 5. Thus, a section that contained excessive yielding could produce convergence rates that exceed the rate limit when measured in one orientation, and rates that are below the limit when measured in a different orientation. The Convergence Solution deals with normalized convergence rates, that are independent of the magnitude of convergence, which eliminates these influences. The behavior of the rock mass is then characterized by the shape of the convergence rate curves rather than their magnitude.

The other major problem with the convergence rate limit criterion is that it ignores the effect that the excavation sequence has on the convergence. If the rate of excavation varies, or the excavation is done in sequential stages,

jumps and drops are produced in the convergence rate curve that render a convergence rate criterion ambiguous. The maximum rate limit could be exceeded due to an increase in excavation rate, or the excavation of a subsequent stage, rather than by unstable behavior of the rock mass that would require additional support. Also, the lower rate criterion could be met temporarily during a slower excavation rate and then exceeded when the excavation rate increases. This would suggest that the final liner could be installed, when it would actually be too early. This is especially true if the influence of the excavation face extends far from the face, as with heavily yielding ground. However, the Convergence Solution fully accounts for the excavation history which permits the identification of changes in the convergence measurements that actually merit concern.

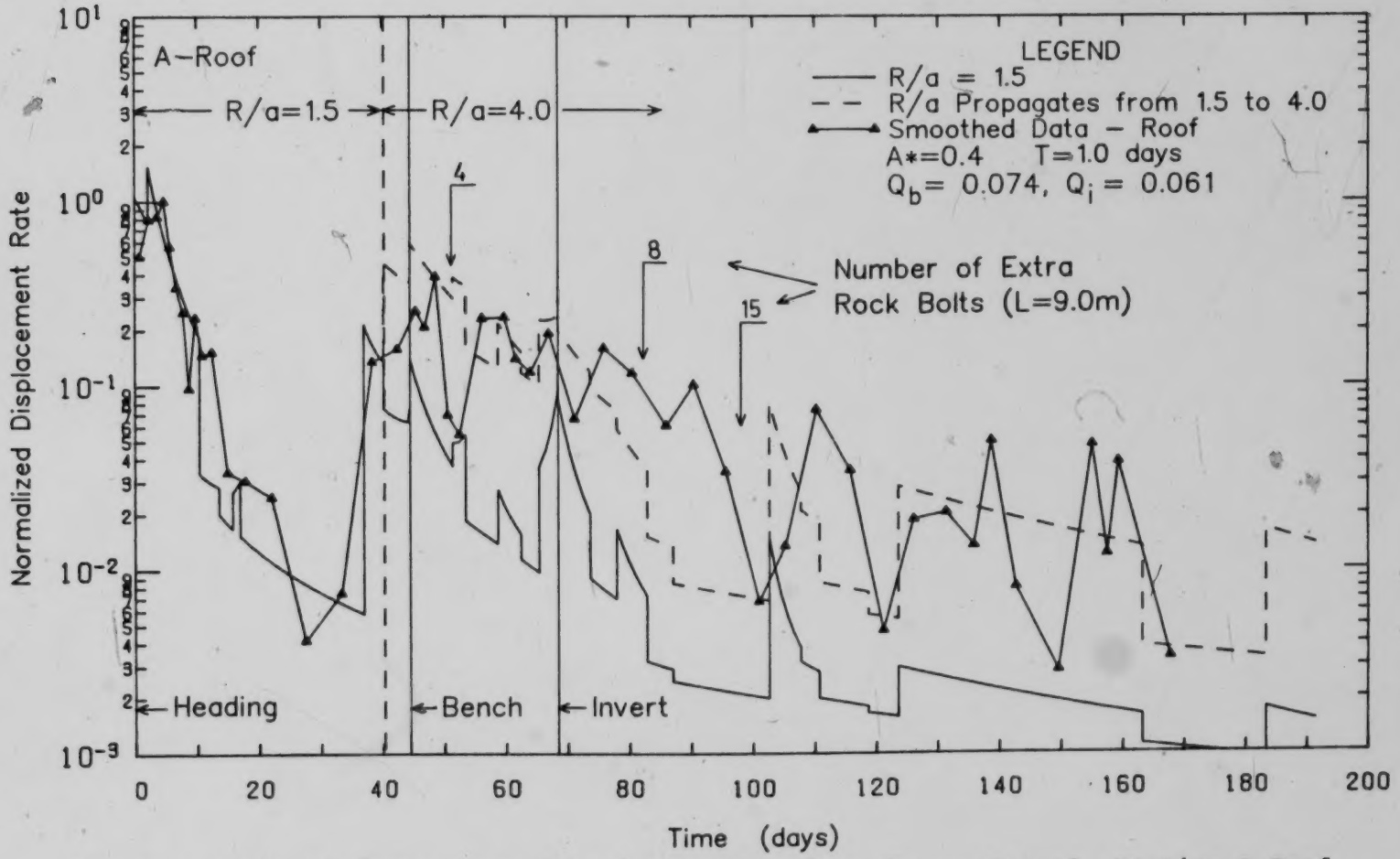

Figure 6.1 Fit of Convergence Solution to Data from Enasan Tunnel, Station A-Roof (same as Fig. 5.17).

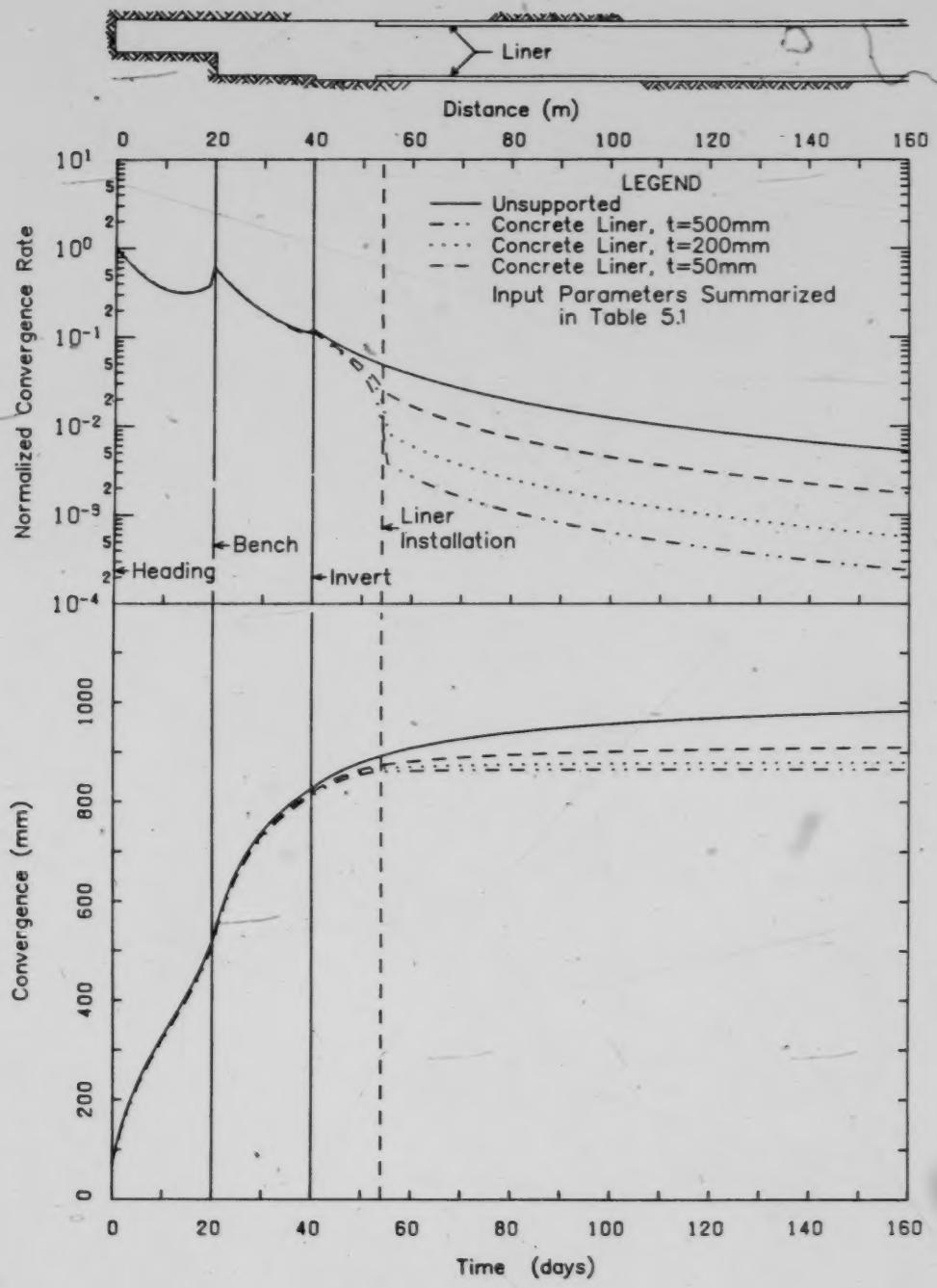

Figure 6.2 Convergence Solution Curves, Liner Thickness Varied; Idealized Excavation.

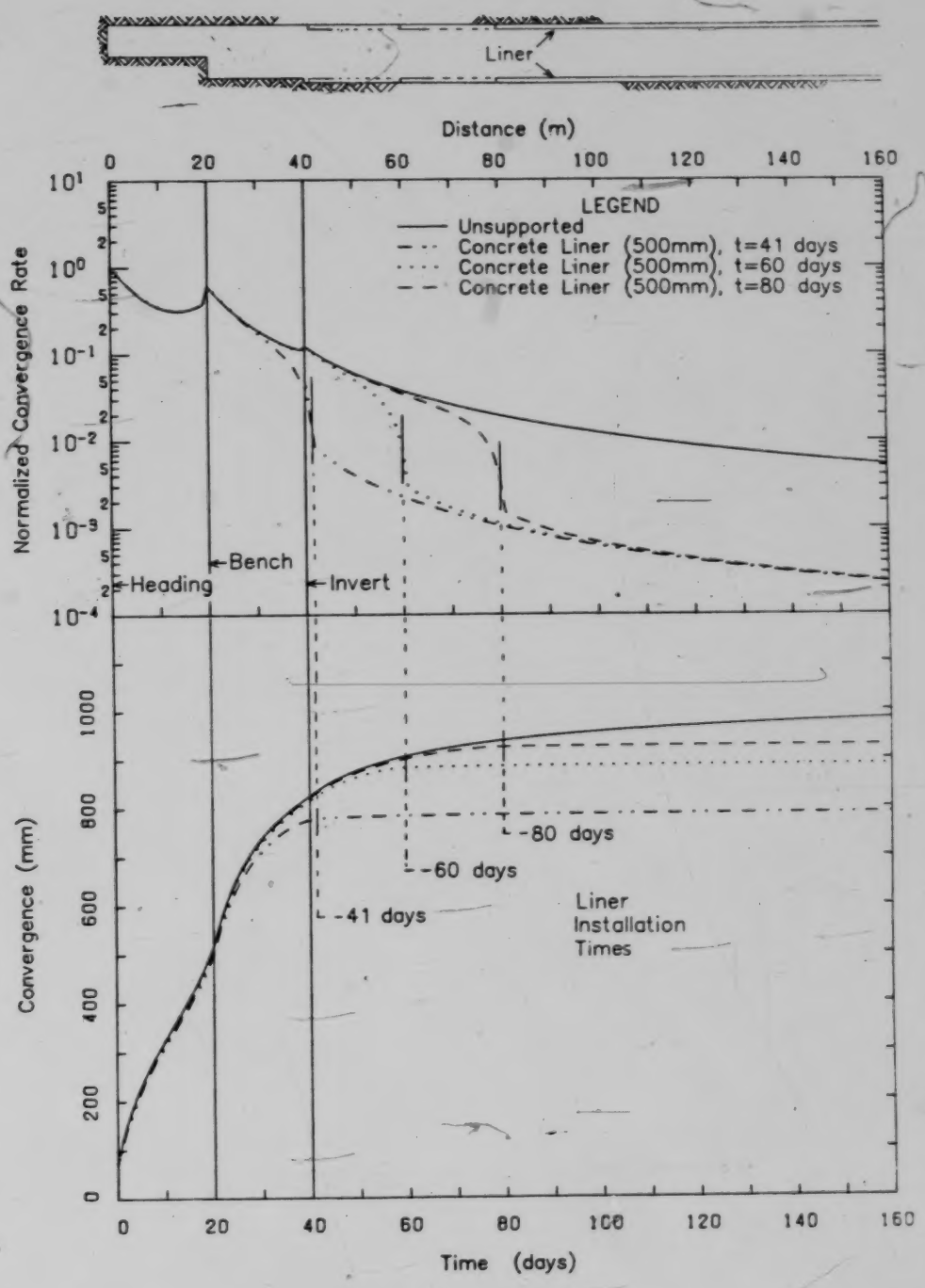

Figure 6.3 Convergence Solution Curves, Liner Placement Varied; Idealized Excavation.

REFERENCES

Chan, D., 1986. Finite Element Analysis of Strain Softening Material. *Ph.D. Thesis, Department of Civil Engineering, University of Alberta*, 282 p.

Cruden, D.M., 1971. The Form of the Creep Law for Rock Under Uniaxial Compression. *International Journal of Rock Mechanics and Mining Science*, 8, pp. 105-126.

Descoeudres, F., 1977.*Mecanique des Roches II*, (Lecture notes) Ecole Polytechnique Federale de Lausanne.

Einstein, H.H. and Schwartz, C.W., 1979. Simplified Analysis for Tunnel Supports. *Journal of the Geotechnical Engineering Division, American Society of Civil Engineers*, 105, pp 499-518.

Guenot, A., Panet, M., and Sulem, J., 1985. A New Aspect in Tunnel Closure Interpretation. *26th US Symposium on Rock Mechanics*, Rapid City, pp. 455-460.

Hoek, E., and Brown, E.T., 1980. *Underground Excavations in Rock*. Institute of Mining and Metallurgy, London, 527 p.

Ito, Y., 1983. Design and Construction by NATM through Chogiezawa Fault Zone for Enasan Tunnel on Central Motorway. *Tunnels and Underground*, 14, pp. 7-14.

John, M., 1977. Adjustment of Programs of Measurements Based on the Results of Current Evaluation. *Proc. International Symposium on Field Measurements in Rock Mechanics*, Zurich, 2, pp. 639-656.,

Kaiser, P.K., 1980.Effect of Stress-History on the

Deformation Behavior of Underground Openings, *Underground Rock Engineering*, Canadian Institute of Mining and Metallurgy, CIM Special Vol. 22, pp. 133-140.

Kaiser, P.K., 1983. Numerical analysis performed while on sabatical at the University of Aachen, West Germany.

Kaiser, P.K., 1984. Personal communication of Enasan Tunnel monitoring data, collected during site visits in Japan.

Kaiser, P.K., Maloney, S., Morgenstern, N.R., 1982. *Support Design for Underground Cavities in Weak Rock*. Report for the Department of Energy and Natural Resources, Government of Alberta, Part 2, 159 p.

Kaiser, P.K., Maloney, S., Morgenstern, N.R., 1983a. Time Dependent Behavior of Tunnels in Highly Stressed Rock. *Proceedings of the International Society for Rock Mechanics Conference*, Melbourne, pp. 329-336.

Kaiser, P.K., Maloney, S., Morgenstern, N.R., 1983b. *Support Design for Underground Cavities in Weak Rock*. Report for the Department of Energy and Natural Resources, Government of Alberta, Part 3, 179 p.

Ladanyi, B. and Gill, D.E., 1984. Tunnel Lining Design in a Creeping Rock. *International Society for Rock Mechanics Symposium on the Design and Performance of Underground Excavations*, Cambridge, pp. 19-26.

Lo, K.Y., Yuen, C.M.K., 1981. Design of tunnel lining in rock for long term effects. *Canadian Geotechnical*

Journal, 18, pp. 24-39.

Maloney, S.M., 1984. An Assessment of Deformation Monitoring Practice in Underground Excavations in Weak Rock by Model Tests. *M.Sc. Thesis, Department of Civil Engineering, University of Alberta*, 282 p.

Otsuka, M. and Kondoh, T., 1981. On the Displacement Forcasting Methods and their Application to Tunnelling by NATM. *Proceedings of the International Symposium on Weak Rock*, Tokyo, pp. 945-950.

Panet, M. and Guenot, A., Analysis of Convergence Behind the Face of a Tunnel. *Tunnelling'82, The Institution of Mining and Metalluryg*, pp. 197-204.

Pelli, F., Kaiser, P.K. and Morgenstern, N.R., 1986. Three-Dimensional Simulation of Rock-Liner Interaction Near Tunnel Face.*Proc 2nd International Symposium on Numerical Models in Geomechanics*, Ghent.

Ranken, R.E. and Ghaboussi, J., 1975. *Tunnel Design Considerations: Analysis of Stresses and Deformations Around Advancing Tunnels.* Department of Transportation, Report of University of Illinois.

Sakurai, S., 1978. Approximate Time-Dependent Analysis of Tunnel Support Structure Considering Progress of Tunnel Face. *International Journal for Numerical and Analytical Methods in Geomechanics*, 2, pp. 159-175.

Sulem, J., 1983. Comportement Differe des Galeries Profondes. *Ph.D. thesis, L'Ecole Nationale des Ponts et Chausées*, 154 p.

Takino, K., Kimura, H., Kamemura, K. and Kawamoto, T., 1983. Three Dimensional Ground Behavior at Tunnel Intersections. *International Symposium on Field Measurements in Geomechanics*, 2, Zurich, pp. 1237-1246.

APPENDIX A

Description of Computer Program SAFE.

SAFE (Soil Analysis by Finite Element) is a computer program developed at the University of Alberta to analyze deformation of soil and (weak) rock structures. The program is written in FORTRAN IV language and has been installed in different types of computer systems including the IBM system, the Amdahl MTS system and the CDC Cyber 205 vector computer system. The program has been applied in analyzing a wide variety of geotechnical problems such as excavation, dam, shaft and tunnel constructions. The initial development of the program was to analyze the post peak deformation of strain softening soil. The program has now been extended to include 2 and 3 dimensional analyses using total and effective stress formulations for fully undrained and drained conditions. A variety of non-linear elastic and plastic models with associated and non-associated flow rules are also available. The following is a list of the main features of the program SAFE.

Basic Formulation

- Displacement finite element formulation assuming small strain and small deformation.

Element Types

- Two dimensional: 3 to 6 nodes triangular, 4 to 8 nodes rectangular

- Three dimensional: 8 to 20 nodes solid elements

Type of Analysis

- Plane stress, plane strain, axisymmetric and three dimensional analysis.

Material Models

1. Linear elastic model.
2. Non-linear elastic hyperbolic model.
3. Elastic perfectly or brittle plastic model using von-Mises, Tresca, Drucker-Prager, and Mohr-Coulomb yield criteria with associated or non-associated flow rule.
4. Elastic plastic strain hardening and softening (weakening) model.
5. Elastic hyperbolic softening model.

Drainage Condition

1. Total stress analysis.
2. Fully undrained effective stress analysis.
3. Fully drained effective stress analysis.

Standard Features

1. Prescribed concentrated point force or distributed pressure boundary condition.
2. Prescribed displacement boundary condition.
3. Changing material properties at any stage of the

analysis.

4. Program restart at any stage of the analysis.

5. Newton Raphson and Modified Newton Raphson iterative scheme for non-linear analysis.

6. Choice of 2x2, 3x3, 2x2x2, and 3x3x3 integration scheme.

7. Load increment subdivision for non-linear analysis.

Special Features

1. Element birth and death option.

2. Automatic application of stress relief due to excavation.

3. Skyline and extended skyline matrix equation solver.

4. Choice of stress calculation for non-linear analysis:

   (i) Euler forward integration scheme;

   (ii) Improved Euler scheme; and

   (iii) Runge-Kutta scheme.

APPENDIX B

Derivation of Equation 3.6.

The manipulations that were performed to obtain Eqn 3.6 from Eqn 3.5 are presented here. Eqn 3.6 describes the convergence that occurs in a tunnel after the installation of a support.

$$C(x,t) = [Q_1+Q_2C_1(x)- \frac{P_s(C(x,t))}{P_o}][C_{x\infty}+AC_2(t)] \qquad \text{Eqn 3.5}$$

where: $P_s(C(x,t)) = K_s \frac{\Delta C_1}{2a}$;

$\Delta C_1 = C(x,t) - C_s$; and

C_s = Convergence at time of liner installation.

Substituting these components into Eqn 3.5, gives:

$$C(x,t) = [Q_1+Q_2C_1(x)-\frac{K_s}{2ap_o}(C(x,t)-C_s)][C_{x\infty}+AC_2(t)] \qquad \text{Eqn B.1}$$

Collecting like terms:

$$C(x,t) = \frac{[(Q_1+Q_2C_1(x)+KC_s][C_{x\infty}+AC_2(t)]}{1 + K(C_{x\infty}+AC_2(t))} \qquad \text{Eqn 3.6.}$$

where: $K = \frac{K_s}{2ap_o}$

APPENDIX C

Documentation of Computer Program CONRATE

The computer program CONRATE calculates convergence vs time, and normalized convergence rate vs time curves according to the final form of the Convergence Solution, given by Equations 3.8, 3.9 and 3.11. When there is no tunnel support, the Convergence Solution reduces to the form given by Equations 3.1 and 3.2. The normalized convergence rate curves are calculated with Equations 4.7 and 4.8 for the no support case, and Equations G.6, G.7 and G.8 for the supported case.

This program is capable of modelling the following conditions:

- The behavior ahead of the tunnel face.
- The effect of a tunnel support.
- Sequentially staged excavations.
- Variable excavation rates.
- Yield zone propagation, according to the method outlined in Appendix H.

C.1 Program Listing

```
CCCCCCCCCCCCCCCCCCCCCCCCCCCCCCCCCCCCCCCCCCCCCCCCCCCCCCCCCCCCCCCCCCCC
CCCCCCCCCCCCCCCCCCCCCCCCCCCCCCCCCCCCCCCCCCCCCCCCCCCCCCCCCCCCCCCCCCC
CCC                                                                CCC
CCC                        "CONRATE"                               CCC
CCC          CALCULATES CONVERGENCE VS TIME                        CCC
CCC          AND NORMALIZED CONVERGENCE RATE                       CCC
CCC          VS TIME CURVES ACCORDING TO THE                       CCC
CCC               CONVERGENCE SOLUTION                             CCC
CCC                                                                CCC
CCCCCCCCCCCCCCCCCCCCCCCCCCCCCCCCCCCCCCCCCCCCCCCCCCCCCCCCCCCCCCCCCCCC
CCCCCCCCCCCCCCCCCCCCCCCCCCCCCCCCCCCCCCCCCCCCCCCCCCCCCCCCCCCCCCCCCCC

      DIMENSION VA(40,3),TI(40),TF(40),BIGT(20),CON(10,300),
     *          CONR(10,300),TT(300),ASTAR(20),TINC(40),
     *          Q1(5),Q2(5),Q(5),TFACE(5),XFACE(5),
     *          XBAR(5),A(5),BIGXP(40),RP(40),CXF(40),
     *          RPC(40),XSUP(5),CS(5),QK(5)
C
C     List of Input Parameters
C
C       NH    - Number of headings in sequential excavation.
C       NP    - Number of parameter sets input.
C       NS    - Number of constant velocity intervals.
C       TOFF  - Offset of initial time.
C       Q1,Q2 - Parameters in Convergence Solution.
C       Q     - Ratio of time-independent convergence
C               of 1st to other headings.
C       TFACE - Time at which face passes monitoring station.
C       XFACE - Position of the monitoring station along
C               the tunnel axis.
C       A     - Radius
C       VA    - Velocity of excavation.
C       TI    - Time at beginning of constant excavation
C               velocity section.
C       TF    - Time at end of constant excavation
C               velocity section.
C       TINC  - Time increment.
C       RP    - Ratio of propagated to non-propagated
C               plastic radius.
C       RPC   - Ratio of propagated to non-propagated CXF
C       BIGXR - R/a
C       BIGT  - T
C       ASTAR - A*
C       TNORM - Convergence rate at this time used to
C               normalize all other rates.
C       FKS   - K
C       F     - Numerical factor for supported tunnel
C               calculation:
C                F = 10. for K<0.002
C                F = 10.-30. for 0.002<K<0.02
C                F = 30. for K>0.02
```

```
C
C      TSUP   - Time of support installation.
C      XSUP   - Position along tunnel axis at which
C               support is installed.
C      QK     - Parameter Qk
C      CXF    - Ultimate Time-independent Convergence.
C
C
C    Read Input Data
C
      READ(5,100)NP,NS,NH,TOFF
  100 FORMAT(3I3,F8.4)
      DO 2 K=1,NH
    2 READ(5,101) Q1(K),Q2(K),Q(K),TFACE(K),
     *             XFACE(K),A(K),CXF(K)
  101 FORMAT(7F8.4)
      DO 3 I=1,NS
      READ(5,102) (VA(I,J),J=1,NH),TI(I),TF(I),TINC(I),
     *             RP(I),RPC(I)
      TI(I) = TI(I) - TOFF
      TF(I) = TF(I) - TOFF
      IF(TI(I).LT.0.) TI(I)=0.
    3 IF(TF(I).LT.0.) TF(I)=0.
  102 FORMAT(8F10.4)
C
      J = 0
    5 JJ = J + 1
      II = 0
      CC = 0.
      CSS = 0.
      CPR = 0.
      READ(5,103)BIGXR,BIGT(JJ),ASTAR(JJ),TNORM,FKS,F,TSUP
      READ(5,104)(XSUP(K),QK(K),K=1,NH)
  103 FORMAT(8F12.5)
  104 FORMAT(2F12.5)
      IF(FKS.GT.0.0) GO TO 6
      TSUP = 1000000.
      DO 4 K=1,NH
      QK(K) = 0.0
    4 XSUP(K) = 1000000.
C
    6 J = J+1
      CNORM = 1.
      IFLAG = -1
    7 T = 0.
      LL = 1
C
      DO 58 M = 1,NS
      TS = TI(M)
      DO 8 K=1,NH
    8 XBAR(K) = 0.
      MM = M-1
      IF(MM.EQ.0) GO TO 11
C
```

```
      DO 9 K=1,NH
      DO 9 I = 1,MM
    9 XBAR(K) = XBAR(K)+VA(I,K)*(TF(I)-TI(I))
C
   11 IF(IFLAG.LT.1) GO TO 20
C
C     Calculates, and Superimposes Convergence
C
   10 CNV = 0.
      DO 30 K=1,NH
C
      BIGX = BIGXR * 0.84 * A(K) *RP(M)
      FT = 1./(1.+T/BIGT(JJ))
      C2 = 1. - FT**0.3
C
C    Pre-Face Convergence
C
      IF(T.GE.TFACE(K))GO TO 21
      FPX = 1./(1.+(XFACE(K)-(XBAR(K)+VA(M,K)*(T-TS)))/BIGX)
      CPF =  FPX**1.2
      FKP = 1./(1.+(XSUP(K) -(XBAR(K)+VA(M,K)*(T-TS)))/BIGX)
      ALPHA = 1. + A(K)/(XSUP(K) -XFACE(K))
      CPKP = FKP**ALPHA
      CXX = (Q1(K)*CPF - CPKP*QK(K)) * CXF(K)
      CT = (Q1(K)*CPF - CPKP*QK(K))*CXF(K)*ASTAR(JJ)*C2
      C = CXX + CT
      GO TO 30
C
C     Post-Face, Pre-Support Convergence
C
   21 FX = 1./(1.+((XBAR(K)+VA(M,K)*(T-TS))-XFACE(K))/BIGX)
      C1 = 1. - FX**2.
      IF(T-TSUP) 23,23,22
   22 IF(TPRE.GE.TSUP) GO TO 24
      T = TSUP
      GO TO 10
   23 FKP = 1./(1.+(XSUP(K) -(XBAR(K)+VA(M,K)*(T-TS)))/BIGX)
      ALPHA = 1. + A(K)/(XSUP(K) -XFACE(K))
      CPKP = FKP**ALPHA
      CXX = (Q1(K) + Q2(K)*C1 - CPKP*QK(K))*CXF(K)
      CT = CXX * ASTAR(JJ) * C2
      C = CXX + CT
      IF(T.NE.TSUP) GO TO 30
      CSS = CSS + C
      CC = CC + C
      GO TO 30
C
C     Post-Support Convergence
C
   24 FKM = 1./(1.+((XBAR(K)+VA(M,K)*(T-TS))-XSUP(K))/BIGX)
      ALPHA = 1. + A(K)/(XSUP(K) - XFACE(K))
      CPKM = FKM**ALPHA
      C = (Q1(K) - CPKM*QK(K) + C1*Q2(K) - FKS*(CC - CSS))
     *     *CXF(K)*(1. + ASTAR(JJ)*C2)
```

```
C
   30 CNV = CNV + C *RPC(M)
C
      IF(T.LE.TSUP.OR.TPRE.LT.TSUP) GO TO 20
      CD = CNV - CC
      IF(CD.GE.CDP) GO TO 20
      CDP = CD
      IF(CD.GT.-0.002.AND.CD.LT.0.002) GO TO 20
      CC = CC+CD/F
      GO TO 10
C
C     Calculates, and Superimposes Convergence Rates
C
   20 CTR = 0.
C
      DO 35 K=1,NH
C
      BIGX = BIGXR * 0.84 * A(K) *RP(M)
      FT = 1./(1.+T/BIGT(JJ))
      C2 = 1. - FT**0.3
      C2P = 0.3/BIGT(JJ)*FT**1.3
C
C    Pre-Face Convergence Rate
C
      IF(T.GE.TFACE(K))GO TO 31
      FPX = 1./(1.+(XFACE(K)-(XBAR(K)+VA(M,K)*(T-TS)))/BIGX)
      CPF =  FPX**1.2
      CPFP = 1.2*VA(M,K)/BIGX*FPX**2.2
      FKP = 1./(1.+(XSUP(K) -(XBAR(K)+VA(M,K)*(T-TS)))/BIGX)
      ALPHA = 1. + A(K)/(XSUP(K) -XFACE(K))
      CPKP = FKP**ALPHA
      CPKPP = VA(M,K)/BIGX*ALPHA*FKP**(ALPHA+1.)
      C = Q1(K)*CPFP + Q1(K)*ASTAR(JJ)*CPFP*C2
     *  + Q1(K)*ASTAR(JJ)*CPF*C2P - QK(K)*CPKPP
     *  - QK(K)*ASTAR(JJ)*CPKPP*C2
     *  - QK(K)*ASTAR(JJ)*CPKP*C2P
      GO TO 35
C
C     Post-Face, Pre-Support Convergence Rate
C
   31 FX = 1./(1.+((XBAR(K)+VA(M,K)*(T-TS))-XFACE(K))/BIGX)
      C1 = 1. - FX**2.
      C1P = 2.*VA(M,K)/BIGX*FX**3.
      IF(T-TSUP) 33,33,32
   32 IF(TPRE.GE.TSUP) GO TO 34
      T = TSUP
      GO TO 20
   33 FKP = 1./(1.+(XSUP(K) -(XBAR(K)+VA(M,K)*(T-TS)))/BIGX)
      ALPHA = 1. + A(K)/(XSUP(K) -XFACE(K))
      CPKP = FKP**ALPHA
      CPKPP = VA(M,K)/BIGX*ALPHA*FKP**(ALPHA+1.)
      C = Q1(K)*ASTAR(JJ)*C2P + Q2(K)*C1P
     *  + Q2(K)*ASTAR(JJ)*C1P*C2 + Q2(K)*C1*C2P*ASTAR(JJ)
     *  - QK(K)*CPKPP - QK(K)*ASTAR(JJ)*CPKPP*C2
```

```
     *  - QK(K)*ASTAR(JJ)*CPKP*C2P
        GO TO 35
C
C     Post-Support Convergence Rate
C
   34 FKM = 1./(1.+((XBAR(K)+VA(M,K)*(T-TS))-XSUP(K))/BIGX)
      ALPHA = 1. + A(K)/(XSUP(K) - XFACE(K))
      CPKM = FKM**ALPHA
      CPKMP = VA(M,K)/BIGX*ALPHA*FKM**(ALPHA+1.)
      C = Q1(K)*ASTAR(JJ)*C2P + Q2(K)*C1P
     *    + Q2(K)*C1*ASTAR(JJ)*C2P
     *    + Q2(K)*C1P*ASTAR(JJ)*C2 + QK(K)*CPKMP
     *    - QK(K)*CPKM*ASTAR(JJ)*C2P
     *    + QK(K)*CPKMP*ASTAR(JJ)*C2
     *    - FKS*CPR*CXF(K) - FKS*CNV*ASTAR(JJ)*C2P
     *    - FKS*CPR*CXF(K)*ASTAR(JJ)*C2
     *    + FKS*CSS*ASTAR(JJ)*C2P
C
   35 CTR = CTR + C/CNORM*Q(K)*RPC(M)
C
      IF(T.NE.TSUP) GO TO 17
      CPR = CTR*CNORM
      GO TO 40
   17 IF(T.LE.TSUP.OR.TPRE.LT.TSUP) GO TO 40
      CD = CPR - CTR*CNORM
      IF(CD.GE.CDD) GO TO 40
      CDD = CD
      IF(CD.GT.-0.000000001.AND.CD.LT.0.000000001) GO TO 40
      CPR = CPR-CD/F
      GO TO 20
C
   40 CDD = 1000.
      CDP = 1000.
      IF(IFLAG) 50,46,48
   46 IF(LL.EQ.2) GO TO 48
      CNORM = CTR
      IFLAG = 1
      GO TO 7
C
   48 II = II+1
      CONR(J,II) = CTR
      CON(J,II) = CNV
      TT(II) = T+TOFF
   50 IF(LL.EQ.2) GO TO 58
      TPRE = T
      T= T+TINC(M)
      IF(T.GT.TFACE(K).AND.TPRE.LT.TFACE(K)) T=TFACE(K)
      IF(IFLAG) 52,54,54
   52 IF(T.LT.TNORM) GO TO 54
      T = TNORM
      IFLAG = 0
   54 IF(T.LT.TF(M)) GO TO 11
      LL = 2
      T = TF(M)
```

```
      GO TO 11
C
   58 LL = 1
C
C    OUTPUT FOR PLOTTING ON DEVICES #6 & #7
C
C    DEVICE #6 - CONVERGENCE VS TIME PLOT
C    DEVICE #7 - NORMALIZED CONVERGENCE RATE
C                VS TIME PLOT
C    OUTPUT IS IN THE FORMAT ACCEPTED BY
C    THE PLOTTING ROUTINE PLOTIT
C
      NDATA = II
      WRITE(6,200) NDATA
  200 FORMAT(I3,',')
      WRITE(6,202) (TT(I),CON(J,I),I=1,NDATA)
  202 FORMAT(F8.2,',',F11.6,',')
      WRITE(7,200) NDATA
      WRITE(7,203) (TT(I),CONR(J,I),I=1,NDATA)
  203 FORMAT(F8.2,',',F13.9,',')
C
C     OUTPUT TABLE OF ALL VALUES
C
      WRITE(8,500)BIGXR,BIGT(JJ),ASTAR(JJ)
  500 FORMAT('1'/' Calculation of Convergence Solution'/
     *       ' for the following parameters:'//
     *' R/a = ',F5.3,3X,'T = ',F5.3,3X,'A* = ',F5.3//)
      WRITE(8,501)
  501 FORMAT('    Time    Convergence     Normalized'/
     *       '   (days)      (mm)      Convergence Rate'/)
      DO 60 L=1,NDATA
   60 WRITE(8,503)TT(L),CON(J,L),CONR(J,L)
  503 FORMAT(1X,F8.3,2X,F11.5,5X,F11.7)
C
      IF(J.LT.NP) GO TO 5
C
      STOP
      END
```

C.2 Sample Input

The sample input file listed below contains the following conditions:

a = 5.0m; advance velocity = 5.0m/day;

face at t=2.0 days; liner installed at 3.0 days;

R/a = 1.0; T=1.0 days; A^*=1.0; $C_{x\infty}$=100.0mm

Q_1 = 0.27; Q_2 = 0.73;

Support Stiffness, K = 0.010/mm; Q_k = 0.05;

Numerical Factor, F = 15.;

Convergence rates are normalized to $\dot{C}$(face);

There is no yield zone , and there is no yield zone propagation at a later stage.

The format required for input into Device #5 is as follows:

```
1,1,1,0.0,
0.27,0.73,1.0,2.0,10.0,5.0,100.0,
5.0,0.0,10.0,0.5,1.0,1.0,
1.0,1.0,1.0,2.0,0.0100,15.,3.0,
15.0,0.050,
```

C.3 Sample Output

The output table from Device #8 is as follows:

Calculation of Convergence Solution
for the following parameters:

R/a = 1.000 T = 1.000 A* = 1.000

Time (days)	Convergence (mm)	Normalized Convergence Rate
0.0	6.01992	0.0193971
0.500	8.44855	0.0253095
1.000	11.99578	0.0404739
1.500	18.32201	0.0797523
2.000	33.24631	1.0000000
2.500	91.07471	0.2531484
3.000	106.93271	0.0455386
3.500	112.80774	0.0350459
4.000	115.78442	0.0204822
4.500	117.65512	0.0138059
5.000	118.97244	0.0101458
5.500	119.96948	0.0079007
6.000	120.76233	0.0064107
6.500	121.41557	0.0053621
7.000	121.96840	0.0045899
7.500	122.44600	0.0040004
8.000	122.86530	0.0035373
8.500	123.23813	0.0031645
9.000	123.57349	0.0028586
9.500	123.87769	0.0026032
10.000	124.15549	0.0023870

Devices 6 and 7 contain convergence and normalized convergence rate vs time curves, respectively, that are in the format for the plotting routine "PLOTIT".

APPENDIX D

Excavation Steps in Finite Element Analyses

The procedure that was followed in the steps of each of the finite element analyses presented in Chapter three are summarized in this section. A diagram of the mesh is given in Fig. D.1 to aid in the description of the excavation steps. This is an enlargement of a portion of the complete mesh shown in Fig. 3.4.

There is an end effect at the left side boundary that has an influence on the convergence results up to Column 8, shown in Fig. D.1. Thus, only the convergence from Column 9 on is valid. This corresponds to a distance after the face of three radii. It is desirable to extend the range of valid results to at least four radii after the face, to model as much of the near face behavior as possible. This can be accomplished by excavating up to column 19. However, the optimum position of the face is at column 16, where the finest portion of the mesh models the region immediately after the face.

The procedure outlined below satisfies these two criteria, producing valid convergence results up to a distance of 4.5 radii from the face, and positioning the face at Column 16 (Station 0).

The final convergence results that have been used to produce the convergence curves in Appendix E are composed of the following components:

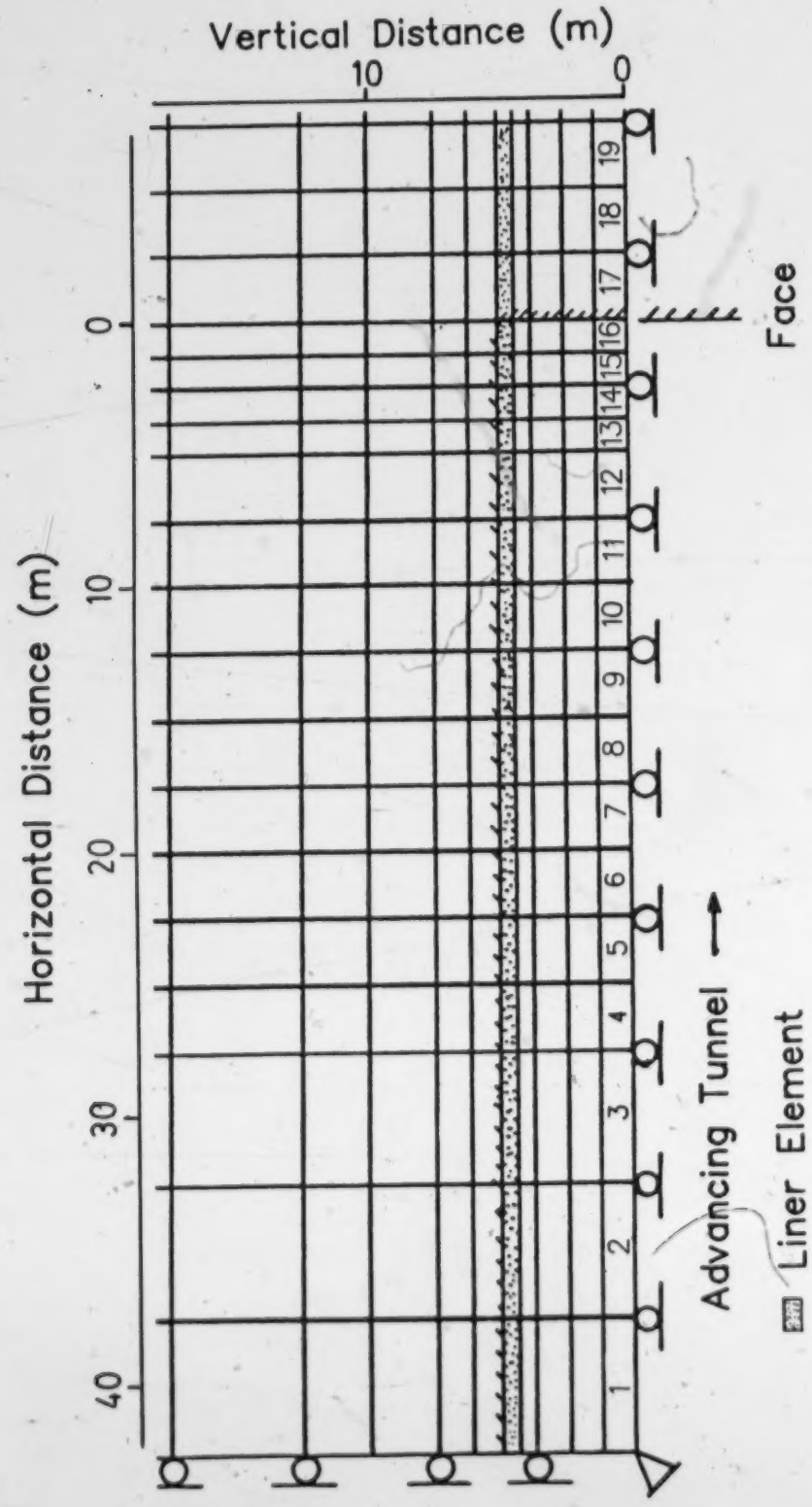

Figure D.1 Portion of Finite Element Mesh.

- The convergence from ahead of the face to 3.0 radii after the face is given by Columns 9 to 21 (not shown in Fig B.1) when the face is at Station 0.
- The convergence from 3.0 to 3.5 radii after the face is given by the convergence of Column 9 when the face is at Station -2.5.
- The convergence from 3.5 to 4.0 radii after the face is given by the convergence of Column 9 when the face is at Station -5.0.
- The convergence from 4.0 to 4.5 radii after the face is given by the convergence of Column 9 when the face is at Station -7.5.

This procedure was followed for each of the analyses, to extend the valid range of convergence results to 4.5 radii after the face. The sequences of excavation and lining placement for each of the cases analyzed are outlined separately below.

Unlined Tunnel

Step 1: Apply a pressure of 12.5 MPa to the top and left side boundaries.

Step 2: Change the left side and top boundaries from no displacement restrictions to no horizontal displacements permitted.

Step 3:* Excavate elements within the tunnel from Columns 1 to 16.

Step 4: Excavate elements in Column 17.

Step 5: Excavate elements in Column 18.

Step 6: Excavate elements in Column 19.

* The convergence results are derived from the position of the face at this step.

Lined Tunnel; Support Delay of 0.25 Radii.

Step 1: Apply a pressure of 12.5 MPa to the top and left side boundaries.

Step 2: Change the left side and top boundaries from no displacement restrictions to no horizontal displacements permitted.

Step 3: Excavate elements in Column 1.

Step 4: Excavate elements in Column 2 and activate liner element in Column 1.

Step 5: Excavate elements in Column 3 and activate liner element in Column 2.

and so on, until: Step 14:

Excavate elements in Column 12 and activate liner element in Column 11.

Step 15: Excavate elements in Columns 13 and 14, and activate liner element in Column 12.

Step 16:* Excavate elements in Columns 15 and 16, and activate liner element in Columns 13 and 14.

Step 17: Excavate elements in Column 17 and activate liner element in Columns 15 and 16.

Step 18: Excavate elements in Column 18 and activate liner element in Column 17.

Step 19: Excavate elements in Column 19 and activate liner element in Column 18.

* The convergence results are derived from the position of the face at this step.

Lined Tunnel; Support Delay of 0.75 Radii.

Step 1: Apply a pressure of 12.5 MPa to the top and left side boundaries.

Step 2: Change the left side and top boundaries from no displacement restrictions to no horizontal displacements permitted.

Step 3: Excavate elements in Column 1.

Step 4: Excavate elements in Column 2 and activate liner element in Column 1.

Step 5: Excavate elements in Column 3 and activate liner element in Column 2.

and so on, until: Step 13:

Excavate elements in Column 12 and activate liner element in Column 10.

Step 14: Excavate elements in Columns 13 and 14, and activate liner element in Column 11.

Step 15:* Excavate elements in Columns 15 and 16, and activate liner element in Column 12.

Step 16: Excavate elements in Column 17 and activate liner

element in Columns 13 and 14.

Step 17: Excavate elements in Column 18 and activate liner element in Columns 15 and 16.

Step 18: Excavate elements in Column 19 and activate liner element in Column 17.

* The convergence results are derived from the position of the face at this step.

Lined Tunnel; Support Delay of 1.25 Radii.

Step 1: Apply a pressure of 12.5 MPa to the top and left side boundaries.

Step 2: Change the left side and top boundaries from no displacement restrictions to no horizontal displacements permitted.

Step 3: Excavate elements in Columns 1 and 2.

Step 4: Excavate elements in Column 3 and activate liner element in Column 1.

Step 5: Excavate elements in Columns 4 and 5, and activate liner element in Column 2.

Step 6: Excavate elements in Column 6 and activate liner element in Column 3.

Step 7: Excavate elements in Column 7 and activate liner element in Column 4.

and so on, until: Step 12:

Excavate elements in Column 12 and activate liner element in Column 9.

Step 13: Excavate elements in Columns 13 and 14, and activate liner element in Column 10.

Step 14:* Excavate elements in Columns 15 and 16, and activate liner element in Column 11.

Step 15: Excavate elements in Column 17 and activate liner element in Column 12.

Step 16: Excavate elements in Column 18 and activate liner element in Columns 13 and 14.

Step 17: Excavate elements in Column 19 and activate liner element in Columns 15 and 16.

* The convergence results are derived from the position of the face at this step.

Lined Tunnel; Support Delay of 1.75 Radii.

Step 1: Apply a pressure of 12.5 MPa to the top and left side boundaries.

Step 2: Change the left side and top boundaries from no displacement restrictions to no horizontal displacements permitted.

Step 3: Excavate elements in Columns 1 and 2.

Step 4: Excavate elements in Column 3 and activate liner element in Column 1.

Step 5: Excavate elements in Columns 4, 5 and 6, and activate liner element in Column 2.

Step 6: Excavate elements in Column 7 and activate liner element in Column 3.

Step 7: Excavate elements in Column 8 and activate liner element in Column 4.

and so on, until: Step 11:

Excavate elements in Column 12 and activate liner element in Column 8.

Step 12: Excavate elements in Columns 13 and 14, and activate liner element in Column 9.

Step 13: Excavate elements in Columns 15 and 16, and activate liner element in Column 10.

Step 14:* Excavate elements in Column 17 and activate liner element in Column 11.

Step 15: Excavate elements in Column 18 and activate liner element in Column 12.

Step 16: Excavate elements in Column 19 and activate liner element in Columns 13 and 14.

* The convergence results are derived from the position of the face at this step.

APPENDIX E

Convergence Curves from Finite Element Analyses

The convergence curves produced by the finite element analyses of the five lined tunnel cases presented in Chapter three are given in Figs E.1 to E.5. Each of these figures shows the data points connected by the solid lines for the unlined tunnel, and four different support delays for the lined tunnel. The dashed curves are visually fitted smoothed curves that approximate each of the cases. Figures E.6 to E.10 contain only the smoothed curves of the five lined tunnel cases presented in Figs E.1 to E.5.

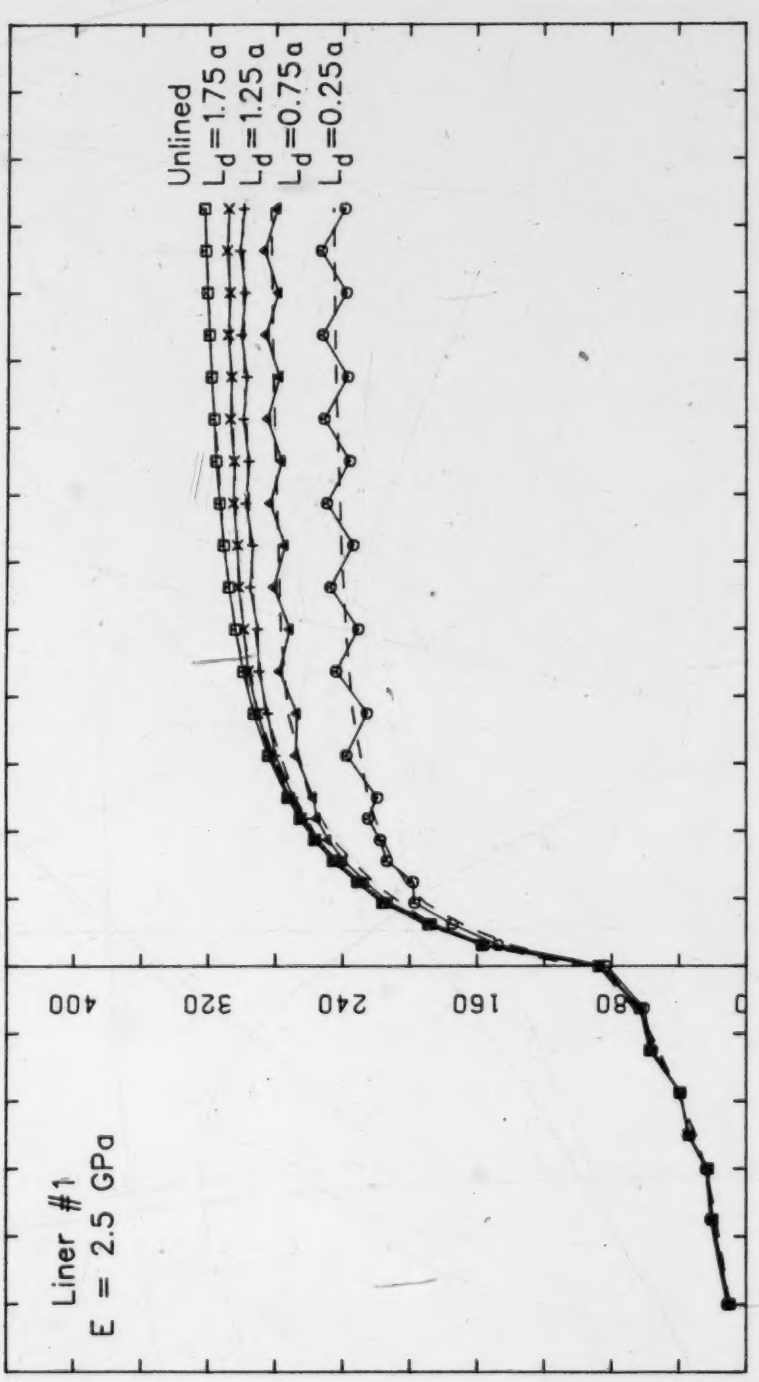

Figure E.1 Convergence Curves from Finite Element Analysis; Liner #1.

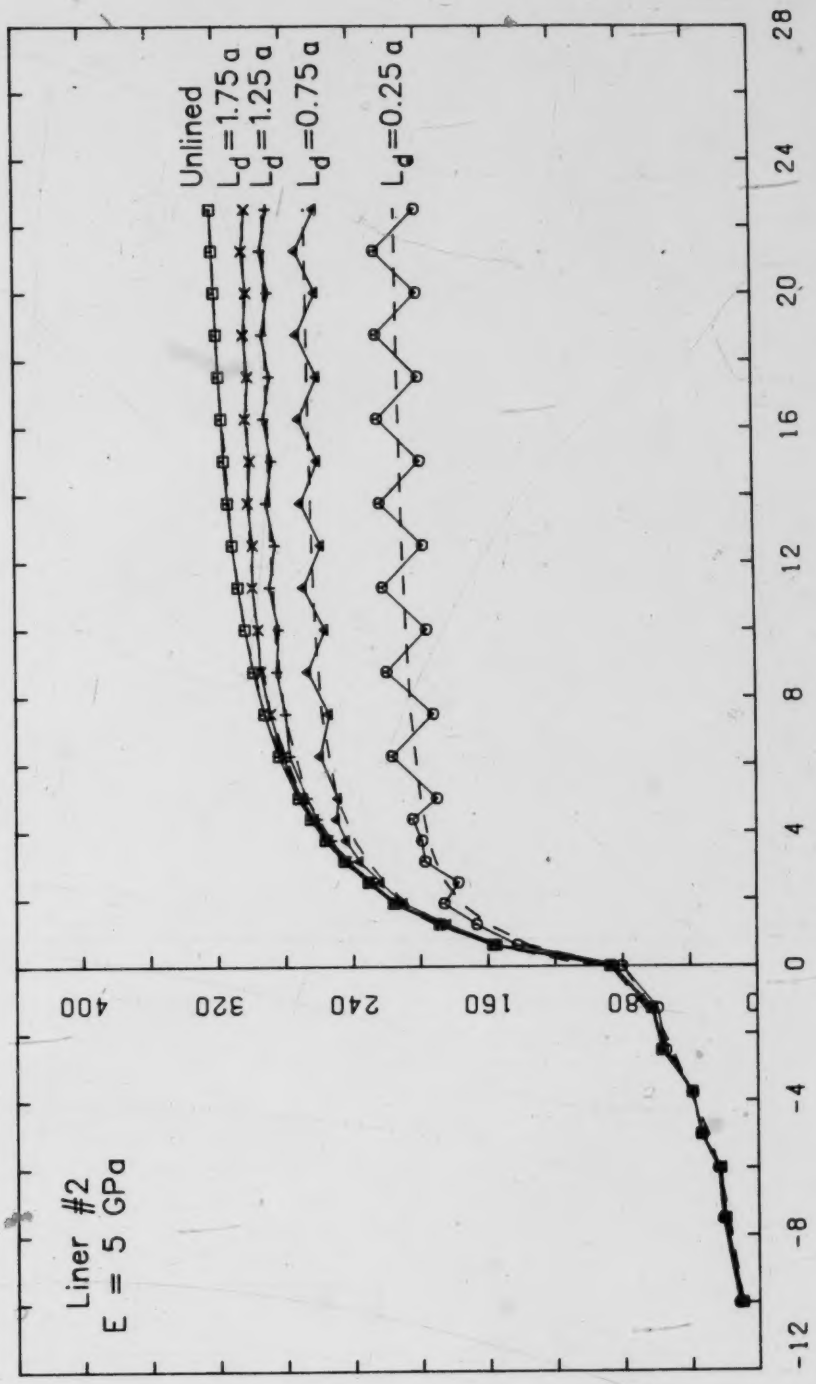

Figure E.2 Convergence Curves from Finite Element Analysis; Liner #2.

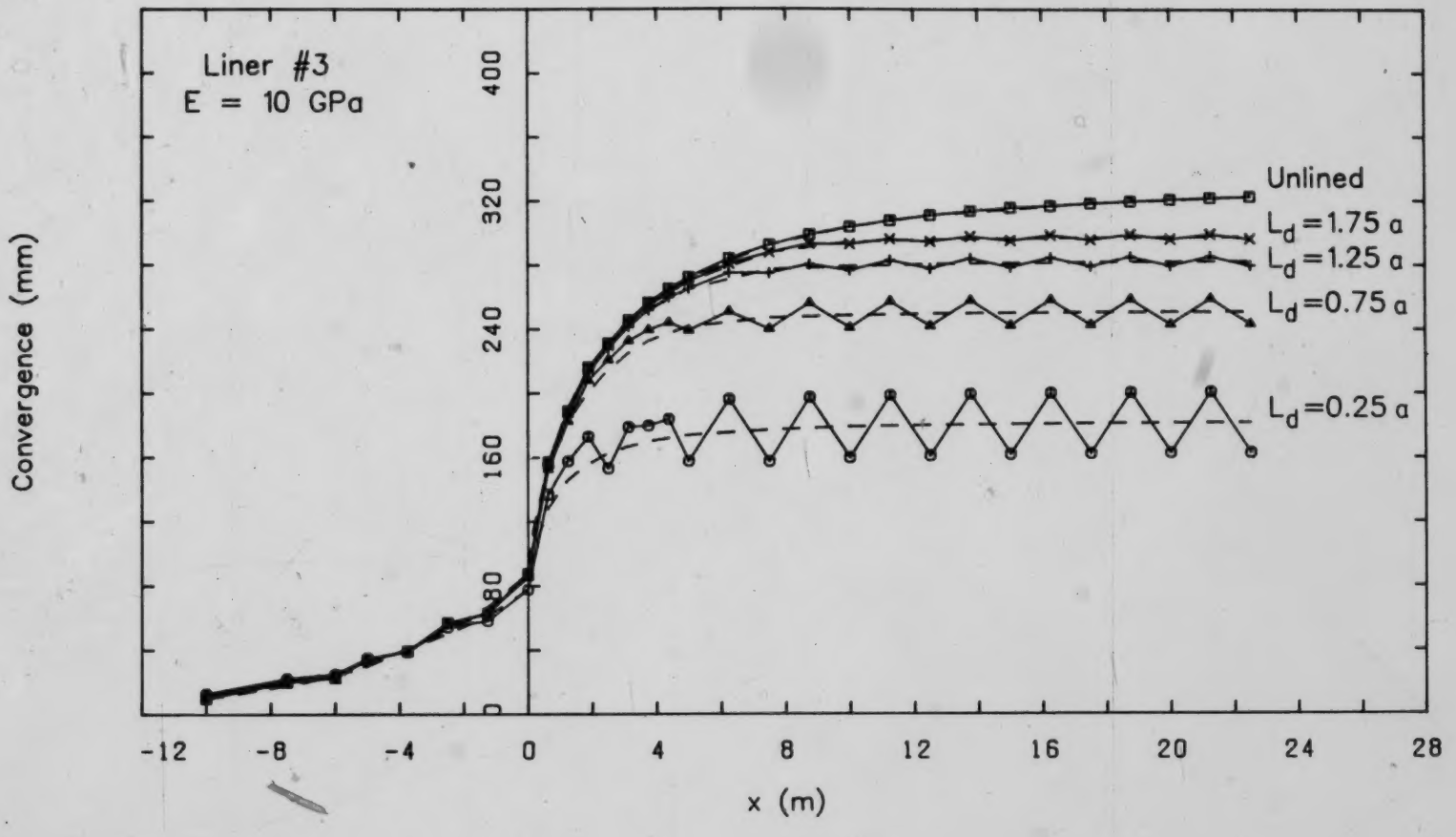

Figure E.3 Convergence Curves from Finite Element Analysis; Liner #3.

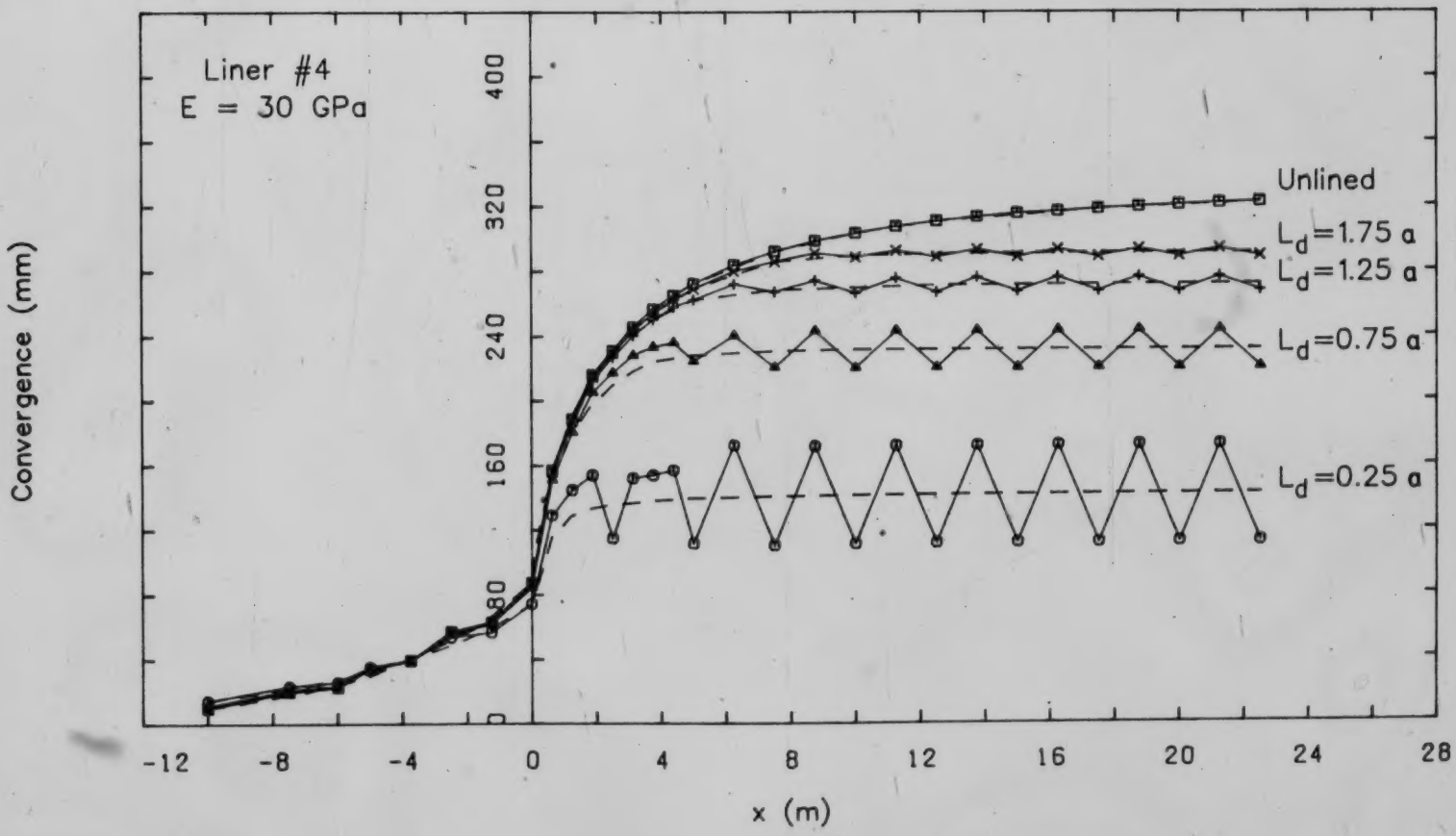

Figure E.4 Convergence Curves from Finite Element Analysis; Liner #4.

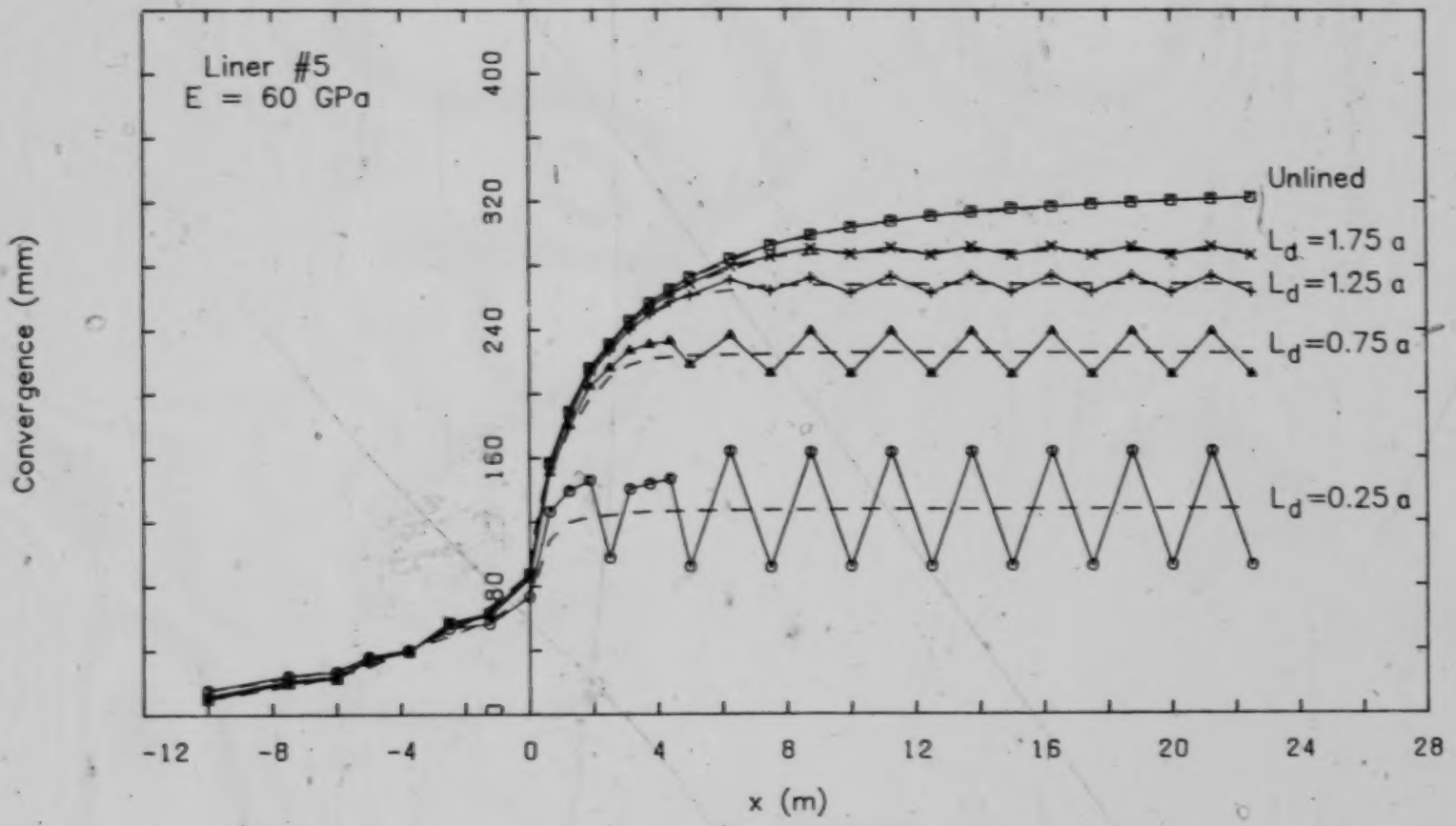

Figure E.5 Convergence Curves from Finite Element Analysis; Liner #5.

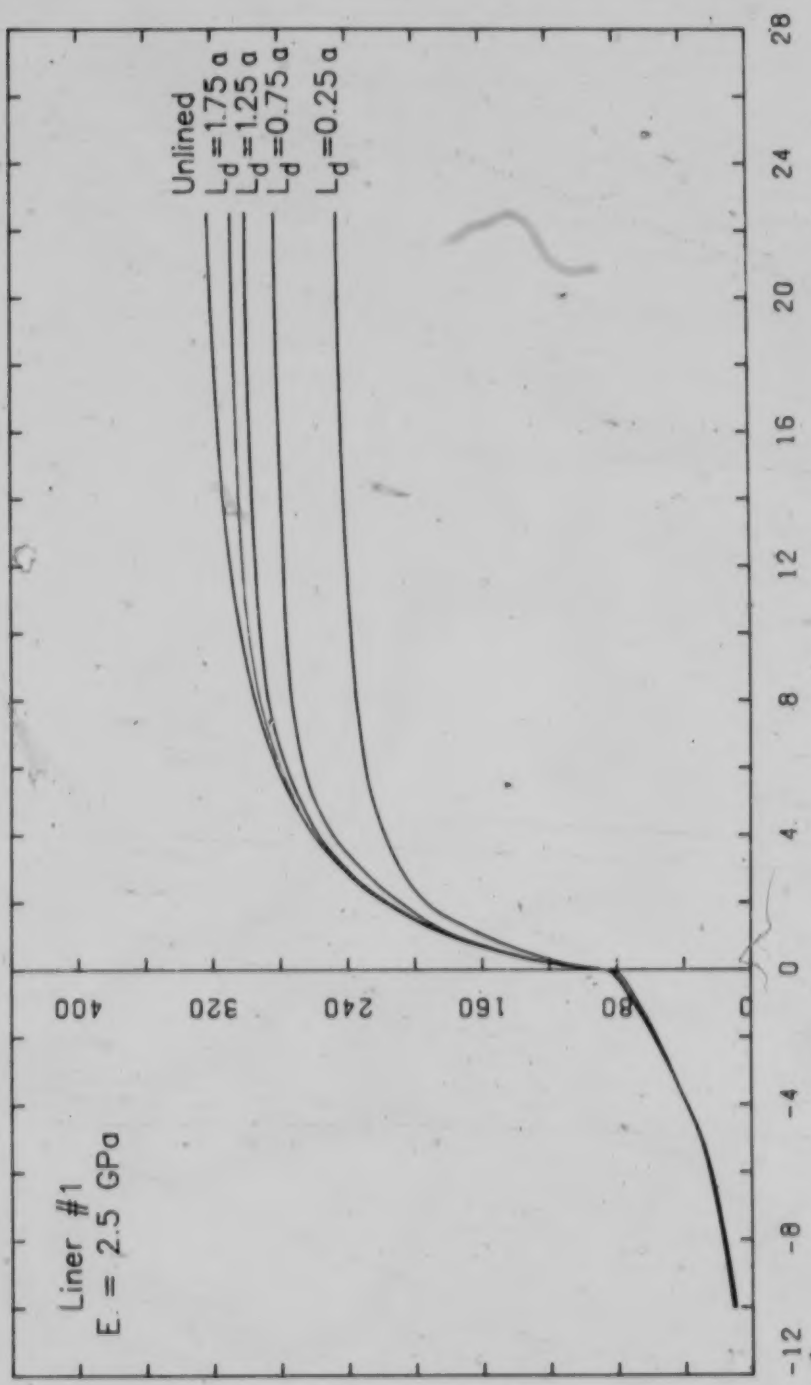

Figure E.6 Smoothed Convergence Curves based on Finite Element Analysis; Liner #1.

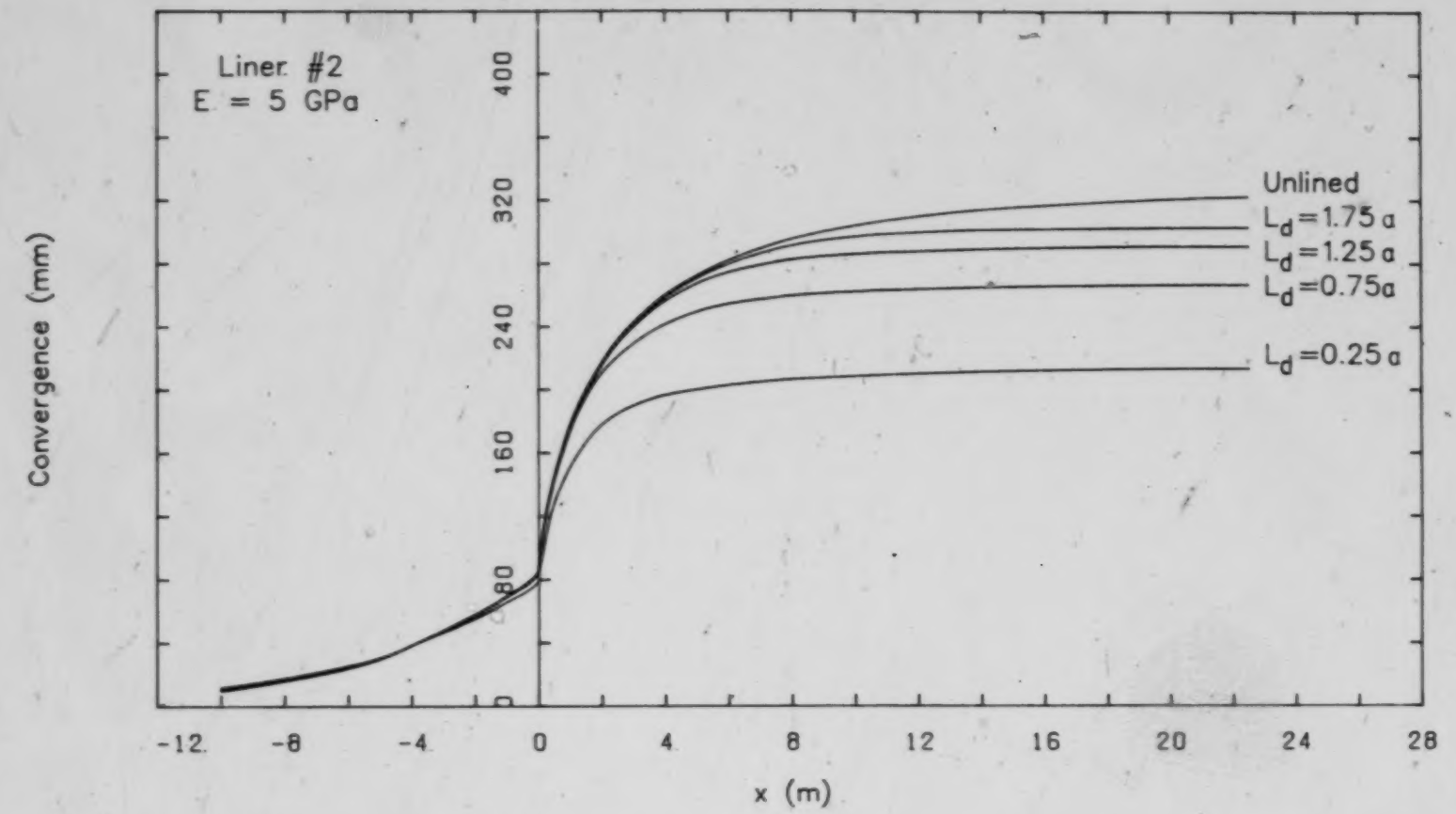

Figure E.7 Smoothed Convergence Curves based on Finite Element Analysis; Liner #2.

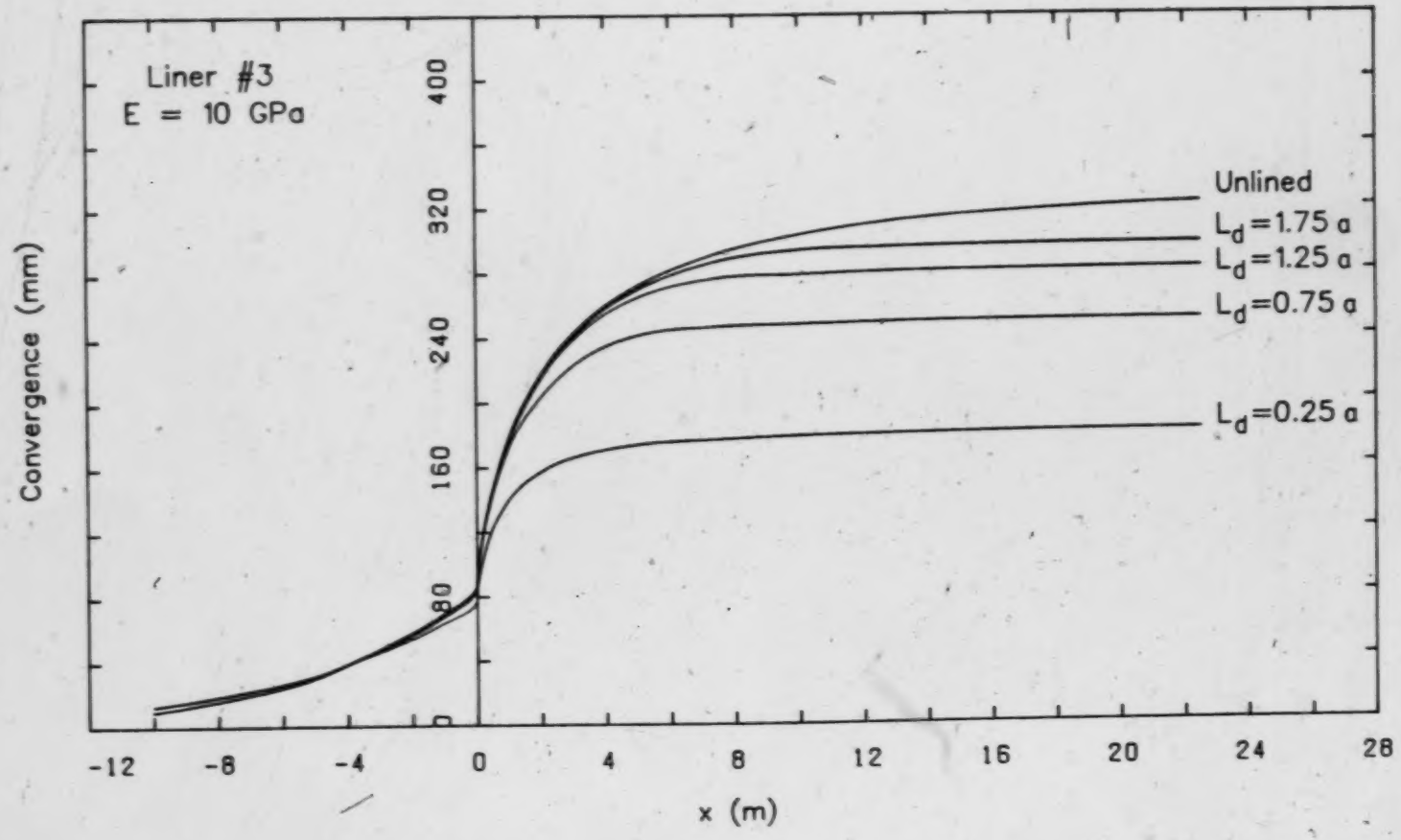

Figure E.8 Smoothed Convergence Curves based on Finite Element Analysis; Liner #3.

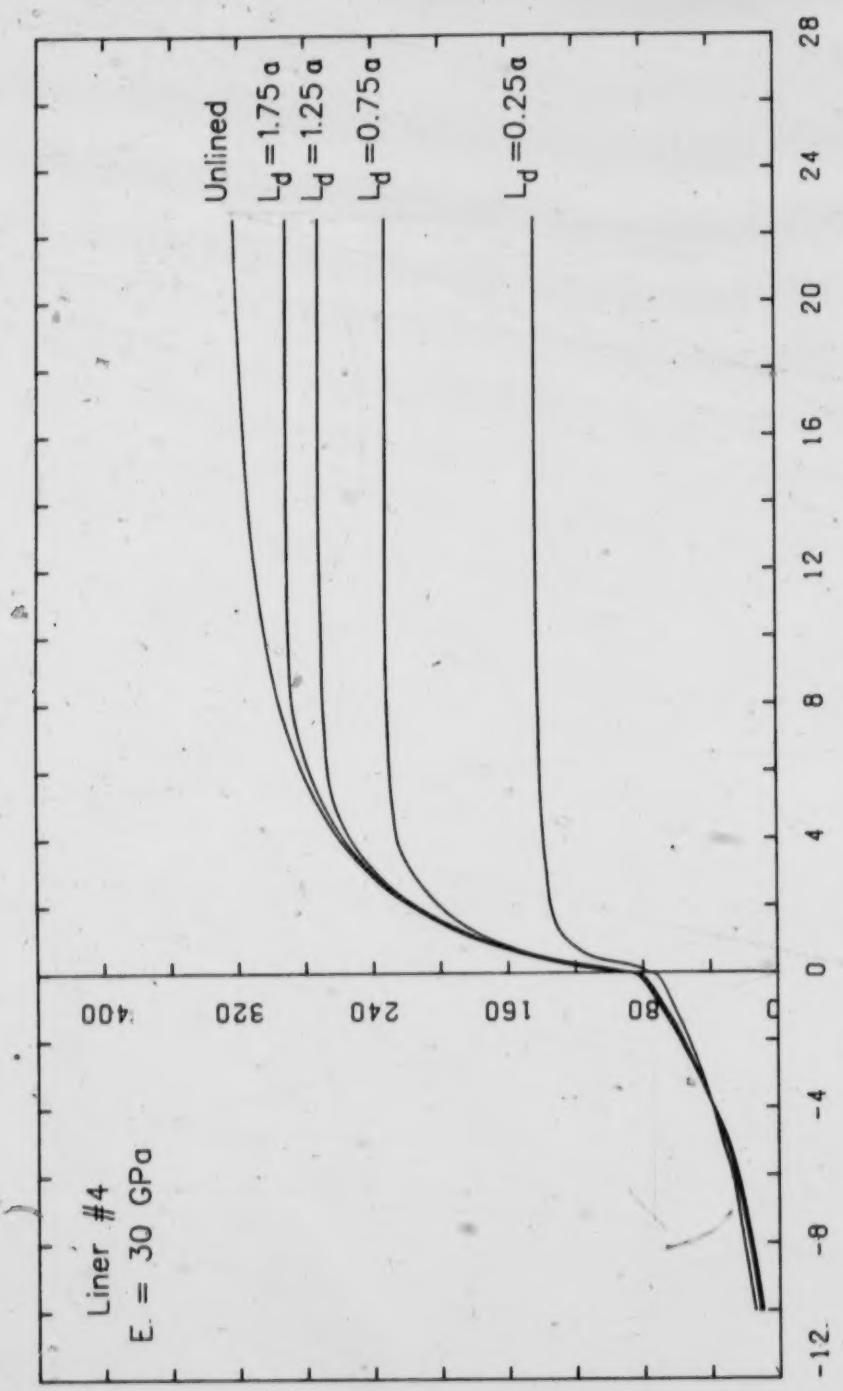

Figure E.9 Smoothed Convergence Curves based on Finite Element Analysis; Liner #4.

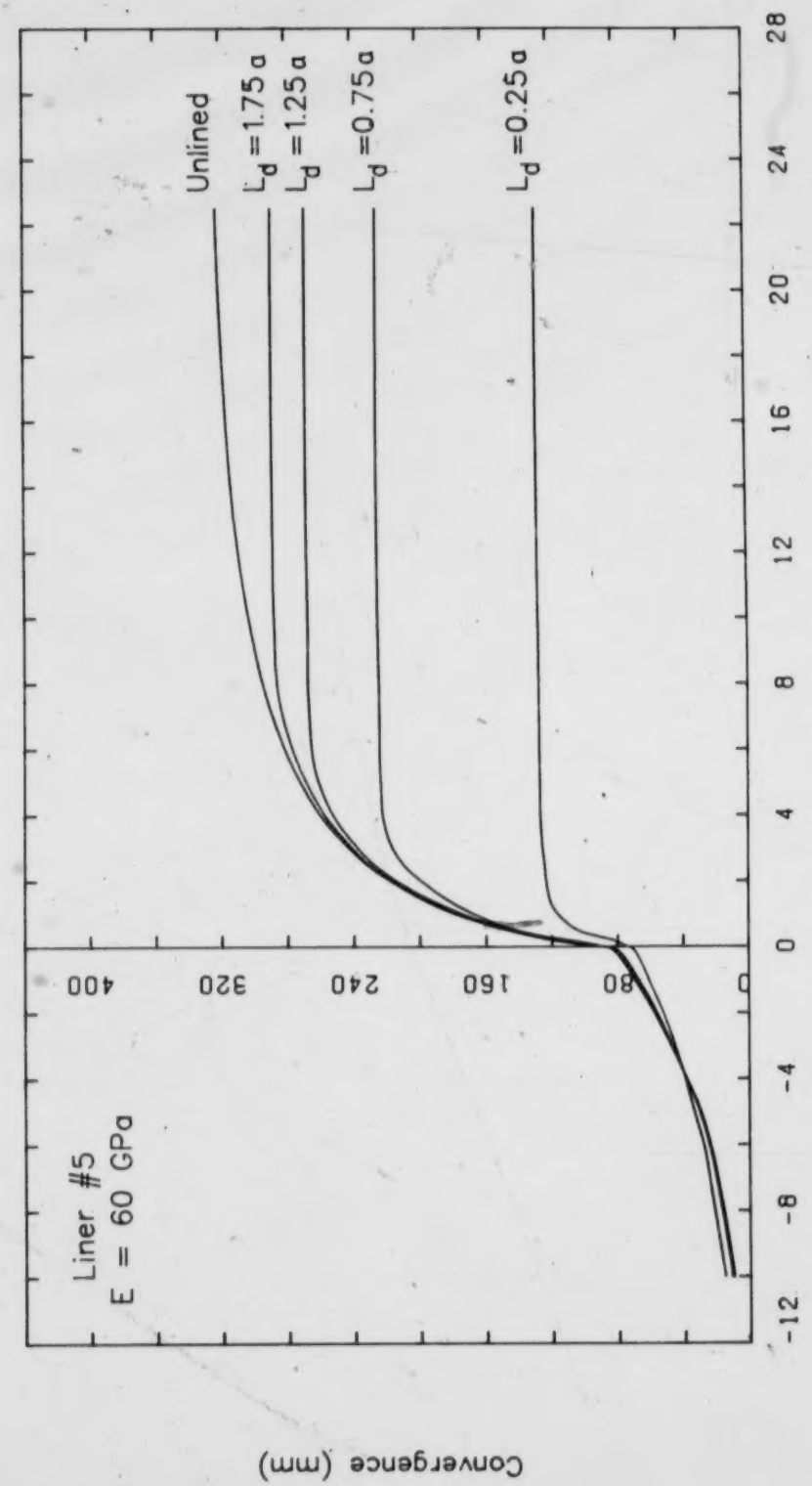

Figure E.10 Smoothed Convergence Curves based on Finite Element Analysis; Liner #5.

APPENDIX F

Plots of Radial Strain vs Time; Excavation Simulation Test 7.13

The radial strain vs time plots for two of the measuring stations of Test MC-7.13 are contained here. Figures F.1 and F.2 display the radial strain curves for the extensometers of Station 81. The results from station 106 are given in Figs F.3 and F.4.

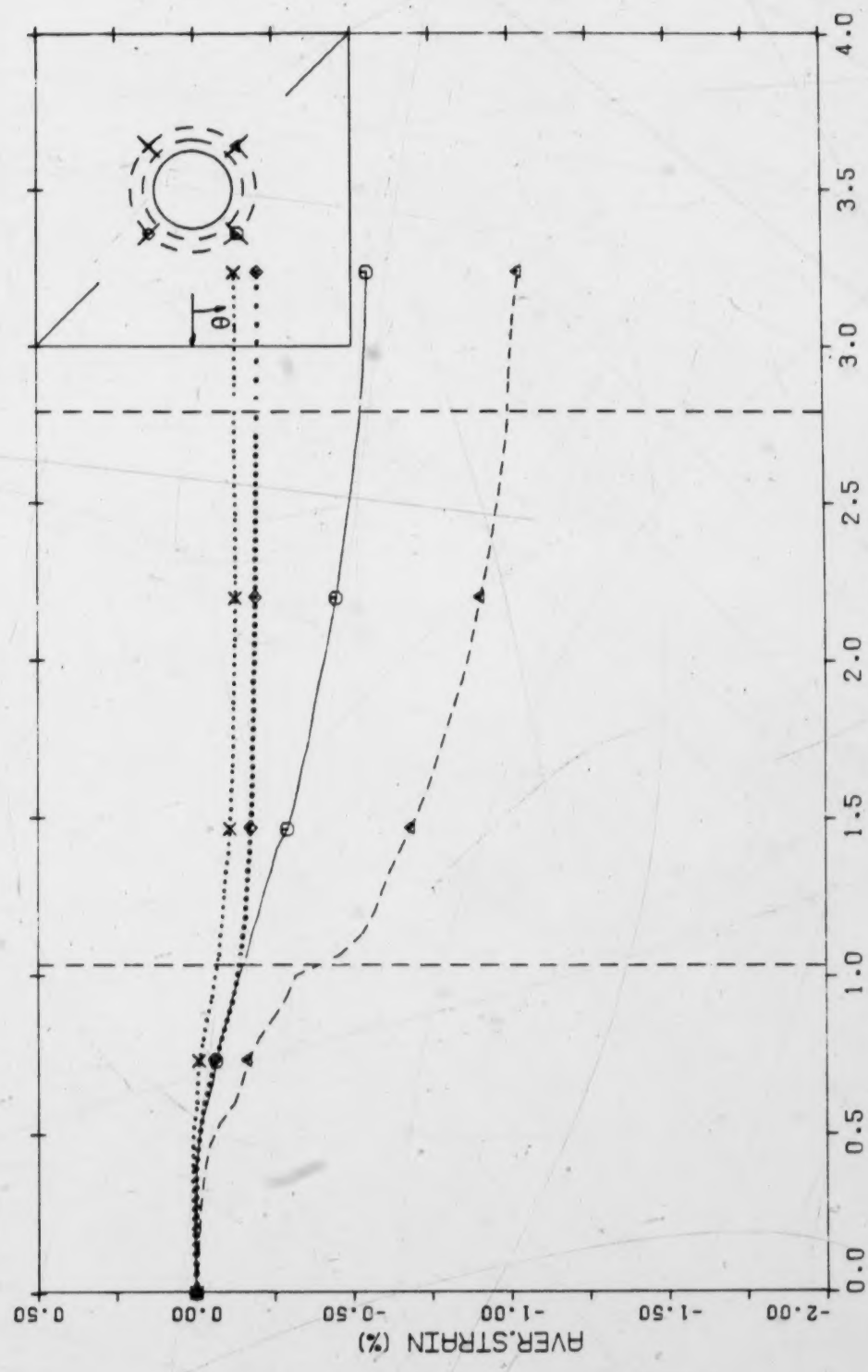

Figure F.1 Radial Strain vs Time - Test MC-7.13; Station 81 (Maloney, 1984).

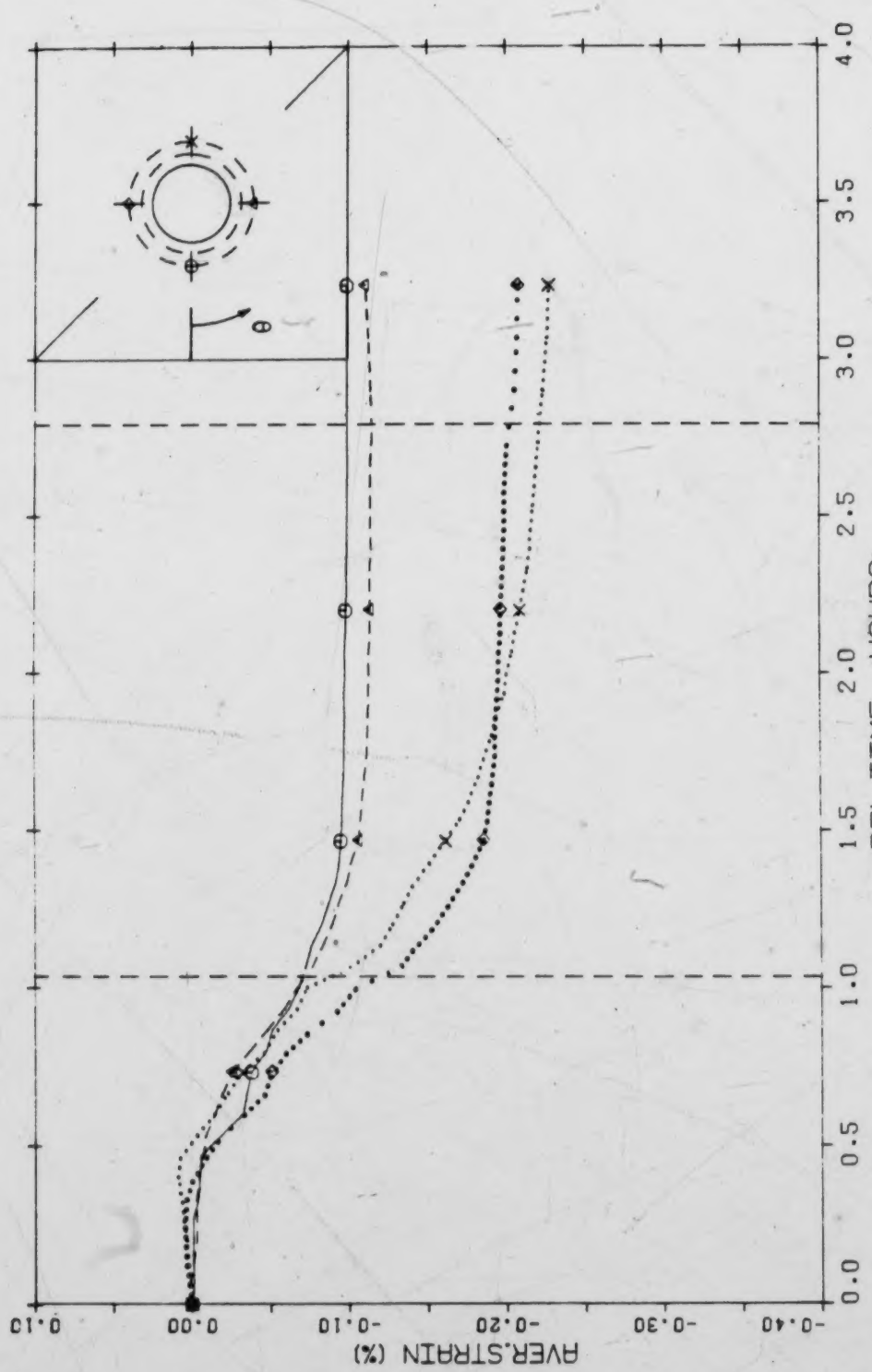

Figure F.2 Radial Strain vs Time - Test MC-7.13; Station 81 (Maloney, 1984).

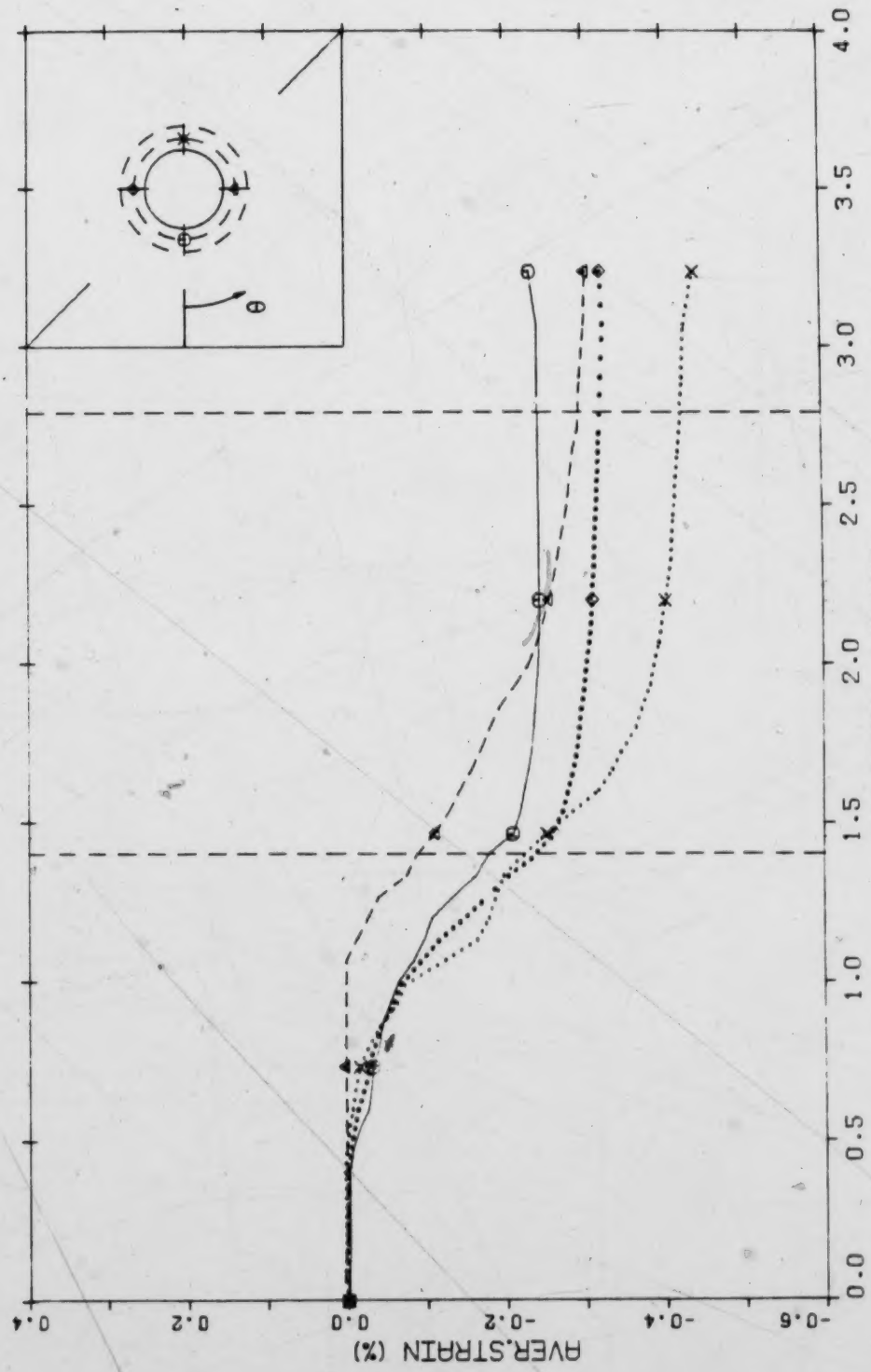

Figure F.3 Radial Strain vs Time - Test MC-7.13; Station 106 (Maloney, 1984).

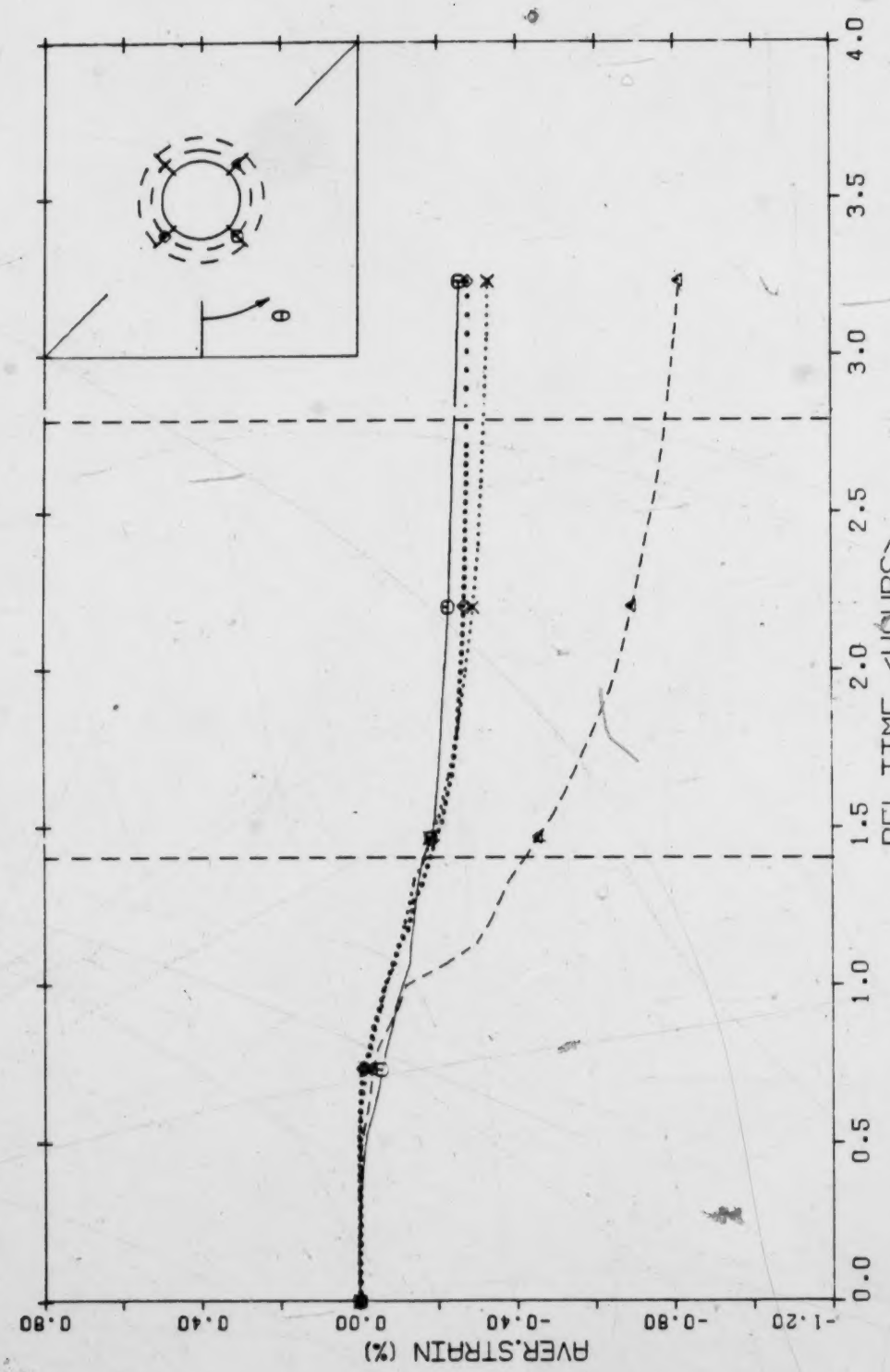

Figure F.4 Radial Strain vs Time - Test MC-7.13; Station 106 (Maloney, 1984).

APPENDIX G

Adaptation of Convergence Solultion for a Supported Tunnel.

The method of adapting the Convergence Solution for a supported tunnel from expressing convergence to expressing normalized convergence rate is summarized below. The purpose of this exercize is to adapt the Solution to fit data presented in the normalized convergence rate format. A similar manipultaion for an unsupported tunnel is given in Chapter four. The Convergence Solution for the supported case is given by Eqns 3.8, 3.9 and 3.11. There are three steps involved in converting these equations from predicting convergence to predicting normalized convergence rate.

First, they must be expressed as a function of time alone. This is accomplished by substituting v*t (velocity*time) for x. If the excavation does not proceed with constant velocity, it must be divided into a series of constant velocity intervals. In this case, the following substitution would be required:

$$x = \bar{x}_{n-1} + v_n t \qquad \text{Eqn 4.2.}$$

where: $\bar{x}_{n-1} = \sum_{i=1}^{n-1} + v_i t_i$

v_i = velocity of i^{th} constant velocity interval.

t_i = time at end of i^{th} interval.

This gives the position of the face in the n^{th} constant velocity interval as a function of time.

Second, these equations must be converted from convergence to convergence rates. This is accomplished by taking the first derivitive with respect to time, as follows:

- Pre-face equation:

$$\dot{C}(t) = \frac{dC(t)}{dt} = Q_1\dot{C}_{pf}(t)C_{x\infty} + Q_1\dot{C}_{pf}(t)AC_2(t) + Q_1C_{pf}(t)A\dot{C}_2(t) - Q_k\dot{P}_{k+}(t)C_{x\infty} - Q_k\dot{P}_{k+}(t)AC_2(t) - Q_kP_{k+}(t)A\dot{C}_2(t) \qquad \text{Eqn G.1}$$

- Post-face, pre-support equation:

$$\dot{C}(t) = \frac{dC(t)}{dt} = Q_1A\dot{C}_2(t) + Q_2\dot{C}_1(t)C_{x\infty} + Q_2\dot{C}_1(t)AC_2(t) + Q_2C_1(t)A\dot{C}_2(t) - Q_k\dot{P}_{k+}(t)C_{x\infty} - Q_k\dot{P}_{k+}(t)AC_2(t) - Q_kP_{k+}(t)A\dot{C}_2(t) \qquad \text{Eqn G.2}$$

- Post-support equation:

$$\dot{C}(t) = Q_1A\dot{C}_2(t) + Q_2\dot{C}_1(t)C_{x\infty}$$

$$+ Q_2 C_1(t)\dot{AC}_2(t) + Q_2\dot{C}_1(t)AC_2(t) + Q_k\dot{P}_{k-}(t)C_{x\infty}$$

$$- Q_k P_{k-}(t)\dot{AC}_2(t) + Q_k\dot{P}_{k-}(t)AC_2(t) - K\dot{C}(t)C_{x\infty}$$

$$-KC(t)\dot{AC}_2(t) - K\dot{C}(t)AC_2(t) + K\dot{AC}_2(t)C_s \qquad \text{Eqn G.3}$$

where: $$C_{pf}(t) = \left[\frac{1}{1 + \left[\frac{x_f - (\bar{x}+vt)}{X}\right]}\right]^{1.2}$$

$$\dot{C}_{pf}(t) = \frac{1.2v}{X}\left[\frac{1}{1 + \left[\frac{x_f - (\bar{x}+vt)}{X}\right]}\right]^{2.2}$$

$$C_1(t) = 1 - \left[\frac{1}{1 + \left[\frac{(\bar{x}+vt) - x_f}{X}\right]}\right]^{2}$$

$$\dot{C}_1(t) = \frac{2v}{X}\left[\frac{1}{1 + \left[\frac{(\bar{x}+vt) - x_f}{X}\right]}\right]^{3}$$

$$\dot{C}_2(t) = \frac{0.3}{T}\left[\frac{1}{1 + \frac{t}{T}}\right]^{1.3}$$

$$P_{k+}(t) = \left[\frac{1}{1 + \left[\frac{x_s - (x+vt)}{X}\right]}\right]^{a}$$

$$\dot{P}_{k+}(t) = \frac{v}{X}a \left[\frac{1}{1 + \left[\frac{x_s - (x+vt)}{X}\right]}\right]^{a+1}$$

$$P_{k-}(t) = \left[\frac{1}{1 + \left[\frac{(x+vt) - x_s}{X}\right]}\right]^{a}$$

$$\dot{P}_{k-}(t) = -\frac{v}{X}a \left[\frac{1}{1 + \left[\frac{(x+vt) - x_s}{X}\right]}\right]^{a+1}$$

The final step is to normalize both equations to the maximum convergence rate; the maximum rate occurs at the face in the second equation. Substituting $t=t_f$ into Eqn G.2:

$$\dot{C}_{max} = \frac{2Q_2 v}{X} C_{x\infty} + \frac{2Q_2 v}{X} AC_2(t_f) + Q_1 \dot{AC}_2(t_f)$$
$$- Q_k \dot{P}_{k+}(t_f) C_{x\infty} - Q_k \dot{P}_{k+}(t_f) AC_2(t_f)$$
$$- Q_k P_{k+}(t_f) \dot{AC}_2(t_f) \qquad \text{Eqn G.4}$$

The magnitude can be factored out of this equation as follows:

$$\dot{C}_{max} = C_{x\infty}[\frac{2Q_2v}{X} + \frac{2Q_2v}{X} A^*C_2(t_f) + Q_1A^*\dot{C}_2(t_f)$$
$$- \frac{Q_k}{Q_2}\dot{P}_{k+}(t_f) - \frac{Q_k}{Q_2}\dot{P}_{k+}(t_f)A^*C_2(t_f)$$
$$- \frac{Q_k}{Q_2}P_{k+}(t_f)A^*\dot{C}_2(t_f)$$
$$= C_{x\infty} \times M \qquad \text{Eqn G.5.}$$

where: $A^* = \frac{A}{C_{x\infty}}$

Normalizing equations G.1, G.2 and G.3 to Eqn G.5 yields:

- Pre-face equation:

$$\frac{\dot{C}(t)}{\dot{C}_{max}} = \frac{Q_1}{M}[\dot{C}_{pf}(t) + \dot{C}_{pf}(t)A^*C_2(t)$$
$$+ C_{pf}(t)A^*\dot{C}_2(t) - \frac{Q_k}{Q_1}\dot{P}_{k+}(t) - \frac{Q_k}{Q_1}\dot{P}_{k+}(t)A^*C_2(t)$$
$$- \frac{Q_k}{Q_1}P_{k+}(t)A^*\dot{C}_2(t)] \qquad \text{Eqn G.6}$$

- Post-face, pre-support equation:

$$\frac{\dot{C}(t)}{\dot{C}_{max}} = \frac{Q_2}{M}[\frac{Q_1}{Q_2}A^*\dot{C}_2(t) + \dot{C}_1(t)$$
$$+ \dot{C}_1(t)A^*C_2(t) + C_1(t)A^*\dot{C}_2(t) - \frac{Q_k}{Q_2}\dot{P}_{k+}(t)$$
$$- \frac{Q_k}{Q_2}\dot{P}_{k+}(t)A^*C_2(t) - \frac{Q_k}{Q_2}P_{k+}(t)A^*\dot{C}_2(t)] \qquad \text{Eqn G.7}$$

- Post-support equation:

$$\frac{\dot{C}(t)}{\dot{C}_{max}} = \frac{Q_2}{M}\left[\frac{Q_1}{Q_2}A^*\dot{C}_2(t) + \dot{C}_1(t) + \dot{C}_1(t)A^*\dot{C}_2(t) + \dot{C}_1(t)A^*C_2(t) + \frac{Q_k}{Q_2}\dot{P}_{k-}(t) - \frac{Q_k}{Q_2}P_{k-}(t)A^*\dot{C}_2(t) + \frac{Q_k}{Q_2}\dot{P}_{k-}(t)A^*C_2(t) - \frac{K}{Q_2}\dot{C}(t)C_{x\infty} - \frac{K}{Q_2}C(t)A^*\dot{C}_2(t) - \frac{K}{Q_2}\dot{C}(t)A^*C_2(t) + \frac{K}{Q_2}A^*\dot{C}_2(t)C_s\right]$$

Eqn G.8

It is important to note that Eqns G.6 and G.7 are independent of magnitude; both the magnitude of ultimate convergence ($C_{x\infty}$), and the magnitude of the maximum convergence rate. However, Eqn G.8 is *not* independent of magnitude, but requires at least an estimate of $C_{x\infty}$. Although these equations have been normalized to $\dot{C}_{max}$, the convergence rate at anytime could have been used, and it would still be independent of magnitude. Also, the solution of Eqn G.8 involves iteration, as $\dot{C}(t)$ appears on both sides of the equation. It has been presented this way because when the Convergence Solution is expanded in Chapter 5 to model sequentially staged excavations, it needs to be calculated in this manner.

APPENDIX H

Extension of Convergence Solution to Model Yield Zone Propagation.

The Convergence Solution has been extended to model the yield zone propagation that occurs in the Enasan Tunnel case history, analyzed in Chapter 5. This extension, outlined below, is only intended as a first approximation of modelling this complex phenominon.

At present, the Convergence Solution models a sequentially excavated tunnel as having a constant R/a ratio. This means that as the tunnel radius (a) increases with the bench and invert excavations, the yield zone propagates to maintain a constant R/a ratio. This assumption is discussed in Chapter 5, and illustrated in Fig. 5.8. The "yield zone propagation" that is to be modelled here is an *additional* propagation to a higher ratio of R/a. The stages of a sequentially excavated tunnel would be modelled separately, each propagating from an initial R/a to a higher R/a at a given time. These results would then be superimposed.

The propagation to a higher R/a can be modelled by changing the parameters X and $C_{X\infty}$. The parameter X is directly proportional to R (X/R = 0.84) and would be altered according to the change in R. The ultimate time-independent convergence ($C_{X\infty}$) also increases as the yield zone propagates, but it is not proportional to R. Note that

eventhough the Convergence Solutionis independent of $C_{x\infty}$, the fact that $C_{x\infty}$ changes requires a knowledge of:

$$\frac{C_{x\infty}(\text{after propagation})}{C_{x\infty}(\text{before propagation})}$$

This ratio can be calculated based on the following equation (Kaiser, 1980), that gives the tunnel wall displacement for a tunnel in yielding ground:

$$\frac{u}{u^e} = \frac{\lambda_e}{1+a}\left[2\left(\frac{R}{a}\right)^{(1+a)} + a - 1\right] \qquad \text{Eqn H.1}$$

where: u^e = displacement of tunnel wall for elastic case;

a = dilation factor of yielded ground; and

$$\lambda_e = \frac{1}{1+m}\left(m - 1 + \frac{\sigma_c}{\sigma_o}\right) \qquad \text{Eqn H.2}$$

where: σ_c = uniaxial compressive strength of the ground;

σ_o = initial ground stress; and

$m = \frac{1+\sin\phi}{1-\sin\phi}$

The following parameters have been used to reflect the conditions at the Enasan Tunnel:

$a = 1.0$ (no dilation of yielded ground);

$\frac{\sigma_c}{\sigma_o} = 0.25$; $\phi = 25$ degrees;

$m = 2.5$; $\lambda_e = 0.5$.

The substitution of these quantities into Eqn H.1 yields:

$$\frac{u}{u^e} = \frac{1}{2}\left(\frac{R}{a}\right)^2 \qquad \text{Eqn H.3}$$

This relationship has been used in Chapter 5 to model the yield zone propagation a the manner that is illustrated below. In the example fit (Section 5.4.1) of the data from Station A, Postion H2, the Convergence Solution indicated that the yield zone propagated from an initial value of R/a=2.5 to R/a=4.5 at t=40 days. This propagation was modelled as follows:

The value of R/a was changed from 2.5 to 4.5 in the Convergence Solution; and

The Convergence Solution was multiplied by the ratio:

$$\frac{C_{x\infty}(\text{after propagation})}{C_{x\infty}(\text{before propagation}}$$

determined in the following manner:

$$\frac{u}{u^e}(\text{before prop.}) = \frac{1}{2}(2.5)^2 = 3.125$$

$$\frac{u}{u^e}(\text{after prop.}) = \frac{1}{2}(4.5)^2 = 10.125$$

Since $C_{x\infty}$ is proportional to tunnel wall displacement, the ratio becomes:

$$\frac{C_{x\infty}(\text{after propagation})}{C_{x\infty}(\text{before propagation}} = \frac{10.125}{3.125} = 3.24$$

All of the cases presented in Chapter 5 were calculated in this manner.